

CFD modeling of combustion of solid waste materials with low melting points

Dissertation

zur Erlangung des akademischen Grades

Doktoringenieur (Dr.-Ing.)

von M.Sc. Muhammad Usman Farid
geb. am 07.05.1990 in Sahiwal, Pakistan

genehmigt durch die Fakultät für Verfahrens- und Systemtechnik
der Otto-von-Guericke-Universität Magdeburg

Promotionskommission:	Prof. Dr.-Ing. habil. Eckehard Specht	(Vorsitz)
	Prof. Dr.-Ing. habil. Evangelos Tsotsas	(Gutachter)
	Prof. Dr.-Ing. Andreas Bück	(Gutachter)
	Dr.-Ing. Nico Zobel	(Gutachter)

eingereicht am: 21.11.2017

Promotionskolloquium am: 01.02.2018

Acknowledgements

This work has been financially supported by **University of Agriculture, Faisalabad-Pakistan** under UAF-FDP project, “Establishment of Sub-Campus of UAF at Depalpur, Okara”. The research work has been conducted with a collaboration and excellent technical support provided by **Fraunhofer Institute for Factory Operation and Automation (IFF) Magdeburg, Germany**. I wish to express my deep gratitude and acknowledgement to the above mentioned institutes for their kind support.

It is a matter of immense pleasure for me to express my earnest gratitude and regards to my supervisor, **Jun.-Prof. Dr.-Ing. Andreas Bück** who provided me an opportunity to work in his research group at the chair of Thermal Process Engineering, Otto von Guericke University Magdeburg, Germany. He encouraged me at every step through valuable and constructive advices which helped me throughout my research work. It was a privilege to work under his enthusiastic and enlightened supervision.

I wish to express my deep gratitude and thanks to the head of the chair, **Prof. Dr.-Ing. habil. Evangelos Tsotsas** for his sublime guidance and encouragement which helped to improve my scientific skills. His valuable remarks and constructive criticism have a remarkable contribution towards the successful completion of my dissertation.

I also wish to record my sincere regards to **Dr.-Ing. Nico Zobel** (Fraunhofer IFF) for his kind guidance and support throughout my research work. The fruitful discussions and innovative ideas contributed to the advancement of my scientific work.

I would also like to show my sincere gratitude and thanks to **Dr.-rer. nat. Wolfram Heineken** (Fraunhofer IFF) for providing excellent technical support during my project. He was always there for help whenever I was stuck in some problem. His support and guidance significantly improved technical and computational skills.

I also pay regards and thanks to all my colleagues at the Chair of Thermal Process Engineering, especially **Dipl.-Ing. Nicole Vorhauer** and my other office colleagues for providing a friendly and wonderful working atmosphere.

I also pay my sincere thanks to my dear friends in Magdeburg as well as in Pakistan for their care and best wishes and making my social life so memorable.

Last but not the least, I would like to thank and assiduously acknowledge my parents, brothers (**Muhammd Zeeshan Farid** and **Muhammad Imran Farid**) and sister (**Anam Sadia**) for continuously supporting, motivating and encouraging me at every step throughout my life. Particularly, I have no words to owe a debt of gratitude to my (Late) father. Without his immense love, care and support, I could never have come so far.

I dedicate this thesis to the loving memory of my father (**Late) Maher Sher Muhammad Dadra**.

Muhammad Usman Farid
Magdeburg, November 2017

Abstract

Energy and environment are global issues worldwide. Disposal of waste, especially in the solid form, has been identified as a major problem around the globe. Solid waste is generated as a result of different domestic, commercial and industrial applications. Large quantities of solid wastes are usually dumped into landfills at substantial costs. Sometimes the solid waste consists of hazardous components which may create adverse environmental degradation and, hence, are not suitable for the landfills. Scarcity in available land for dumping of continuously increasing solid waste is another challenge faced in the current era of rapidly accelerating urbanization. There is a dire need to introduce alternative techniques for the management of these huge quantities. Thermal treatment, or in other words combustion, is an attractive way to get rid of possibly hazardous wastes. It reduces the large volumes of the solid waste materials for relatively easy disposal while generating low levels of secondary pollution. Handling of huge quantities of solid (waste) materials becomes much easier through this technique. Energy generation is an additional benefit of this technique. Different waste-to-energy techniques have shown promising outcomes to meet the challenges of energy scarcity in the recent years. With the technological advancements, different combustion techniques have been introduced. However, there is always a question of efficient and complete burning of the solid fuel along with low levels of flue gas emissions. Pulverized fuel combustion (PFC) is one of the latest combustion technologies in which solid materials are burnt in the form of small particles, injected pneumatically into the combustion furnace. PFC technology has been proved to be an efficient combustion technique and, hence, widely being used in the industrial furnaces and boilers. However, severe challenges are faced if the solid (waste) material contains components with low melting point. Having a low melting point, it becomes difficult to manage and convey the pulverized material to the hot combustion chamber. Faced to high temperatures from the combustion zone, fuel particles are melted within the nozzle. The melting of fuel causes clogging in the fuel transport nozzle used to convey the material into the combustion chamber. The present study was conducted in order to address this issue. In this work, a new technology for combustion of materials with low melting points ($< 60^{\circ}\text{C}$) is proposed, focusing on apparatus and nozzle design to prevent clogging. For this purpose, different nozzle designs were evaluated through multiphase CFD simulations. The effect of different operating conditions on the combustion process and, particularly, on nozzle temperature was studied with different nozzle designs. It was concluded from the outcomes that air flow rates supplied through the fuel nozzle have a significant influence on nozzle temperature. Nozzle temperature decreases by approximately 20 K by increasing the nozzle air flow rate by a factor of 1.75. A parametric study was conducted with different fuel particle sizes. It was revealed that small fuel particle size results in wider combustion zone near the fuel nozzle exit while large fuel particles produce a rather long combustion zone further away from the nozzle exit. Hence, a high temperature near the injection point is observed with small

fuel particle size. An optimum particle size of 10 μm was proposed for the combustion of solid materials with low melting point. Moreover, an optimization study with different air flow rates supplied to the combustion furnace resulted that besides significantly decreasing the nozzle temperature, high air flow rates also have a cooling effect on the combustion zone resulting in low combustion temperatures. The optimum results have been obtained with a nozzle air flow rate of $40 \text{ m}^3 \text{ h}^{-1}$ (with Nozzle 2). The effect of heat flux from the furnace was also studied. It is resulted that the combustion temperature significantly decreases by the heat loss from the furnace walls. This is in favor of the usage of simpler fuel nozzles for the transportation of solid materials with low melting point. Installing the primary air inlet near to the fuel nozzle also reduces the temperature near the nozzle exit. The major finding of the current work is the optimized fuel nozzle design and air flow suitable for the transportation of pulverized material with low melting point ($< 60^\circ\text{C}$).

Kurzzusammenfassung

Energie und Umwelt sind Themen von globaler Bedeutung. Müllentsorgung, insbesondere die von Müll in Form von Feststoffen, gilt weltweit als ernstzunehmendes Problem. Feststoffmüll entsteht als Ergebnis verschiedenster Gebräuche im häuslichen, gewerblichen und industriellen Bereich. Die enormen Mengen an Müll werden üblicherweise mit einem hohen Kostenaufwand auf Deponien verbracht. Es kommt vor, dass im Müll gefährliche Stoffe enthalten sind, die der Umwelt schaden und daher auf herkömmlichen Deponien nicht fachgerecht entsorgt sind. Eine weitere Herausforderung in dieser Zeit der fortlaufenden Urbanisierung ist der Mangel an Land der zur Deponierung der steigenden Müllmassen zur Verfügung steht. Es ist dringend notwendig alternative Techniken für die Bewältigung dieser Massen anzuwenden. Wärmebehandlung und Verbrennung sind geeignete Formen der Entsorgung von möglicherweise gefährlichem Müll. Sie reduzieren die hohen Mengen an Feststoffmüll mit einer nur geringen sekundären Verschmutzung, weshalb sie sich für den Umgang mit großen Müllmassen eignen. Ein weiterer Vorteil dieser Technik ist die Energieproduktion. Verschiedene Energie-aus-Abfall Techniken erzielen vielversprechende Ergebnisse um den Herausforderungen der Energieknappheit in den folgenden Jahren zu begegnen. Dank technischer Fortschritte wurden verschiedene Techniken zur Verbrennung eingeführt. Nichtsdestotrotz bleibt die Frage der effizienten und kompletten Verbrennung von festen Brennstoffen in Zusammenhang mit möglichst gering schadstoffbelasteten Abgasen bestehen. Die Verbrennung von pulverisiertem Brennstoff (PFC) ist eine der neuesten Techniken, bei der feste Stoffe als kleine Partikel pneumatisch in die Verbrennungskammer geblasen und dort verbrannt werden. PFC hat sich als effiziente Verbrennungstechnik erwiesen und findet daher viel Anwendung in industriellen Feuerungen und Kesseln. Dennoch entstehen hier ernsthafte Herausforderungen wenn die Feststoffe Bestandteile mit einem geringen Schmelzpunkt enthalten. Bei Bestandteilen mit geringem Schmelzpunkt ist es schwierig die pulverisierten Stoffe zu der heißen Verbrennungskammer zu befördern, da die Brennstoffpartikel aufgrund der hohen Temperaturen bereits in der Düse schmelzen und der Stofftransport in ihr blockiert wird. Die vorliegende Arbeit wurde erstellt um sich eben jenem Punkt zu widmen. Es wird eine neue Technologie zur Verbrennung von Stoffen mit einem niedrigen Schmelzpunkt ($< 60^{\circ}\text{C}$) vorgestellt, bei der der Fokus auf einem Apparat- und Düsensdesign liegt, welches die Blockierung der Düsen verhindert. Hierfür wurden verschiedene Formen von Düsen anhand von mehrphasigen CFD Simulationen bewertet. Der Einfluss von verschiedenen Betriebsbedingungen auf den Verbrennungsprozess und insbesondere die Düsentemperatur wurde anhand der unterschiedlichen Düsenformen untersucht. Aus den Ergebnissen lässt sich schließen, dass der Luftstrom der Brennstoffdüse einen erheblichen Einfluss auf die Düsentemperatur hat. Die Düsentemperatur reduziert sich um ungefähr 20 K, wenn der Düsenluftstrom mit dem Faktor 1.75 erhöht wird. Eine Parameterstudie mit verschiedenen Brennstoffpartikelgrößen wurde durchgeführt. Sie zeigte, dass kleinere Brennstoffpartikelgröße zu einer breiteren Verbrennungszone in der Nähe des

Düsenausgangs führt, während größere Brennstoffpartikel eine eher längere Verbrennungszone vergleichsweise weit entfernt vom Düsenausgang produzieren. Somit wird eine hohe Temperatur in der Nähe des Eintrittspunkts in Verbindung mit kleineren Brennstoffpartikelgrößen beobachtet. Eine optimale Partikelgröße von 10 μm wurde für die Verbrennung von Feststoffen mit geringem Schmelzpunkt vorgeschlagen. Zudem zeigte die Untersuchung verschiedener Luftströme zur Versorgung der Verbrennungskammer dass, während die Düsentemperatur signifikant reduziert wird, hohe Luftströme ebenso einen kühlenden Effekt auf die Verbrennungszone haben, was zu niedrigeren Verbrennungstemperaturen führt. Die optimalen Ergebnisse wurden mit einem Luftstrom von 40 $\text{m}^3 \text{h}^{-1}$ (mit Düse 2) erzielt. Außerdem wurde der Einfluss von Wärmeübertragung aus der Kammer untersucht. Es wurde gezeigt, dass sich die Verbrennungstemperaturen bei einem Wärmeverlust der Verbrennungskammerwände deutlich reduzieren. Das spricht auch für den Einsatz von einfacheren Bauformen der Brennstoffdüse für den Transport von Feststoffen mit einem geringen Schmelzpunkt. Ist der erste Lufteintritt in der Nähe der Brennstoffdüse eingebaut wird auch die Temperatur in der Nähe des Düsenausgangs reduziert. Den Kern dieser Arbeit bilden das optimierte Brennstoffdüsendesign sowie die feststellung des Luftstroms, der sich für den Transport von pulverisierten Stoffen mit niedrigem Schmelzpunkt ($< 60^\circ\text{C}$) eignet.

Nomenclature

Symbols

A	Area	m^2
C_p	Specific heat capacity	$J\ kg^{-1}\ K^{-1}$
d	Diameter	m
E	Energy flow rate	$J\ s^{-1}$
HV	Heating value	$J\ kg^{-1}$
k	Thermal conductivity	$W\ m^{-1}\ K^{-1}$
\dot{M}	Mass flow rate	$kg\ s^{-1}$
Pr	Prandtl number	-
q	Heat flow rate	$J\ s^{-1}$
Re	Reynolds number	-
Sc	Schmidt number	-
Sh	Sherwood number	-
T	Temperature	$^{\circ}C$
u	Velocity	$m\ s^{-1}$
V	Volume	m^3
W	Weight	kg
X	Mass fraction	-

Greek letters

ε	Emissivity coefficient	-
λ	Excess air ratio	-
ν	Specific volume	$m^3\ kg^{-1}$
ρ	Density	$kg\ m^{-3}$
σ	Stefan Boltzmann constant	$W\ m^{-2}\ K^{-4}$

Subscripts/superscripts

A	Air
ad	Adiabatic
C	Carbon
Comb.	Combustion
cv	Convection
f	Fuel
fr	Fraction
G	Gas
H	Hydrogen

i	Species/initial
N	Nitrogen
O	Oxygen
P	Particle
r	Residue
rd	Radiation
S	Sulfur
t	Total/time
w	Wall

Abbreviations

AD	Air demand
ASH	Ash content
CA	Cooling air
CAD	Computer aided design
CFD	Computational fluid dynamics
CV	Calorific value
DO	Discrete ordinates
DPM	Discrete phase modeling
EDM	Eddy dissipation model
FBC	Fluidized bed combustion
FC	Fixed carbon
FLOX	Flameless oxidation
FTA	Fuel transport air
GCV	Gross calorific value
HiTAC	High temperature air combustion
HV	Heating value
HHV	Higher heating value
LHV	Lower heating value
MC	Moisture content
MILD	Moderate or intense low oxygen dilution
MSW	Municipal solid waste
NCV	Net calorific value
NO _x	Nitrogen oxides
OD	Oxygen demand
PE	Polyethylene
PET	Polyethylene terephthalate
PFC	Pulverized fuel combustion

PP	Polypropylene
RDF	Refused derived fuel
SBM	Species balance model
SRF	Solid recovered fuel
SST	Shear stress transport
VM	Volatile matter
WtE	Waste to energy

Table of Contents

Acknowledgements	i
Abstract	ii
Kurzzusammenfassung	iv
Nomenclature	vi
Table of Contents	ix
1. Introduction and Motivation	1
1.1 Overview	1
1.2 Solid waste management	1
1.3 Combustion of solid waste	2
1.4 Waste-to-energy	3
1.5 Combustion of solid materials: methods and technologies	4
1.6 The new work.....	6
1.7 Outline of the thesis.....	7
2. Combustion of Solid Materials	9
2.1 Introduction	9
2.2 Fuel classification.....	10
2.3 Solid fuels: chemical and thermal characteristics.....	11
2.3.1 Proximate analysis.....	11
2.3.2 Ultimate analysis	13
2.3.3 Heating value of solid fuel	14
2.4 Types of solid fuels	15
2.5 Modeling of combustion process.....	18
2.6 Species balance model (SBM).....	18
2.6.1 Oxygen demand (OD)	19
2.6.2 Air demand (AD).....	19
2.6.3 Air supply and excess air ratio (λ).....	20
2.6.4 Combustion gases/flue gases composition	21
2.6.5 Calculation sheet for species balance model (SBM)	22
2.7 Mass and energy balance model.....	24
2.7.1 Mass balance	24
2.7.2 Energy balance	24
2.7.3 Adiabatic combustion temperature.....	25
2.8 Results and discussion.....	26

2.8.1 Oxygen demand (OD)	26
2.8.2 Air demand (AD).....	27
2.8.3 Adiabatic combustion temperature.....	28
2.8.4 Effect of excess air on adiabatic temperature	30
2.8.5 Effect of air preheating.....	34
2.8.6 Composition of combustion gases.....	35
2.8.7 Formation of nitrogen oxides (NO _x).....	38
2.9 Summary	40
3. Pulverized Fuel Combustion (PFC) Technology	41
3.1 Pulverized fuel combustion (PFC)	41
3.2 Combustion mechanism in PFC	43
3.2.1 Fuel transportation or injection	44
3.2.2 Drying.....	44
3.2.3 Devolatilization	46
3.2.4 Char combustion.....	46
3.2.5 Ash formation.....	47
3.3 State of the art in PFC technologies	48
3.3.1 PFC of solid materials: coal and other solid materials	48
3.3.2 Burner designs and furnace aerodynamics	50
3.3.3 Pre-heating and MILD combustion technology	53
3.3.4 Melting phenomena of solid particles during PFC.....	57
3.3.5 Computational fluid dynamics (CFD) modeling of PFC.....	62
3.4 Outcomes and further challenges in PFC	66
4. CFD Modeling of PFC for Solid Materials with Low Melting Points	68
4.1 Introduction	68
4.2 A case study of paint residue.....	68
4.3 Combustion plant for pulverized waste.....	71
4.3.1 Fuel transport nozzle	73
4.4 CFD modeling methodology	74
4.4.1 Modeling approach.....	76
4.4.2 CFD computational domain and boundary conditions	82
4.4.3 Operating conditions	84
4.5 Results and discussion.....	85
4.5.1 Mesh sensitivity analysis.....	85
4.5.2 Temperature distribution in the furnace	87
4.5.3 Nozzle temperature.....	90

4.6 Summary and outcomes	91
5. Optimization of Fuel Nozzle for PFC	93
5.1 Overview and motivation	93
5.2 Fuel nozzle designs	94
5.3 Operating conditions	97
5.3.1 Nozzle air	97
5.3.2 Primary air	97
5.3.3 Secondary air	98
5.4 CFD modeling approach	99
5.5 Results with Data Set 1: Study of different nozzle geometries	99
5.5.1 Temperature distribution	99
5.5.2 Nozzle 1	101
5.5.3 Nozzle 2	101
5.5.4 Nozzle 3	103
5.5.5 Nozzle 4	104
5.6 Modifications in nozzle air	104
5.7 Results with Data Set 2: Study with modified nozzle air flow rates	104
5.7.1 Temperature distribution	104
5.7.2 Nozzle 1	107
5.7.3 Nozzle 2	108
5.7.4 Nozzle 3	109
5.7.5 Nozzle 4	110
5.8 Study of different fuel particle sizes	112
5.8.1 Temperature distribution with small fuel particle size	113
5.8.2 Temperature distribution with large fuel particle size	113
5.9 Optimization of nozzle air with Nozzle 2	121
5.9.1 Variations in nozzle air	121
5.9.2 Sectional air flow rate increase	126
5.10 Effect of excess air ratio (λ)	132
5.11 Comparison of CFD results with the literature	134
5.12 Summary	135
6. Simplification of the Fuel Transport Nozzle	136
6.1 Overview and motivation	136
6.2 Effect of nozzle air flow rate: A case of water cooling	136
6.3 Primary and secondary air	137
6.4 Simulation results with different nozzle air flow rates	138

6.5 Effect of water cooling and primary air injection position.....	140
6.6 Simulation results.....	141
6.7 Effect of heat losses through furnace walls: A case of air cooling.....	143
6.8 Simulation results with heat flux through walls: Heat losses to ambient air.....	145
6.9 A case of materials with melting point at 60°C.....	146
6.10 Summary.....	149
7. Partial Validation of CFD Model for PFC.....	150
7.1 Overview.....	150
7.2 Experimental investigations.....	150
7.3 CFD simulation results.....	153
7.4 Comparison between experimental and simulation results.....	155
7.5 Outcomes and reasons for discrepancies.....	156
7.6 A case of optimized nozzle: Comparison with calculated results.....	156
7.7 Summary.....	158
8. Conclusions and Outlook.....	159
Bibliography.....	163
Appendices.....	174
Appendix A: Tabulated data of SBM model and mass and energy balance model.....	174
Appendix B: Domain of furnace with different nozzles and CFD simulation results.....	179
Appendix C: CFD Simulation results of simplified nozzle (Chapter 6).....	195
Appendix D: Contours of flue gases (Chapter 7).....	200
Appendix E: List of CFD simulations.....	201
List of Own Publications and Student Theses.....	203
Curriculum Vitae.....	204

Introduction and Motivation

1.1 Overview

Energy and environment are attaining special focus these days and are considered among the major issues worldwide. The rapid increase in population, booming urbanization and modern advancements in living standards has brought a significant enhancement in the generation of different kinds of wastes which harm the natural environment in different ways. Waste may be defined as anything which is left over and inessential having no marginal value for the owner. Solid waste is a form of waste which is considered to be in solid phase, however, it is also found in other forms like liquid-chemical waste and semi-solid phase e.g. sludge etc. [1]. Solid waste, if not managed efficiently, imparts a major contribution in the overall environmental degradation and depletion of natural resources. Major problems associated with the solid waste, in particular, include occupation of large space/volume, nuisances and public health problems (e.g. formation of odors, unpleasant environment, insects, pathogens etc. due to accumulation and aggregation of solid waste materials), economy, environmental contamination and depletion of resources [1]. The global volume of solid waste has been reported as 11 billion tons per year. The quantity of solid waste is estimated to be 1.74 tons per year per capita worldwide [2]. Solid waste is generated in different domestic, commercial and industrial production and application processes and activities. However, it is categorized depending upon the production source, e.g. domestic waste, commercial waste, industrial waste, biomedical waste, agricultural waste, construction waste etc. Handling and management of these huge quantities of solid waste is becoming an emerging global environmental issue around the globe. Waste generation is, indeed, a depiction of energy losses in a system and hence imparts additional costs to the community in terms of collection, transportation, management/treatment and adequate disposal [3]. Furthermore, it imposes diverse effects on the equilibrium of natural ecosystem and living conditions in a community [4]. Attentions must be given to introduce latest solid waste management techniques to dispose these large volumes of wastes.

1.2 Solid waste management

Due to the rapid solid waste generation and problems associated with these huge quantities of solid wastes, it has become essential to effectively manage solid waste for environmental, economical and social sustainability [3,4]. Waste management strategy, in general, includes different stages like identification, separation and characterization, collection, treatment and disposal of solid waste. Type of waste material and its composition play an important role while designing a solid waste management system. Complex problems are faced in solid waste management systems because of different compositions of waste materials [5]. Hence,

selection of any solid waste management system mainly depends on type, composition and amount of solid waste. In recent decades, attentions have been directed towards modern methods and systems for management of solid waste. Conventionally, a huge quantity of solid waste is being disposed in open fields and landfills. Dumping of solid waste requires a large space and technical expertise for the construction of landfill site as it threatens the environment if not designed and constructed efficiently. Efforts are being made to reduce the quantity of solid waste to be dumped and to enhance recycling, re-use and alternative methods for management of solid waste materials [3][6].

Landfill is not a suitable option, especially, when the waste material contains hazardous constituents. Due to improper lining and construction material, hazardous and reactive constituents may leach down and pollute the ground water. According to EU Landfill Directive (1999/31/EC), origin, source, production, constituents, chemical and physical properties and structure of waste materials are the basic requirements for landfill directive and therefore, hazardous properties of waste materials must be analyzed according to Hazardous Waste Directive 1991/689/EEC before disposing into the landfills. Industrial by-products produced in different production and application processes have a major contribution to commercial and industrial waste. In some cases, these wastes contain hazardous constituents and are considered to be toxic in nature and hence, become difficult to dump in landfills. Moreover, these waste materials have a very complex compound structure. Ecotoxicological tests also showed that these kinds of materials consist of hazardous components; therefore, landfill is not an appropriate method for the disposal [7]. There is a dire need to introduce alternative methods to manage this kind of solid wastes.

1.3 Combustion of solid waste

Thermal treatment is one of the solid waste management techniques. It is emerging as an attractive way to get rid of larger volumes of solid waste materials and allows disposal to landfills at comparatively less space as well as lower cost. Combustion or incineration is one of the thermal conversion methods in which the combustible constituents of solid waste materials are burnt at high temperatures in order to produce ash and gaseous products. It has been found to be an appropriate technique for the management of wastes especially when it is not suitable to dispose them into landfills directly e.g. hazardous wastes. The main advantage of this method is the reduction of larger and bulky volumes of waste materials for easy handling, transportation and disposal. It reduces the initial volume of the solid waste up to 85% while eliminating the odor and leachate present in the solid waste materials [8-10]. Additional aim of burning of solid waste is to remove the toxicity of the hazardous constituents present in it. Combustion of solid materials is found to be appropriate for materials which are dispersed, volatile, resistive to decomposition, and cannot be degraded biologically. Combustion or incineration is typically carried out for materials like industrial wastes, refinery wastes, materials containing grease and waxes, waste oils and oil emulsions and other organic waste materials [11]. Beside the reduction of large volumes and removal of

toxic constituents, combustion of solid waste also generates a large amount of thermal energy which can be used for power generation or heating purposes within the industry or local community. In modern waste management systems, strategies are being shifted from landfill methods to the thermal treatment of the solid wastes to recover the useful energy contained in the solid materials.

1.4 Waste-to-energy

With the latest evolution in modernization and rapidly depleting fossil fuels, the gap between available energy and the energy requirement is constantly expanding. According to an estimate, around 2 billion people in the world still lack in available electrical energy [12]. There is a need of introducing alternative and sustainable sources of energy to close this gap. Energy sources can be mainly classified into fossil fuels, nuclear energy sources and renewable sources of energy. The former two sources are significantly expensive while the later, being affordable, reliable and environmentally stable, provides a sustainable solution for the generation of energy. During recent years, energy generation systems have been shifted from conventional methods to the renewable energy generation methods. Currently, about 23.7% of the total world's energy demand is generated through renewable energy sources, while in 1998 the total contribution of renewable energy sources was only 2% [12]. Research is being carried out in order to introduce and evaluate the alternative and renewable sources to produce energy.

Waste-to-energy (WtE) techniques have become popular in recent years. Energy generation from combustion of waste material also provides a reliable and alternative solution for energy scarcity. Generation of electricity and heat or in other words energy recovery through thermal treatment of solid (waste) materials, e.g. combustion of waste materials, is termed as waste-to-energy (WtE) technique (Fig. 1.1). Waste-to-energy (WtE) techniques play an important role in the management of solid waste by destroying the toxic and harmful materials and reducing the burden on landfills and over-all waste management system [13,14]. WtE technology is more advantageous for waste materials containing components with higher calorific value and, ultimately, generating high amount of energy, e.g. plastics etc. Moreover, consumption of fossil fuels is significantly reduced along with preservation of natural environment using such technologies [15,16]. There are several WtE techniques and energy conversion methods, for example incineration/combustion, biodegradation, solid recovered fuels and refused derived fuels. However, power generation through incineration is one of the most dominant technologies. Furthermore, selection of any WtE technique highly depends upon the chemical and physical characteristics of the material [9,17]. The early processes for energy recovery were simply to join an incinerator and a boiler to get the thermal energy. However the differentiation between conversion and energy recovery is still a point to ponder [18].

Solid recovered fuel (SRF) or sometimes termed as refuse derived fuel (RDF) technology is an advanced WtE technology. It is used to enhance the combustion ability of a solid waste material through mechanical operations. Generation and utilization of solid recovered fuels

(SRF) is an alternative solution for those waste materials which cannot be recycled. SRF is the safest way to manage non-sustainable waste fractions. Special attention is being diverted to such technologies by different energy intensive industries in order to save primary fuels and substantial costs for energy utilization. However, it is necessary to enhance the quality of solid recovered fuels (SRF) in order to burn them in coal fired power plants and cement or lime producing industries so that operative and technical problems can be avoided. Commercial and industrial waste materials consist of a significant amount of energy content which should be recovered. The proper sorting and separation can ensure a good quality of solid recovered fuels [19-22].

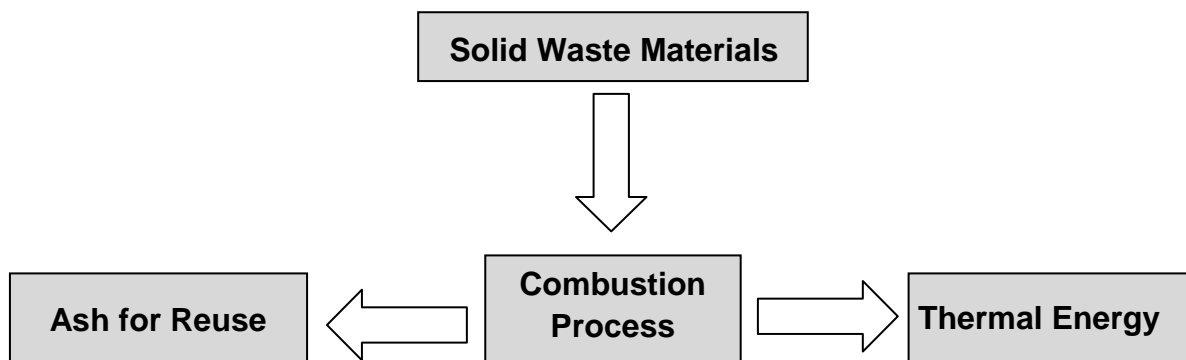


Fig. 1.1: Efficient management of solid waste materials

Besides the generation of thermal energy, the combustion process of solid waste materials also results in bottom ash as a by-product which can be processed and used for further purposes. It contains many valuable constituents like phosphor, potassium, iron scarp, aluminum and copper, which can be utilized for useful purposes. However, utilization of ash produced for a specific purpose depends on the type of (waste) fuel combusted. For example, ash produced in the combustion process of biomass and sewage sludge is used as fertilizer as it is rich in many nutrients and mineral fractions. Similarly, ash generated by the combustion of municipal and industrial solid waste materials consists of stony material, ceramics, glasses and ceramic constituents and, hence, can be utilized as additive in cement, bricks, ceramics and other construction materials. Therefore, there is a need to not only recover energy but also to extract valuable products generated from the incineration/combustion of waste materials [23-28].

1.5 Combustion of solid materials: methods and technologies

Conventionally, solid wastes used to be burnt in open fields. This method was most common for agricultural waste produced after the harvesting season. Due to its simplicity and ease of use, it has also been used to handle refuse from municipal, yard, garden and construction sources. However, uncontrolled combustion methods were found to occur at low temperatures and were one of the major factors for environmental pollution and global warming [29,30].

Utilization of raw materials obtained from different waste materials in the form of briquettes has imparted a significant improvement in the combustion of solid wastes. In this method,

solid waste materials are densified, i.e. density of the bulky materials is increased by mechanical forces in order to form briquettes or pellets of solid waste material, which are then burned in fixed bed combustors or kilns. In addition, briquetting technology also contributes in reducing the emission levels and environmental hazards. Densification of coal and solid waste materials has been the most common technology in the past few years [31,32]. However, this technique also faces problems with efficient and complete burning such as poor ability to ignite and smoking etc.

Fluidized bed combustion (FBC) and gasification technology has imparted a broad advancement in the field of solid fuel combustion, particularly for solid waste materials like sewage sludge etc. In this method, solid fuel particles are suspended by primary air provided in upward direction from the bottom of the bed. The particles are continuously agitated and mixed by secondary air provided from the side walls. At the outlet of the fluidized bed, solid particles are removed from the flue gas with the help of cyclone separators. Recirculation of solid fuel particles with longer residence time results in efficient burning of materials with even high moisture contents. This technology is suitable for low-cost and low-quality solid fuels and for those solid materials which are very hard to burn [15,16]. However, this technology has certain drawbacks like additional equipment for separation, agglomeration etc. [33-35].

Pulverized fuel combustion (PFC) technology is one of the modern combustion technologies, which is widely used in industrial furnaces and boilers. In PFC technology, finely crushed fuel particles are injected into the combustion chamber along with the stream of air which is termed as transport air. In other words, powdered solid fuel is transported pneumatically to the combustion furnace through a fuel injection nozzle. In this way, combustion takes place at very high level of air-fuel mixing ratio. After burning of the solid fuel, flue gases leave through the outlet pipe and ash residue is collected by the ash collector provided at the bottom of the furnace.

In pulverized fuel combustion, the residence time of the fuel particles is relatively short and particles are not circulated as in case of fluidized bed combustion (FBC). The pulverized fuel combustion method is becoming the dominant combustion technology and is widely being implemented in blast furnaces, improving combustion efficiencies and reducing the overall costs. Attention is directed to improve the plant design and combustion processes to ensure higher thermal efficiencies [33][36-40].

Figure 1.2 represents the schematic view of a typical pulverized fuel combustion (PFC) system with different components, e.g. fuel nozzle, burner, combustion chamber, flue gas outlet and ash collector.

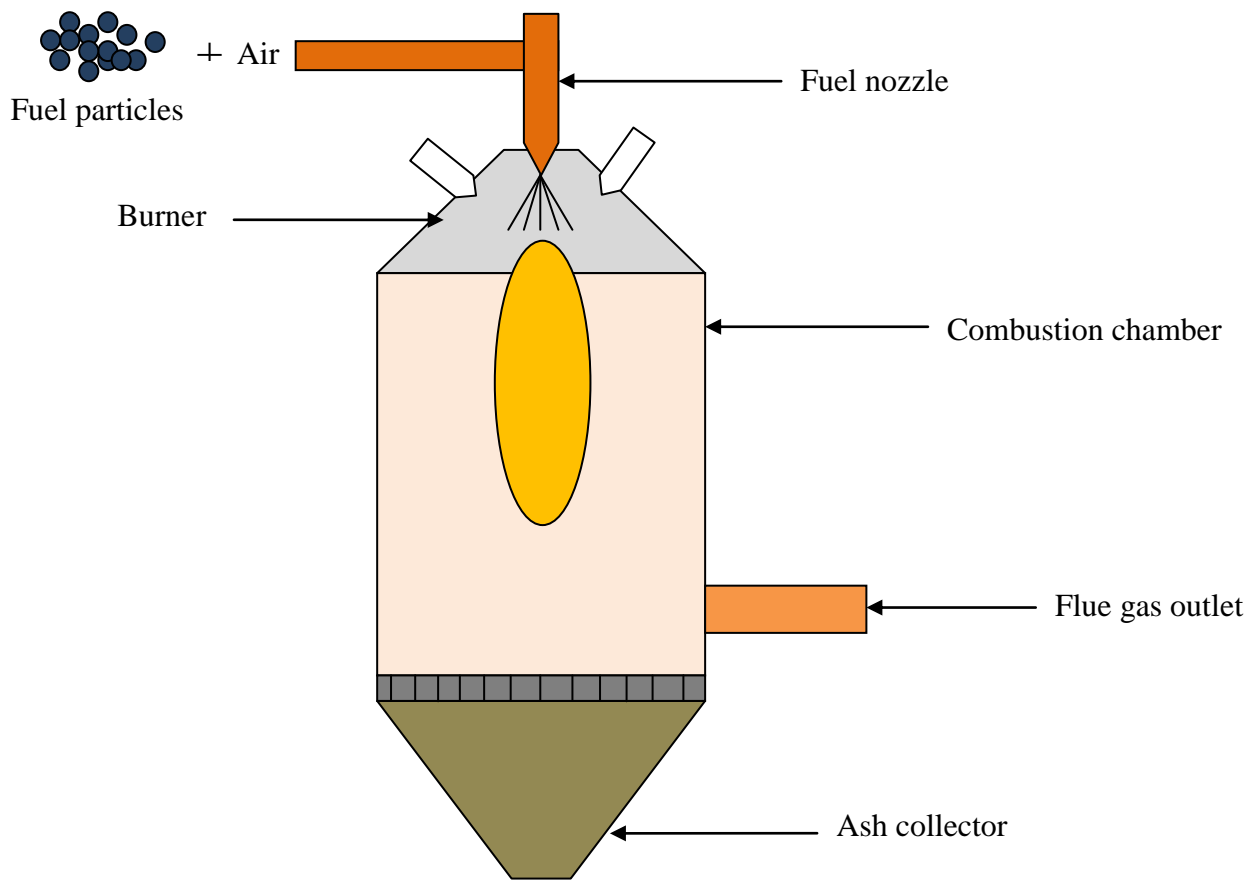


Fig. 1.2: Schematic diagram of pulverized fuel combustion (PFC) system

Currently, PFC technology is most commonly applied to coal as a fuel. Co-firing of coal along with secondary fuel is also an emerging method in PFC, however, utilization of other fuels in coal fired system requires certain optimization and modifications [33][36-40]. There is a need to apply such latest combustion technologies to other types of (waste) materials with improved combustion processes and energy recovery systems.

A review on state of the art technologies for pulverized fuel combustion will be presented later on in Chapter 3.

1.6 The new work

Based on recent reviews, it is evident that there is a dire need to study, improve and implement the latest combustion technologies, e.g. PFC technology for various solid materials. As described before, several technical challenges are faced while using different solid waste materials as a fuel in the traditional (PFC) furnaces. Chemical and thermal properties play an important role in the (PFC) combustion of solid waste materials. One of the most important properties, in this context, is the melting point of solid materials. Severe problems occur during the pulverized fuel combustion (PFC) process if the fuel (solid waste material) has constituents with low melting point. It becomes difficult to manage and convey such type of material in the combustion apparatus, particularly during transportation of fuel

particles into the combustion chamber through the fuel nozzle. Exposed to very high temperatures, the fuel particles start melting (already) in the fuel nozzle and transform into a semi-molten and sticky matter through agglomeration. This sticky material can block the fuel nozzle. A very efficient system is required for the transportation of such solid materials to the combustion furnace which should prevent the pre-melting of fuel particles in the fuel nozzle.

The present work has been planned to study the combustion behavior and characteristics of such solid materials during the pulverized fuel combustion (PFC) process. Special focus has been given to the characteristics and fate of solid (waste) materials with low melting point during combustion (PFC) process. It should be noted that no study was found so far in an extensive literature study about the combustion of such kind of materials which contain constituents with low melting points. Hence, the main objective of the conducted research was to present an optimized combustion system for such materials, i.e. solid materials with low melting point. A case of paint residue from spray paint industry is taken as it contains constituents with low melting point, i.e. around 60°C. Nozzle and apparatus design will be considered in detail.

Research strategy and objectives of the present work are given in the following:

1. Study of chemical and thermal characteristics of different solid materials.
2. General (mathematical) modeling of combustion phenomena of different solid materials.
3. Identification of the parameters influencing the overall combustion process.
4. Comprehensive CFD model for combustion of pulverized solid materials.
5. Optimization of fuel nozzle design for PFC of materials with low melting point.
6. Simplification of fuel nozzle for PFC of materials with low melting point.
7. Experimental validation of CFD model for PFC with low melting point.

1.7 Outline of the thesis

The thesis is organized into following contents:

Chapter 2 highlights the process parameters which influence the overall combustion process. A unified modeling approach is presented for the combustion of different solid fuels. Solid fuels are categorized into four classes, i.e. coal, biomass, municipal solid waste and industrial waste. For each category three samples are taken for analysis. Chemical compositions and thermal characteristics of these materials are discussed. Species balance model (SBM) is presented to analyze the reactants and products of the combustion process. A mass and energy balance model is also derived in order to investigate the inputs and outputs of the combustion process. Adiabatic temperature is computed from the proposed model. Moreover, the effects of different excess air numbers and preheat temperatures on the adiabatic temperature are also discussed.

Chapter 3 presents the fundamentals and characteristics of pulverized fuel combustion (PFC) technology. Application of pulverized fuel (PFC) technology to different solid fuels is

described. State of the art technologies for pulverized fuel combustion are presented. Process parameters and apparatus design influencing the pulverized fuel combustion (PFC) are also discussed. Moreover, problems and challenges associated with pulverized fuel combustion (PFC) for solid materials, especially materials with low melting point, are addressed.

In Chapter 4, application of computational fluid dynamics (CFD) modeling for the combustion process of pulverized fuel materials (with low melting point) is presented. Different sub-models and their application in PFC are discussed. A combustion system, i.e. furnace geometry and its components for the combustion of solid materials with low melting point, is presented. A base case is investigated with the stated operating conditions and geometry. As an outcome, the parameters affecting the combustion process are obtained for further work.

In Chapter 5, the study about optimization of different nozzle designs with respect to the problem stated, i.e. low melting point of fuel particles, is presented. Four different nozzle designs are evaluated through multiphase CFD simulations. Moreover, based on the base case, modifications are made in the operating conditions. In order to check the effect of fuel particle size, a case study about different particle sizes is presented. Optimization of nozzle air flow rates is also presented with the best case of fuel nozzle design obtained from the CFD simulation results. The effect of excess air on combustion characteristics is also analyzed.

Chapter 6 is a continuation of Chapter 4 and Chapter 5. In this chapter, a simplified design of fuel transport nozzle is presented in an effort to reduce the nozzle temperature. The effect of nozzle air flow rate in the proposed nozzle is discussed along with further technical, construction and operating aspects. An alternative method for reduction of nozzle tip temperature is presented. The effect of water cooling as well as heat flux is discussed with the suggested (simplified) nozzle design.

Chapter 7 is dedicated to a partial validation and comparison of simulation results of the proposed comprehensive computational fluid dynamics (CFD) model for the combustion of pulverized fuel with low melting point with a pilot plant combustion facility. For this purpose CFD simulations are conducted with the operating conditions of a real pulverized fuel combustion plant. The experimental measurements generated in the plant are compared with the simulation results. A comparison between results of mass and energy balance and simulation results is also presented for the optimized fuel nozzle. The outcomes from both investigations are discussed.

Chapter 8 presents a summary and conclusions about the novel technology for the combustion of materials with low melting point, along with an outlook about future work.

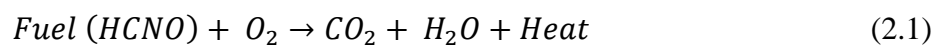
Combustion of Solid Materials

This chapter highlights the process parameters which influence the overall combustion process. A unified modeling approach is presented for the combustion of different solid fuels. Solid fuels are categorized into four classes i.e. coal, biomass, municipal solid waste and industrial waste. For each category three samples are taken for the analysis. Chemical compositions and thermal characteristics of these materials are discussed. A species balance model (SBM) is presented to analyze the reactants and products of the combustion process. A mass and energy balance model is also constructed in order to investigate the inputs and outputs of the combustion process. Adiabatic temperature is computed from the proposed model. Moreover, the effect of different excess air numbers and preheat temperatures on the adiabatic temperature is analyzed.

2.1 Introduction

Power generation by means of combustion is one of the oldest and most effective methods in energy sector. According to an estimate, combustion process (by using fossil fuels and renewable sources such as biomass etc.) contributes to about 90% of the total worldwide energy requirement for traffic, electricity and heating systems etc. Development and improvement of efficient combustion systems have been under consideration for several years. However, design of an efficient combustion system and quantitative investigations of the combustion processes require understanding of both technical aspects and combustion fundamentals [40,41].

Combustion is an energy conversion process in which energy bonded within the fuel is converted into thermal energy through an exothermic reaction. The combustion process involves a combustion reaction of fuel combustibles with air or oxygen, i.e. oxidation, heat production, and combustion gases/flue gas generation etc.



The basic goal of combustion is to extract the maximum amount of energy from the fuel or combustible material. In order to increase the efficiency of the combustion process it is necessary to burn all the combustible components present in the fuel. A certain amount of oxidizer is required to burn/oxidize the fuel. Air or sometimes pure oxygen is used as oxidizer in the combustion reaction. The combustion reaction is considered to be complete and efficient if fuel and oxidizers are in perfect balance conditions. In other words, enough air must be available to burn all the fuel combustibles. This can be explained chemically by “stoichiometric state of combustion”. A combustion reaction is assumed to be stoichiometric when fuel and oxidant are in a balanced ratio that corresponds to total oxidation [42]. Combustion processes and undergoing reactions can be explained and modeled mathematically using laws of conservation of energy, conservation of mass as well as

thermodynamics. Mass and energy balances are considered to be the basic elements when designing large and complex models for combustion processes. Therefore, it is necessary to study mass and energy balances for the combustion of different solid materials before implementing them in the combustion systems.

In order to understand the fundamentals of combustion phenomena and identify the factors affecting the combustion process in general, the present work addresses different types of solid fuel. Chemical and thermal properties of different solid fuels and their effects on the combustion process, particularly on combustion temperature, are studied. Mass and energy balances are formulated for the solid fuels. As an outcome of this work, air demand, adiabatic combustion temperatures and combustion products are computed from the mass/energy balance models. Effect of excess air on combustion temperature is also discussed, in order to be implemented later in Chapter 4.

2.2 Fuel classification

A fuel is a substance which chemically reacts with the oxidant (oxygen/air) to produce heat and secondary products, e.g. combustion gases. The choice of fuel depends upon the combustion facility to be used, heating values, ignition temperature, combustible and non-combustible constituents, combustion products, cost and transportation of fuel [43]. Type and characteristics of fuel play a leading role in the combustion process. Table 2.1 presents different types of fuels. Fuels are, generally, classified according to the physical state in which they are found such as solid, liquid or gas. Furthermore, according to their source of generation, fuels are usually divided into two categories, fossil fuels and renewable or alternative fuels. Fossil fuels are formed by long term weathering, accumulation and decomposition processes, while renewable fuels are generated as by-products in the domestic, commercial or industrial processes. Other sources of renewable energy include wind, solar, hydro- and geo-thermal power. However, all these sources mainly depend on the climatic conditions and geographic position on the earth and are difficult to store [43,44]. As described in Chapter 1, most of the energy generation systems are nowadays being shifted towards renewable and alternative fuels due to the rapid depletion of fossil fuels.

Table 2.1: Classification of fuels [44]

Physical state	Fossil fuels	Renewable/Alternative fuels
Solid	Coal	Biomass, woods, manure, residues, solid wastes etc.
Liquid	Petrol, diesel, kerosene oil etc.	Bio-diesel, vegetable oil, bio-ethanol etc.
Gas	Natural gas	Bio-gas, pyrolysis and digester gases etc.

However, it is quite essential in the present era to introduce modern technologies which can provide sustainable and efficient solutions for utilization of alternative fuels in place of

conventional (fossil) fuels. Different researches are being conducted in regard of specific types of fuel in solid, liquid or gaseous state. The present work describes, particularly, the combustion characteristics of different solid fuels for their adoption in energy generation systems.

2.3 Solid fuels: chemical and thermal characteristics

The structure of solid fuels is complex and differs among them depending upon the mixture of compounds present. Design of a combustion system highly depends on physical, chemical as well as thermal properties of solid fuels. Characteristics of solid materials are of key importance, especially when selecting a thermal treatment system for solid waste material. These properties assist in the determination and assessment of feasibility and compatibility of the specific material with the combustion facility in terms of air requirement and emission levels. Process operating conditions are also significantly influenced by these properties [45,46]. Therefore, identification and analysis of chemical and thermal characteristics is the first step in the selection, designing and implementation of a solid waste combustion technology.

Solid fuels consist of different combustible as well as non-combustible constituents. The typical solid fuel can be chemically described as $C_xH_yS_zO_wN_v$ where C, H, S, O, N are carbon, hydrogen, sulfur, oxygen and nitrogen contents, respectively [47]. Carbon and hydrogen are considered to be the main components of the solid fuel which on provision of specific temperature, i.e. ignition temperature, react with oxygen to produce thermal energy according to following chemical reactions:



Chemical and thermal properties of the solid fuels are commonly described by two analyses:

1. Proximate analysis
2. Ultimate analysis

Both analyses are considered as standard tests for solid fuels, e.g. coal etc. However, certain problems emerge during the analysis of biomass or other waste material due to the non-homogeneity of the material. Therefore, it is necessary to use appropriate sampling techniques in order to ensure the true representation of the fuel (solid material) [48].

2.3.1 Proximate analysis

Proximate analysis includes determination of moisture content, volatile matter, fixed carbon and ash content present in the fuel. The measurements are carried out by individual tests and expressed in mass percentages or mass fractions. Detailed description of the analysis is given in the following.

Moisture content (MC) is the amount of water present in the solid material. Amount and nature of moisture depend upon the type of material. Commonly, water is expressed in two forms: 1- intrinsic water and 2- extrinsic water. The former is the amount of water naturally

present in the solid material (under controlled atmosphere) without the effect of weather conditions (i.e. temperature etc.) whereas the latter is the total moisture present in the solid materials with external factors such as temperature, rain, soil contamination. Hence, moisture contents (MC) are expressed in the terms of as received, air dried and oven dried basis [49-51]. High amount of moisture present in the fuel reduces the heating value and increases the heating time. Hence a low level of moisture content is always desirable in order to increase the quality of fuel [43]. As a standard method for the determination of moisture content (MC), a unit quantity (1 gram) of solid (fuel) material is heated to a temperature of 104 to 110°C for one hour and MC is computed as [43][48][52]:

$$MC (\%) = \frac{W_i - W_f}{W_i} \times 100 \% \quad (2.4)$$

where, MC is moisture content in (%), W_i is the initial weight of the sample and W_f is the final weight of the sample after drying in the oven at a temperature of 104 to 110°C.

Volatile matter (VM) is a mixture of gases which are released due to the heating of fuel particles. The gases contained in the volatile matter include carbon monoxide (CO), carbon dioxide (CO₂), water vapor, hydrogen (H₂), tar and other hydrocarbons. Volatile matter is generated upon the thermal decomposition of the solid material and hence plays an important role in the ignition and overall combustion reaction. Typically, volatile matter is found at about 80-90% in wood, 30% in bituminous coal and 5-10% in anthracite [50]. Ignition is directly associated with the volatile matter present in a solid fuel. Ignition temperature decreases with the increase in volatile matter, which makes the fuel easily ignitable. For the determination of volatile matter (VM) present in a solid material, the sample of solid material (fuel) is slowly heated to a temperature of 850°C to 950°C (commonly in a muffle furnace) for seven minutes. The gases evolving during this process are termed as volatile gases or volatile matter [43][48-52]. Their amount can be described by the following expression:

$$VM (\%) = \frac{W_L}{W_i} \times 100 \% \quad (2.5)$$

where, VM is volatile matter in (%), W_L is the weight loss in the fuel sample and W_i is the initial weight of the sample.

Ash content (ASH) is the residue left behind after the complete burning of the solid material. It contains many inorganic and mineral constituents. Production and composition of ash content by the combustion of solid material is also significantly important for the design of combustion system as many operational problems are associated with this matter e.g. slagging, erosion, fouling, corrosion as well as transportation cost. Re-use and recycling of ash content also depend upon the type and constituents of ash. This is one of the important parameters which influence boilers and industrial furnaces at elevated temperatures. Therefore, it is necessary to determine the properties and nature of ash content of a specific fuel material. The standard method for the determination of ash content involves complete burning of a unit quantity of fuel at a temperature of 500-700°C for 30 minutes depending upon the type of material [43][48-52]. The ash content (ASH) is determined by:

$$ASH (\%) = \frac{W_r}{W_i} \times 100 \% \quad (2.6)$$

where, *ASH* is ash content in (%), *W_r* is the weight of residue left behind after burning of the fuel sample and *W_i* is the initial weight of the sample.

Fixed carbon (FC) is the amount of pure carbon present in the solid material. It is actually the combustible proportion excluding moisture content (MC), volatile matter (VM) and ash content (ASH) [43][48-52]. Hence fixed carbon can be determined by the following expression:

$$FC (\%) = 100 \% - (MC \% + VM \% + ASH \%) \quad (2.7)$$

where, *FC* is fixed carbon in (%), *MC* is moisture content in (%), *VM* is volatile matter in (%) and *ASH* is ash content in (%), which are computed from expressions (2.4), (2.5) and (2.6) respectively.

All these indices can also be determined by thermogravimetric analysis (TGA) in which all components of proximate analysis can be determined by a single operation; TGA analysis is considered to be more suitable for coal samples [48].

2.3.2 Ultimate analysis

Ultimate analysis is also known as elemental analysis of a solid material. It provides information about the elements composition present in the solid fuel. It includes determination of amount of carbon (C), hydrogen (H), oxygen (O), nitrogen (N) and sulfur (S). Carbon (C), hydrogen (H) and sulfur (S) are the main components of the combustion reaction. The overall heat generation during the combustion process mainly depends upon carbon (C) and hydrogen (H). A lower level of oxygen is desirable in solid fuels as it increases the capacity of fuel material to hold moisture and ultimately reduces the heating value of the material. Nitrogen does not possess heating value and, hence, does not take part in the combustion process in this sense. However secondary reactions, e.g. production of nitrous oxides, are influenced by the quantity of nitrogen present in the fuel. A good fuel must contain low amount of nitrogen to avoid (fuel) NO_x formation. Sulfur is found in two forms in solid fuels, burnable and non-burnable. As a result of combustion reaction, burnable sulfur becomes a part of the flue gas mixture while non-burnable sulfur is contained in the ash. Less sulfur present in the fuel material ensures its good quality [44].

Ultimate or elemental analysis is helpful in combustion calculations, e.g. stoichiometric combustion calculations for a specific type of solid fuel. The outcome of this analysis can be expressed as [44]:

$$C \% + H \% + O \% + S \% + N \% \rightarrow 100 \% \quad (2.8)$$

where, *C* %, *H* %, *O* %, *S* % and *N* % are the percentage contents of carbon, hydrogen, oxygen, sulfur and nitrogen respectively present in the solid fuel.

Ultimate analysis is carried out by different experimental techniques. In order to determine carbon, hydrogen and sulfur contents (%) present in fuel, a unit quantity of solid fuel is burnt in the presence of oxygen and under controlled conditions. The content of the respective

element is obtained through combustion gas analysis and empirical correlations. Nitrogen content is estimated by the well known Kjeldahl method for nitrogen determination [43][53].

2.3.3 Heating value of solid fuel

Heating value (HV) or calorific value (CV) is the amount of thermal energy released when a unit quantity of solid material is burnt in the presence of air. It is measured as amount of energy per unit mass of fuel (MJ kg^{-1}). It is the most important property of a fuel and is based on the composition of solid material (i.e. proximate and ultimate analysis). Hence, it differs among solid materials that contain different constituents. Calorific value or heating value is further classified into two types: 1- Higher heating value (HHV) or Gross calorific value (GCV) and 2- Lower heating value (LHV) or Net calorific value (NCV). Higher heating value (HHV) is the amount of heat generated when a unit quantity of fuel is burnt along with the latent heat possessed by the water vapor produced as a result of the combustion reaction [43,44]. It is the maximum amount of energy contained in a solid fuel. Hence, it is also termed as gross calorific value (GCV). On the other hand, lower heating value is obtained when a known quantity of the solid fuel (material) is burnt completely in the presence of air excluding the latent heat contained in the water vapor of the combustion gases. Hence, it is also known as net calorific value (NCV) [48,49][52]. Moisture content (MC) has a strong influence on the heating value. Therefore, moisture content must be stated when describing the heating value of a material. Lower heating value (LHV) can be obtained from the higher heating value (HHV) by subtracting the latent heat of water vapor. It can be mathematically expressed as [48]:

$$LHV = HHV - 2.45(MC_{fr} + 9H_{fr}) \quad (2.9)$$

where, LHV is lower heating value (MJ kg^{-1}), HHV is higher heating value (MJ kg^{-1}), MC_{fr} and H_{fr} the mass fractions of moisture and hydrogen, respectively.

Heating value is determined experimentally by using an apparatus known as “bomb calorimeter”, which provides a cost effective method for determination of the heating value. Much research was conducted in order to estimate the heating value of different solid fuels using the correlations established from the proximate and elemental analysis. However, selection of a correlation for the computation of heating value of a specific type of material depends on the physical and chemical characteristics of the fuel in order to ensure accuracy.

Other properties like density, porosity, hardness, swelling etc. are also important when considering the overall efficiency of combustion phenomena. However, the importance of such properties is specific to the method or system of combustion utilized. For example, particle size and swelling property are important in case of fluidized bed combustion (FBC) and pulverized fuel combustion (PFC). Similarly, bulk density is an important parameter for storage, handling, mechanical operations as well as transportation [48].

2.4 Types of solid fuels

In this work, a modeling approach for the combustion of different solid fuels is presented in order to analyze the process parameters influencing the combustion process. The model is composed of species balances, mass and energy balances. For this purpose, solid fuels are categorized into four types, i.e. coal, biomass, municipal solid waste and industrial waste (Fig. 2.1).

Three fuels (samples) were selected from each category of solid fuels for analysis in the frame of the suggested modeling approach. For coal, brown coal, bituminous coal and anthracite were selected. Coal is formed from the thermal decomposition and conversion of wood and decay of plants for a very long period of time. The process of thermal conversion of coal from wood is commonly known as coalification. With the passage of time, the properties of decaying material are changed and different types of coal (material) are produced with different quantities of oxygen and carbon (and other constituents) present. This phenomenon is expressed by the “rank” of coal [48]. Coal is classified into different types depending upon the rank, i.e. peat, lignite, bituminous coal, anthracite. Peat is the coal at initial stage, whereas the highest grade of coal is anthracite [43]. Three coal ranks were selected in this work in order to address the effect of different qualities of coal when using coal as a reference for comparison with other solid materials (Fig. 2.1) in regard of combustion properties and ability.

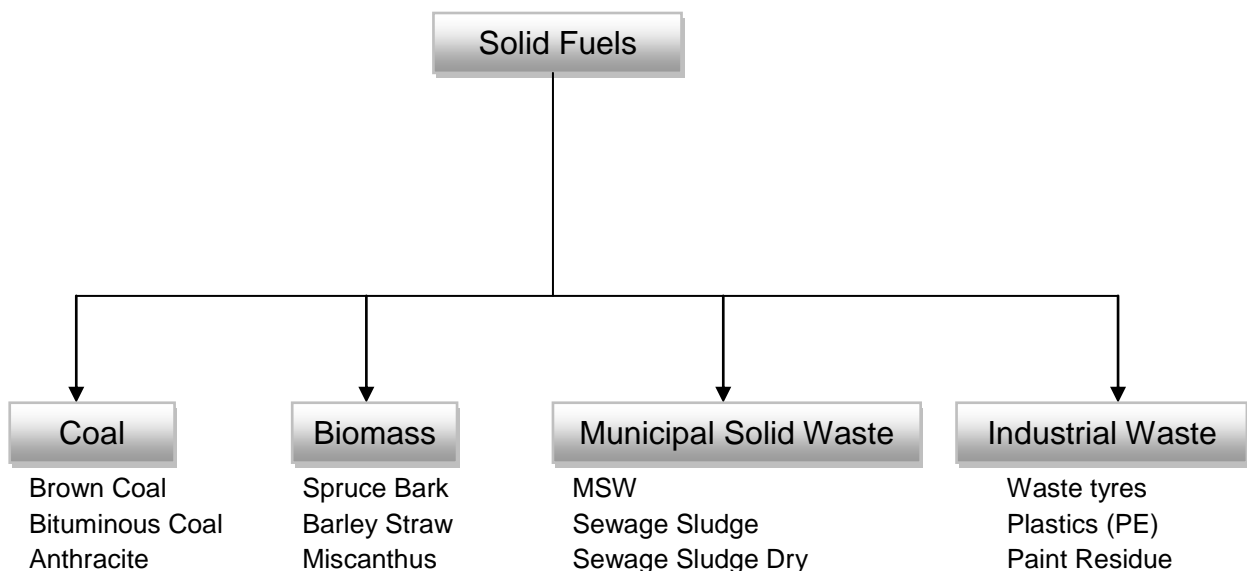


Fig. 2.1: Selection of solid fuels

Biomass is classified into different groups, such as woody material, herbs and grasses, agricultural residues, aquatic material, animal wastes etc. [49][51]. In the present study only three categories of biomass are defined, namely woody material, agricultural residues and grasses/energy crops. Spruce bark is selected from the category of wood, barley straw is

selected from agricultural residues and miscanthus is selected among the grasses/energy crops.

Municipal solid waste is also divided into three types, i.e. MSW in general, sewage sludge generated from waste water and sewage sludge in dry form. Waste tyres, plastics (PE) and paint residue are adopted for the analysis from the category of industrial waste (Fig. 2.1). Table 2.2 presents the chemical and thermal properties of the selected solid materials obtained from open literature [54]. It should be noted that the higher heating value (HHV) is obtained at the respective level of moisture content (MC) as given by Table 2.2.

It can be noted that brown coal has the lowest heating value (22.34 MJ kg^{-1}) among the coal samples while anthracite has the highest heating value, i.e. 33.94 MJ kg^{-1} . This is because of high moisture content (11%) in case of brown coal; with that of anthracite reported to be less i.e. 1.90 %. Brown coal has less carbon content as compared to the other coal types; hence, it has the lowest heating value as compared to the other coal samples. It can be noted that quality and rank of coal (fuel) increases with increase in carbon content and decrease in oxygen content. On the other hand, anthracite is observed to have high sulfur content in comparison to other coal samples.

In case of biomass, the highest heating value is achieved by the woody biomass material, i.e. spruce bark, whereas barley straw has the lowest heating value (16.53 MJ kg^{-1}). This is due to higher carbon content in spruce bark (51.10%) than in barley straw in which carbon content is found to be 49.09%. Hence, it can be stated that woody (biomass) material has higher energy value than the straws or grasses.

Similarly, in the samples of municipal solid waste, the general category of municipal solid waste with the highest carbon content (59.19%) possesses the highest calorific value of $19.22 \text{ (MJ kg}^{-1}\text{)}$ among all three samples. In this category, two types of sewage sludge were also selected. It should be noted that the heating value of dry sludge is 14.56 MJ kg^{-1} which is greater than for sewage sludge (12.24 MJ kg^{-1}) with more moisture content (as given by Table 2.2).

A significant diversity is found among the fuel materials selected in case of industrial waste. Waste tyres are the scrap and used tyres which are usually used in the pyrolysis process to extract energy. With a moisture content of 1.30% and the highest carbon content of 86.40 %, they have a large heating value (39.48 MJ kg^{-1}). In case of plastics PE (poly-ethylene), the lowest moisture content is found, i.e. 0.17%, while no trace of oxygen was reported in this material. Hence, a high calorific value, i.e. 40.56 MJ kg^{-1} , is found in the plastics (PE).

Table 2.2: Chemical and thermal characteristics of different solid fuels

Category	Fuel samples	Ref.	Proximate analysis (ar)				Ultimate analysis (daf)					HHV (MJ kg ⁻¹)
			(%)				(%)					
			MC	VM	FC	ASH	C	H	N	O	S	
Coal	Brown coal	54	11.00	47.17	38.00	3.83	66.67	4.81	0.84	27.36	0.31	22.34
	Bituminous coal	54	2.50	31.69	59.77	6.05	81.80	5.00	1.50	11.21	0.43	30.81
	Anthracite	54	1.90	7.55	87.70	2.84	91.60	3.50	1.60	2.39	0.83	33.94
Biomass	Spruce bark	54	5.25	71.25	21.28	2.22	51.10	6.04	0.41	42.42	0.03	18.79
	Barley straw	54	11.53	67.33	15.94	5.20	49.09	6.06	0.64	44.14	0.08	16.53
	Miscanthus	54	8.40	84.00	5.10	2.50	49.66	6.07	0.59	43.39	0.11	17.69
Municipal solid waste	MSW	54	6.16	68.13	9.93	15.78	59.19	9.80	2.19	28.53	0.29	19.22
	Sewage sludge	54	8.65	47.27	4.66	39.42	54.32	7.67	8.37	27.46	2.18	12.24
	Sewage sludge dry	54	5.20	57.54	9.29	27.97	50.70	7.40	4.90	36.00	1.02	14.56
Industrial waste	Waste tyres	54	1.30	61.39	30.30	7.01	86.40	8.00	0.50	3.40	1.70	39.48
	Plastics (PE)	54	0.17	99.77	0.00	0.06	86.23	13.69	0.06	0.00	0.02	40.56
	Paint residue	55*	0.42	69.98	0.76	28.84	62.44	6.02	0.49	28.80	2.25	18.34

*The analysis for different kinds of pulverized (paint) wastes generated from different processes of spray paint industries was conducted by Fraunhofer Institute for Factory Operation and Automation (IFF) Magdeburg, Germany. The sample of paint residue considered in this work is one of these materials.

Similarly, paint residue has a moisture content of 0.42% which is significantly lower than in the other types of (selected) solid fuels. However, the heating value of paint residue, i.e. 18.34 MJ kg⁻¹, is less than in the plastic because of lower carbon content of paint residue (62.44%) than in the plastic sample (i.e. 86.23%). A high value of volatile matter, i.e. 69.98%, is also present in this fuel sample which makes it a very suitable burning material. It should also be noted that paint residue has different compositions of constituents contained, depending upon the type and composition of material used in the production and preparation process. However, the paint residue considered in this work is one of these types.

2.5 Modeling of combustion process

From the above proximate and ultimate analysis, it is concluded that constituents present in the fuel material (especially moisture and carbon content) have a significant influence on the overall heating value. A modeling study is presented using the chemical and elemental compositions of the selected solid fuels (Table 2.2) in order to check their influence on the combustion process. The overall objective of this study is to present a unified model (using different sub-models) for the combustion process in order to assess the process parameters influencing the combustion temperature.

2.6 Species balance model (SBM)

The species balance model is based on the balances between reactants and the products of the combustion reaction. It is the basic step in the modeling of the combustion process. Solid fuel is burnt in the presence of air to produce combustion gases. In case of solid fuels, hydrogen (H), carbon (C) and sulfur (S) present in the fuel react with oxygen to produce water (H₂O), carbon dioxide (CO₂) and sulfur dioxide (SO₂). Hence, the amount of these elements present in the fuel plays an important role in the generation of combustion products [56].

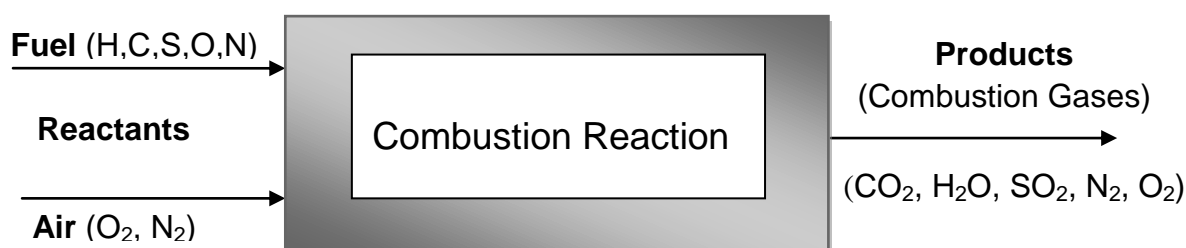


Fig. 2.2: General species balance model for solid fuels

Similar to a simple chemical reaction model, SBM is also divided into reactants as the input species and products as the output species. Input species include fuel and oxidant. Either air or pure oxygen is used as oxidation agent in the chemical reaction. Output species contain the combustion gases resulting from the combustion reaction (Fig. 2.2). As described in the previous section (Section 2.1), a specific amount of oxygen/air is required to completely burn a unit quantity of solid fuel. Therefore, composition and quantity of the incoming fuel as well as the kind of oxidation agent (air or oxygen) have significant influence on the combustion

products. For instance, as air is composed of oxygen (ca. 23% by mass) and nitrogen (ca. 77% by mass), the quantity of nitrogen in the reactants increases by increasing the amount of air. As nitrogen is not combustible, the quantity of nitrogen and its products also increases in the combustion/flue gases. On the other hand, a low amount of air supplied to the combustion reaction results in unburnt fuel. Similarly, composition and type of fuel also influence the composition of products/flue gases obtained in the combustion reaction. Therefore, fuel and oxidant (air) should be in perfect balance to ensure complete combustion. In the present work, a unified SBM model is proposed in order to compute the amount of air required to burn a given amount of fuel as well as the composition of resulting flue gases for different solid fuels. The SBM model is further divided into the following parts.

2.6.1 Oxygen demand (OD)

The amount of oxygen required for complete burning of all constituents of the solid fuel is termed as “oxygen demand”. Computation of oxygen demand is based on the assumption that the whole quantities of carbon (C), hydrogen (H) and sulfur (S) present in the fuel are converted to carbon dioxide (CO₂), water (H₂O) and sulfur dioxide (SO₂) respectively [56]. Following reactions of oxygen occur during the combustion process of solid fuels:

Reaction with carbon (C):



Reaction with hydrogen (H):



Reaction with sulfur (S):



Hence, oxygen demand (OD) for a given solid fuel (X) is obtained from the following expression [56]:

$$OD = \sum X_{if} v_i \frac{M_{O_2}}{M_i} - X_{O_2,f} . \quad (2.13)$$

In this expression OD is the oxygen demand (kg O₂/kg fuel), X_{if} is the mass fraction of a component “i” present in the fuel, v_i is the stoichiometric number for complete oxidation of component “i”, M_{O_2} and M_i are the molar masses of oxygen and component “i” respectively, and $X_{O_2,f}$ is the mass fraction of oxygen already contained in the fuel.

Oxygen demand (OD) can also be described as [43]:

$$OD = O_{2,stoich} - O_f \quad (2.14)$$

where, $O_{2,stoich}$ is the total amount of oxygen required for stoichiometric combustion of a solid fuel and O_f is the amount of elemental oxygen already contained in the solid fuel.

2.6.2 Air demand (AD)

Air demand (AD) is the amount of air which is theoretically required for a complete combustion reaction. It includes the oxygen theoretically required for a stoichiometric

combustion reaction, i.e. oxygen demand (OD). In other words, air demand is the minimum air required in order to convert carbon to CO₂, hydrogen to H₂O and sulfur to SO₂. It is computed by dividing the oxygen demand (OD) by the quantity of oxygen present in the air [56]:

$$\textit{Theoretical air demand} = \frac{\textit{Theoretical oxygen demand}}{\textit{oxygen concentration in air}} . \quad (2.15)$$

It should be noted that the amount of air i.e. air demand (AD) depends upon the concentration of oxygen contained in air. If the concentration of oxygen is less in the air stream provided to the combustion chamber, more air is required for complete combustion of solid fuel and, similarly, if the concentration of oxygen is more, air demand is lower. Air demand (AD) can be expressed by the following equation [56]:

$$AD = \frac{OD}{X_{O_2,A}} . \quad (2.16)$$

In this expression, AD is the air demand for a given solid fuel (kg air/kg fuel), OD is the oxygen demand computed from Eq. 2.13 or Eq. 2.14, and $X_{O_2,A}$ is the mass fraction of oxygen in air (based on concentration of oxygen in air).

Air demand (AD) determines the minimum requirement of air to be supplied to the combustion system for complete combustion. However, it should be noted that in real combustion systems, furnace air is provided in some excess to certainly avoid incomplete combustion of the fuel.

2.6.3 Air supply and excess air ratio (λ)

Fuel and air are both necessary components of a combustion system (Fig. 2.2). It is always necessary to ensure the availability of air at least required for the given amount of solid fuel (air demand AD). However, in actual practice there is some uncertainty in regard of the availability of air to all particles of the solid fuel, due to leakage of air, improper mixing and other factors. To avoid this risk, it is always desirable to supply some extra amount of air, i.e. in excess to the required air, to provide better conditions for complete mixing of air and fuel and, hence, to ensure complete combustion reaction. This can be described by the excess air ratio, sometimes also termed as excess air number and denoted by the Greek letter lambda (λ). Excess air ratio is defined as the ratio of air supplied to the combustion system to the stoichiometric air demand (AD). It can be mathematically described as [48][56]:

$$\textit{Excess air ratio}, \lambda = \frac{\dot{M}_{A,S}}{\dot{M}_{A,AD}} . \quad (2.17)$$

In Eq. 2.17, $\dot{M}_{A,S}$ is the mass flow rate of air (kg s⁻¹) supplied to the combustion system and $\dot{M}_{A,AD}$ is the mass flow rate of air (kg s⁻¹) necessary for stoichiometric combustion of a given solid fuel, corresponding to the theoretical air demand.

Excess air ratio (λ) is one of the important parameters which influence the overall combustion process. If the amounts of required air and air supplied to the combustion system are equal, then $\lambda = 1$. This is termed as stoichiometric condition of the combustion reaction (Section

2.1). Values of $\lambda > 1$ result in over-stoichiometric conditions which means that more air is available than the required air (AD). The flame produced at this state is termed as “lean flame”. On the other hand, values of $\lambda < 1$ describe sub-stoichiometric conditions of the combustion reaction. This implies that less air is present in the combustion chamber than the required amount of air (AD). The flame generated at this state is termed as rich flame [56]. This condition results in a more or less portion of unburnt fuel in the combustion process. Therefore, it is necessary to provide air with λ greater than one. In the present study, different levels of excess air number λ are studied with respect to combustion temperatures.

2.6.4 Combustion gases/flue gases composition

Combustion gases, or sometimes termed flue gases, are a gaseous mixture composed of different gases produced as a result of combustion reaction at a given condition and fuel. The mixture of these gases typically includes carbon dioxide (CO₂), water vapor (H₂O), sulfur dioxide (SO₂), oxygen (O₂) and nitrogen (N₂). Composition mainly depends upon the type of fuel and air supplied to the combustion system, e.g. furnace. Moreover, generation of other gases like carbon monoxide (CO) and oxides of nitrogen depends on the state of reaction and temperature conditions of the combustion facility.

Composition is usually measured in terms of specific gas volumes (m³ of gas *i* per kg of fuel) and denoted by v_i . The specific volume of carbon dioxide (CO₂) can be obtained directly from the balanced stoichiometric combustion reaction of the given fuel using (Eq. 2.10). In case of solid fuels, some amount of water is already present in the fuel; hence, the specific volume of water vapor (H₂O) is estimated by adding the stoichiometric specific volume and specific volume of water already contained in the solid (raw) fuel. The former is obtained from the balanced stoichiometric combustion equation of hydrogen while the latter is computed from the moisture content (MC) of solid fuel from the equation [56]:

$$v_{H_2O,f} = MC_{fr} \frac{1}{(1-MC_{fr}-ASH_{fr})} \frac{1}{\rho_{H_2O}} \quad . \quad (2.18)$$

Here, $v_{H_2O,f}$ is the specific volume of water vapor already present in the raw fuel (in m³ H₂O/kg fuel), MC_{fr} is the mass fraction of moisture in the solid fuel, ASH_{fr} is the mass fraction of ash and ρ_{H_2O} is density of water vapor (kg m⁻³).

Stoichiometric water specific volume ($v_{H_2O,stoich}$) is obtained from the balanced combustion reaction equation of hydrogen for the given solid fuel and, hence, the specific volume of water vapor (v_{H_2O}) is obtained from the following equation [56]:

$$v_{H_2O} = v_{H_2O,stoich} + v_{H_2O,f} \quad . \quad (2.19)$$

Similarly carbon dioxide (CO₂), sulfur dioxide (SO₂) is also obtained directly from combustion Eq. 2.12.

When air is provided in excess, i.e. λ is greater than one ($\lambda > 1$), combustion gases also include some oxygen. The specific volume of O₂ in combustion gases is computed from the following expression [56]:

$$v_{O_2} = (\lambda - 1) AD \frac{X_{O_2,A}}{\rho_{O_2}} \quad (2.20)$$

where, v_{O_2} is oxygen specific volume in the combustion gases ($m^3 O_2/kg$ fuel), λ is excess air ratio, AD is air demand, $X_{O_2,A}$ is oxygen mass fraction in air and ρ_{O_2} is the density of oxygen ($kg m^{-3}$).

It should be noted that oxygen in the mixture of combustion gases is only found when air is provided in excess. At stoichiometric state of combustion, i.e. $\lambda = 1$, all the oxygen present in air is utilized in the combustion process and, hence, no trace of oxygen is obtained in the combustion gases.

As described in the previous section, air also contains a large portion of nitrogen. When air is provided as oxidant in the combustion reaction, oxygen present in the air reacts with the combustible species to produce combustion products; however, nitrogen being not combustible does not take part in the combustion reaction and remains in the mixture of combustion gases. The amount of nitrogen gas in the mixture of flue gases is computed by using the following relation [56]:

$$v_{N_2} = \lambda AD \frac{X_{N_2,A}}{\rho_{N_2}} + \frac{X_{N_2,f}}{\rho_{N_2}} \quad (2.21)$$

where, v_{N_2} is the specific volume of nitrogen gas in the combustion gases ($m^3 N_2/kg$ fuel), λ is excess air ratio, AD is the air demand, $X_{N_2,A}$ and $X_{N_2,f}$ are mass fractions of nitrogen in air and raw fuel, respectively, and ρ_{N_2} is density of nitrogen ($kg m^{-3}$).

Equation (2.21) shows that the concentration of nitrogen in combustion gases is directly influenced by the excess air ratio (λ) and the air demand. The quantity of nitrogen gas in the mixture of combustion gases increases with increase in excess air ratio. On the other hand, nitrogen gas generation depends upon the air demand (AD) which is directly linked with the elemental composition of the fuel. It should also be noted that in certain temperature conditions, nitrogen is converted into nitrous oxides. The conditions and conversion of nitrogen into secondary products are discussed later in this chapter.

2.6.5 Calculation sheet for species balance model (SBM)

A unified calculation sheet has been developed for different solid fuels. Figure 2.3 represents this calculation sheet of the species balance model (SBM) with brown coal as an example for the various fuels of Table 2.2. The elemental composition of the solid material, properties of air/oxidant and excess air ratio are given as input, and oxygen demand, air demand and the composition of the flue gas mixture resulting from the combustion process are obtained as output. Different solid fuels (as represented in Table 2.2) have been analyzed by means of this model and results will be reported in Section 2.8.

Species Balance Model (SBM) For Different Solid Fuels				
Input parameters				Input
Fuel				output
Brown Coal				
XC (Mass fraction of carbon)	0.6667	Balance	Reaction	
XH (Mass fraction of hydrogen)	0.0481		C + O ₂ → CO ₂	
XN (Mass fraction of nitrogen)	0.0084		1 kmol C 1kmol O ₂ 1 kmol CO ₂	
XS (Mass fraction of sulfur)	0.0031		12.00 kg C 32 kg O ₂ 22.4 m ³ CO ₂	
XO (Mass fraction of oxygen)	0.2736		1 kg C 2.66666667 kg O ₂ 1.8666667 m ³ CO ₂	
			0.67 kg C 1.77786667 kg O ₂ 1.2445067 m ³ CO ₂	
XO ₂ in air (Mass fraction of oxygen in air)	0.23	Balance	Reaction	
Density of O ₂ (kg/m ³) at STP	1.428		H + O ₂ → H ₂ O	
XN ₂ in air (Mass fraction of nitrogen in air)	0.77		1 kmol H 0.25 kmol O ₂ 0.5 kmol H ₂ O	
Density of N ₂ (kg/m ³) at STP	1.25		1 kg H 32 kg O ₂ 22.4 m ³ H ₂ O	
Lambda (Excess air number)	1.3		1 kg H 8 kg O ₂ 11.2 m ³ H ₂ O	
MC (Mass fraction of moisture in fuel)	0.11		0.0481 kg H 0.3848 kg O ₂ 0.53872 m ³ H ₂ O	
Ash (Mass fraction of ash in fuel)	0.0383	Balance	Reaction	
Density of water vapor (kg/m ³)	0.8		S + O ₂ → SO ₂	
M (1/(1-MC-ASH))	1.174122		1 kmol S 1 kmol O ₂ 1 kmol SO ₂	
H ₂ O already contained in fuel	0.129153		32 kg S 32 kg O ₂ 22.4 m ³ SO ₂	
Specific volume of water in fuel (m ³ H ₂ O/kg fuel)	0.161442		0.0031 kg S 0.0031 kg O ₂ 0.00217 m ³ SO ₂	
		O Demand Stoich.	2.1658	
		Oxygen Demand (OD)	1.8922 (kg of O ₂ /kg of fuel)	
		Air Demand (waf-fuel)	8.2268 (kg of air/kg of fuel)	
		Air Demand (AD)	7.0068 (kg of air/kg of fuel)	
		Composition of Flue Gas		
		CO ₂	1.2445 m ³ of CO ₂ /kg of fuel	
		H ₂ O	0.7002 m ³ of H ₂ O/kg of fuel	
		SO ₂	0.00217 m ³ of SO ₂ /kg of fuel	
		O ₂	0.3386 m ³ of O ₂ / kg of fuel	
		N ₂	5.6177 m ³ of N ₂ / kg of fuel	
		Total Gas Volume	7.9031 m ³ of CG/ kg of fuel	

Fig. 2.3: Species balance model (SBM)

2.7 Mass and energy balance model

In order to estimate the required flow rate of air for a given amount of fuel and to compute the adiabatic temperature as result of combustion of different solid fuels, a mass and energy balance model is formulated in relation to the proposed species balance model. Figure 2.4 represents different components of the mass and energy balance model.

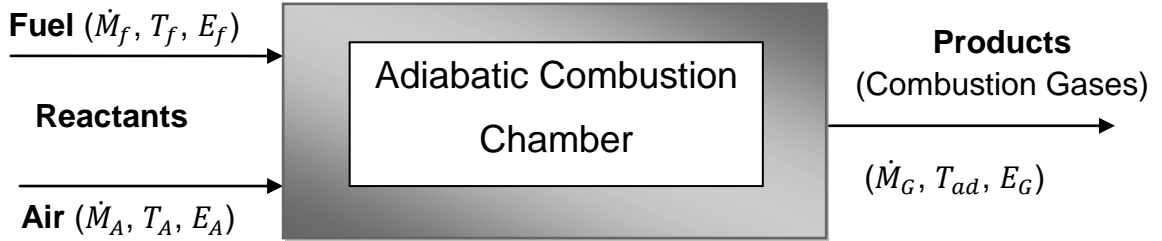


Fig. 2.4: Mass and energy balance model

2.7.1 Mass balance

According to a common mass balance, the total amount of incoming mass should be equal to the matter leaving the system if there are no losses and no accumulations in the system. Figure 2.4 illustrates the typical mass balance of an adiabatic combustion system. \dot{M}_f and \dot{M}_A are the mass flow rates of incoming fuel and air, respectively. Mass flow rate of the output is represented by the mass flow rate of combustion gases (\dot{M}_G).

Without losses, it is:

$$\dot{M}_{in} = \dot{M}_f + \dot{M}_A = \dot{M}_G = \dot{M}_{out} \quad (2.22)$$

where, \dot{M}_{in} is the mass flow rate of the incoming streams of materials and \dot{M}_{out} is the mass flow rate of the materials leaving the system.

The mass flow rate of air for a specific amount of fuel is computed from the following equation [56]:

$$\dot{M}_A = \lambda AD \dot{M}_f \quad (2.23)$$

In Eq. 2.23, \dot{M}_A is the mass flow rate of air, λ is excess air number, AD is air demand and \dot{M}_f is the mass flow rate of the given fuel.

From Eq. 2.22 and Eq. 2.23, the mass flow rate of combustion gases is also obtained to:

$$\dot{M}_G = \dot{M}_f (1 + \lambda AD) \quad (2.24)$$

2.7.2 Energy balance

According to the law of conservation of energy, the total energy entering to the system should be equal to the energy leaving the system assuming no energy loss through the system. In adiabatic combustion system (Fig. 2.4), the energy contained in the fuel and air is converted into energy of the combustion gases which is expressed by the adiabatic combustion temperature. Here, the energy content of the fuel is represented by the energy flow rate E_f , air energy by the enthalpy flow rate E_A and flue gas energy by E_G (all in kJ h^{-1}). It is:

$$E_f + E_A = E_G \quad . \quad (2.25)$$

The energy flow rate of solid fuel is expressed by the following relation [56]:

$$E_f = \dot{M}_f (HV + c_{pf} T_f) \quad (2.26)$$

where, \dot{M}_f is mass flow rate of fuel, HV is the heating value, c_{pf} is the specific heat capacity of the fuel and T_f is the initial temperature of fuel.

Energy (enthalpy) flow rate of the air is estimated as:

$$E_A = \dot{M}_A c_{pA} T_A \quad (2.27)$$

where, \dot{M}_A is mass flow rate of air, c_{pA} is specific heat capacity of air and T_A is the inlet temperature of air.

After combustion reaction, energy flow rate of the combustion gases is given by:

$$E_G = \dot{M}_G \bar{c}_{pG} T_{ad} \quad . \quad (2.28)$$

In this expression, \dot{M}_G is the mass flow rate of combustion gases, \bar{c}_{pG} is the mean specific heat capacity of combustion gases and T_{ad} is the adiabatic combustion temperature.

It should be noted that combustion products obtained as a result of combustion reaction consist of a mixture of different gases. Therefore, an average specific heat capacity of all the combustion products is taken in order to compute the energy of combustion gases. The mean specific heat capacity (\bar{c}_{pG}) is expressed as [56]:

$$\bar{c}_{pG} = \sum X_{iG} c_{pi} = \frac{1}{\rho_G} \sum X_i \rho_i c_{pi} \quad (2.29)$$

where, X_{iG} is the fraction of the gas component i in the combustion gas mixture, and c_{pi} is the specific heat capacity of the gas component i , ρ_G is the density of gas mixture, and ρ_i is the density of the gas component i in the combustion gas mixture.

Combining the mass and energy balance models, the following expression for coupled mass and energy balance is obtained [56]:

$$\dot{M}_f (HV + c_{pf} T_f) + \dot{M}_A c_{pA} T_A = \dot{M}_G \bar{c}_{pG} T_{ad} + \dot{M}_G \Delta H_{diss} \quad (2.30)$$

where, all parameters are same as expressed in Eqs. 2.26, 2.27 and 2.28. In the additional term ΔH_{diss} is the enthalpy of dissociation of combustion gases.

2.7.3 Adiabatic combustion temperature

Adiabatic combustion temperature (T_{ad}) is the maximum temperature produced as a result of combustion reaction of a given (amount of) fuel (material) considering no heat loss through the combustion system to the surrounding and getting the maximum energy of the combustion products at the outlet. Maximum temperature of the combustion gases, i.e. adiabatic combustion temperature, can be computed from the mass and energy balance model Eq. 2.30 [56]:

$$T_{ad} = \frac{HV}{(1+\lambda AD) \bar{c}_{pG}} + \frac{\lambda AD}{1+\lambda AD} \frac{c_{pA}}{\bar{c}_{pG}} T_A - \frac{\Delta H_{diss}}{\bar{c}_{pG}} \quad . \quad (2.31)$$

In Eq. 2.31, the term $\frac{\lambda AD}{1+\lambda AD} \frac{c_{pA}}{\bar{c}_{pG}}$ is ≈ 1 and $\frac{\Delta H_{diss}}{\bar{c}_{pG}}$ can be neglected for λ greater than one, resulting in lean combustion; hence, the adiabatic combustion temperature for a given fuel can be obtained as [56]:

$$T_{ad} = \frac{HV}{(1+\lambda AD) \bar{c}_{pG}} + T_A \quad (2.32)$$

where, HV is the higher heating value of the given fuel or solid material, λ is excess air number, \bar{c}_{pG} is specific heat capacity of the combustion gas mixture and T_A is the inlet temperature of air.

Equation 2.32 shows that the adiabatic temperature mainly depends on the heating value and air demand. The greater the heating value, the greater will be the adiabatic temperature of the combustion gases. On the other hand, adiabatic temperature decreases with increase in the air demand of the solid fuel. The temperature of the inlet air stream also affects the adiabatic temperature of the combustion system.

2.8 Results and discussion

Three samples from each category of solid materials are analyzed using species balances and the mass and energy balance model.

2.8.1 Oxygen demand (OD)

Oxygen demand (OD) for different solid fuels is calculated using the species balance model (provided in Section 2.6). First, the calculations are made for the reference sample, i.e. brown coal, and then the same procedure is applied to all other fuel samples of different solid materials. The unified species balance model has been presented in Fig. 2.3 for the calculation of oxygen demand for any solid material.

Oxygen demand (OD) for different solid materials is represented in a bar chart (Fig. 2.5). The results reveal that oxygen demand (OD) or in other words oxygen required in order to completely burn a solid fuel mainly depends upon the type and composition of solid material. The main constituents which influence oxygen demand are carbon, hydrogen, sulfur and oxygen (already contained in the solid material). Application of the species balance model (SBM) to different solid materials resulted in that oxygen demand (OD) is larger for anthracite among the three samples of coal (Appendix A, Table A1). This is because of the larger amount of carbon and smaller amount of oxygen present in anthracite as compared to brown coal and bituminous coal. The difference in the oxygen demand (DO) among biomass samples is observed to be smaller because they have similar amount of carbon and oxygen constituents. However, the comparison of the three samples shows that spruce bark has a somewhat higher value of oxygen demand as compared to barley straw and miscanthus.

The comparison among the three samples of municipal solid waste shows that the general category of municipal solid waste (i.e. MSW) has higher oxygen demand, i.e. 2.08 kg O₂/kg

fuel, while dry sewage sludge has lower oxygen demand due to smaller carbon content, i.e. 50.70% as compared to other samples (Table 2.2).

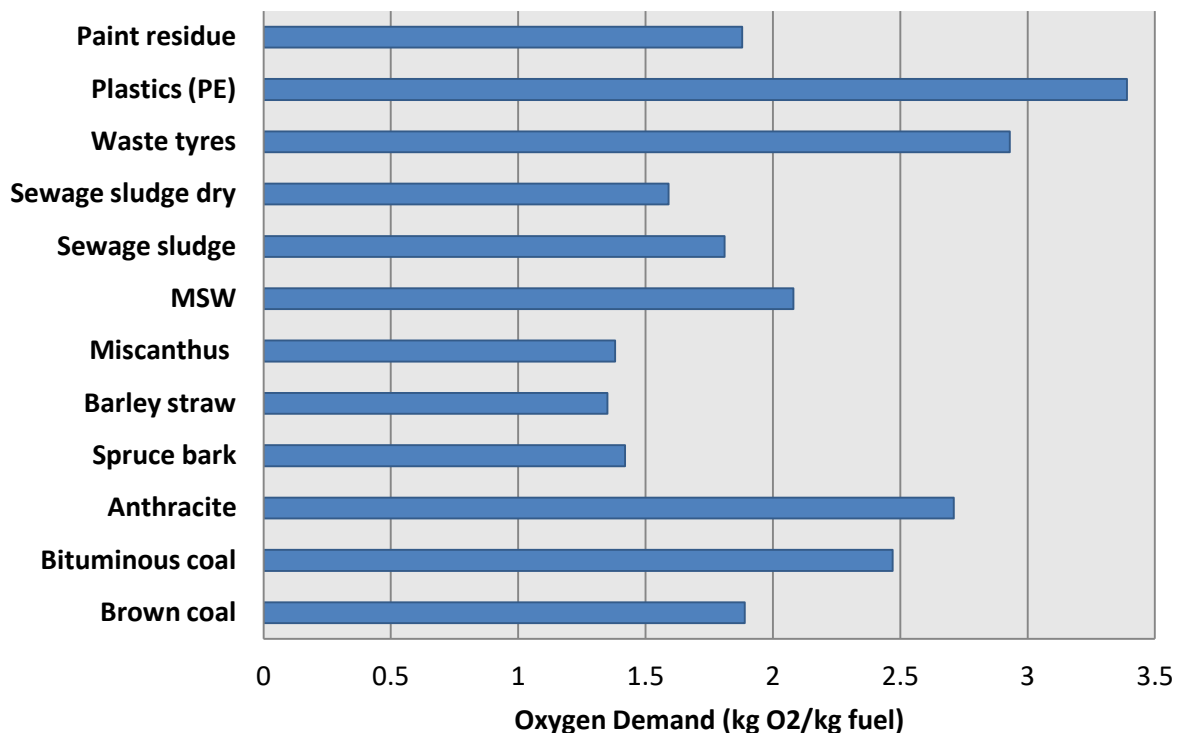


Fig. 2.5: Oxygen demand (OD) for different solid fuels

Industrial waste contains very diverse materials, hence, very different results are observed. Oxygen demand for plastic (PE) is resulted as the highest, i.e. 3.39 kg O₂/kg fuel, among all other samples. This is due to the fact that in this sample no oxygen is found. Carbon content is also found to be higher as compared to other samples of industrial fuel. The oxygen demand of waste tyres and paint residue was obtained resulted as 2.93 kg O₂/kg fuel and 1.88 kg O₂/kg fuel respectively (Appendix A, Table A1).

The overall comparison shows that plastics have a higher amount of carbon and hydrogen constituents; hence, the industrial fuel sample of plastics has the highest oxygen demand of 3.39 kg O₂/kg fuel while the lowest oxygen demand is found in the case of biomass sample of barley straw, i.e. 1.35 kg O₂/kg fuel (Fig. 2.5). It can be concluded that the higher the value of carbon and hydrogen present in the solid material, the higher will be the oxygen demand. This implies that increased presence of both constituents requires more oxygen to burn the solid material. On the other hand, higher amount of inherit oxygen present in the solid material reduces the total oxygen required for complete combustion.

2.8.2 Air demand (AD)

Air demand is an important parameter when air is considered as the oxidation medium. According to the SBM model, air demand (AD) has a direct relation with the oxygen demand (OD). However, it also depends on the concentration of oxygen present in the air. Air demand

has been computed for the different solid materials using the proposed species balance model. Figure 2.6 illustrates the results for ambient air with 23 mass % of oxygen (see also Appendix A, Table A2). As expected, the results are similar to those concerning the oxygen demand (OD) in Fig. 2.5, but differences among the various investigated solid fuels are amplified.

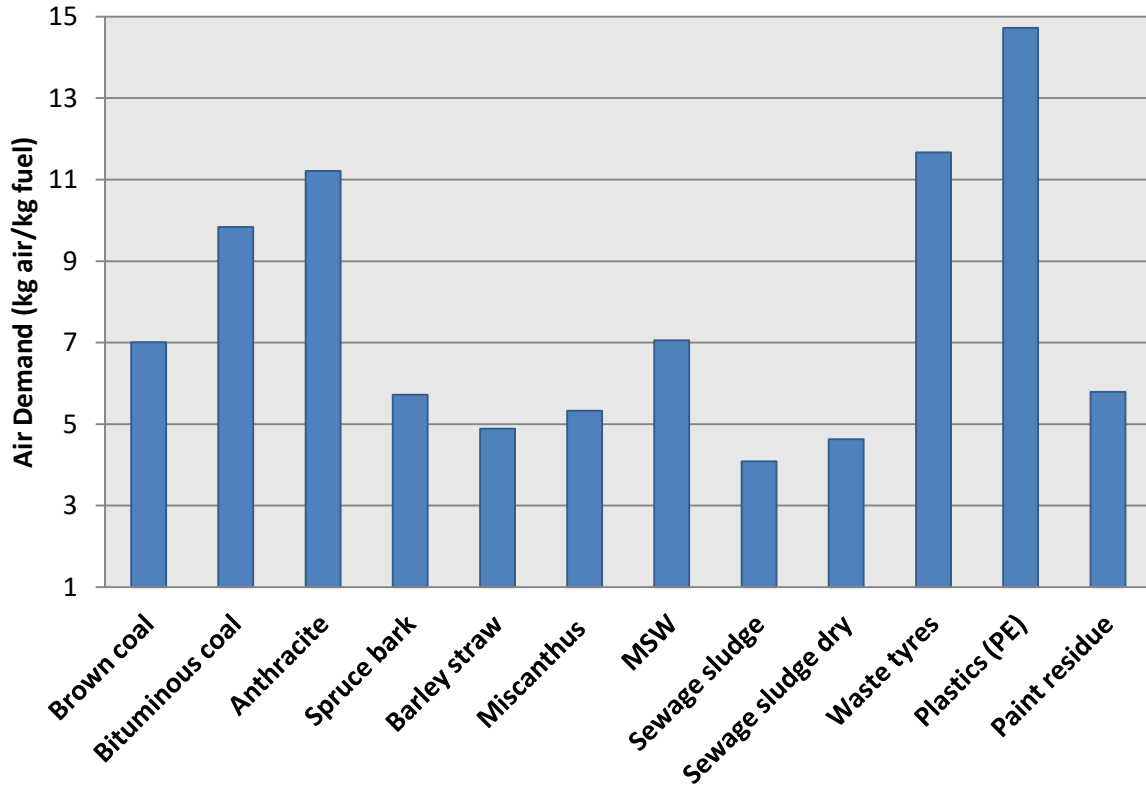


Fig. 2.6: Air demand (AD) for different solid fuels

2.8.3 Adiabatic combustion temperature

Adiabatic temperature is the maximum temperature produced as a result of combustion of any solid material in an insulated or in other words adiabatic combustion chamber. This is one of the most important parameters for describing the energetic conversion of solid material to heat. In this work, adiabatic combustion temperature for different solid materials is computed from the mass and energy balance model coupled with the species balance model (SBM). The calculations are based on a reference value of excess air ratio of $\lambda = 1.3$ (Appendix A, Table A3). Figure 2.7 shows the adiabatic flame temperature for different solid materials at the reference value of excess air number. It should be noted that the adiabatic temperature resulting from the combustion of a solid material depends on the heating value (HV) of the solid material, air demand (AD) and excess air number (λ), Eq. 2.32. Maximum temperature produced also slightly depends on the mean specific heat capacity of combustion gases. As described before, the combustion products are a mixture of different gases, hence, an average value of heat capacity of the gas mixture is taken into account in the combustion calculations. In the present calculations, the value of the mean specific heat capacity of combustion gases is assumed as $1.2 \text{ kJ kg}^{-1} \text{ K}^{-1}$. The higher the heating value of the fuel material, the higher is the

adiabatic temperature. Contrarily, a higher value of air demand reduces the adiabatic temperature.

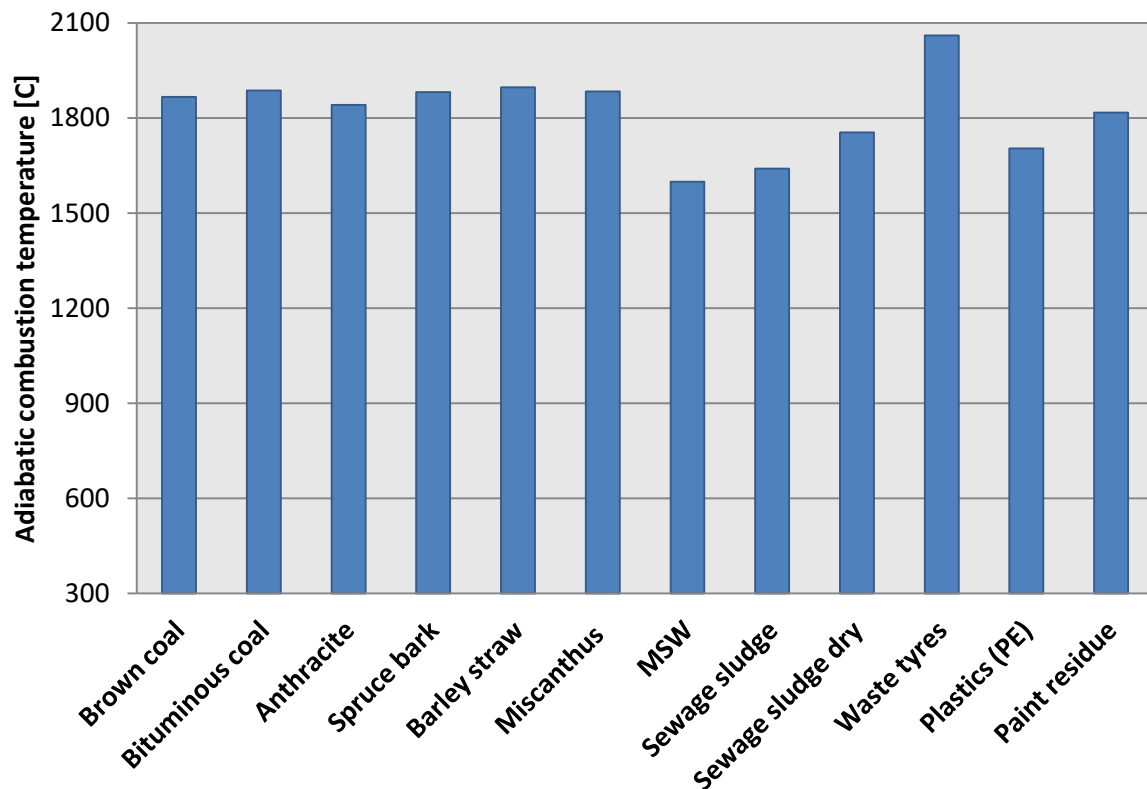


Fig. 2.7: Adiabatic combustion temperature for different solid fuels ($\lambda = 1.3$)

In the present study, higher heating values were obtained from the literature (Table 2.2) and air demand (AD) was computed from the species balance model (SBM). It should also be noted that in this work complete combustion of all the constituents into final products is assumed and the heat of dissociation to various intermediate compounds is neglected. It can be observed that the highest temperature is obtained from the combustion of bituminous coal among the three samples of coal. This is because of the lower air demand (AD) of bituminous coal as compared to anthracite and higher heating value than for brown coal. In the category of biomass, air demand (AD) is approximately 5 kg air/kg fuel for all types of biomass materials studied and the higher heating value is also approximately equal (Table 2.2), hence only a very minor difference in adiabatic temperature among biomass samples can be observed (Fig. 2.7).

In case of municipal solid waste, the highest adiabatic temperature resulted from the combustion of dry sewage sludge as compared to the other samples. This is because of lower value of air demand (AD) and higher heating value than for the wet sewage sludge. In case of industrial waste, the highest value of adiabatic temperature is obtained for waste tyres as compared to the other two fuel samples. Although, the fuel sample of plastics (PE) has a heating value higher than the other two fuels, it has also very high air demand (AD), which results in a significantly lower value of adiabatic combustion temperature. This implies that more air is required to completely burn this type of fuel due to the presence of more carbon.

The adiabatic temperature in case of plastics (PE) and paint residue resulted as 1704°C and 1817°C, respectively. A higher value of adiabatic temperature of paint residue than of the plastics (PE) sample is due to the greater air requirement (air demand AD) in case of plastics. Therefore, from this analysis it can be stated that both heating value and air demand have significant influence on the adiabatic combustion temperature. The higher the air demand (AD) of solid fuel, the lower is the adiabatic temperature attained by the combustion gases and vice versa.

2.8.4 Effect of excess air on adiabatic temperature

The above results have shown the adiabatic combustion temperature of different solid fuels at a reference value of excess air ratio, i.e. $\lambda = 1.3$, and the effect of air demand and heating value on this temperature for different solid materials. In order to quantify the effect of excess air on the adiabatic temperature, this section provides a parametric study for the different solid fuels with different levels of excess air ratio, starting with the reference value of $\lambda = 1.3$ and then going up to $\lambda = 3.7$ in intervals of 0.3. The results (see also Appendix A, Table A4) emphasize that excess air has a significant influence on the adiabatic combustion temperature. Adiabatic temperature of the combustion gases decreases strongly with an increase in excess air, irrespective of the fuel used.

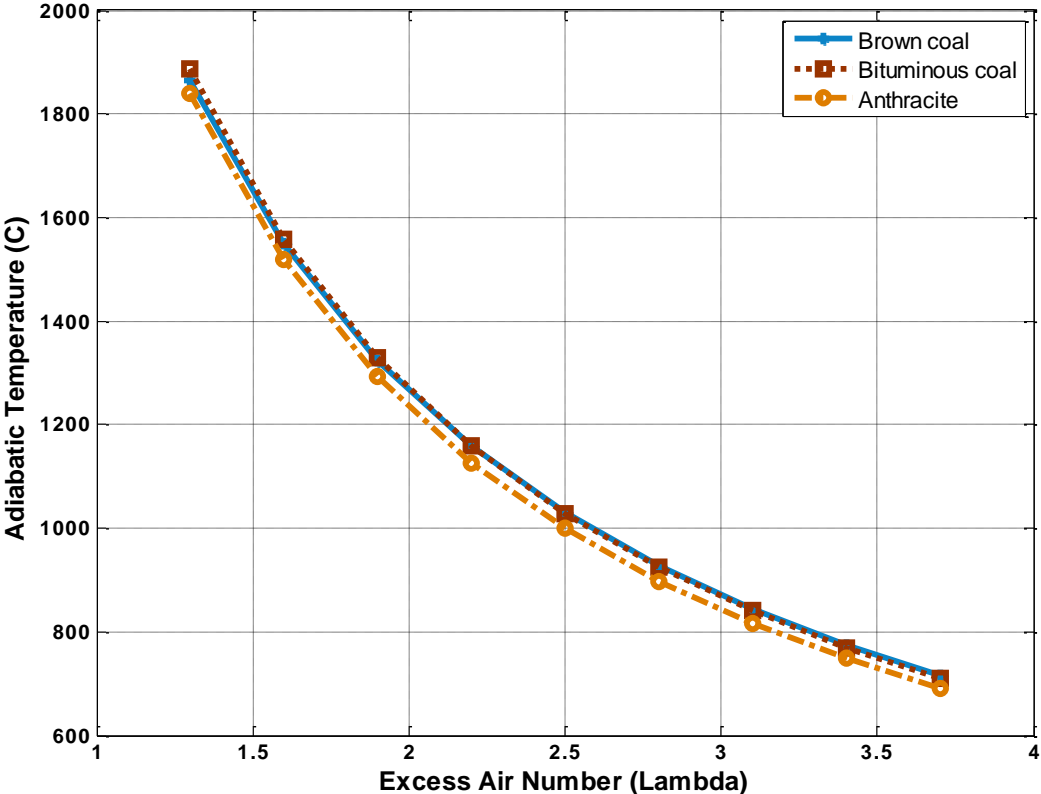


Fig. 2.8: Effect of excess air ratio (λ) on adiabatic temperature of coal

Figure 2.8 illustrates the effect of excess air ratio on adiabatic temperature for the three samples of coal, i.e. brown coal, bituminous coal and anthracite. The maximum value of adiabatic temperature, achieved at the lowest value of excess air number ($\lambda = 1.3$), is with

1887°C highest in case of bituminous coal. However, this temperature decreases significantly to 711°C by increasing the excess air number to $\lambda = 3.7$. The curve for brown coal and bituminous coal are almost overlapping, with anthracite placed slightly lower.

Differences in adiabatic temperature are also very minor for the three investigated biomass fuels (Fig. 2.9).

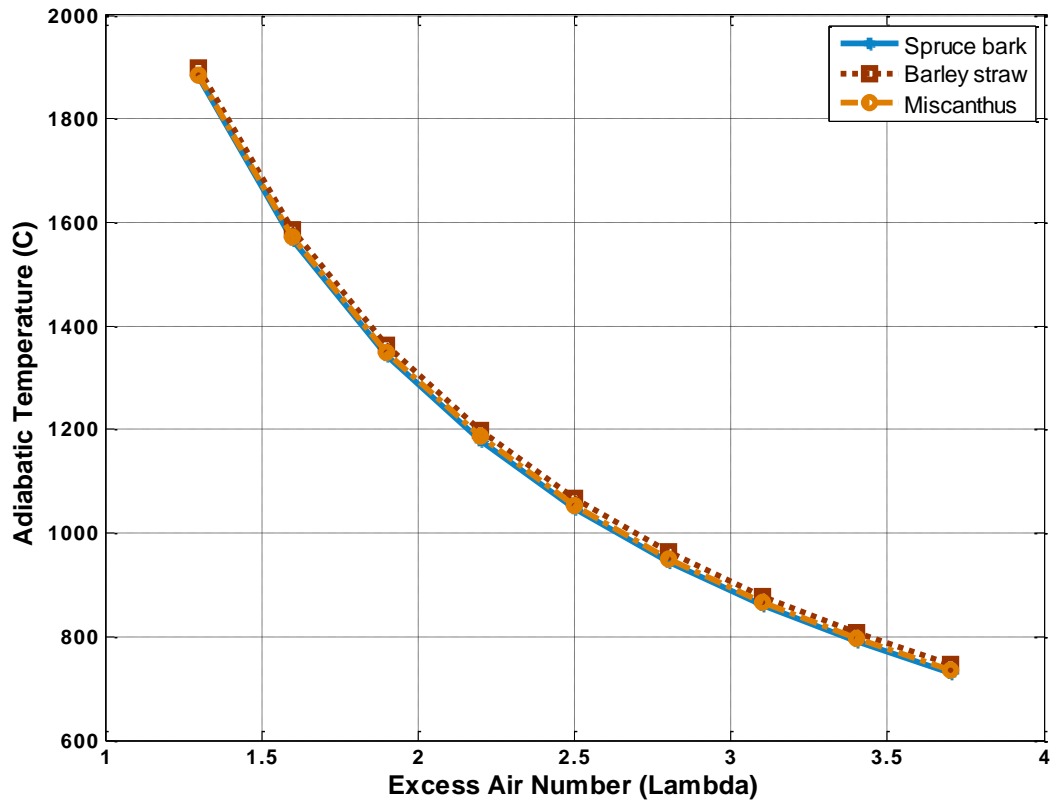


Fig. 2.9: Effect of excess air ratio (λ) on adiabatic temperature of biomass

Figure 2.10 represents the adiabatic temperature of different samples of municipal solid waste with different levels of excess air. As municipal solid waste consists of different materials with different physical and thermal properties, different heating values and air demands (AD) result for complete combustion. Hence, different adiabatic temperature is obtained for the different types of municipal solid waste. However, the trend of adiabatic combustion temperature is similar to the other solid materials, i.e. adiabatic combustion temperature decreases with increase in excess air number. It is also observed that although dry and wet samples of sewage sludge have similar value of air demand (AD), the two samples result in different adiabatic temperatures. This is due to the different heating values, since the heating value of solid material increases by decreasing the moisture content. As dry sewage sludge has lower water content than wet sewage sludge, its heating value is higher, resulting in a higher value of adiabatic temperature. On the other hand, general MSW has a heating value greater than the other two samples, but it requires more air for complete combustion, i.e. air demand (AD) is higher, hence, adiabatic temperature of MSW is lower than for the sewage sludge samples (Figs. 2.7, 2.10).

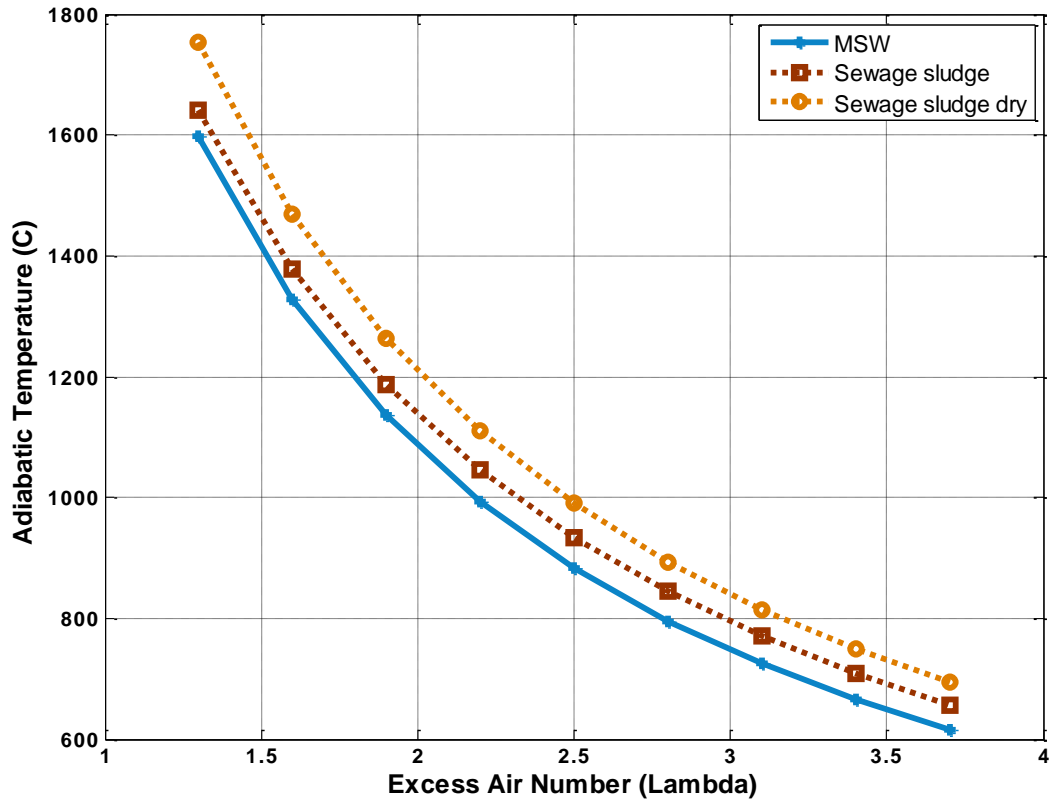


Fig. 2.10: Effect of excess air ratio (λ) on adiabatic temperature of MSW

Similar to the municipal solid waste, industrial waste also consists of different constituents in each category, so that different heating values as well as air demands are obtained. This results in different adiabatic temperature in all three cases, i.e. waste tyres, plastics (PE) and paint residue (Fig. 2.11).

The maximum adiabatic temperature is obtained in case of waste tyres, as these have a significantly higher heating value of 39.48 MJ kg^{-1} . On the other hand, plastics (PE) also have a high heating value; however, in this case air demand (AD) is the highest among all the fuel samples. Hence, a minimum value of adiabatic temperature is obtained in this case. As expected, adiabatic temperature of all three samples of industrial waste decreases significantly by increasing the excess air ratio. For example, adiabatic temperature of waste tyres at $\lambda = 1.3$ resulted as 2060°C , which decreases to 1115°C at $\lambda = 2.5$ and 770°C at $\lambda = 3.7$. The respective values for paint residue are 1817°C at $\lambda = 1.3$ and 707°C at $\lambda = 3.7$ (Fig. 2.11).

To compare materials of different type, one fuel from each category is chosen: anthracite is selected from coal, miscanthus from biomass, dry sewage sludge from municipal solid wastes, and paint residue from the group of industrial wastes. Figure 2.12 illustrates that all four solid fuels have very similar values of adiabatic temperature. Interestingly, such different fuels as paint residue and anthracite have a very similar pattern of adiabatic temperature (see also Appendix A, Table A4).

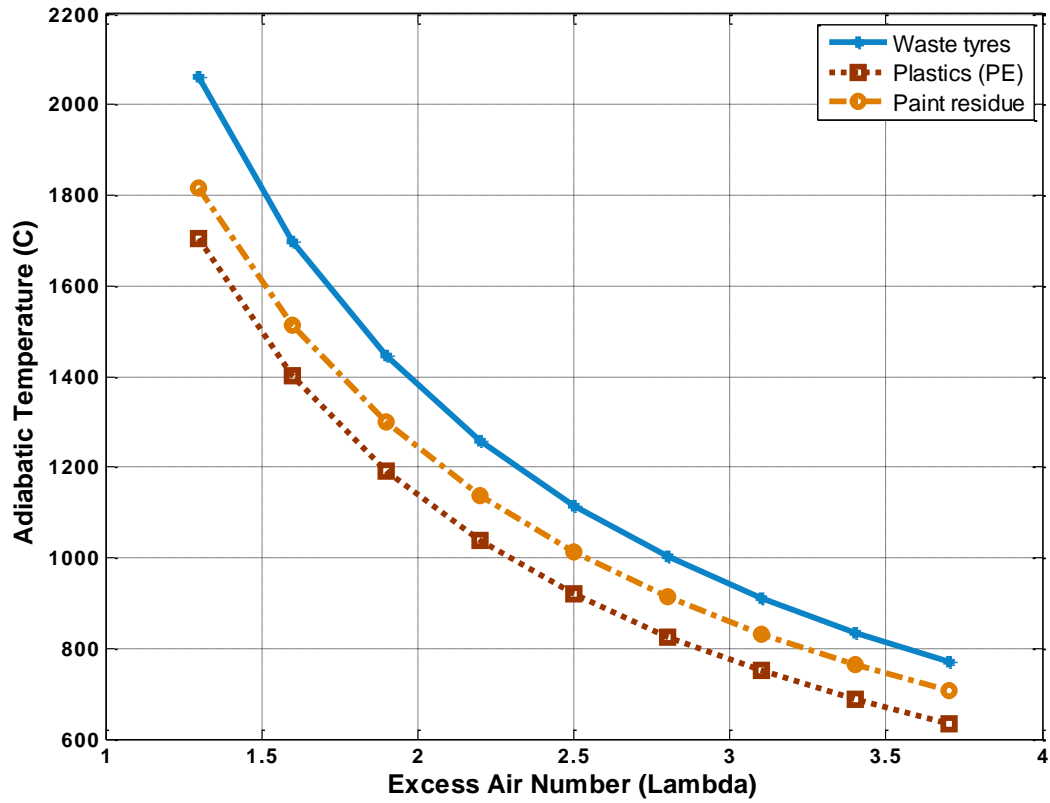


Fig. 2.11: Effect of excess air ratio (λ) on adiabatic temperature of industrial waste

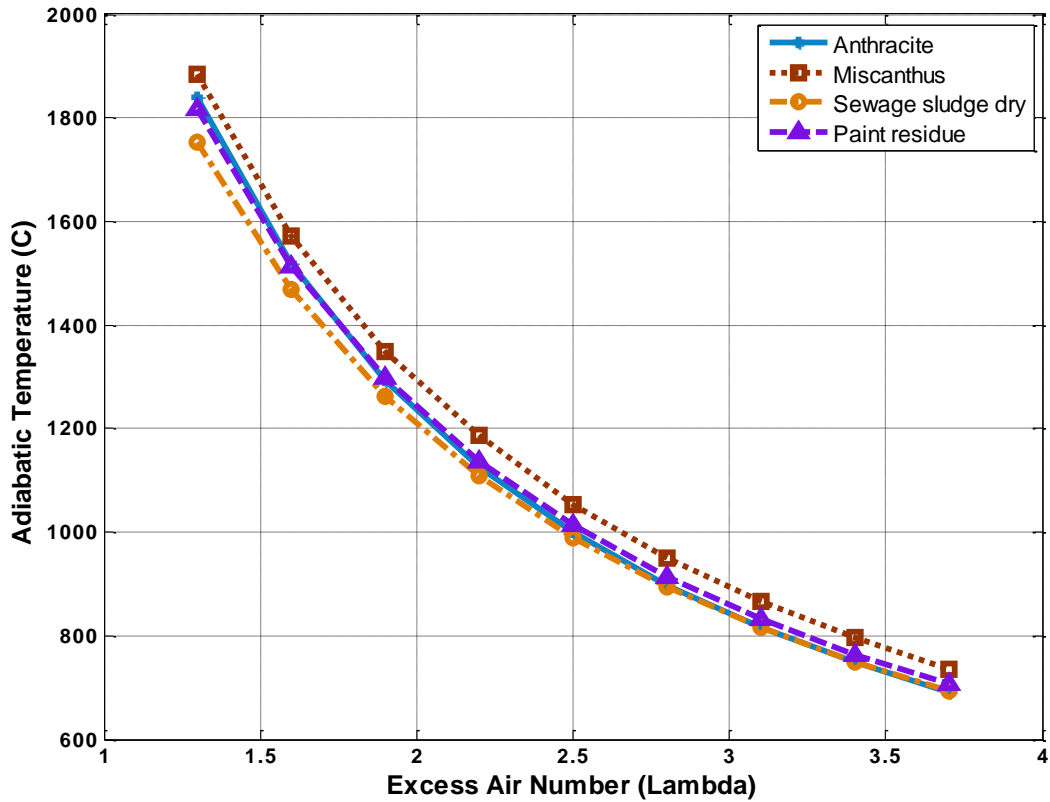


Fig. 2.12: Effect of excess air ratio (λ) vs adiabatic temperature for different solid fuels

The similar pattern is also found in the experimental investigations conducted by Jain [57]. He experimentally investigated the effect of excess air on adiabatic combustion temperature. He stated that excess air is always necessary to burn all the combustible constituents of fuel.

However, beside reduction of unburnt fuel in the combustion gases at the outlet of the combustion chamber, a larger quantity of excess air also results in large amount of air/oxygen in the combustion gases. Moreover, the adiabatic temperature decreases with increase in excess air in the combustion chamber. However, this problem can be avoided by preheating of air entering to the combustion system. Furthermore, an optimum amount of excess air should be used in combustion systems to ensure high efficiencies [57]. A similar trend of the influence of excess air ratio on the adiabatic temperature was described in the investigations by Asl and Salem [58], Quaak et al. [59], Martinez et al. [60], and Amini and Samani [61].

2.8.5 Effect of air preheating

The previous section described the influence of excess air on the adiabatic temperature of different solid fuels. It can be concluded from the results that supply of air in excess to the stoichiometric demand is necessary in order to ensure complete combustion. However, it is also noted that adiabatic temperature significantly decreases with increase in excess air, hence, reducing the thermal output. Preheating of inlet air provides a promising solution to cope with this issue. In order to quantify the effect of preheating of air on the adiabatic combustion temperature for different solid fuels, a further parametric study is presented in this section. For this purpose, a reference case is defined as shown in Table 2.3: one fuel from each category is selected and the excess air ratio is set to $\lambda = 2.5$ for the investigation of preheating of inlet air. Initial air temperatures (preheating of air) from 25°C to 400°C are considered.

Table 2.3: Reference case for analysis of preheating effect on adiabatic temperature

Fuel	Excess air number (λ)	Adiabatic temperature (°C)
Anthracite	2.5	999
Miscanthus	2.5	1054
Sewage sludge dry	2.5	990
Paint residue	2.5	1013

Figure 2.13 illustrates the adiabatic temperature of the combustion gases for four different solid fuels at different levels of air temperature (Appendix A, Table A6). As, Eq. 2.32 shows, any increase in air inlet temperature can approximately be simply added to the adiabatic combustion temperature. In this way, by increasing the air temperature from 25°C to 100°C, the combustion temperature of, for example, anthracite increases from 999°C to 1074°C; preheating the air to a temperature of 400°C, an adiabatic temperature of 1374°C is obtained. It should be noted that specific heat capacity of air and combustion gases may also vary by changing the inlet air temperature, which slightly affects the adiabatic temperature. However, in the present calculations, the adiabatic temperature of solid fuels is approximated by neglecting these effects.

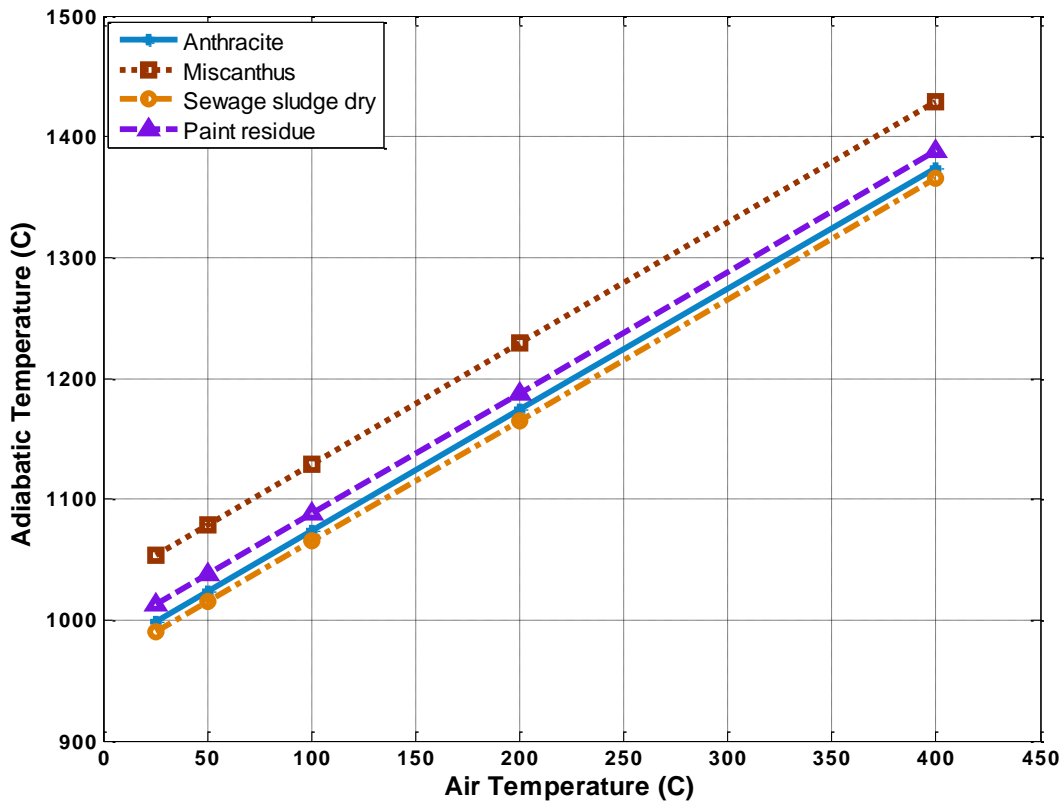


Fig. 2.13: Effect of air temperature on adiabatic temperature

Preheating of air is one of the most effective methods which are utilized at industrial scale to increase the efficiency of combustion systems. On the other hand, preheating of air increases the operational cost of the combustion system. As a common technique, the temperature of air is increased by exchanging the heat of combustion gases leaving the system [62]. However, attention must be given to the preheating techniques when designing the combustion systems i.e. boilers, furnaces etc.

2.8.6 Composition of combustion gases

As described in previous sections, combustion gases are a mixture of different species which are generated as a result of the combustion reaction. Combustion gases are produced at different rates and compositions depending upon the type and constituents of the fuel burnt. The proposed species balance model (SBM) helps to determine the composition of different gases obtained after the combustion reaction of the given fuel material. In order to investigate the influence of fuel composition and excess air number (λ) on the combustion gas composition, a further study is presented. Similar to the previous section, one fuel from each category of the given solid materials is selected, i.e. anthracite from coal, miscanthus among biomass, dry sewage sludge from municipal solid waste and paint residue from the category of industrial waste. It should be noted that the present analysis is based on the assumption of “complete combustion ($\lambda \geq 1$)” in case of all solid fuels. This implies that all carbon present in the solid fuel is burnt to carbon dioxide (CO_2) and hydrogen is converted to water vapor (H_2O) as a result of combustion reaction.

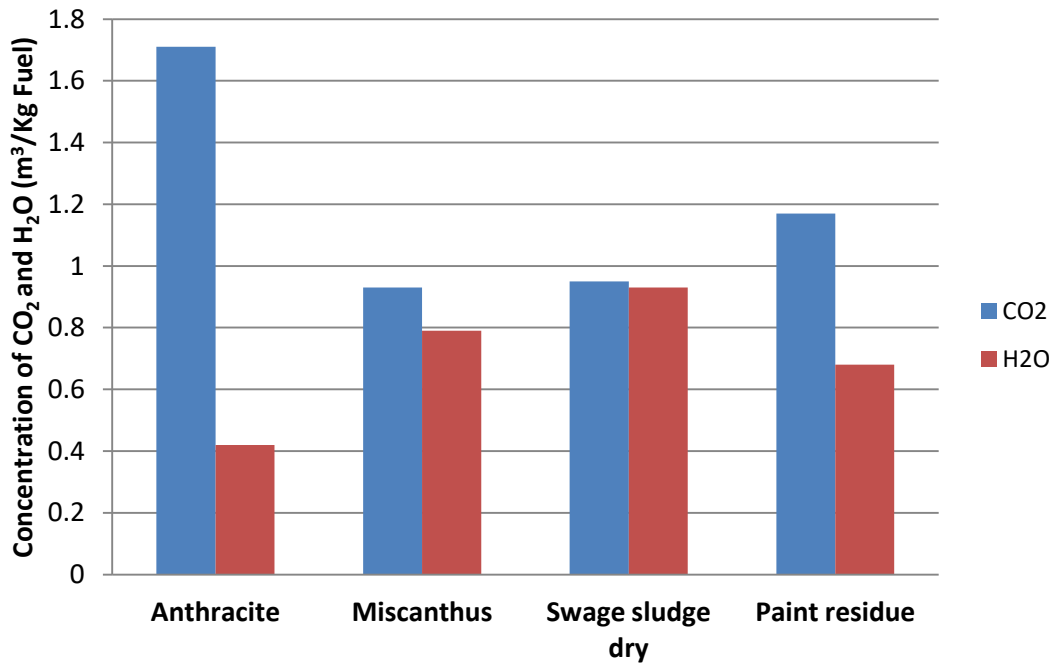


Fig. 2.14: Concentration of CO₂ and H₂O resulting from combustion reaction

Figure 2.14 illustrates the concentration (more precisely specific volume m³/kg fuel) of carbon dioxide (CO₂) and water vapor (H₂O) produced as a result of combustion reaction for different solid fuels at excess air ratio of 1.5. It is observed that anthracite gives the highest quantity of carbon dioxide (CO₂), i.e. 1.71 m³ CO₂/kg fuel while the biomass sample (miscanthus) results in the lowest amount of carbon dioxide (CO₂), i.e. 0.93 m³ CO₂/kg fuel. This is due to the fact that anthracite consists of the highest amount of carbon (91.60%), whereas miscanthus has the lowest carbon content (49.66%). Similarly, water vapor concentration is highest in case of sewage sludge. However, it should be noted that concentration of water (vapor) also depends upon the moisture content initially present in the fuel.

The computed effect of excess air on the composition of the combustion gas mixture is shown in Table 2.4 at five levels of excess air number for different solid fuels. It is observed that at complete combustion, i.e. lean combustion ($\lambda > 1$), excess air has no influence on the specific volumes of carbon dioxide (CO₂), water vapor (H₂O) and sulfur dioxide (SO₂) as all combustible (carbon, hydrogen and sulfur) are completely burnt and converted into secondary products (combustion gases). However, the specific volumes of oxygen and nitrogen are significantly affected by the supply of air in excess. At $\lambda = 1$, no trace of oxygen is found in the mixture of the combustion gases as all the available oxygen is utilized to burn the combustible constituents of the fuel.

Table 2.4: Concentrations of combustion gases (m³/kg fuel)

Fuel	λ	CO₂	H₂O	SO₂	O₂	N₂	Total
Anthracite	1.0	1.71	0.42	0.0058	0	6.92	9.05
	1.5	1.71	0.42	0.0058	0.90	10.37	13.41
	2.0	1.71	0.42	0.0058	1.81	13.83	17.76
	2.5	1.71	0.42	0.0058	2.71	17.28	22.12
	3.0	1.71	0.42	0.0058	3.61	20.73	26.48
Miscanthus	1.0	0.93	0.79	0.00077	0	3.29	5.02
	1.5	0.93	0.79	0.00077	0.43	4.93	7.09
	2.0	0.93	0.79	0.00077	0.86	6.58	9.16
	2.5	0.93	0.79	0.00077	1.29	8.22	11.23
	3.0	0.93	0.79	0.00077	1.72	9.86	13.31
Sewage sludge dry	1.0	0.95	0.93	0.00714	0	2.89	4.77
	1.5	0.95	0.93	0.00714	0.37	4.32	6.57
	2.0	0.95	0.93	0.00714	0.75	5.75	8.37
	2.5	0.95	0.93	0.00714	1.12	7.17	10.17
	3.0	0.95	0.93	0.00714	1.49	8.59	11.97
Paint residue	1.0	1.17	0.68	0.0158	0	3.57	5.43
	1.5	1.17	0.68	0.0158	0.47	5.35	7.68
	2.0	1.17	0.68	0.0158	0.93	7.13	9.93
	2.5	1.17	0.68	0.0158	1.39	8.91	12.17
	3.0	1.17	0.68	0.0158	1.86	10.69	14.42

However, by increasing the excess air number from 1.0 to 3.0, the specific volume of oxygen also gradually increases in the flue gas mixture. This is due to the fact that when air/oxygen is supplied to the combustion system, the required amount of oxygen is consumed in the burning of combustible contents and the remaining portion of the supplied oxygen is discharged along with the other combustion by-products. Similarly, excess air also significantly affects the specific volume of nitrogen in the combustion gas mixture of any solid fuel. As nitrogen is not a part of combustion reaction, all of the nitrogen which is supplied along with oxygen (in case of air) is contained in the combustion gas (outlet) mixture. However, it is noted that nitrogen contained in the solid fuel also influences the composition of the combustion gas mixture.

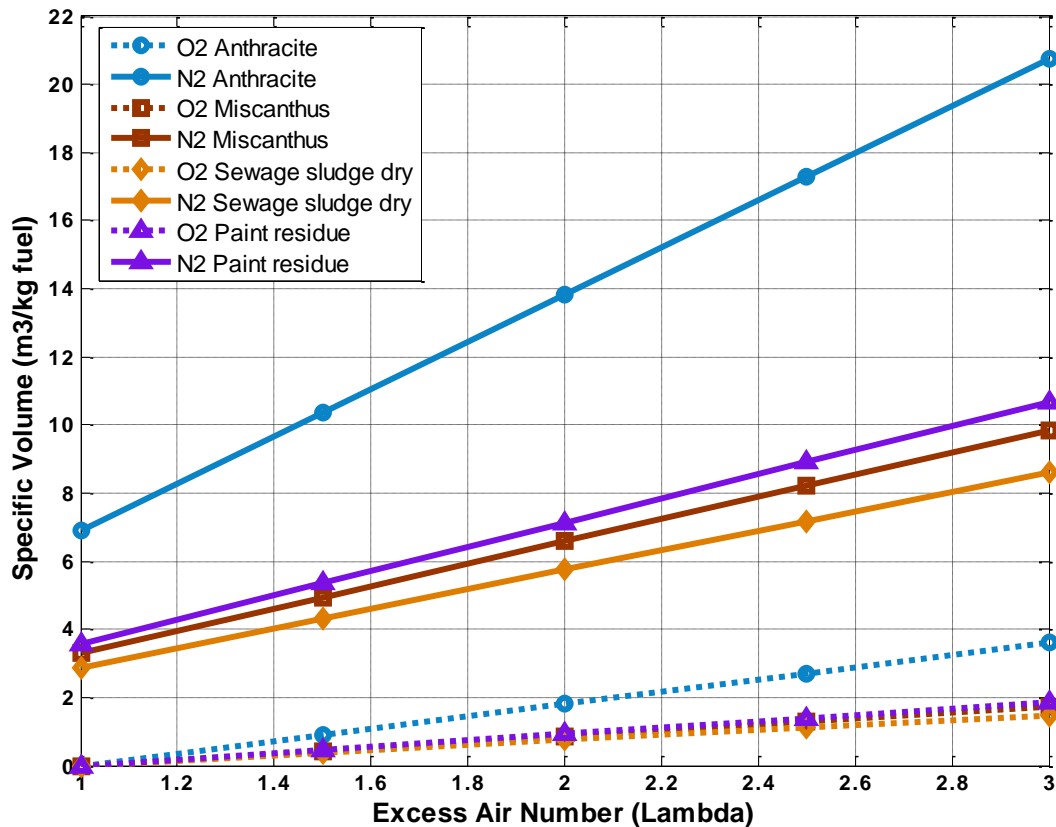


Fig. 2.15: Effect of excess air on specific volumes of O₂ and N₂

Figure 2.15 represents the concentration of oxygen (O₂) and nitrogen (N₂) at different levels of excess air ratio (λ). It can be observed that the specific volumes of both nitrogen and oxygen in the combustion gas mixture increase with increase in excess air. However, nitrogen has a larger portion in the combustion gas mixture as compared to oxygen. This is due to the fact that air is composed of much more nitrogen than oxygen. Moreover, the composition of solid fuel also affects the nitrogen concentration in the combustion gas mixture. Fuel with higher air demand (AD) requires more air for complete combustion, which results in more nitrogen in the flue gases. For example, combustion reaction of anthracite results in the highest quantity of nitrogen gas in the combustion gas mixture among the selected solid fuels. Higher air demand in case of anthracite, i.e. 11.21 kg air/kg fuel, is the reason for this behavior. At the opposite end, sewage sludge (dry) results in a minimum quantity of nitrogen due to lower air demand.

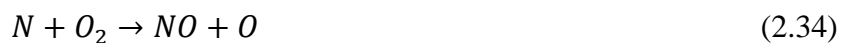
2.8.7 Formation of nitrogen oxides (NO_x)

Nitrogen is found in the atmosphere and makes up a major portion of air, as it also makes up a large part of flue gases after combustion in air. Therefore, it is important to study the behavior of nitrogen during combustion phenomena, especially at elevated temperatures. Under favorable conditions, nitrogen may react with other species (commonly oxygen) to produce secondary products, i.e. oxides of nitrogen (NO_x). Nitrogen oxides (NO_x) are of different types and structures; however, three among these oxides are important when studying combustion processes: nitrogen monoxide (NO), nitrogen dioxide (NO₂) and di-nitrogen

oxide (N₂O). In common practice, NO_x mainly consists of nitrogen monoxide (NO) along with a small quantity of nitrogen dioxide (NO₂). However, it is necessary to analyze the formation of both gases for the selection of a proper NO_x reduction technique. There are three general mechanisms leading to NO_x formation in a common combustion system [42][63], denoted by:

1. Thermal NO_x
2. Fuel NO_x
3. Prompt NO_x

Thermal NO_x is formed as a result of chemical reaction between atmospheric nitrogen (N₂) and oxygen (O₂) at high temperature. This is considered to be the most dominant source of NO_x production in a combustion process. Generation of NO_x through this process depends upon the temperature and nitrogen residence time. Hence, formation of thermal NO_x increases with increase in flame temperature. The mechanism of thermal NO_x formation can be described by following reactions [42][63,64]:



The first reaction (Eq. 2.33) is the limiting reaction which requires high activation energy, i.e. 314 kJ mol⁻¹. Therefore, a very high temperature is required for the onset of this reaction. Formation of thermal NO_x can thus be avoided by lowering the temperature and diluting the available oxygen in the combustion chamber.

Fuel NO_x is produced when nitrogen contained as a constituent of the solid fuel reacts with the (excess) oxygen present in the combustion chamber. Conversion of nitrogen present in the solid fuel to NO_x is based on very complex processes and reaction schemes, i.e. several reversible reactions are involved. The general mechanism of NO_x formation involves releasing of nitrogen from the solid fuel in the form of volatile hydrogen cyanide HCN which forms further intermediate species, i.e. NCO, CN, HNCO, after reacting with free radical species, e.g. O, OH. NO_x is formed by a further series of reactions among these species. Staged combustion is suggested to be the most effective method for minimization of fuel NO_x [42][63].

Reaction of atmospheric nitrogen with hydrocarbon radicals results in the formation of prompt NO_x. This is formed at the early stages of the combustion process. However, prompt NO_x contributes as a very small portion of the total NO_x production. Therefore, it is only considered when exceptionally low emission levels are desired [42][63].

NO_x are secondary products in the combustion process and are termed pollutants. Hence, reduction of NO_x levels is very important. There are several methods for minimizing the emission levels such as flue gas recirculation, staged combustion, catalytic converters, steam

injection etc. However, selection of the appropriate method depends greatly on the type of fuel used in the combustion system [42][64].

2.9 Summary

In this chapter, a unified model consisting of sub-models (species balance model (SBM), mass balance and energy balance model) was presented for the combustion of different solid fuels. It is concluded that thermal characteristics and chemical composition of the solid materials play an important role in the combustion phenomena. Carbon and hydrogen are the combustible constituents present in the solid fuel which burn to release energy. However, carbon has more influence on the combustion characteristics. Air demand (AD) depends upon the species composition of the solid fuel. Concentration of oxygen present in the air also significantly influences the air demand (AD). More oxygen in the air, less will be the air demand and vice versa. The SBM model coupled with the mass and energy balance model showed that the maximum temperature generated in the adiabatic combustion chamber is mainly influenced by heating value, air demand and excess air ratio.

Comparing different fuels at the reference level of excess air ratio ($\lambda = 1.3$), the highest temperature is obtained in case of waste tyres, i.e. 2060°C, while municipal solid waste has the lowest temperature, i.e. 1599°C. However, similar to coals, waste tyres also result in high levels of carbon dioxide emission due to the presence much carbon. It is interesting to note that paint residue has approximately the same adiabatic temperature (around 1800°C) as anthracite coal, with comparably lower emission levels. This is due to the smaller air demand and higher amount of volatiles (resulting in a higher calorific value) in case of paint residue. Moreover, the presence of a high amount of volatile matter (VM) also indicates its suitability for combustion (ignition). Furthermore, the investigations also revealed that air supplied to the combustion chamber also has a significant effect on the adiabatic temperature. Adiabatic temperature is reduced significantly by increasing the excess air number (λ). For example, adiabatic temperature in case of paint residue is reduced from 1800°C to 700°C by increasing the excess air number from 1.3 to 3.7. Since air supply is always necessary in excess in order to achieve complete combustion, preheating of inlet air provides a promising solution to achieve high temperature despite of a high level excess air (as usually done in industrial furnaces).

As an outlook of current findings, paint residue turned out to be an alternative solid fuel with significant energy content. Hence, there is a need to further investigate this type of fuel with the latest combustion technologies, especially with pulverized fuel combustion technology (PFC).

Pulverized Fuel Combustion (PFC) Technology

This chapter presents the fundamentals and characteristics of PFC technology. Application of PFC to different solid fuels is discussed. State of the art technologies for pulverized fuel combustion are presented. Process parameters and apparatus design influencing the pulverized fuel combustion are also discussed. Moreover, problems and challenges associated with PFC for solid materials, especially materials with low melting point, are also discussed.

3.1 Pulverized fuel combustion (PFC)

Pulverized fuel combustion is one of the modern combustion technologies. The basic principle of the PFC technology involves combustion of solid fuel in the form of particulate matter, i.e. in powder/pulverized form. Hence, pulverized fuel combustion technology includes different mechanical unit operations and thermal processes, i.e. crushing, milling or grinding, sieving, fuel transportation or injection, combustion, heat extraction, discharge of flue gas with safe concentrations and processing of ash for further use. Figure 3.1 represents the flow chart of different processing steps involved in PFC technology.

Solid waste or fossil fuel (i.e. coal) is a bulky material in raw form. The raw material (having large size and non-uniform shape) is first crushed into smaller pieces. The smaller pieces are milled to fine particles afterwards. Selection of size and number of mills and grinders depends upon type of the material and desired particle size for the combustion system, i.e. PFC plant. The fine particulate material is allowed to pass through different sieves in order to separate the main fraction from oversize and undersize material. The solid particles of the main fraction are then fed to the combustion furnace. These particles are injected into the (combustion) firing chamber with the help of an air jet stream. In other words, powdered solid fuel is transported pneumatically to the combustion furnace through a fuel injection nozzle.

Combustion of solid particles takes place in the combustion chamber resulting in the release of a very high amount of thermal energy at high temperature, along with combustion gases (Chapter 1). Heat is extracted from the combustion gases using heat exchangers and flue gases are discharged from the stack at permissible emission levels. Residue left behind is collected for the further processing [33][40][48].

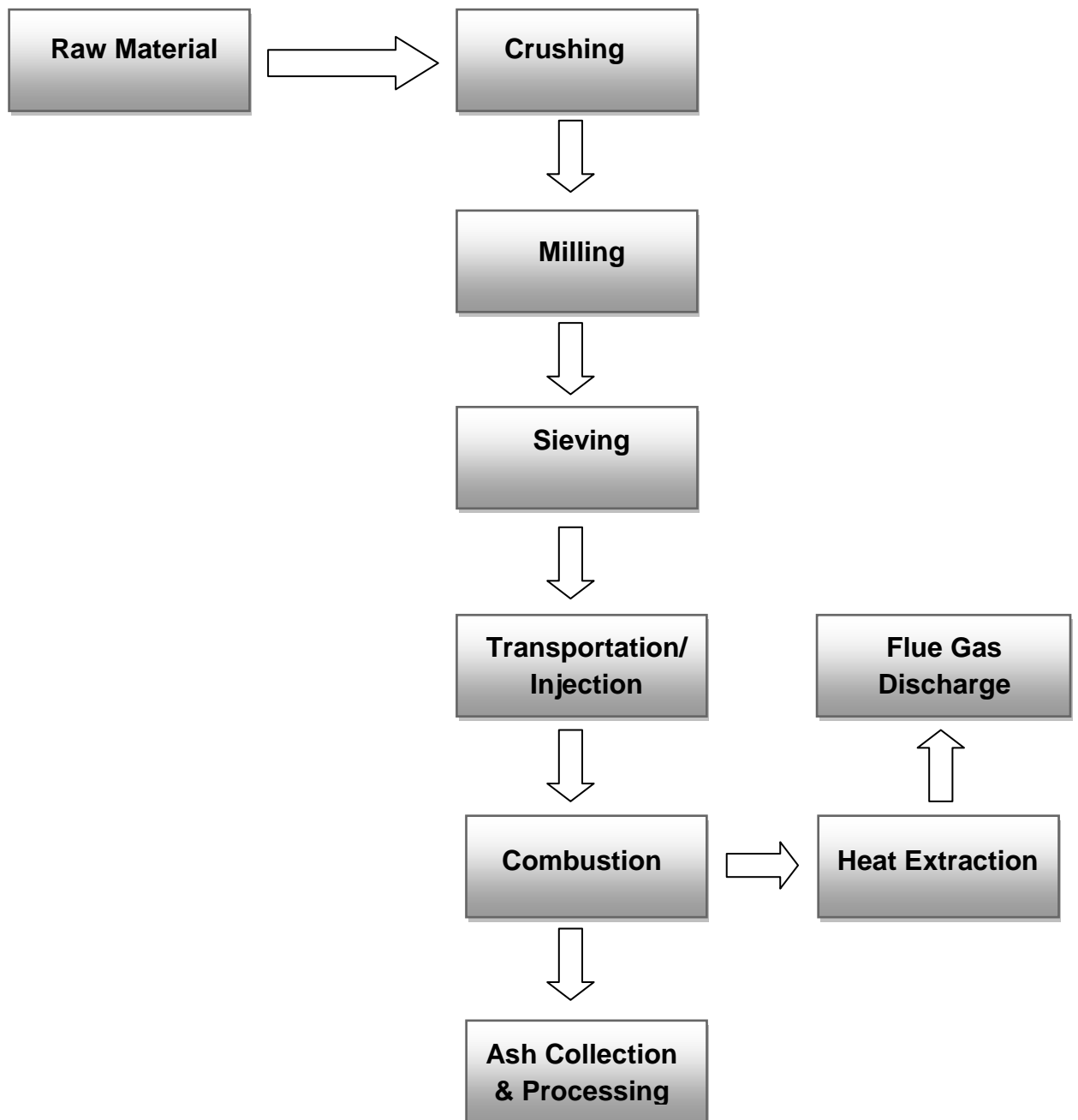


Fig. 3.1: Steps involved in pulverized fuel combustion technology

The main objective of the pulverization of solid material is to increase the specific (surface) area of the solid particles so that maximum area can be exposed to the oxidant (commonly air) which results in optimum conditions for ignition and combustion of the solid (fuel) particles. Due to this ability, it is one of the most reliable and effective methods for combustion of solid materials. However, feeding method as well as design of combustion system, i.e. furnace, burner etc. significantly influence the combustion process. In pulverized fuel combustion, the residence time of the fuel particles is relatively short and particles are not circulated as in case of fluidized bed combustion (FBC). Fuel along with air is fed from the top of the combustion plant and flue gases are released from the outlet very fast, after typically only 2 s.

A typical PFC plant has following components:

1. Fuel nozzle
2. Burner
3. Secondary air nozzle
4. Combustion chamber or firing chamber
5. Ash collector
6. Flue gas outlet

Figure 1.2 has already presented a schematic diagram of pulverized fuel combustion system. Fuel particles are transported by the air stream with high velocity through the fuel nozzle available at the top of the combustion furnace. The air used to transport the pulverized/powdered solid material is termed as transport air or sometimes also named as primary air. After injection of the solid particles into the combustion furnace along with air, combustion takes place at very high level of air-fuel mixing ratio. Sometimes more air is also provided after the injection of solid fuel. The air provided in this way is termed as secondary air. The purpose of secondary air is to enhance the air-fuel mixing ratio and to provide optimum (temperature) conditions for ignition. The device which controls the mixing of fuel and air jets is termed as burner.

Design of burners plays a key role in pulverized fuel combustion systems. Combustion of the pulverized solid material takes place in the combustion chamber with a very short residence time of fuel particles. However, sufficient time should be provided for complete burning of the solid particles to avoid unburnt fuel at the outlet. This can be accomplished by efficient design of the combustion chamber. After burning of the solid fuel, flue gases leave via an outlet pipe and ash residue is collected by the ash collector placed at the bottom of the furnace [33][40].

3.2 Combustion mechanism in PFC

In pulverized fuel combustion (PFC) solid fuel is injected and burnt in the form of small particles. Hence, it is important to understand the behavior of combustion phenomena at individual particle level. After the injection of pulverized fuel into the combustion chamber, the particles undergo different effects, phases and reactions. These processes or, in other words, sub-phases of the PFC typically take a very short period of time for completion.

Though short, this time must be provided by the combustion system in form of sufficient residence time of the solid particles. Moreover, the nature and duration of involved processes depend upon the type of material and size and shape of the solid particles [65].

In general, PFC involves the following different phases and processes (Fig. 3.2) occurring for individual particles [66-69]:

1. Fuel transportation or injection
2. Drying
3. Devolatilization and volatile burning
4. Char combustion
5. Ash formation

3.2.1 Fuel transportation or injection

This is the first step in pulverized fuel combustion. In this step, powdered or pulverized solid fuel is injected into the combustion chamber. The injected solid particles are diluted by the hot gases in the combustion chamber. In this stage mixing of injected particles and hot gases takes place by particle-gas interaction phenomena. Particle size and shape play a key role in the aerodynamics and mixing behavior in the combustion chamber. In most cases, the solid particles are assumed to be spherical in shape; however, in actual conditions the particles possess non-spherical shape and non-uniform sizes, which leads to complex mixing behavior and characteristics [65].

3.2.2 Drying

This process starts just after the injection of solid particles into the combustion chamber (hot gases environment). During this phase, the moisture present in the solid particles is evaporated by the heat provided by the surrounding hot gases present in the combustion chamber (Fig. 3.2). Drying of fuel particles is initiated at comparatively low temperatures (e.g. 373 K) [68]. However, the evaporation of moisture from the solid particle depends upon the type of material and its properties (i.e. porosity etc.). For example in case of biomass (wood) particles, the release of moisture is initialized at approximately 25°C at very slow rate depending on saturation pressure. Release of moisture from solid fuel particle increases with increase in temperature until this reaches the boiling point of water. Drying of solid particles is governed by particle temperature and vapor concentration gradient [67,68][70].

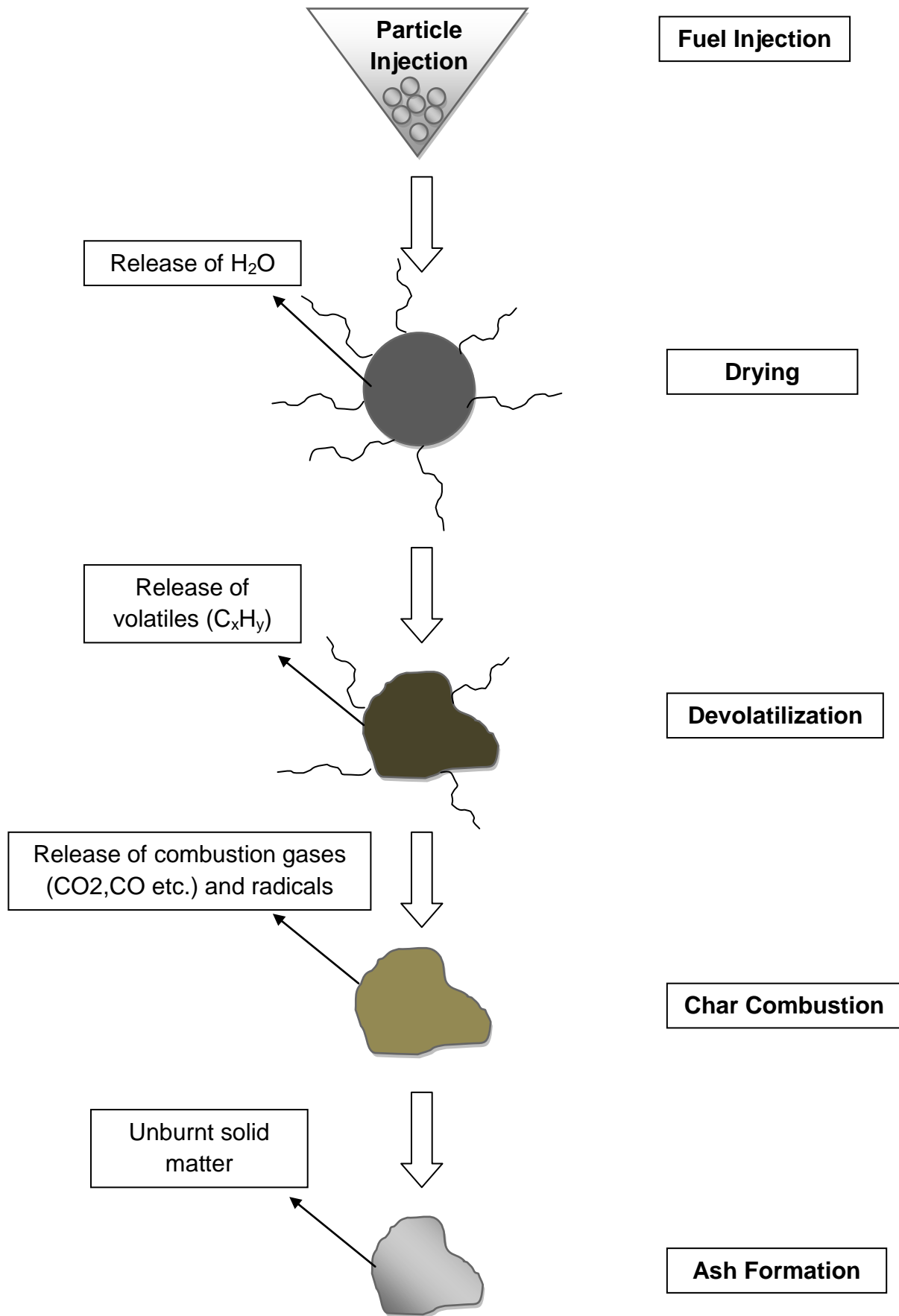


Fig. 3.2: Mechanism of pulverized fuel combustion (PFC) [66-69]

3.2.3 Devolatilization

Devolatilization is the release of volatile species from the solid particle in the form of gases (Fig. 3.3). After drying of the moisture present in solid fuel, the fuel particle undergoes the devolatilization phase. However, both processes are very rapid and occur simultaneously. This is the most important stage during pulverized fuel combustion (PFC). During this stage, the combustible species are transported from the pores of the solid particle in the form of C_xH_y (and also CO , CO_2 , H_2 etc.), water vapor (by the inherited water content) and inorganic radicals.



Fig. 3.3: Devolatilization process

The composition of volatiles is influenced by the chemical analysis of the specific type of fuel (Chapter 2). Devolatilization of a solid particle commonly starts at a temperature range of $160^{\circ}C$ to $300^{\circ}C$. However, this temperature may vary depending upon the type and size of the fuel particle. Size of the fuel particle also has a significant influence on the volatiles release. Devolatilization is faster in case of smaller particles as compared to larger ones [70]. After the release of volatile gases, the organic portion of the volatile species released during the devolatilization process are burnt to produce carbon dioxide (CO_2) and water vapor (H_2O) $Volatiles + O_2 \rightarrow CO_2 + H_2O$ (3.1) while other species (inorganic) undergo other transformations [66-70].

During PFC, combustion is initiated when the combustible species released from the solid particle achieve the ignition temperature. Air streams and chemical heat release rates result in the structure of the flame. However, stability of the flame is determined by the burning of volatile gases. Hence, release of volatiles is considered to be one of the most important factors controlling the overall combustion process. Stability problems may occur due to variation in devolatilization characteristics. These problems can be overcome by optimization of operating conditions (i.e. air stream velocities) and by burner design [69].

3.2.4 Char combustion

After the release of volatiles from the solid particle, the solid residue left behind from the devolatilization process is termed as “char”. Char has a very complex structure and composition which is determined by the development and conditions of the devolatilization phase. The formation of char is also dependent on the type of material. For example, biomass fuel particles maintain their irregular shape during char formation, while coal particles become soft and spherical. Hence, complex combustion phenomena result which are determined by the size, shape and composition of char [70]. Oxidation of char consists of complicated mechanisms. In general, combustion of char is divided into different regimes

which are determined by the penetration of oxygen into the pores of the fuel particle. Hence, difficulties are faced to define the exact combustion zone. The reactivity of the char is also largely dependent on the type of fuel material. Time required to burn the char proportion of a solid fuel particle is one of the important factors which affect the overall design of combustion systems, especially the combustion chamber [66-71].

3.2.5 Ash formation

Ash is the unburnt fraction of the solid fuel particle. It contains different inorganic and mineral constituents. Ash formation is the last step in pulverized fuel combustion (PFC) which occurs during the burning of char. Ash is further categorized into two types, i.e. fly ash and bottom or residual ash. During char combustion, a fraction of constituents is volatilized and leaves a layer of ash on the surface of the char particle. This layer is removed by attrition and forms fine particles of ash through condensation, coagulation and agglomeration. The fly ash particles are dispersed in the flue gas mixture. Diameter of fly ash particles varies from 0.01 μm to 1 μm . The mineral compounds contained in the particle after char combustion result in residual ash formation. The particle size of residual ash ranges from 1 to 100 μm . Formation of either type of ash in the combustion process of pulverized fuel depends on the characteristics of the material as well as the combustion conditions, i.e. particle residence time in the combustion chamber, temperature, oxygen concentration etc. [72,73]. Composition of ash generated by the combustion of solid material is significantly important for the design of combustion system as many operational problems are associated with this matter, e.g. slagging, erosion, fouling, corrosion as well as transportation cost. Re-use and recycling of ash contents also depend upon the type and constituents of ash (Chapters 1 and 2).

All these processes occur simultaneously in the combustion furnace. Temperature is the key factor which influences all steps in several ways. The solid fuel particle is exposed to high temperature after injection from the fuel nozzle. After reaching a certain temperature, i.e. devolatilization temperature, the volatile species are evolved from the particle and ignition is started. However, it should be noted that this temperature varies depending on the type and constituents present in the solid fuel. Hence, ignition and combustion of volatiles may start close to the fuel nozzle or near the burner exit. The temperature of the solid particle increases significantly after the ignition of volatile matter and reaches to its maximum value. Afterwards, combustion of char takes place; however, it occurs at slower rate than the combustion of volatiles. In PFC, high efficiencies, e.g. 90% are achieved, making PFC to an attractive technology for the combustion of solid material [74].

3.3 State of the art in PFC technologies

This section provides a selective review about the advancements made so far in pulverized fuel combustion (PFC). The technological and scientific progresses presented so far are categorized as following:

1. PFC of solid materials: coal and other solid materials
2. Burner designs and furnace aerodynamics
3. Preheating and MILD combustion technology in PFC
4. Melting phenomena of solid particles during PFC
5. Computational fluid dynamics (CFD) modeling of PFC

3.3.1 PFC of solid materials: coal and other solid materials

Pulverized fuel combustion (PFC) is emerging as a dominant combustion technology which has become the preferable mode of combustion in many industrial furnaces with improved combustion efficiencies.

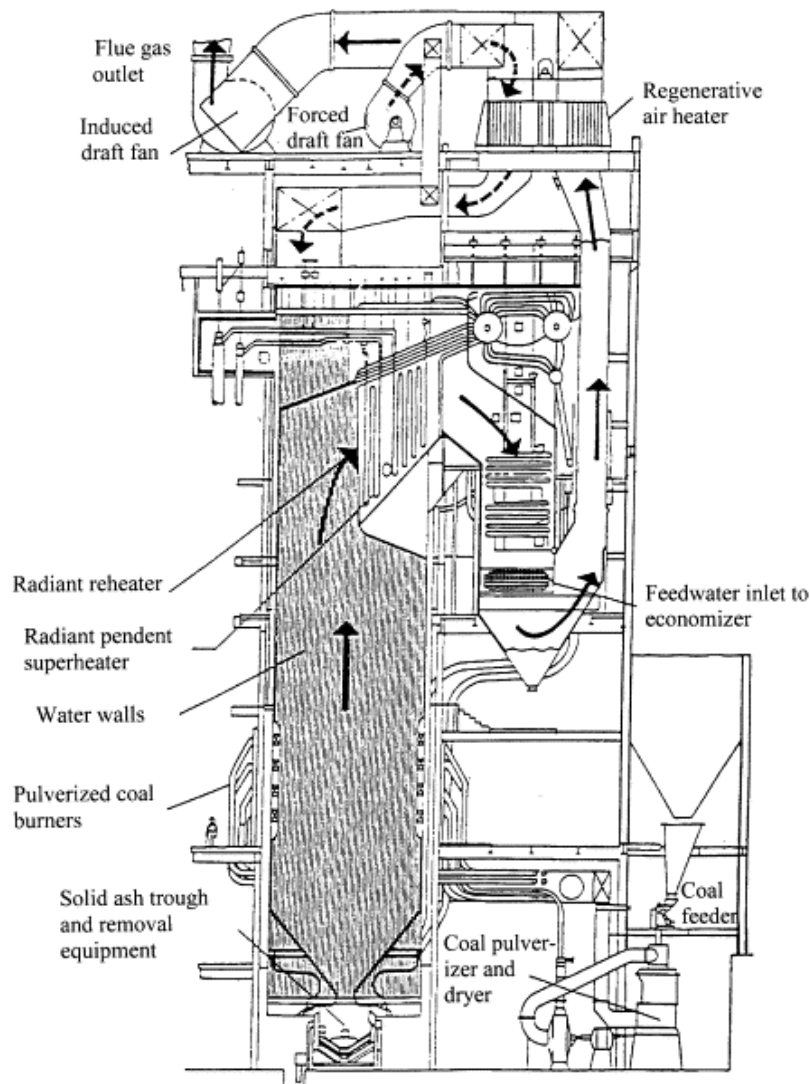


Fig. 3.4: Pulverized coal fired utility boiler [40] (with permission from Elsevier)

PFC has achieved special attention by the research community as well as the industrial sector during the last years. During this era, different technological advancements have been made in pulverized fuel combustion technology in terms of plant design, material processing, modeling and insight of combustion processes; thus, combustion efficiencies have been significantly improved. During past years, pulverized fuel combustion technology was applied to coal as a fuel (Fig. 3.4). Pulverized coal power plants with approximately 2000 GW are being operated around the globe [33].

Beer [40] presented a comprehensive study about the developments in combustion technologies. He mentioned that combustion of pulverized coal has been a common power generation technology during recent years. However, there is a need to develop advanced clean coal combustion technologies due to increasing emissions. The new technologies should be developed accompanied by efficient modeling and lab scale experimental approaches which are useful for designing of combustion systems at large scales. Combustion of coal with secondary fuel is one of the advancements made so far in the sector of pulverized fuel combustion. Combustion of alternative solid material in the conventional combustion furnace also provides a sustainable solution to replace the fossil fuels. However, utilization of other fuels in coal fired systems requires certain optimization and modifications [36-40] [75].

Lempp [76] reported that combustion of alternative solid materials, e.g. biomass etc., along with coal has many advantages as compared to conventional (coal) power generation systems, such as high efficiency, less pollutant emissions, economical feasibility and capability of multiple material firing. Co-firing includes combustion of biomass with not only coal but also with natural gas as a primary fuel. However, co-firing with the former is the most common technology. Lempp [76] further stated that co-firing may be classified into three technologies, i.e. direct co-firing, indirect co-firing and parallel co-firing. In direct co-firing technology, solid material, e.g. biomass, is ground to fine particles and then injected into the combustion system (boiler etc.). Individual or common burner can be used for this purpose, however, transportation of solid fuels in separate burner results in more flexible and economical designs of furnaces. This is the most common method in co-firings of coal with other materials. On the other hand, in indirect co-firing technology, solid (biomass) material is converted into gas with the help of a gasifier and the resulting gas is burnt with coal in the combustion furnace. This technology is applicable to a wide range of materials allowing the maximum ratios of alternative solid fuels with primary fuel (e.g. coal). However, this technology is more expensive than the direct firing as it requires an additional setup (gasification system). Moreover, problems of gas cleaning and ash depositions are also faced. Parallel co-firing involves combustion of alternative solid material (e.g. biomass) in separate combustion chamber and supplying heat energy to the main heating system. It also enables high throughputs of solid materials to be combusted. This method is mostly suitable for industrial applications in which industrial by-products are burnt for heating purposes. However, technical challenges such as handling, transportation, combustion characteristics, slagging,

fouling and corrosion are faced, which need to be rectified to enhance combustion efficiencies [76].

Wu et al. [38] also stated that combustion of secondary fuels (solid wastes etc.) along with coal has emerged to be one of the most sustainable and convenient solutions for the minimization of coal consumption. However, there is a need to analyze the combustion characteristics of co-firings of coal and other solid materials to avoid technical and operation problems in the boilers. For this purpose they investigated the co-combustion of SRF (solid recovered fuels) with coal in an entrained flow reactor (Fig. 3.5).

In a 2-m high reactor, both fuels were injected from the top of the reactor along with primary air. The injection rate of solid materials was adjusted in such a way that an excess air ratio of 1.43 was maintained. They concluded from the experimental investigation that combustion of coal with secondary fuel, i.e. SRF, does not exert any additional load on the emission levels of NO and SO₂. However, burnout can be affected in the combustion furnace. Moreover, they emphasized that a suitable particle size and improvement in the quality of SRF is desirable for optimum combustion characteristics.

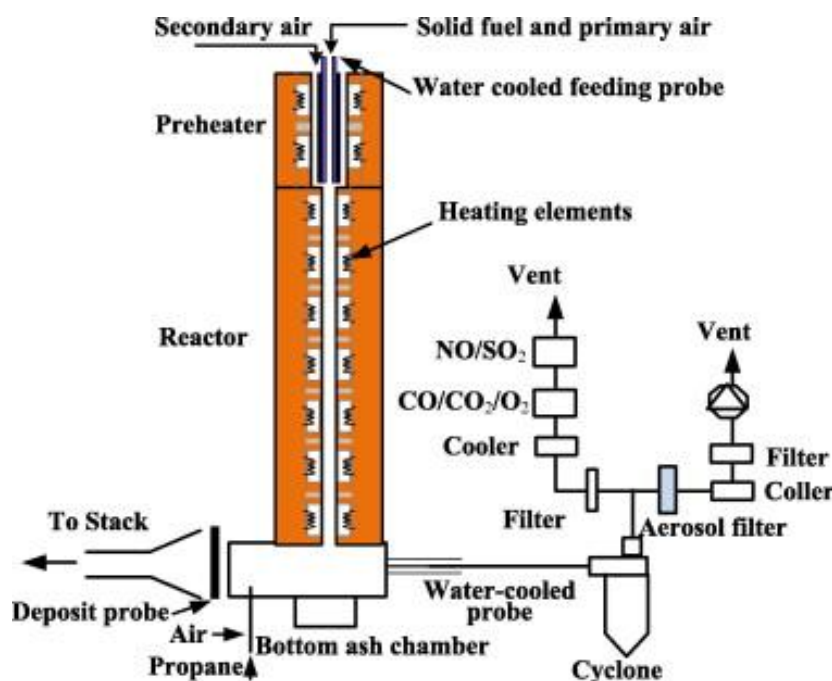


Fig. 3.5: Entrained flow reactor by Wu et al. [38] (with permission from Elsevier)

3.3.2 Burner designs and furnace aerodynamics

The burner is a supporting apparatus attached to the combustion furnace. It is utilized to convey the fuel and air to the combustion chamber of the furnace (Fig. 1.2). These systems are capable to mix the fuel and air streams entering to the furnace. Commonly, fuel is injected with a velocity range of approximately 15-25 m s⁻¹ based on the design and type of material in order to prevent settling of particles. Burners are installed in the pulverized fuel combustion (PFC) furnaces in different ways, e.g. downs-hot firing, horizontal firing and tangential firing. In downs-hot firing, pulverized fuel is fed in downwards direction to the combustion furnace.

This provides a comparatively long path for the flame. Hence, it is suitable for those materials which take long residence time to complete the combustion process (usually low volatile materials). In case of horizontal firing burners, pulverized fuel particles are injected horizontally to the combustion furnace resulting in high turbulence gas streams to enhance the combustion process. In this type of arrangement, an individual flame/combustion zone is produced by each burner. Hence, a sufficient amount of air is always required through secondary air inlet. In tangential firing arrangements of burners, fuel particles are conveyed to the combustion furnace with the help of burners installed at the corners to form a tangent to the combustion zone circle. The swirl produced by the burners creates a relatively high degree of turbulence. Design of burner plays an important role in the performance of a combustion system, i.e. PFC furnace. It is used to adjust the mixing ratios and to minimize the emissions by controlling the injection rates. Depending upon design, the burners for pulverized fuel combustion are further classified into wall burners, corner burners, low NO_x burners etc. Selection of burner arrangement and design of burner depends upon the capacity of the combustion system as well as the fuel used for the PFC combustion [77].

Mullinger and Jenkins [78] reported that combustion of pulverized fuel (coal) is alike the combustion of liquid fuels. However, burner's flexibility is highly desirable for combustion of solid materials. In most of the cases, burners for pulverized fuel combustion are similar to those used in the combustion of oils. However, atomizer present in the liquid fuel burners is replaced by the fuel nozzle in case of pulverized solid fuels. The powdered fuel is transported into the combustion system through this nozzle. A typical burner includes an open end pipe for the pulverized fuel transportation, as shown in Fig. 3.6.

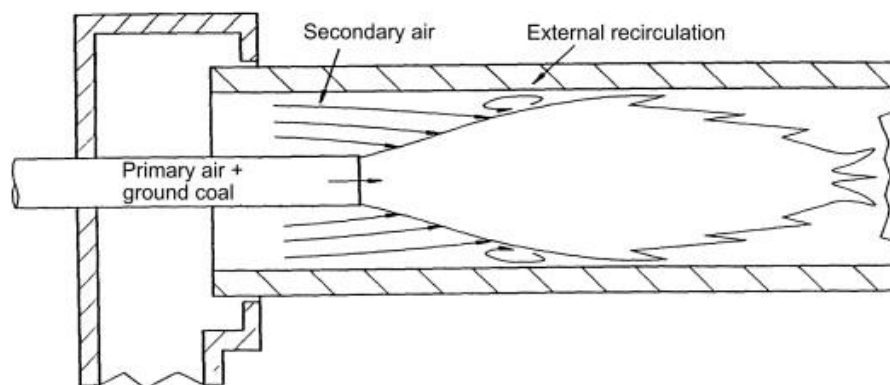


Fig. 3.6: Typical open end burner for pulverized coal combustion [78] (with permission from Elsevier)

With the transformation of technology from combustion facilities operated with liquid fuels to solid fuel combustion furnaces/kilns, modifications were made of the conventional burners to develop new burner designs which were capable of solid fuel injection. However, optimized mixing of air and fuel particles is still a problem to be addressed. For example, poor mixing ratios and flow velocities may cause non-uniform concentration of solid particles in the channels used for the transportation of solid fuel particles. High concentrations of powdered material in the multiphase (air and fuel particles) flows result in accumulation and settlement

of fuel particles in some parts of the nozzle (pipe) which cause operational problems of the combustion facility. This phenomenon is termed commonly as roping. An efficient burner must prevent roping during fuel injection. This can be achieved by providing optimum air flow for the required mass loading of fuel particles. Swirling is another way to improve mixing patterns of the reactants in the burner. Multi-channel burners have also been found to be advantageous and economical, where an oil burner can also be installed for start-up purposes (Fig. 3.7) [78].

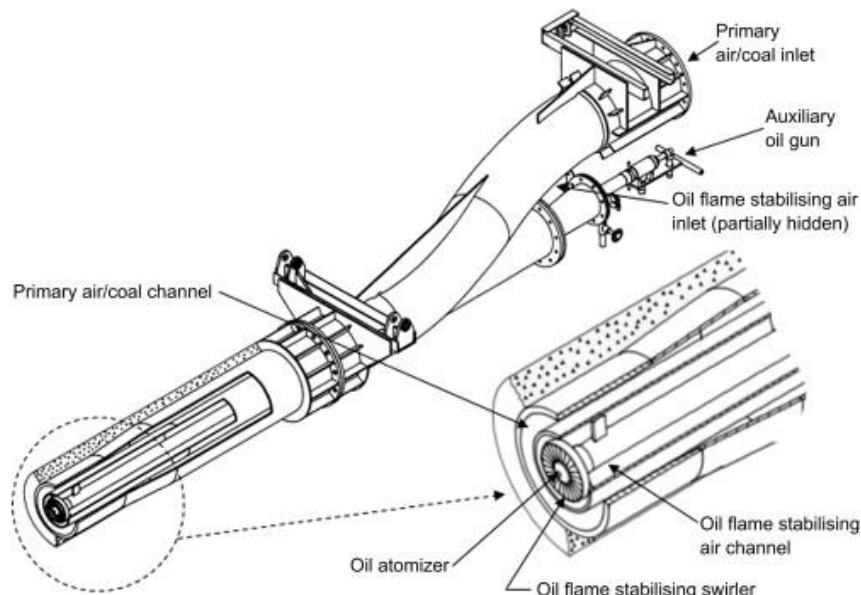


Fig. 3.7: Pulverized coal burner with oil firing facility [78] (with permission from Elsevier)

Katzer et al. [79] investigated the relationship between swirl burner and flame length for pulverized coal. They reported that structure and operating conditions of the burner are important process parameters involved in power generation from solid fuels (i.e. coal). They contribute to achieve stable ignition and combustion conditions. Stability of flame is not only important in case of gas fuels but also plays a critical role in pulverized fuel combustion in terms of flame location and resistivity to blow-off. There are two types of burners used in power generation units, i.e. jet burners and swirl burners. However, in case of swirl burners, different strategies are required in order to address the flame characteristics (especially near the outlet of the burner) than the conventional methods used in jet burners. Moreover, challenges are faced when trying to describe the location of flame beginning from the burner outlet. They concluded from experimental investigations that flame stability depends upon the main reaction zone which can be described by different parameters, i.e. flame length and flame fluctuations in length and flame brightness and its deviation. An increase in the number of swirls resulted in improvements in flame stability. Further they suggested that the current methods should also be applied to analyze new burners with different operating conditions [79].

Sung et al. [80] recently presented a study about a methane assisted burner for pulverized coal. They stated that different aerodynamic factors such as air flows, staging, swirling

significantly influence the structure and behavior of combustion flames. NO_x emissions can be reduced by maintaining low oxygen quantities (rich flame environment) in the primary combustion zone. They investigated a swirl burner (Fig. 3.8) containing two inlets and two axial swirling annuli. Six vanes are mounted at angles of 30° , 40° , 50° and 60° on each swirling annulus. Pulverized coal was transported by a mixture of methane and air through inlet 1 while pipe 2 was used to supply methane and air mixture. The results revealed that flame lift (i.e. distance of flame beginning from burner) decreases by increasing the swirl numbers. Greater mixing (swirling) intensities result in rather radial than axial flows, creating a large internal reticulating zone. Increase in swirl number as well as larger internal recirculating zone also result in improvement in flame stability. Furthermore, Sung et al. [80] also concluded that formation of an exhaust tube vortex is greatly dependent on swirl number.

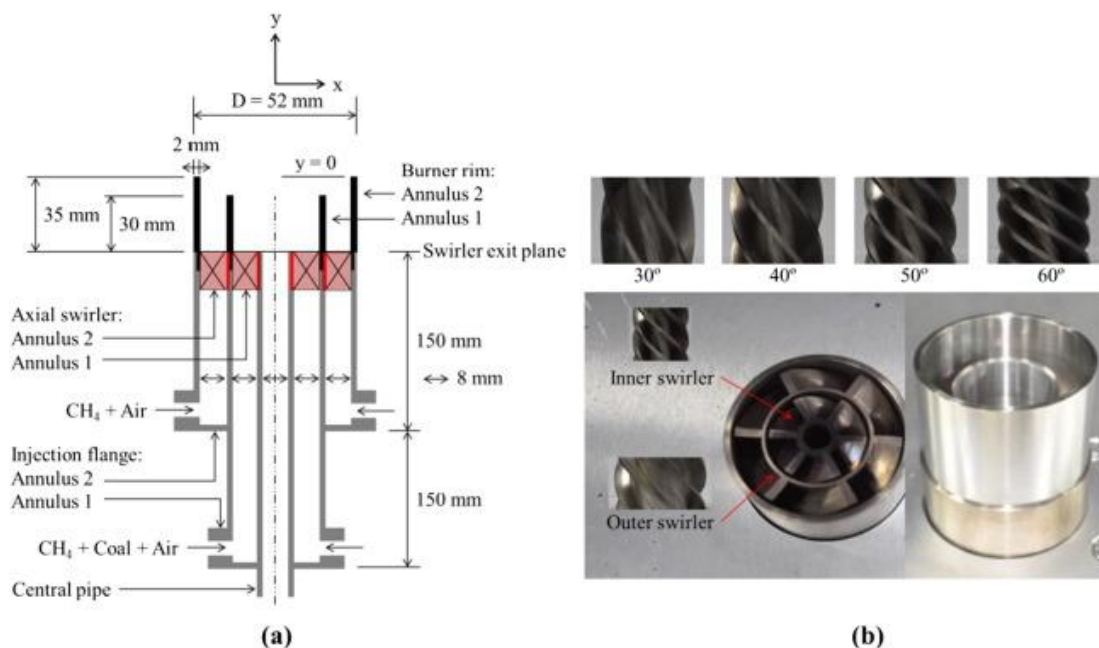


Fig. 3.8: Swirl burner for pulverized fuel (coal) [80] (with permission from Elsevier)

Similarly, aerodynamics and design of burners have been discussed in various studies reported by Tamura et al. [81], Li et al. [82] and Zhou et al. [83]. However, most of the studies have focused on pulverized coal as a fuel. There is a need to discuss the aerodynamic behavior of other types of fuel material, i.e. solid wastes during injection. Moreover, staging of air and fuel has also been found to be an appropriate technique for the combustion of pulverized solid fuels. However, the effect of different flow rates at different inlets should also be discussed for the understanding of combustion patterns in PFC systems.

3.3.3 Pre-heating and MILD combustion technology

Different aerodynamic and thermodynamic factors influence the combustion process in several ways. Temperature is of key important among these factors. Combustion processes are, roughly, categorized on the basis of high, intermediate and low temperatures. When fuel and oxidant (typically air) are mixed together in the combustion chamber, a certain temperature (called ignition temperature) is required to initiate the combustion process.

Heating the combustible substances prior to mixing provides an effective solution for the combustion of materials with relatively low heating values. The heat is supplied by flue gases; hence, this type of combustion is termed as heat-recirculating combustion [84]. In this frame heating of air (among the reactants) has been considered as the most common technique. A respective technology is denoted by HiTAC (high temperature air combustion) and is based on the previous concepts, i.e. combustion by use of highly preheated air with large enthalpy. In this method, temperature of air is enhanced to a higher level than the auto-ignition temperature of the mixture. HiCOT, i.e. high temperature combustion technology, is another way to conduct a combustion process at elevated temperatures. However, this technique is not limited to the utilization of air as in case of HiTAC.

MILD combustion, i.e. moderate or intense low oxygen dilution, is emerging as a modern form of combustion. It is a combination of elements from high temperature combustion techniques, i.e. HiTAC and HiCOT. MILD combustion conditions are achieved by elevating the reactant temperature in the incoming stream beyond the self-ignition temperature of the fuel mixture, provided that temperature during the combustion process remains less than the auto-ignition temperature. The basic purpose of MILD combustion is to reduce the combustion temperatures below the threshold at which formation of different pollutants starts. This mode of combustion is, sometimes, also termed as flameless combustion (FLOX) [85].

Saha et al. [86] presented a study about the MILD combustion of pulverized coal. They reported that MILD combustion is recognized as a modern and efficient combustion technology. This technology has significantly improved the thermal efficiencies and reduced the combustion based emissions. The combustion occurs at lower temperatures and formation of pollutants, i.e. NO_x , is minimized under such a low temperature combustion environment. As no apparent flame is produced in the combustion process, this technique is also termed as flameless oxidation. They investigated two types of coal under MILD conditions in a self-recuperative furnace. From numerical and experimental results they concluded that a NO reburning process is involved in MILD combustion which significantly reduces the emission of NO. In general, numerous studies are available on MILD combustion for gaseous fuels. However, just a few data is available for solid fuels under such new technologies. Furthermore, more elaborate models should be presented for the complex mechanisms involved.

Weber et al. [87] investigated the combustion of different fluid and solid fuels under MILD conditions. They conducted experiments in a 0.58 MW furnace with preheating the combustion air to a temperature of 1300°C . They concluded that although air was supplied in excess of 10%, the combustion happened under sub-stoichiometric conditions. In their findings, light oil and gaseous fuel showed a similar combustion behavior, while heavy oil and coal showed similar combustion patterns. Moreover, significant reduction in NO_x emission was obtained for a highly volatile fuel with nitrogen content of 1.49%.

Saha et al. [88] presented a study for pulverized coal with different particle sizes. They reported various benefits of the MILD combustion technology, i.e. high thermal efficiencies, lower emission levels, stability of combustion and its wide application range. They conducted experiments with a vertical MILD combustion furnace with total heat capacity of 60 kW. Air and natural gas were supplied through swirl burner for a premixed combustion and pulverized fuel was injected using a 19 mm central jet into the furnace. The measurements were recorded at several locations along the central line ($x = 0$) described as the ratio of vertical distance from the fuel jet exit and diameter of fuel jet, i.e. Y/D_j (Fig. 3.9). Their results showed MILD combustion conditions prevailed irrespectively of the particle size, as no visible flame was observed. Higher combustion temperature was resulted in case of smaller particles; especially in the close vicinity of fuel exit.

Saha et al. [88] also concluded that devolatilization of large particles takes place downstream in the furnace, which implies that larger particles require longer residence time for complete combustion. However, the results also showed that the flow pattern of combustion gases in the combustion furnace is more influenced by the injection velocities than by the size of fuel particles.

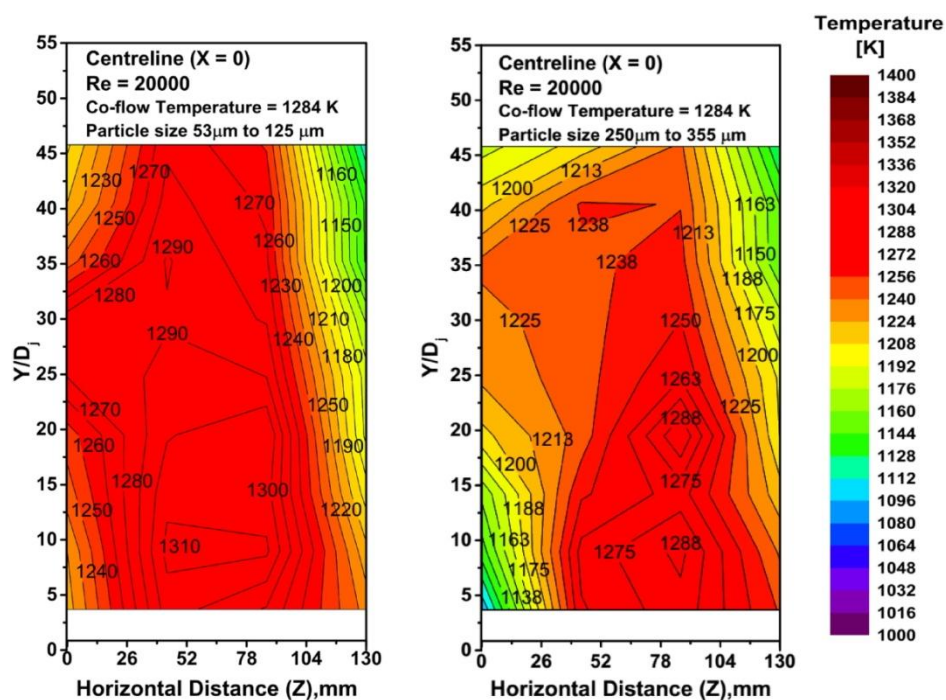


Fig. 3.9: Temperature distribution in MILD combustion furnace [88] (with permission from Elsevier)

Weidmann et al. [89] presented a comprehensive study about MILD combustion of pulverized coal in a pilot-scale combustion facility. They reported that FLOX (flameless oxidation) has been found to be an appropriate technique for the reduction of pollutants particularly generated from thermal conversion of nitrogen. Preheating of reactants and controlled supply of oxygen are the key factors in MILD combustion. However, implementation of higher levels

of preheating is, sometimes, difficult in case of solid fuels. It is also noted that MILD combustion conditions can be obtained even with moderate reactant temperatures. This can be achieved by recirculation of flue gases with the fuel particles. In this context, preheating of the fuel and air is not always necessary, and diluted regimes of MILD combustion are obtained. Such patterns can be obtained by supplying the incoming air stream with high velocity. Experimental investigations were conducted with a 500 kW cylindrical combustion furnace (Fig. 3.10).

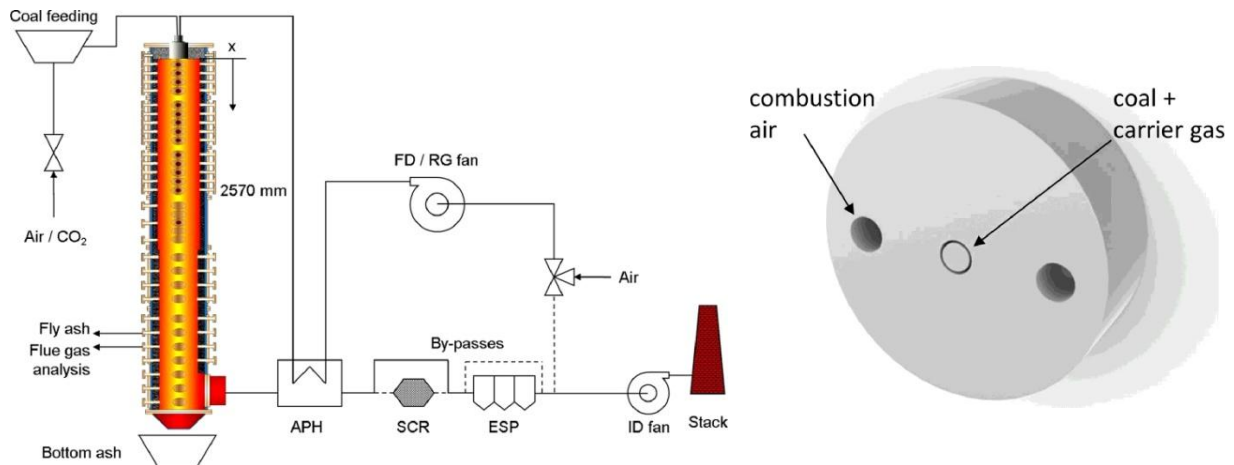


Fig. 3.10: FLOX combustion furnace and burner design [89] (with permission from Elsevier)

Pulverized fuel was conveyed through the central pipe (nozzle) of the FLOX burner while combustion air was supplied via two eccentrically mounted nozzles. Stream velocities were very high, however not greater than 100 m s^{-1} . Weidmann et al. [89] stated that pre-heating the air entering to the combustion furnace to a temperature of 300°C is considered as the state of the art in common boilers. In their study however, they used a preheating of air not greater than 150°C . Furthermore, two FLOX conditions were studied, i.e. $\text{FLOX}_{\text{CO}_2}$ and FLOX_{air} . In the first case, 79% by volume CO_2 + 21% by volume air was used as carrier stream while in the second case air was used to convey the fuel. The two cases were compared in regard of standard flame conditions generated by low NO_x burner.

The measurements were recorded at several locations, starting 80 mm from the burner exit to a distance of 2500 mm vertically in the furnace. The structure and intensity of reaction zones were measured through chemiluminescence imaging technique. The local (flame) velocity was measured using laser Doppler velocimetry and combustion gas temperature was recorded with the help of a suction pyrometer (with shielded thermocouple). Figure 3.11 shows the photographs of three flame conditions at 80 mm from the burner exit. Weidmann et al. [89] concluded that use of carbon dioxide (CO_2) as a carrier gas delayed the combustion process showing a visible stream of (fuel) particles. On the other hand, an irregular flame zone was observed in case of FLOX_{air} unlike to the reference case (FLAME) in which a stable flame is obtained. Hence, flameless conditions were confirmed in both cases $\text{FLOX}_{\text{CO}_2}$ and FLOX_{air} . The actual reaction zone was found to be in the diluted mixing regime away from the burner.

The comparison of temperature distribution in the furnace showed that FLOX_{air} has higher local temperatures than $\text{FLOX}_{\text{CO}_2}$. Hence, NO production was also found to be larger in FLOX_{air} . Furthermore, they also emphasized to validate the numerical results with the reported experimental flameless combustion conditions [89].

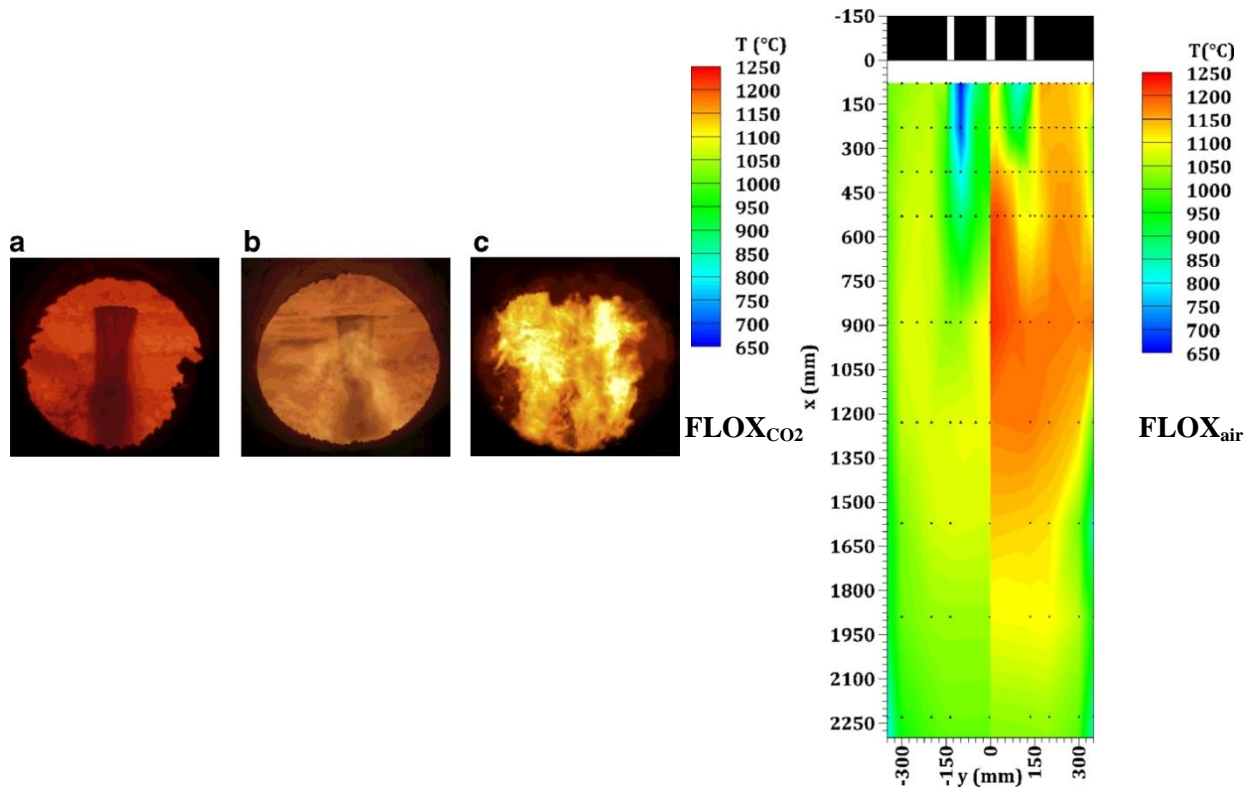


Fig. 3.11: Flame conditions at burner exit $\text{FLOX}_{\text{CO}_2}$ (a), FLOX_{air} (b) and FLAME (c) and temperature profiles of $\text{FLOX}_{\text{CO}_2}$ and FLOX_{air} in the furnace [89] (with permission from Elsevier)

3.3.4 Melting phenomena of solid particles during PFC

In PFC, solid fuel is injected into the combustion furnace in the form of small particles; therefore, the physical properties of solid particles also play an important role in the combustion process. Melting of solid particles is one of the important physical phenomena which significantly influence the operation of PFC systems. At high temperatures, solid particles melt to form a molten and sticky matter, which creates difficulties in different plant operations. Such difficulties are related to agglomeration and deposition processes. Agglomeration is the combination of two or more solid particles, through thermal treatment, to form larger particulate matter. Agglomeration is desired in many industrial applications, such as pellet formation of pharmaceuticals. However, it is highly undesirable in various other plant operations, e.g. gasification, combustion, drying, fluidization (in FBC) and heat exchange. Formation of sticky matter creates severe problems in the reactor, especially depositions at the reactor walls. As agglomeration occurs due to the melting of constituents present in the fuel, type and composition of the fuel play a vital role in this phenomenon.

However, operating conditions, e.g. air velocity, reaction mechanism, particle size and operating temperature, are also important in this context. Numerous studies have been conducted in order to describe this phenomenon; however, most of the studies are focused on agglomerate formation in reactor (fluidized) beds [90].

Similarly, in pulverized fuel combustion (PFC) melting and deposition of fuel particles on the walls of the furnace is a major issue. In most of the cases, these problems are related to melting of ash content of the fuel. Ash is produced as a result of combustion of solid particles (Section 3.2.5). Ash is retained at the bottom of the furnace (bottom ash) or in the flue gases (fly ash) after the combustion process. However, some of the ash may undergo physical deformation, e.g. agglomeration, due to high temperatures in the combustion furnace. Various operational problems occur due to melting and agglomeration of ash particles in the combustion system. For example, fouling and slagging are caused by the deposition of molten or semi-molten ash particles at the heat transfer surfaces. These depositions hinder the heat transfer and, hence, result in lower thermal efficiencies of the combustion systems. High quantities of specific constituents of solid fuels, i.e. Na, K, S, Si and Cl, are main factors involved in such mechanisms (Fig. 3.12 reported by Niu et al. [91]). The analysis of ash produced after the combustion of solid materials helps to understand and mitigate such formation of molten material in the furnace [92].

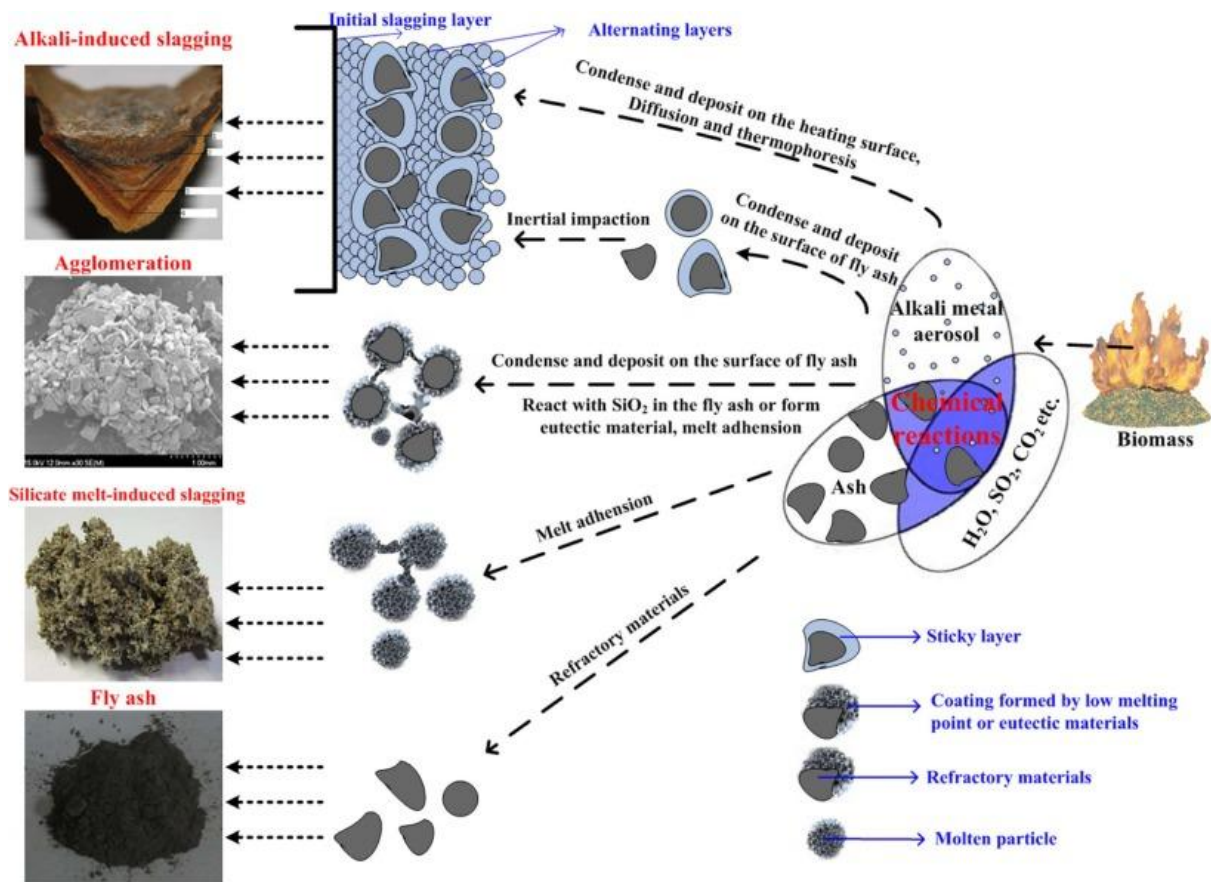


Fig. 3.12: Behavior of ash melting and deposition [91] (with permission from Elsevier)

It is also reported elsewhere [93] that the behavior of fuel ash at high temperature is one of the important factors to be addressed in combustion processes. Different operational problems occur due to fusion, sintering and agglomeration of the melted material, such as slagging, fouling and corrosion (at high temperatures). Fouling is the deposition of fused layer at the heat transfer surface while slagging occurs due to ash deposition on furnace walls. As a result degradation of the furnace material may occur (termed as corrosion). However, corrosion may also be caused by gaseous species reactions. Besides decreasing the overall efficiency, these problems also cause operational costs and reduce the lifetime of the combustion system. Different strategies are adopted in order to eradicate such problems. For example, in the grate firing method, water cooled grates and reduced preheating temperatures are used to minimize the melting of ash, while in fluidized beds, different additives (lime, kaolin, alumina, dolomite etc.) are used to alter the composition of ash and, ultimately, to reduce the agglomeration and slagging processes. Co-firing of different fuel blends also presents a suitable solution for the prevention of ash fusion [93].

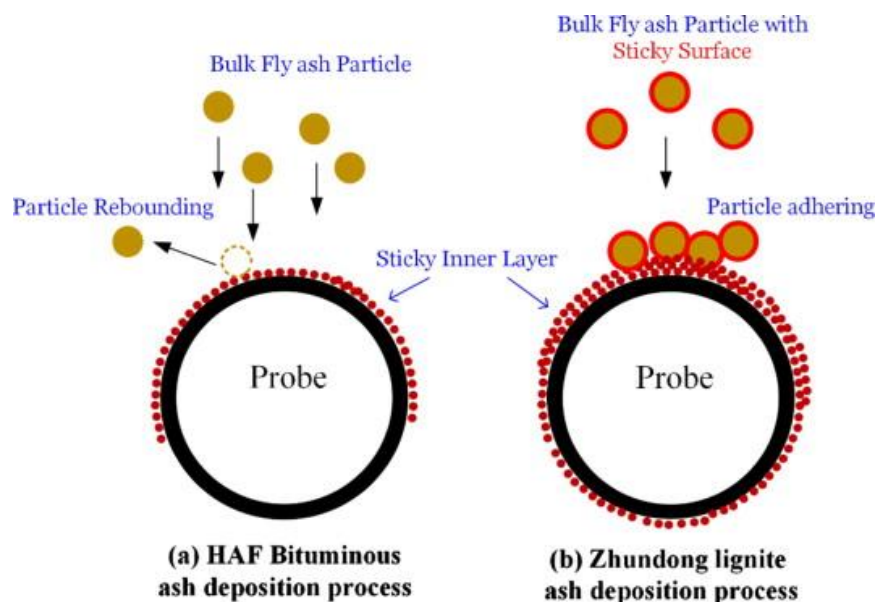


Fig. 3.13: Deposition phenomena of sticky layer [94] (with permission from Elsevier)

Li et al. [94] presented a study about the fine particulate deposition in pulverized coal combustion in a down-fired furnace. They investigated the slagging and deposition phenomena of lignite with higher content of sodium and alkaline earth metals and bituminous (high ash fusion) coal. They reported that alkaline earth metals are present in larger quantities in coal (lignite) in water soluble form. During the combustion of fine fuel particles, this matter evaporates and forms small sticky particles leading to slagging in the furnace walls. The melting and slagging behavior of the two samples was analyzed near the burner and comparison between the two fuels revealed that the slag formed in case of lignite coal is completely molten while with bituminous coal slag in the form of solid layer is rather obtained, which is easy to remove. This due to the fact that lignite contains constituents with

lower melting points than bituminous coal, i.e. approximately 900°C. Moreover, the slag layer is formed due to two factors, i.e. formation of sticky layer on the wall and coating of bulky particles with the sticky layer (Fig. 3.13). Furthermore, it is suggested in [94] that pretreatment of the fuel and addition of alumina and kaolin can reduce the formation of sticky layers in the furnace.

Naganuma et al. [95] presented a study about the mitigation of particle (ash) deposition in solid fuel boiler. They reported that particle deposition is formed due to adhesion on the inner surface of the boiler at high temperatures and causes major operational problems. They presented a surface treatment method, i.e. thermal spraying method, in order to reduce the adhesion between metal and melting material. The concluded from experimental investigations that the adhesion phenomena and surface reaction between metal and ash particles can be prevented by using Ni alloy coating, sprayed on the walls of the boiler with the help of arc-plasma. It was proven by the comparison (Fig. 3.14) that areas with thermal spray coating resulted in no surface deposition of the molten particles. According to [95], this technique is applicable for different types of fuels and the coating does not appreciably hinder the heat transfer mechanism in the boilers.

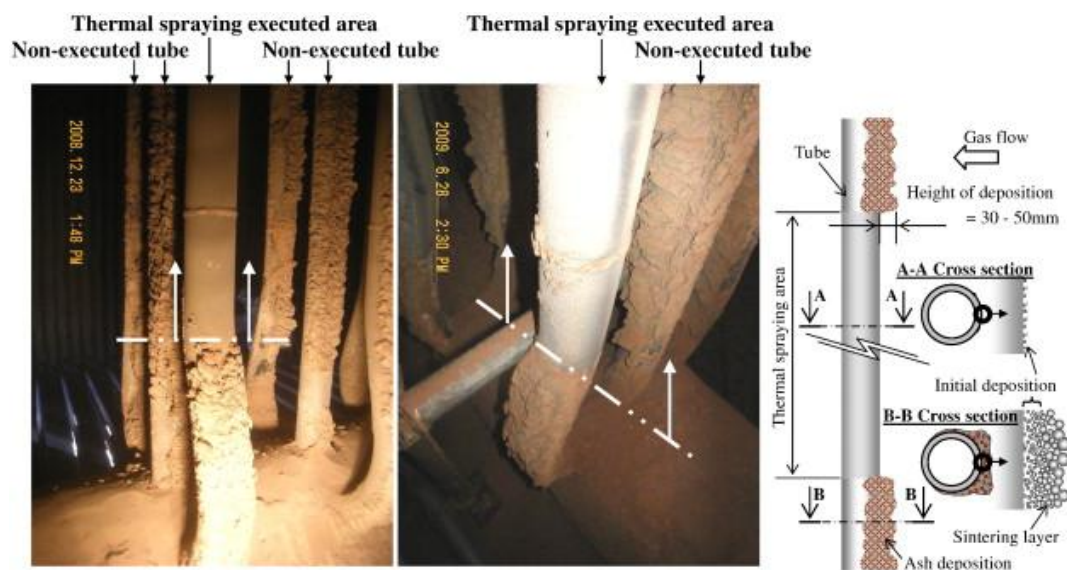


Fig. 3.14: Effect of thermal spraying on particle deposition [95] (with permission from Elsevier)

Bartels et al. [96] presented a comprehensive overview about the formation, identification and mitigation of agglomeration. The mechanism of agglomeration is very complex, depending upon the aerodynamics, particle-particle interactions and chemical reactions. However, reactant type and composition has a key role in agglomerate formation. For example, in case of fluidized beds, inorganic fraction of the solid fuel (i.e. alkali) reacts with silica present in sand to form silicates with considerably low melting point as compared to the parent components. This results in a sticky layer on the reactor bed. Formation of ash during combustion or gasification of solid fuel is the basic step in the formation of agglomerates and is highly dependent on the quantities of constituents present in the fuel. For example, solid

materials having larger proportions of sodium (Na) and potassium (K) result in ash with considerably lower melting point. The sticky (ash) material serves as glue in the combination of solid particles, i.e. agglomeration. Similarly, during char burning, the temperature of the fuel particles increases and inorganic constituents with low melting point escape from the interior of char particles in form of molten sticky matter that helps to form the agglomerates upon collisions.

Furthermore, Bartels et al. [96] also reported that different strategies are applied for the mitigation or prevention of agglomeration. As high temperature is the key factor for the melting of fuel particles, lowering the operating temperature (by altering air and fuel ratios) is one of the basic measures to avoid agglomeration. Other strategies include increasing inlet gas velocity, controlling the fuel loading, pulsation, pre-treatment of fuel, blending of fuel materials, introduction of additives and improving the design of reactors. However, there is still space for further development of new technologies for the mitigation of agglomerate formation [96].

Another study about the agglomeration of solid materials was reported by Arena and Mastellone [97]. They studied the pyrolysis of plastic wastes (polyethylene (PE) and polyethylene terephthalate (PET)) in a fluidized bed. They reported that adhesive properties and contact area are the major factors affecting agglomeration. Related processes are complicated when plastic waste is used in energy recovery systems. The material analysis of both types of plastic waste has shown that devolatilization is faster in case of PE than for PET. The faster devolatilization results in the reduction of polymer viscosity. Hence, sticky material required for aggregation is also reduced. Similarly, another study was presented by Mastellone and Arena [98] about a mixture of plastic wastes (polyethylene (PE), polypropylene (PP) and polyethylene terephthalate (PET)) having low softening and melting temperature. In both of the studies, de-fluidization was addressed during the pyrolysis process, i.e. for thermal conversion at relatively lower temperatures in fluidized beds.

Recently, Pedersen et al. [99] presented a study about deposition and agglomeration during the combustion of solid recovered fuels (SRF). They conducted batch-wise experiments in a small scale rotary drum kiln (Fig.3.15 a) using different solid fuels, i.e. SRF and different types of plastics (PE, PP and PET). They reported that SRF consists of heterogeneous solid materials including paper, glass, wood and different types of plastics. However, the share of plastics is relatively large in the composition of solid recovered fuels. Having a very high volatile matter content, plastics (PE and PP) possess a very high calorific value which increases the overall quality of SRF. However, different problems e.g., agglomeration, wall deposition, are faced due to the presence of these materials.

Pedersen et al. [99] pointed out that plastic (PE) granules have a very low melting point; hence, it was difficult to feed them to the kiln, although experiments were conducted batch-wise with a very small quantity (i.e. 0.5 g). PE granules melted and deposited on the surface of the feed hopper at a temperature of approximately 100-200°C (Fig. 3.15 b). Due to this

issue, they used PE beads/large pellets for the further investigations. Two types of deposit formed in the combustion process of SRF, i.e. deposit at low temperature due to melting of polymers and plastics present in the fuel and deposits formed at high temperature due to melting of ash constituents. Moreover, the comparison of different kinds of plastic materials revealed that PET resulted in char residue containing carbon while PP and PE were fully devolatilized. Presence of glass (in case of PET) increased the fusion and sticking of residue at high temperature (approximately 800°C). Addition of cement raw meal (including SiO₂, CaCO₃ and Al₂O₃) in the drum contributed to reduced deposit formation by absorbing the melted material (polymer). Furthermore, the necessity to design the equipment for feeding of such materials (plastics etc.) is stressed [99].

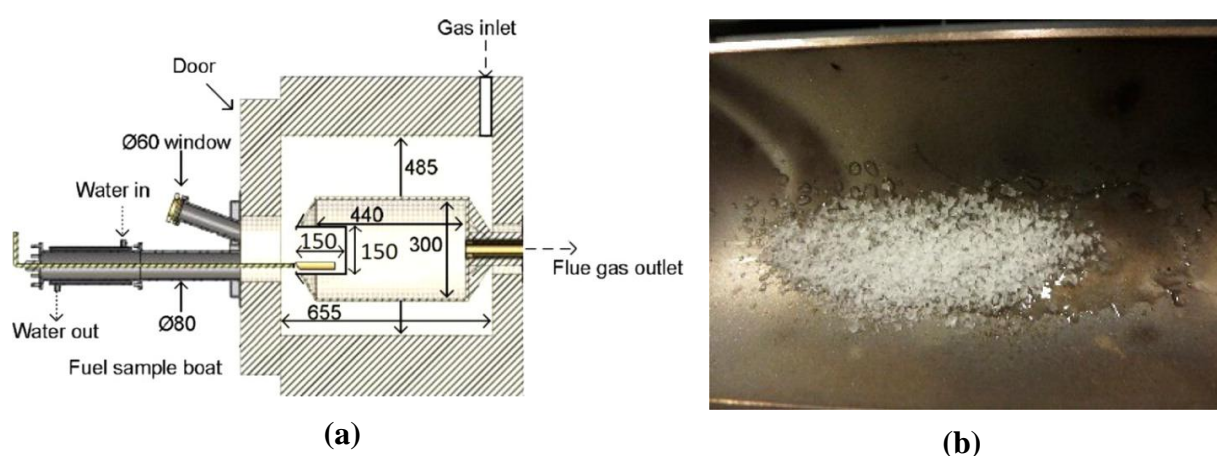


Fig. 3.15: Rotary drum furnace (a) and melting of plastics, here PE (b) [99] (with permission from American Chemical Society (ACS) Publications)

Further studies were presented by Venturini et al. [100], Akiyama et al. [101], Liu et al. [102] and Zhou et al. [103]. However, most of the studies focused on the behavior of ash melting and fusion during the combustion process. There is a lack of available data about the transportation of pulverized material to the combustion chamber (in PFC). As pointed out by Pedersen et al. [99] there is a dire need to introduce modern combustion technologies, especially fuel transport systems, for the combustion of materials which immediately melt when exposed to high temperature. Moreover, combustion phenomena of such materials also vary from other solid fuels, which should be addressed. Therefore, there is still need to investigate the combustion process in PFC systems for solid fuels with low melting point.

3.3.5 Computational fluid dynamics (CFD) modeling of PFC

Combustion research is an integrated and multidisciplinary field of science which consists of various physical, chemical and thermodynamic aspects. A superior combustion system must be enabled to provide high combustion efficiency, maximum energy recovery, low (pollutant) emission level and better reliability. In order to fulfill these criteria, a combustion system undergoes different steps of designing and optimization. It is important to study the physical

and chemical processes involved in the combustion process to ensure the optimum design of a combustion plant (Fig. 3.16).

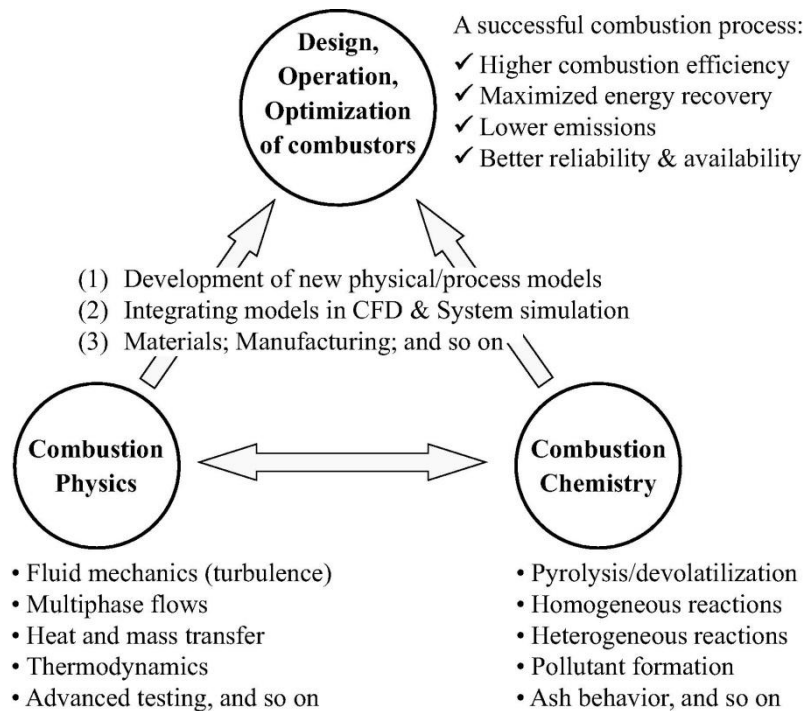


Fig. 3.16: Steps involved in designing the combustion system [67] (with permission from Elsevier)

Computational fluid dynamics (CFD) modeling is an important tool used to describe different combustion processes. CFD has been proven to be a very appropriate tool for the design, simulation and optimization of various fluid flow systems even without building any experimental/physical setup. CFD modeling of the combustion process is, in general, composed of different sub-models which describe different parts of the combustion process, i.e. particle motion, turbulence and aerodynamics, drying and pyrolysis, chemical reactions, char combustion, and heat transfer (Fig. 3.17). Computational fluid dynamics modeling of combustion has also been found to be a cost-effective method for the optimization of different operational parameters. Simulations of the combustion operation can be repeated so many times as necessary until optimized operational conditions have been achieved at relatively low costs compared to experiments. However, it is necessary to use appropriate modeling technique in order to ensure the validity of the predicted results obtained from the CFD approach [67][104,105].

A number of sub-models have been developed in order to be incorporated in the CFD modeling of solid fuel combustion; however, most of these models have been originally developed for pulverized coal. There is a need to analyze and implement these models on different types of solid fuel (solid waste materials) for better exploitation of new technologies.

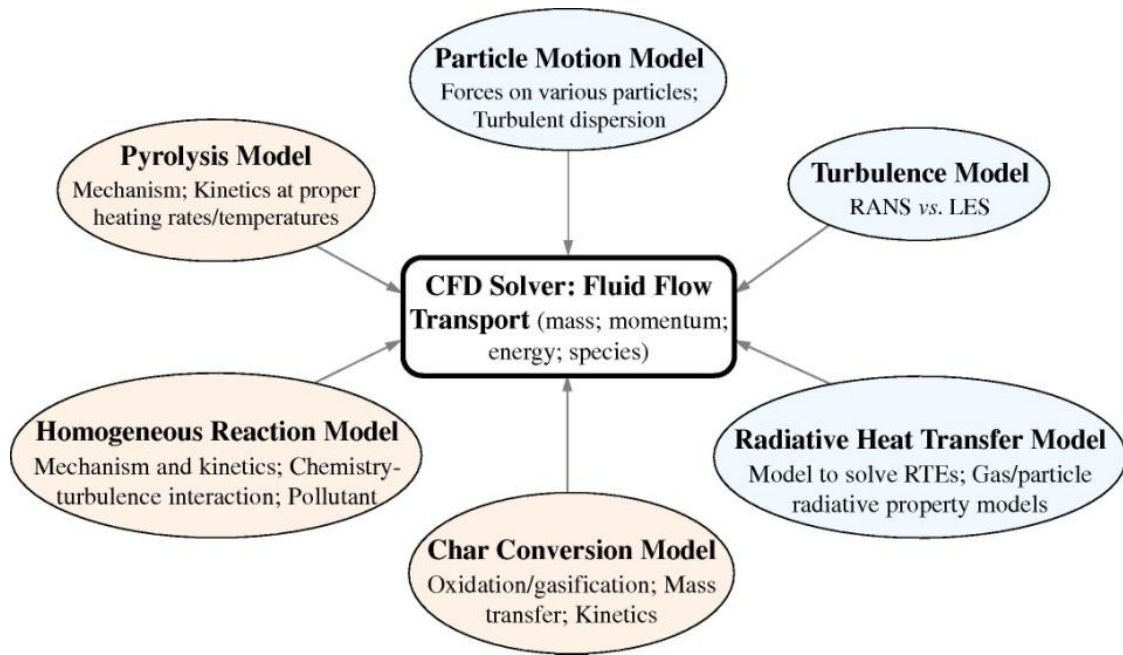


Fig. 3.17: CFD modeling of combustion process [67] (with permission from Elsevier)

Some CFD studies of the combustion of pulverized fuels have been reported. For example Stroh et al. [106] presented a numerical simulation approach for co-fired pulverized fuel combustion chamber. They pointed out the potential of CFD modeling to provide insight of co-firing combustion processes and support up-scaling of combustion setups to industrial units. They simulated three different cases of solid fuel input, i.e. pure coal, co-firing with 9% biomass and co-firing with 17% biomass. They conducted CFD simulations on ANSYS with different sub-models, i.e. k-omega for modeling the turbulence phenomena, eddy dissipation model for gas phase reactions and discrete ordinates for the modeling of heat transfer by radiation. The simulation results showed the maximum temperature to be at 1500°C near the burner for the case of coal. Temperature decreases significantly at positions far away from the burner. In case of biomass co-firing, the maximum temperature was noted to be at 1300°C (Fig. 3.18). This is due to the difference in heating value of the biomass fuel to the coal. Moreover, it was concluded that the maximum temperature is reduced by increasing the quantity of biomass in the co-fire stream. Good agreement between numerical and experimental results was found.

Silaen and Wang [107] presented a CFD modeling study in order to check the effect of different turbulence and devolatilization models in an entrained flow coal gasifier. Eulerian-Lagrangian approach was applied in the numerical simulations with a computational domain of 969 k cells. The comparison between different models revealed that the constant rate model results in the fastest devolatilization, while the Kobayashi model gives lower devolatilization rates. Moreover, they also found that 3-D results provide better insight than the 2-D simulation cases.

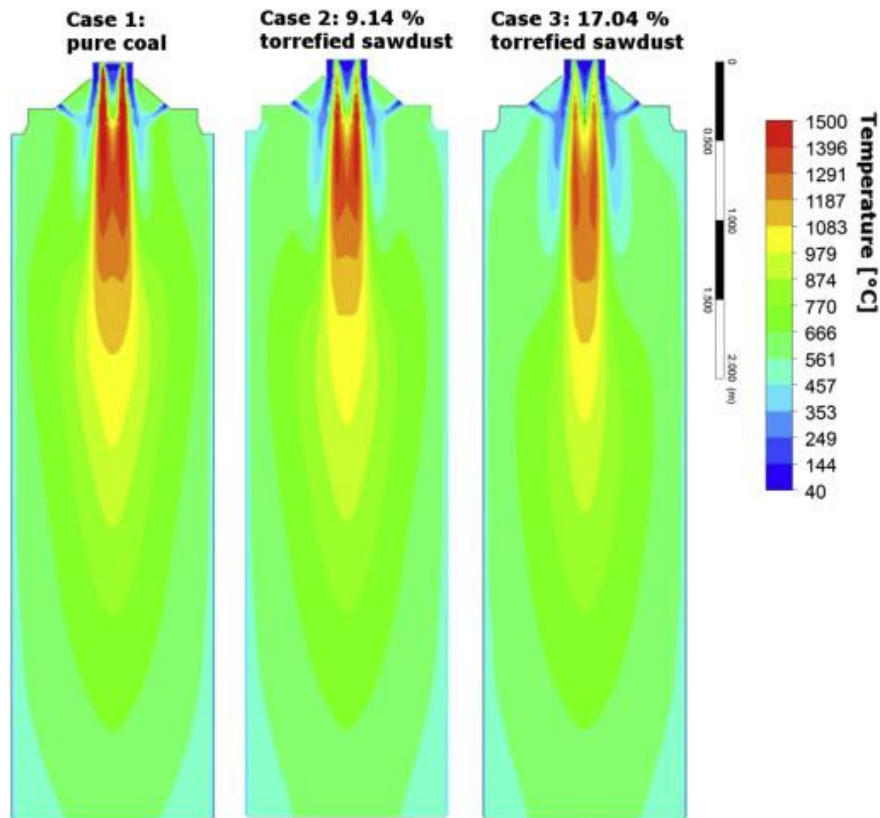


Fig. 3.18: Temperature distributions with different fuel ratios [106] (with permission from Elsevier)

Jeldres et al. [108] reported a modeling technique for the co-firing of biomass and coal. They stated that CFD simulations applied to study the different combustion behavior of coal and biomass at small scale need to be also applied on larger scale. Thus, they conducted a CFD modeling study for a 150 MW boiler with co-firing of coal and sawdust. Discrete phase modeling approach was presented along with different sub-models, i.e. discrete ordinates (DO), k-epsilon, two-competing rates model and eddy dissipation model (EDM). It was reported that EDM provides a promising solution for the prediction of combustion processes at industrial scale. The biomass share in the coal fuel supply was found to increase the temperature due to early burning of the biomass particles. Yin [109] presented a CFD modeling approach in order to check the effect of particle vaporization and radiation during pulverized fuel combustion. He used two-competing rates model for devolatilization and discrete ordinates (DO) for modeling the radiation effect. He concluded that gas radiation is overlapped by the particle radiation in the pulverized fuel combustion process, hence, it is important to account for particle radiation precisely. More studies should be carried out for the investigation of radiation phenomena.

Kumar and Sahu [110] reported a study about different operating positions of the burner in a 210 MW coal fired combustion furnace (boiler). They investigated furnace performance with four different positions (tilt angles) and concluded that combustion characteristics (i.e.

residence time and temperature profile) are significantly influenced by changing the burner position (tilt) from +15° to -15°.

Numerous other modeling approaches also have been reported for the evaluation of combustion characteristics. For example, Schaffel et al. [111] presented a CFD model for MILD combustion; Gubba et al. [112] studied numerically the co-firing of coal and straw, whereas investigations on oxy-MILD combustion were reported by Perrone and Amelio [113]. Ghalleti et al. [114] presented a modeling approach for MILD combustion using CFX code, and Paulrud and Nilsson [115] presented a study about the effect of particle size during the combustion of wood. However, majority of the studies are focused on the combustion of either coal or co-firing of coal with biomass. There is a need to apply the advanced and improved modeling techniques proposed by various researches to the combustion of other types of solid material, i.e. solid waste, by-products etc.

3.4 Outcomes and further challenges in PFC

Based on recent literature, it is evident that pulverized fuel combustion (PFC) has gone through different technical development phases during the past few years. This modern technology enables the efficient combustion of solid materials and is becoming popular in many industrial applications. However, most of the studies conducted so far were focused on the combustion of either coal or a combination of coal with biomass materials. Other solid materials, such as municipal solid waste, domestic wastes and industrial by-products and residues, should also be investigated to foster their better exploitation by the latest combustion technology. Large advantages can be expected when energy (heat) requirements of the industry can be met by the combustion of its own by-products.

The majority of previous work focused on the combustion behavior, burning characteristics and resulting by-products of the combustion process. However, transportation and injection of solid fuel into the combustion chamber is the basic as well as the most important step in the pulverized fuel combustion (PFC) process which should be further elaborated. Several challenges are faced during the transportation of fuel particles to the combustion chamber, especially when the material has a low melting point. Problems are faced while conveying the solid (fuel) particles into the PFC furnace. Exposed to a very hot combustion zone, the solid particles (with low melting point) are melted in the fuel nozzle and converted into a molten and sticky matter. This matter starts accumulating on the walls of nozzle/burner and causes blocking of the nozzle, which means interruption of the entire combustion process. There are studies on thermal conversion, recycling of polymers and pyrolysis of plastics. However, research on the transportation and combustion of solid materials with low melting point (in PFC furnaces) is still missing. In this regard, there is a need to develop new burners and fuel nozzle designs which are capable of transporting such materials without pre-melting.

Computational fluid dynamics (CFD) modeling has been proven to an appropriate tool for the solution of different combustion problems. However, CFD modeling still needs to be applied to analyze the behavior of alternative solid fuels with low melting point during PFC.

In order to address the problem stated, the present work highlights the behavior of PFC combustion of solid materials with low melting point. Special focus is set on the design of the fuel nozzle for transportation of such solid materials. The study is conducted by means of computational fluid dynamics (CFD) modeling approaches. Optimization of different operating conditions is also presented for better adoption of the proposed fuel nozzle design.

CFD Modeling of PFC for Solid Materials with Low Melting Points

This chapter is an extended version of parts of a manuscript entitled “Study on nozzle design for combustion of solid materials with low melting points” published in Applied Thermal Engineering [116]. In the current chapter, application of computational fluid dynamics (CFD) modeling to the combustion process of pulverized fuel materials with low melting point is presented. Different sub-models and their applications in PFC are discussed. A combustion system, i.e. furnace geometry and its components for the combustion of solid materials with low melting points, is presented. A base case is investigated with the stated operating conditions and geometry. As an outcome, the parameters affecting the combustion process are obtained for further work.

4.1 Introduction

As described in the previous Chapter 3, pulverized fuel combustion (PFC) has been accepted as an efficient technology for the combustion of solid fuels. However, several challenges are faced during combustion of different solid materials. Transportation of solid particles with low melting point is one of the major issues during PFC. Many operational problems occur during the transportation of such material to the combustion chamber. The temperature of furnace and nozzle walls increases by the heat transfer (radiation) from the combustion zone. When solid particles are fed into the combustion chamber, they come across with high temperature either from the nozzle wall or from the combustion (flame) zone. Hence, the solid particles start melting once temperature reaches to the melting point of the solid material. A sticky and molten material is produced as a result of melting and agglomeration of solid particles. This may cause clogging of the fuel nozzle and cease the operation of the combustion system. Hence, an appropriate system is required for the combustion of such material.

In order to address this problem, a comprehensive study is conducted of the combustion of pulverized waste materials with special focus on solid materials with low melting point (as respective data was lacking in the literature). Investigations are carried out using multiphase CFD simulations with the overall objective of evaluation and optimization of nozzle designs for the transportation of solid materials with low melting point.

4.2 A case study of paint residue

As described in the previous chapters, different solid materials consist of different constituents with low melting point. Solid (waste) materials containing plastics have very low melting point and are difficult to burn in conventional combustion systems. However, plastics are further classified into different groups depending upon the type of polymer used in the manufacturing processes and, thus, have different melting points. For example, polyethylene

(PE) has a melting point of 137°C while softening of the solid material starts at a temperature of 100°C. Polypropylene (PP) and polyethylene terephthalate (PET) have melting temperatures of 183°C and 265°C, respectively, and softening temperatures of 165°C and 260°C, respectively [98]. In another study [99], the melting temperature of polyethylene (PE) was reported as low as 90°C. Solid paint residue generated from spray coating of metals in, e.g., the automobile and furniture industry also contains constituents with low melting point, i.e. around 60°C, and is a compound mixture with very complex compositions.

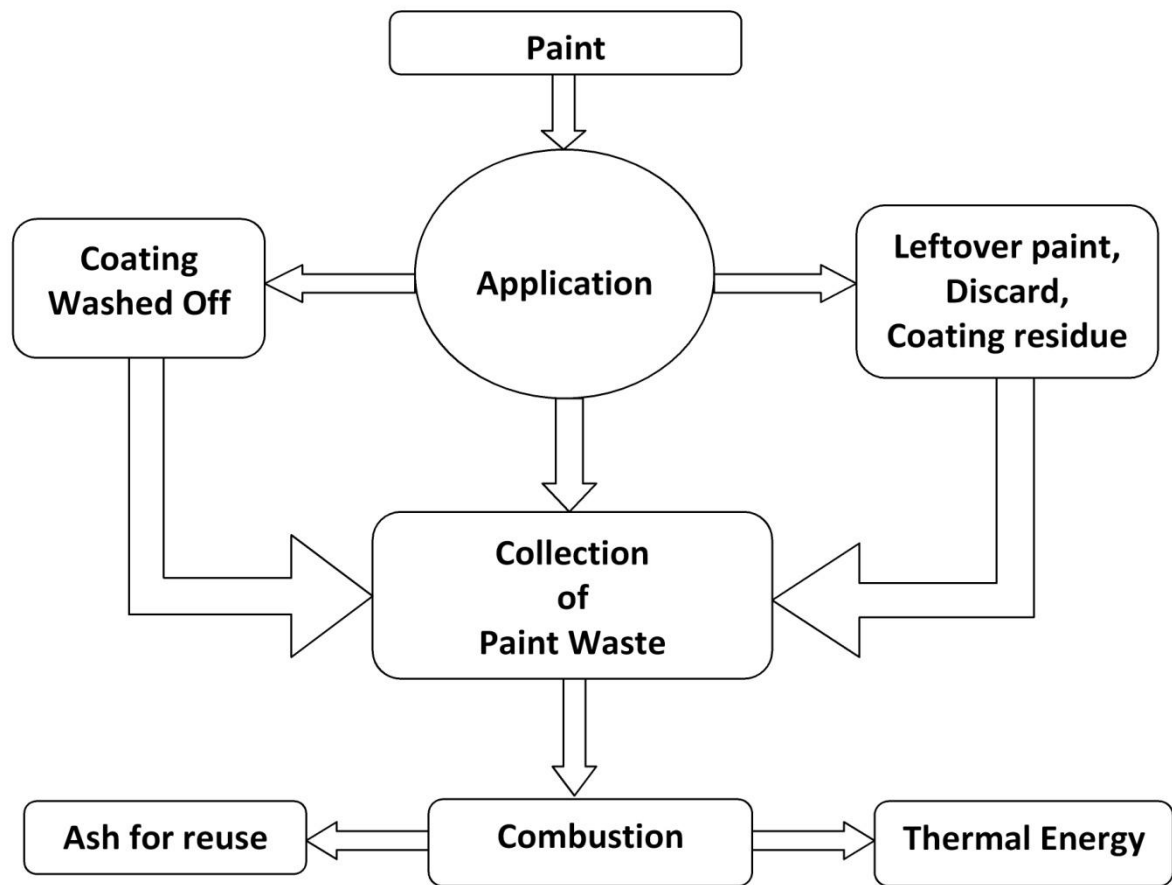


Fig. 4.1: Proposed management of paint residue

Ecotoxicological tests showed that, as paint waste contains hazardous components, landfill is not an appropriate method for the disposal of paint waste produced by spray application in industry [7]. On the other hand, paints are handled in very diverse ways during their life cycle. The paint applied on different spots of buildings can be disposed with the brickwork in the landfills. Paint coating can also be washed off using sandblasting when the facade is renovated. The paint coating is added to the environment directly or indirectly by moving in the wastewater. This is considered to be hazardous due to the presence of toxic metals and organic solvents [117]. An appropriate and suitable system is required in order to manage this

kind of waste. Figure 4.1 shows the proposed management which is based on the combustion of solid paint residues.

The comparison of paint with other solid waste materials shows that it has the lowest melting point (less than 60°C). On the other hand, paint residue is formed due to the solidification of sprayed (over-sprayed) paints. Hence, it consists of very fine particles. Figure 4.2 shows the typical particle size distribution of paint residue.

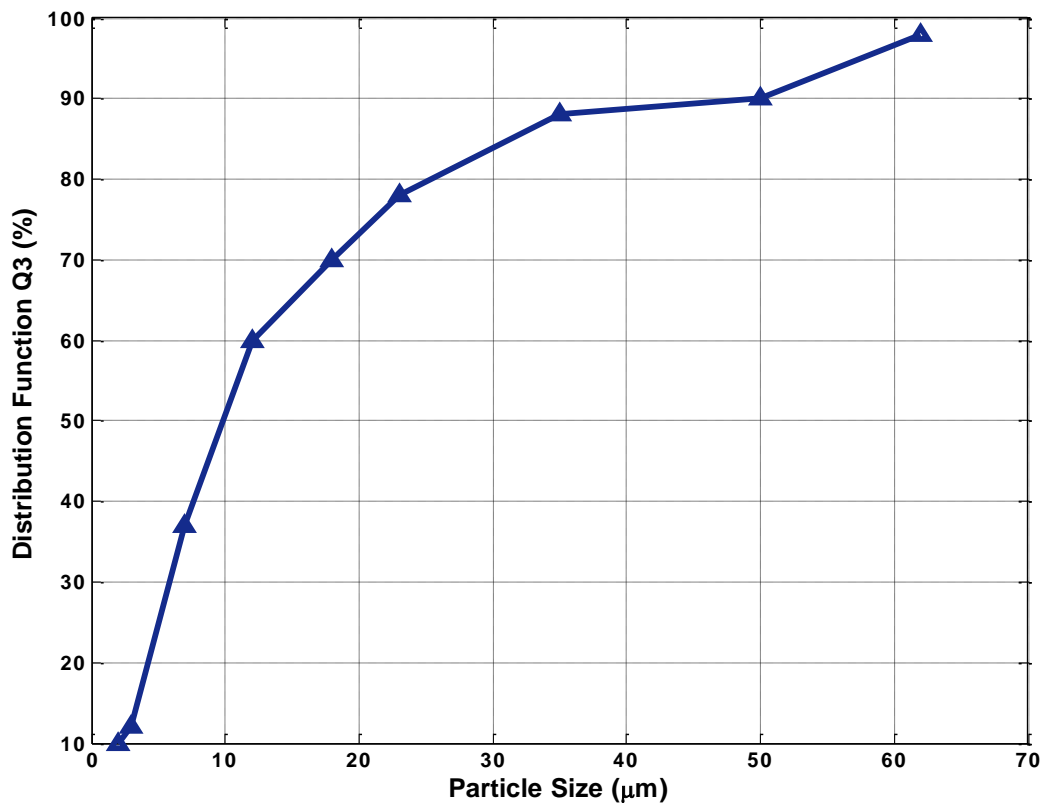


Fig. 4.2: Particle size distribution of paint residue (Fraunhofer IFF, Magdeburg [55])

It can be observed that about 50% particles have a particle size $\leq 10 \mu\text{m}$. A particle size of less than $50 \mu\text{m}$ was found in about 90% of the paint residue. This implies that paint residue consists of very fine particles, which eliminates the additional burden of mechanical processes, i.e. grinding, milling of solid fuel, required for PFC.

The material analysis of spray paint residue showed that it has a higher heating value of $18.336 \text{ MJ kg}^{-1}$. The proximate and elemental compositions are presented in Table 4.1. It is important to note that melting of solid paint particles is initiated when they are exposed to a temperature of 60-65°C and agglomerates are formed from 65°C to 150°C. A further increase in temperature causes droplet formation. Hence, at higher temperature, the particles are converted into sticky material which may clog the fuel nozzle. Therefore, the temperature must be kept below 60°C during the transportation in the feeding and spray system. Hence, an appropriate nozzle is required for the transportation of this material to the hot combustion chamber.

Table 4.1: Proximate and ultimate analysis of paint residue

Experimental Analysis	Mass Fraction
(a) Proximate analysis	
Volatiles	0.6998
Fixed carbon	0.0076
Water/moisture	0.0042
Ash	0.2884
(b) Ultimate analysis	
Carbon (C)	0.6244
Hydrogen (H)	0.0602
Oxygen (O)	0.2880
Nitrogen (N)	0.0049
Sulfur (S)	0.0225

4.3 Combustion plant for pulverized waste

A system for the combustion of pulverized materials was designed at Fraunhofer Institute for Factory Operation and Automation (IFF), Magdeburg, Germany. The system has a total thermal power capacity of 100 kW. Pulverized waste material is burnt and heat (energy) obtained is used for water heating purposes. The system has different parts, i.e. fuel container and feeder, combustion plant, heat exchanger, gas cooler, dust filter, residue collector and stack (Fig. 4.3).

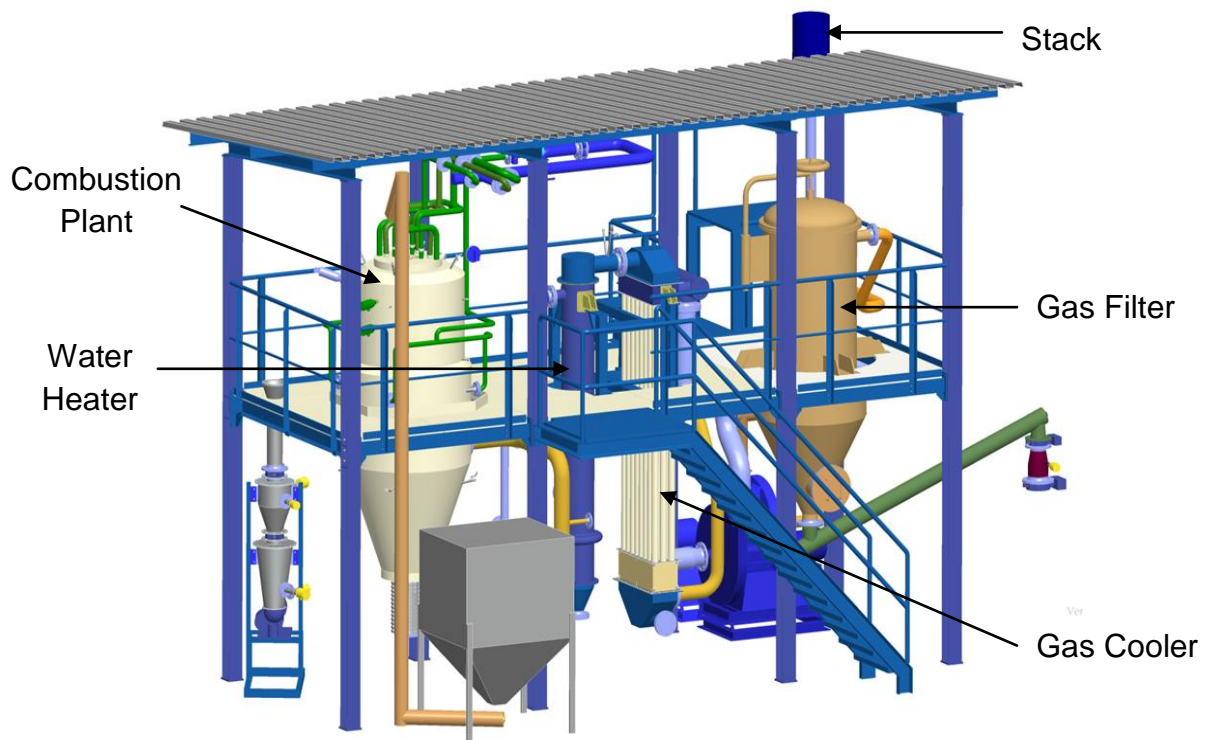


Fig. 4.3: Combustion facility for pulverized materials (Fraunhofer IFF, Magdeburg)

However, the PFC combustion plant, being the most important part of the combustion facility, is our main focus. Pulverized/powdered paint residue generated by the coating industry is used as the fuel. It should be noted that the residues generated by metal coating applications have a different compositions depending upon the origin of the paint material. The material discussed in this work is one of these paint residues (Table 4.1). However, the CFD modeling is developed as a unified approach which is applicable to different types of materials especially with low melting points. The pulverized paint (waste) considered in the present study are assumed to have particles with a mean diameter of 10 μm . Paint residues are formed by the solidification of droplets of paint (liquid) which are emitted by an atomizer/sprayer but do not meet the target (substrate to be painted) or rebound from it (over-spray). Hence, any paint residue particles are expected to have a small particle size (Fig. 4.2).

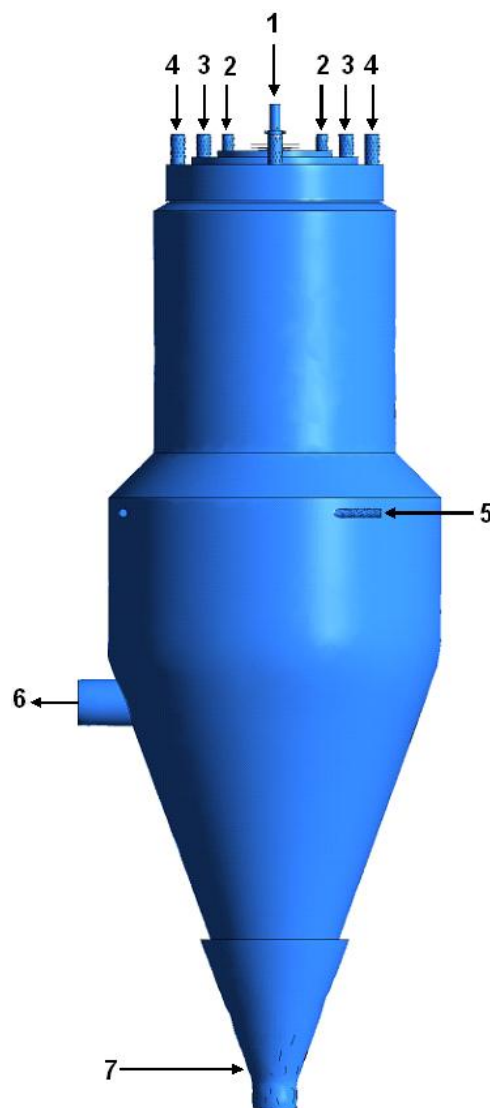


Fig. 4.4: Combustion plant for pulverized (waste) materials (1 = Fuel nozzle, 2 = Primary air inlet inner, 3 = Primary air inlet middle, 4 = Primary air inlet outer, 5 = Secondary air inlet, 6 = Flue gas outlet, 7 = Ash collector)

Figure 4.4 represents the pulverized fuel combustion plant for the combustion of pulverized materials. In the 3 m high vertical combustion furnace, fuel is injected into the pulverized fuel

combustion plant through a central nozzle (fuel nozzle). Fuel transport air (FTA) at a temperature of 25°C and a specified mass flow rate is used to convey the fuel particles. Primary air is supplied via primary air inlets mounted in the form of rings at the top of the combustion furnace (Fig. 4.5). Primary air inlets are categorized according to the ring to which they belong as inner, middle and outer. In this way, a better mixing environment is generated in the combustion chamber. Primary air is provided with a temperature of 300°C to start the combustion process.

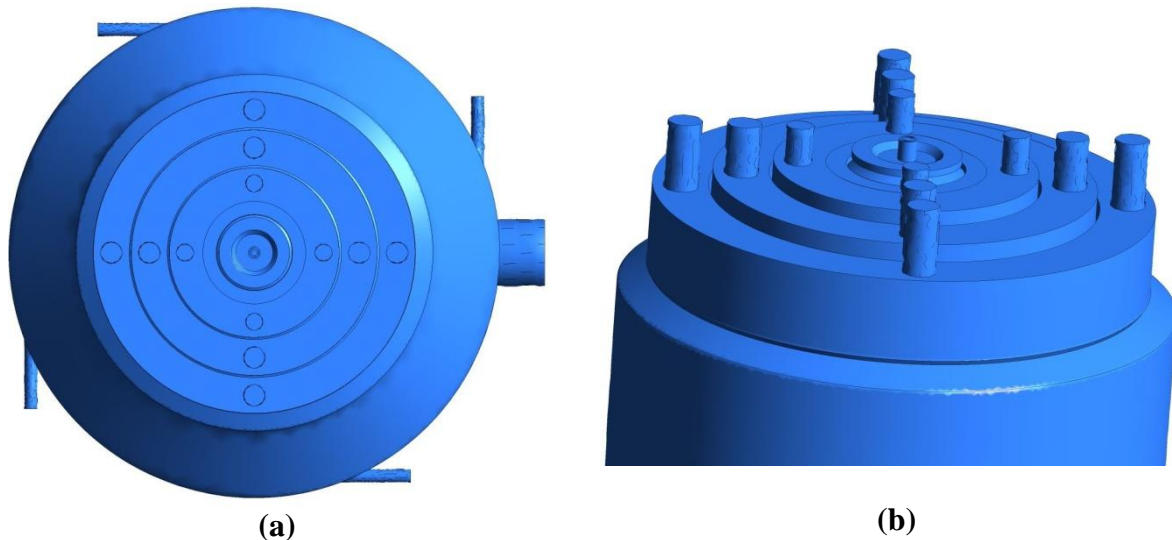


Fig. 4.5: Top view of the PFC furnace

To ensure complete combustion of the fuel, secondary air having a temperature of 300°C is provided from four tangential inlets placed in equal distances along the periphery of the combustion chamber. Too low temperature of primary and secondary air may cause incomplete combustion while too high temperature will increase the operational cost. After combustion of the fuel, flue gases are exhausted via the flue gas outlet. The residue which is left behind after the combustion is collected in the ash collector mounted at the bottom of the combustion chamber.

4.3.1 Fuel transport nozzle

The fuel nozzle is the most critical part of the combustion plant. Combustion and flame characteristics are significantly influenced by nozzle geometry and design. Nozzle designs and inlet parameters have a strong influence on the combustion process [118-120]. However, the existing designs are mainly suitable for the transportation of pulverized coal. In order to introduce latest technologies for the injection of pulverized solid fuels (with relatively low melting point) different nozzle designs are investigated in the present work. Firstly, a simplified structure of fuel nozzle is taken containing two sections (or pipes), i.e. inner section and outer section (Fig. 4.6).

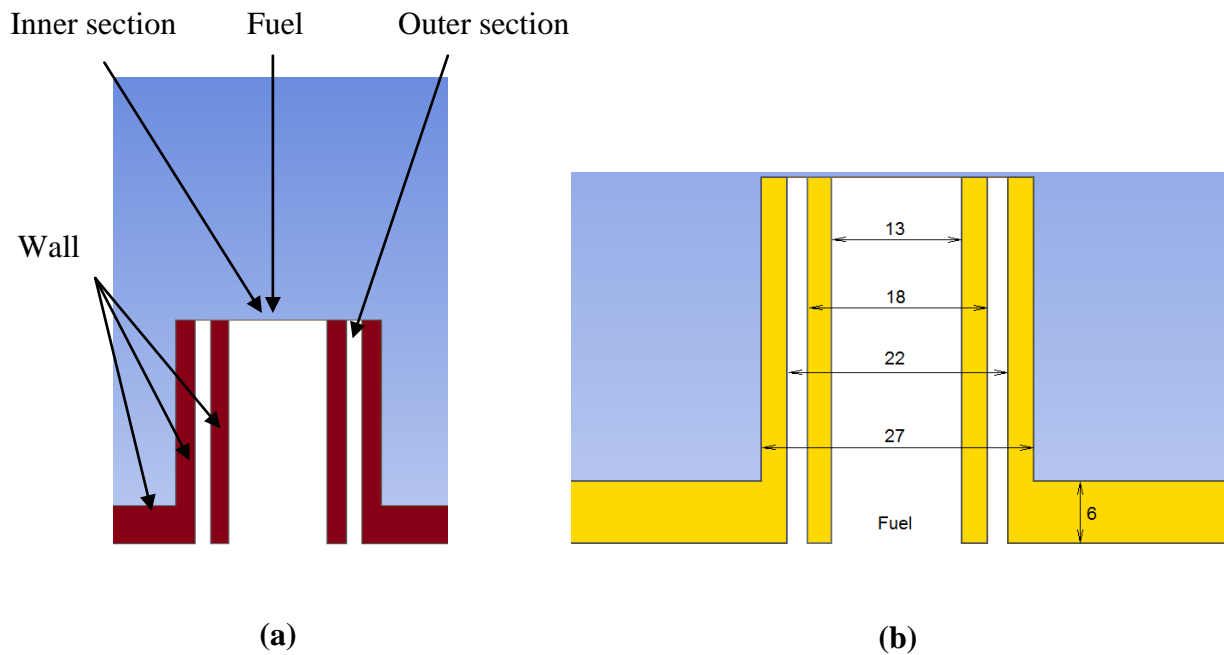


Fig. 4.6: Fuel nozzle (a) structure (b) dimensions (mm)

The inner section is used to convey the solid fuel particles with the help of fuel transport air (FTA) while the outer section is used for supplying of cooling air (CA). The primary purpose of cooling air is to lower the temperature of the nozzle walls. Additionally, it also contributes for better fuel and air mixing after the injection of fuel particles. The inner section has an internal diameter of 13 mm while the outer section is constructed around the inner pipe with an internal diameter of 22 mm. The two sections are separated by a metal wall of 2.5 mm thickness as shown in Fig. 4.6 (b).

4.4 CFD modeling methodology

There are several steps involved in computational fluid dynamics modeling of a certain (combustion) system. First of all, a general sketch of the system is prepared by preliminary data and views. After necessary editions, a digital geometry of the object is prepared through computer aided (CAD) drawings with the help of available platforms, i.e. AutoCAD (Autodesk), Solid Works, Design Modeler (ANSYS) etc. Choice of 2-dimensional or 3-dimensional geometry depends upon the available computational resources as well as the system configurations. The geometry (computational domain) is then divided into small computational cells or grids. Surfaces, e.g. inlet, outlet, walls etc., are also defined for better adaption to real operation by appropriate boundary conditions. The mesh is then imported into the solver, e.g. ANSYS (Fluent). Care must be taken while constructing the mesh of the flow system in order to ensure the compatibility with the respective solver (Fig. 4.7). Different models are applied according to the requirements and type of material to be analyzed. However, it should be noted that the original models available in the solver are based on specific (reference) materials.

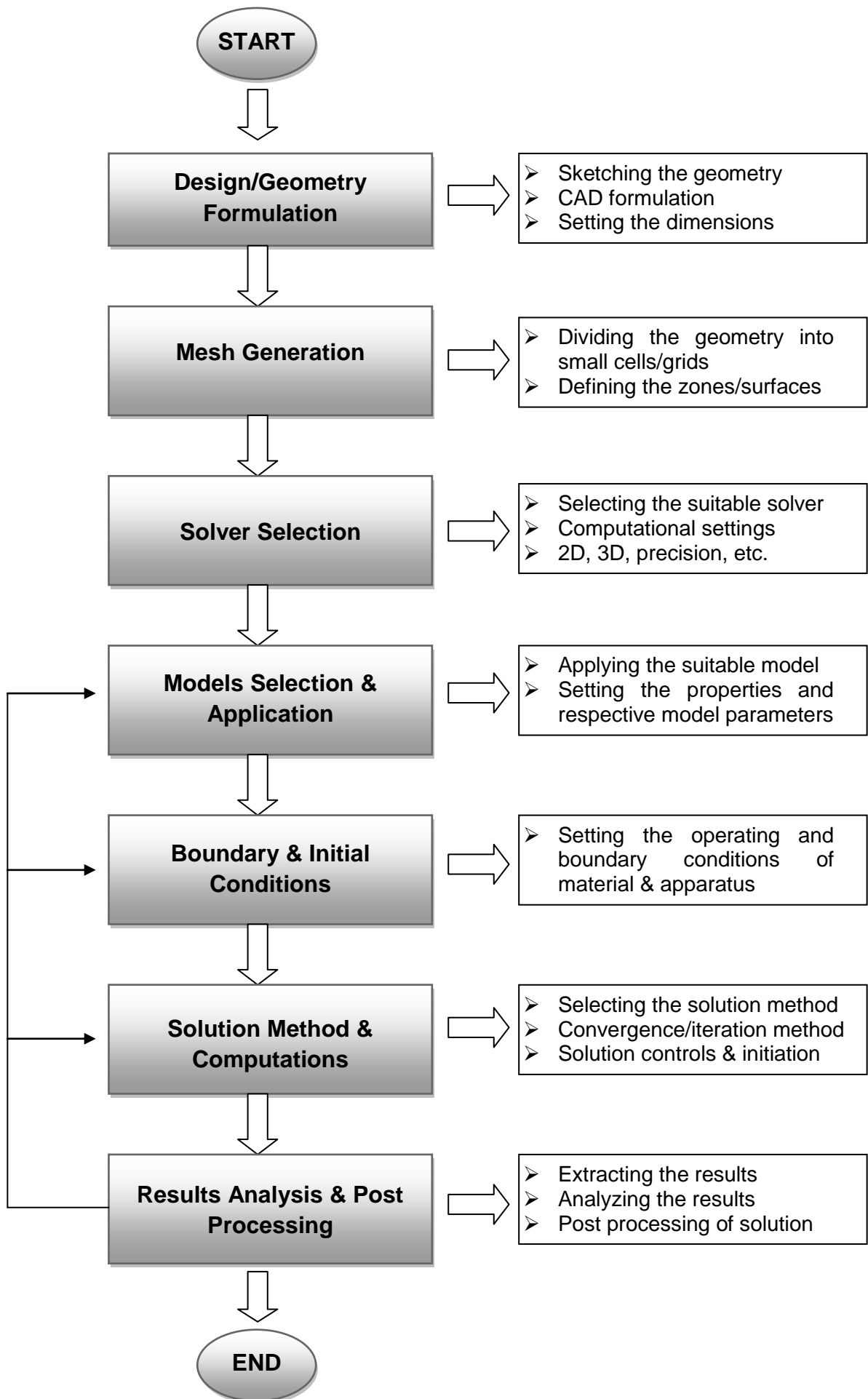


Fig. 4.7: Methodology of CFD modeling

Therefore, it is, often, necessary to provide the required values and properties in regard of the real materials used for more accurate solutions. A suitable solution method is selected along with an iteration method in order to solve the problem in hand. After convergence, i.e. completing of solution, the results are extracted and further processed and analyzed. Figure 4.7 represents the general stepwise methodology for CFD modeling of flow systems.

A similar modeling approach has been used in the present work. The numerical analysis has been conducted in ANSYS (Fluent) version 14 and 16.1.

4.4.1 Modeling approach

The combustion process includes different phenomena such as fluid flow, heat transfer, species transport, multiphase reactions etc. In order to model them, computational fluid dynamics (CFD) simulations are carried out using the commercial software package ANSYS (Fluent). Polyhedral meshing is used in all cases. To ensure an accurate solution and achieve good convergence, special discretization techniques and a fine grid mesh are required. Both requirements lead to a complex code and high memory demand for computing the solution. Polyhedral meshing has the capability to provide automatic mesh benefits. The major advantages of the polyhedral mesh are (i) each cell has more neighbors than in tetrahedral mesh for best approximation of gradients, (ii) less sensitive to stretching (than tetrahedral mesh), limitless possibilities by smart grid generation and optimization techniques, (iii) useful for handling recirculating flows, more accurate with less computation time etc. [121,122].

The motion of particles/fluid is modeled using the discrete phase model (DPM) which is based on the Eulerian-Lagrangian approach. In this method, the fluid phase is solved by Navier-Stokes equations whereas the dispersed phase is solved by particle/droplet tracking in the calculated field. Inter-phase momentum, energy and mass exchanges are also taken into account. During fluid phase calculations, this model computes the trajectories of particles/droplets individually at specific intervals. Due to this, it is considered to be suitable for the modeling of spray dryers and solid/liquid combustion. Particle trajectories are computed by momentum balancing between inertia and other forces, i.e. gravity force, drag force and other body forces [39][123-125]:

$$\frac{d\vec{u}_p}{dt} = \frac{18\mu_g C_D Re}{\rho_p d_p^2} (\vec{u}_g - \vec{u}_p) + \frac{\vec{g}(\rho_p - \rho_g)}{\rho_p} + \vec{F} , \quad (4.1)$$

where, \vec{u}_g and \vec{u}_p are gas and particle velocities, ρ_g and ρ_p are densities of gas and particles, respectively, and \vec{F} represents other body forces. The term $\frac{18\mu_g C_D Re}{\rho_p d_p^2}$ is drag force (F_D) where μ_g is gas viscosity, d_p is particle diameter, Re is Reynolds number and C_D is drag coefficient expressed by the correlation ($C_D = a_1 + \frac{a_2}{Re} + \frac{a_3}{Re^2}$) presented by Morsi and Alexander [123, 126]. The particles are assumed to be monosized, spherical and smooth; hence “spherical drag law” was used in the present study.

In the Reynolds Averaged Navier-Stokes (RANS) approach, particle trajectories are calculated by using time averaged gas velocity which neglects the turbulence effect due to

particle motion. This effect can be predicted by using stochastic tracking. Stochastic tracking was modeled by “Discrete Random Walk Model (DRW)” in which the particle, during its trajectory, is supposed to interact with a succession of fluid phase eddies characterized by a time scale (t_e). The fluctuating velocity is considered to be a function of local turbulence kinetic energy (k) [123,125]:

$$u' = \zeta \sqrt{\frac{2k}{3}} \quad (4.2)$$

and the interaction time of particle-eddy is given by minimum eddy lifetime (t_e) and eddy cross-section time t_{cross} as follows:

$$t_e = 2C_L \frac{k}{\varepsilon} \quad (4.3)$$

$$t_{cross} = -\tau \ln \left[1 - \left(\frac{L_e}{\tau |u - u_p|} \right) \right] \quad (4.4)$$

where, ζ is a normally distributed random number, L_e is eddy length scale given by $L_e = C_L \frac{k^{1.5}}{\varepsilon}$, τ is particle relaxation time defined as $\tau = \frac{\rho_p d_p^2}{18\mu_g}$ and C_L is a time scale constant. The value of C_L was taken as 0.15 in this work [123,125].

Highly turbulent flows are produced in the combustion chamber due to high velocities and chemical reaction rates. The k- ω (SST) model is applied to simulate the turbulence in the combustion process. In CFD, the k- ω turbulence model is based on the Wilcox k- ω model. This model predicts turbulence by two partial differential equations for two variables, k and ω . The first variable is turbulence kinetic energy (k) and the second is specific rate of dissipation of turbulence kinetic energy (ω). Both are obtained from following transport equations [123]:

$$\frac{\partial}{\partial t} (\rho_g k) + \frac{\partial}{\partial x_i} (\rho_g k u_i) = \frac{\partial}{\partial x_j} (\Gamma_k \frac{\partial k}{\partial x_j}) + G_k - Y_k + S_k \quad (4.5)$$

and

$$\frac{\partial}{\partial t} (\rho_g \omega) + \frac{\partial}{\partial x_i} (\rho_g \omega u_i) = \frac{\partial}{\partial x_j} (\Gamma_\omega \frac{\partial \omega}{\partial x_j}) + G_\omega - Y_\omega + S_\omega \quad (4.6)$$

where, G_k is generation of turbulence kinetic energy, G_ω is generation of ω , Γ_k and Γ_ω are effective diffusivities of k and ω respectively, Y_k , Y_ω are dissipation of k and ω due to turbulence, and S_k and S_ω are defined source terms. The k- ω model is suitable for the simulation of viscous sub-layers; however it is unable to efficiently predict the turbulence behavior in wake regions as well as under adverse pressure gradient [127,128]. Menter [127] presented a modified model, namely the k- ω shear stress transport (SST) model by combining the Wilcox k- ω and the k- ε model. The resulting model provides similar benefits as the standard k- ω model and is, additionally, more accurate, reliable and able to predict adverse pressure gradient flow conditions. Therefore, the k- ω shear stress transport model is a suitable model for many aerodynamics and industrial applications [128].

Table 4.2: Models used for different processes in PFC

Process/Effect	Model	Model parameters
Multiphase flow	Discrete particle phase (DPM) model	Maximum number of tracking steps = 5000 Injection type = Surface Particle type = Combusting Particle size distribution = Uniform Particle diameter = 10 μm Temperature = 25°C Evaporating species = H ₂ O
Stochastic tracking	Discrete random walk (DRW) model	Number of tries = 2 Time scale constant = 0.15
Fluid flow/ turbulence	k- ω shear stress transport (SST) model	With model constants set by Fluent
Drying/Particle evaporation	Diffusion controlled model	Latent heat = 2442585 J kg ⁻¹
Particle devolatilization and combustion	Constant rate (devolatilization) model Diffusion-limited (combustion) model	C _p = 1000 J kg ⁻¹ K ⁻¹ Swelling coefficient = 1.4 Heat of reaction for burnout = 32754000 J kg ⁻¹ Particle dry density = 1400 kg m ⁻³
Radiation	Discrete ordinates (DO) model	Theta divisions = 2 Phi divisions = 2 Theta pixels = 1 Phi pixels = 1 Energy iterations per radiation iteration = 10
Gas phase reactions	Eddy dissipation (EDM) model	Reactions = Volumetric Volatile mol. weight = 30 kg kmol ⁻¹ Fraction N in char = 0 Coal/fuel dry density = 1400 kg m ⁻³

Combustion of pulverized fuel can be described by three main steps, i.e. drying of fuel particles, devolatilization and combustion of volatiles, and char combustion. In the first step, fuel particles are heated in the hot combustion zone and moisture is removed from their surface. The release of volatile species from the fuel particle due to thermal decomposition is termed devolatilization. This step plays an important role in the combustion process as it controls the overall reaction rate and ignition. After being released from the fuel particle, volatile species undergo an oxidation process. The composition of gaseous volatile species

depends upon the elemental composition of the fuel. Char combustion involves the combustion of solid char which is left after the complete evaporation of volatiles from the fuel particles [129]. These processes are modeled by using respective sub-models and model parameters in the present study as given in Table 4.2.

The diffusion controlled model is used to describe the drying. After the evaporation of moisture, water vapor diffuses into the main flow stream. The molar flux of vapor depends on the difference in vapor concentration at the droplet surface to that of the bulk gas [39][107][123]:

$$N = k_c(C_s - C_\infty), \quad (4.7)$$

where, N is molar flux of vapor ($\text{kmol m}^{-2} \text{s}^{-1}$), k_c is mass transfer coefficient (m s^{-1}), and C_s and C_∞ are vapor concentrations (kmol m^{-3}) at the particle surface and in the bulk flow stream, respectively. The value of C_s is determined by assuming the surface as saturated while C_∞ is obtained from the transport equations. Mass transfer coefficient (k_c) is computed from the empirical correlation stated as:

$$Sh_d = \frac{k_c d}{D} = 2.0 + 0.6Re^{0.5}Sc^{0.33} \quad (4.8)$$

where, D is the diffusion coefficient of water vapor in bulk gas ($\text{m}^2 \text{s}^{-1}$), d is particle diameter (m), Sh , Sc , and Re are Sherwood number, Schmidt number and Reynolds number, respectively [39][107][123].

The temperature of the drying particle changes due to heat transfer between the particle and the continuous phase. Energy balance related to the convective, latent and radiant heat transfer is given by [39][107][123]:

$$m_p c_p \frac{dT_p}{dt} = hA_p(T_\infty - T_p) - \frac{dm_p}{dt} h_{fg} + A_p \varepsilon_p \sigma (\theta_R^4 - T_p^4) \quad (4.9)$$

where, m_p is particle mass (kg), c_p is heat capacity of particle ($\text{J kg}^{-1} \text{K}^{-1}$), T_∞ and T_p are temperatures of continuous phase and particle, respectively, h is convective heat transfer coefficient ($\text{W m}^{-2} \text{K}^{-1}$), A_p is surface area of particle (m^2), $\frac{dm_p}{dt}$ is the rate of evaporation (kg/s), h_{fg} is latent heat of evaporation (J kg^{-1}), ε_p is emissivity of the particle, σ is Stefan-Boltzmann constant ($5.67 \times 10^{-8} \text{ W m}^{-2} \text{K}^{-4}$) and θ_R is radiation temperature (K).

After the evaporation of moisture, the fuel particle undergoes devolatilization, which is the release of volatiles from fuel particles subjected to high temperature. Silaen and Wang [107] presented a comparison for many devolatilization models and concluded that the constant rate model provides the fastest devolatilization. Based on their findings [107], the constant rate devolatilization model is applied in the present work. In this model, volatiles are assumed to be released at constant rate [107][123] [130]:

$$A_0 = -\frac{1}{f_{v,0}(1-f_{w,0})m_{p,0}} \frac{dm_p}{dt}. \quad (4.10)$$

In this model, A_0 is devolatilization rate (s^{-1}), $f_{v,0}$ is mass fraction of volatiles present in the particle initially, $f_{w,0}$ is mass fraction of moisture (water) initially present in the fuel, and $m_{p,0}$ is the initial mass of particle. In the present simulations, the wet combustion sub-model

was also included, which enables the combustion of a wet and evaporating particle. The wet combustion model (in ANSYS Fluent) requires the amount of water in the fuel in terms of volume fraction. Hence, a volume fraction of liquid (water) is provided as 0.0058561 (based on the mass fraction of moisture in the fuel). A single volatile species is assumed in the present work as actual volatiles are not known for this specific fuel. Moreover, this work is focused on qualitative investigations for the selection of best nozzle geometry. Combustible fraction (volatiles) is calculated by coal calculator (based on the thermal properties and species model in Fluent). In the present simulations, a one-step reaction scheme for the combustion of fuel volatiles is selected:



The particle energy balance of convection, radiation and heat consumed during the devolatilization process can be expressed by following equation [123,124]:

$$T_p(t + \Delta t) = \frac{1}{hA_p + \varepsilon_p A_p \sigma T_p^3} (hA_p T_\infty + \frac{dm_p}{dt} h_{fg} + A_p \varepsilon_p \sigma \theta_R^4) + [T_p(t) - \frac{1}{hA_p + \varepsilon_p A_p \sigma T_p^3} (hA_p T_\infty + \frac{dm_p}{dt} h_{fg} + A_p \varepsilon_p \sigma \theta_R^4)] e^{-\frac{A_p (h + \varepsilon_p \sigma T_p^3) \Delta t}{m_p c_p}} \quad (4.12)$$

After completion of the removal of volatiles present in the fuel particle, char combustion starts to consume the remaining combustible fraction of the particle. In order to model char combustion, the diffusion-limited surface reaction model is applied. This considers that the advancement of char combustion is determined by oxidant diffusion to the particle surface i.e. [123,124]:

$$\frac{dm_p}{dt} = -4\pi d_p D_{i,m} \frac{m_o T_\infty \rho_g}{S_b (T_p + T_\infty)} \quad (4.13)$$

$D_{i,m}$ is diffusion coefficient of the oxidant ($m^2 s^{-1}$), m_o is local mass fraction of oxidant, ρ_g is the density of gas ($kg m^{-3}$) and S_b is the stoichiometric factor.

Radiation is a dominant heat transfer mechanism in the combustion environment. This mode of heat transfer is solved by using the radiative transfer equation (RTE) for absorption, emission and scattering medium as follows [123]:

$$\frac{dI(\vec{r}, \vec{s})}{ds} + (\alpha + \sigma_s) I(\vec{r}, \vec{s}) = \alpha n^2 \frac{\sigma T^4}{\pi} + \frac{\sigma_s}{4\pi} \int_0^{4\pi} I(\vec{r}, \vec{s}') \Phi(\vec{s} \cdot \vec{s}') d\Omega' \quad (4.14)$$

where, $I(\vec{r}, \vec{s})$ is the radiative intensity depending upon position (\vec{r}) and direction (\vec{s}), s is path length, α is absorption coefficient, σ_s is scattering coefficient, n is refractive index, σ is the Stefan-Boltzmann constant ($5.67 \times 10^{-8} W m^{-2} K^{-4}$), T is local temperature, Φ is phase diffusion and Ω' is solid angle.

Based on recent studies conducted by Yin [109] and Khodabandeh et al. [131], the discrete ordinates (DO) model is applied to solve the radiative heat transfer equation (RTE) in the present CFD simulations along with the weighted sum of gray gases model (WSGGM) for the computation of absorption coefficient. The discrete ordinate (DO) model is applicable to

a wide range of optical thicknesses and accounts for particle radiation efficiently [109]. Moreover, it has been found to be in good agreement with the experimental results reported by Khodabandeh et al. [131]. This model has the ability to solve the RTE equations for a finite number of discrete solid angles associated with vector direction (\vec{s}) fixed in the global Cartesian system (x,y,z) [123]. Hence the radiative transfer equation (RTE) (Eq. 4.14) can be written as:

$$\nabla \cdot (I(\vec{r}, \vec{s})\vec{s}) + (\alpha + \sigma_s)I(\vec{r}, \vec{s}) = \alpha n^2 \frac{\sigma T^4}{\pi} + \frac{\sigma_s}{4\pi} \int_0^{4\pi} I(\vec{r}, \vec{s}') \Phi(\vec{s} \cdot \vec{s}') d\Omega'. \quad (4.15)$$

In the presence of a discrete particulate phase (second phase), the RTE equation changes to [123]:

$$\nabla \cdot (I\vec{s}) + (\alpha + \alpha_p + \sigma_p)I(\vec{r}, \vec{s}) = \alpha n^2 \frac{\sigma T^4}{\pi} + E_p + \frac{\sigma_p}{4\pi} \int_0^{4\pi} I(\vec{r}, \vec{s}') \Phi(\vec{s} \cdot \vec{s}') d\Omega'. \quad (4.16)$$

Here, α_p , σ_p and E_p are termed as equivalent absorption coefficient, equivalent scattering factor and equivalent emission of the particles. These coefficients can be obtained for N particles in a volume V as [123][131]:

$$\alpha_p = \lim_{V \rightarrow 0} \sum_{n=1}^N \varepsilon_{pn} \frac{A_{pn}}{V} \quad (4.17)$$

$$\sigma_p = \lim_{V \rightarrow 0} \sum_{n=1}^N (1 - f_{pn})(1 - \varepsilon_{pn}) \frac{A_{pn}}{V} \quad (4.18)$$

$$E_p = \lim_{V \rightarrow 0} \sum_{n=1}^N \varepsilon_{pn} A_{pn} \frac{\sigma T_{pn}^4}{\pi V} \quad (4.19)$$

In Eqs. 4.17, 4.18 and 4.19 ε_{pn} , T_{pn} , A_{pn} and f_{pn} are emissivity, temperature, projected area and scattering factor of the nth particle, respectively.

Gas phase reactions are modeled using the eddy dissipation model (EDM). EDM in ANSYS (Fluent) is based on the findings by Magnussen and Hjertager [132] in which turbulence mixing of the gas is assumed. It considers that the chemical reaction is faster as compared to the time scale of turbulence eddies. Thus, the reaction takes place immediately after mixing of the reactants. The net production rate of species i as a result of reaction r , denoted by $R_{i,r}$, is given by the smaller of the following expressions [107][123]:

$$R_{i,r} = v'_{i,r} M_{w,i} A \rho \frac{\varepsilon}{k} \min_R \left(\frac{Y_R}{v'_{R,r} M_{w,R}} \right) \quad (4.20)$$

$$R_{i,r} = v'_{i,r} M_{w,i} A B \rho \frac{\varepsilon}{k} \frac{\sum_P Y_P}{\sum_j^N v''_{j,r} M_{w,j}} \quad (4.21)$$

where, $v'_{i,r}$ is the stoichiometric coefficient of the reactant i , $v''_{j,r}$ is the stoichiometric coefficient of the product in reaction r , $M_{w,i}$ is molecular weight of species i , Y_R and Y_P are mass fractions of reactant and product, respectively, and A and B are empirical constants (4.0 and 0.5 respectively). The smaller of the above two expressions (Eq. 4.20 and Eq. 4.21) is taken as the limiting value to determine the reaction rate [107][123]. EDM has many advantages when solving engineering and industrial problems; it is applicable to highly turbulent flows and can then ignore chemical kinetics without influencing the predicted temperatures, as stated by Kassem et al. [133]. Moreover, studies presented by Achim et al.

[134] and Saqr et al. [135] also revealed a good agreement between predicted and measured results using this model.

4.4.2 CFD computational domain and boundary conditions

In the present simulations, a 3-dimensional geometry of the combustion furnace has been used for all computations. The domain extents of combustion furnace with the fuel nozzle are shown in Table 4.3. The Z-coordinates represent the vertical/axial distance of the furnace with origin at the injection point. The negative value indicates the distance away from the injection while positive value represents the length of the mounted nozzle. This value varies depending upon the size of fuel nozzle (Appendix B, Table B1, Fig. B1).

Table 4.3: Domain extents of combustion furnace (all dimensions in m)

X min.	-0.549	X max.	0.65
Y min.	-0.549	Y max.	0.549
Z min.	-3.17	Z max.	0.05

Figure 4.8 shows the outline and mesh structure of the computational domain of the PFC combustion furnace used in the present simulations. Initially, a tetrahedral mesh structure is formulated for all cases using the ANSYS meshing tool which is then converted to a polyhedral mesh based on its several advantages as described in Section 4.4.1. It should be noted that the side walls and bottom wall of the furnace are assumed to be perfectly insulated walls, i.e. no heat is transferred to the ambient. However, the region near the nozzle is the main focus in the present study, hence, the top of the furnace is divided into different wall zones in order to study the heat transfer mechanism responsible for increasing the nozzle temperature. Heat is transmitted by radiation from the combustion zone to the wall strip available along the ring of the primary air inlets. This heat is transferred to the upper furnace wall through conduction (Fig. 4.8, Appendix B, Fig. B2).

The top plate of the furnace (near the nozzle) is assumed to be cooled by water. For this purpose, a wall (water cooling wall) is placed above the top furnace wall and the temperature of this wall is set to 30°C (assumed to be provided by water) as shown in Fig. 4.9. The heat flux to the top plate is computed on the basis of fluid local conditions such as gas velocity, turbulence and temperature of furnace [123]. Hence, a value of heat transfer rate at this section can be obtained at the end of the calculation. As described before, fuel and air are provided in the specified inlets predefined during meshing. These inputs are provided from the prescribed mass flow inlets in a direction normal to the boundary with the defined operating conditions (Section 4.4.3).

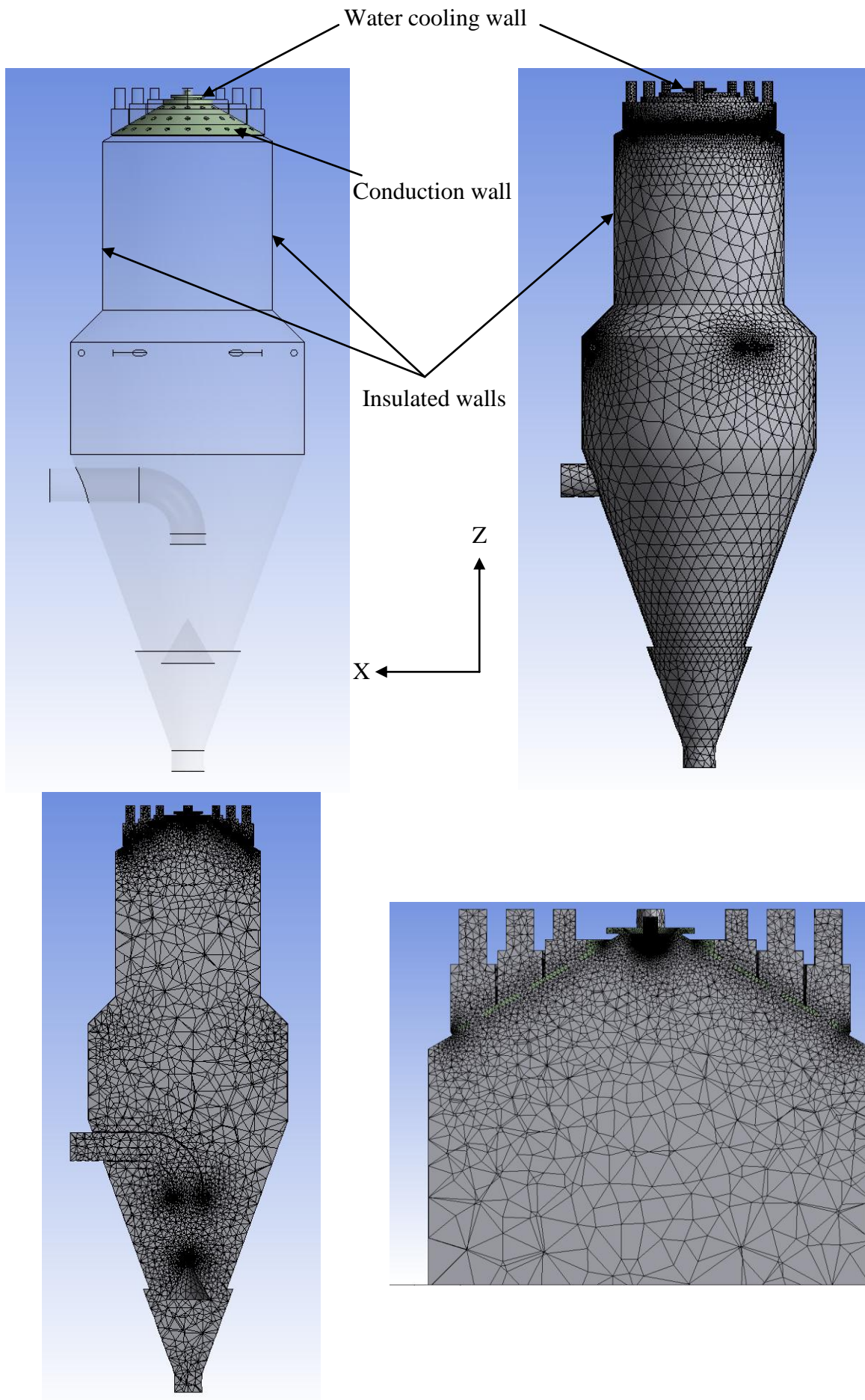


Fig. 4.8: Computational domain of combustion furnace

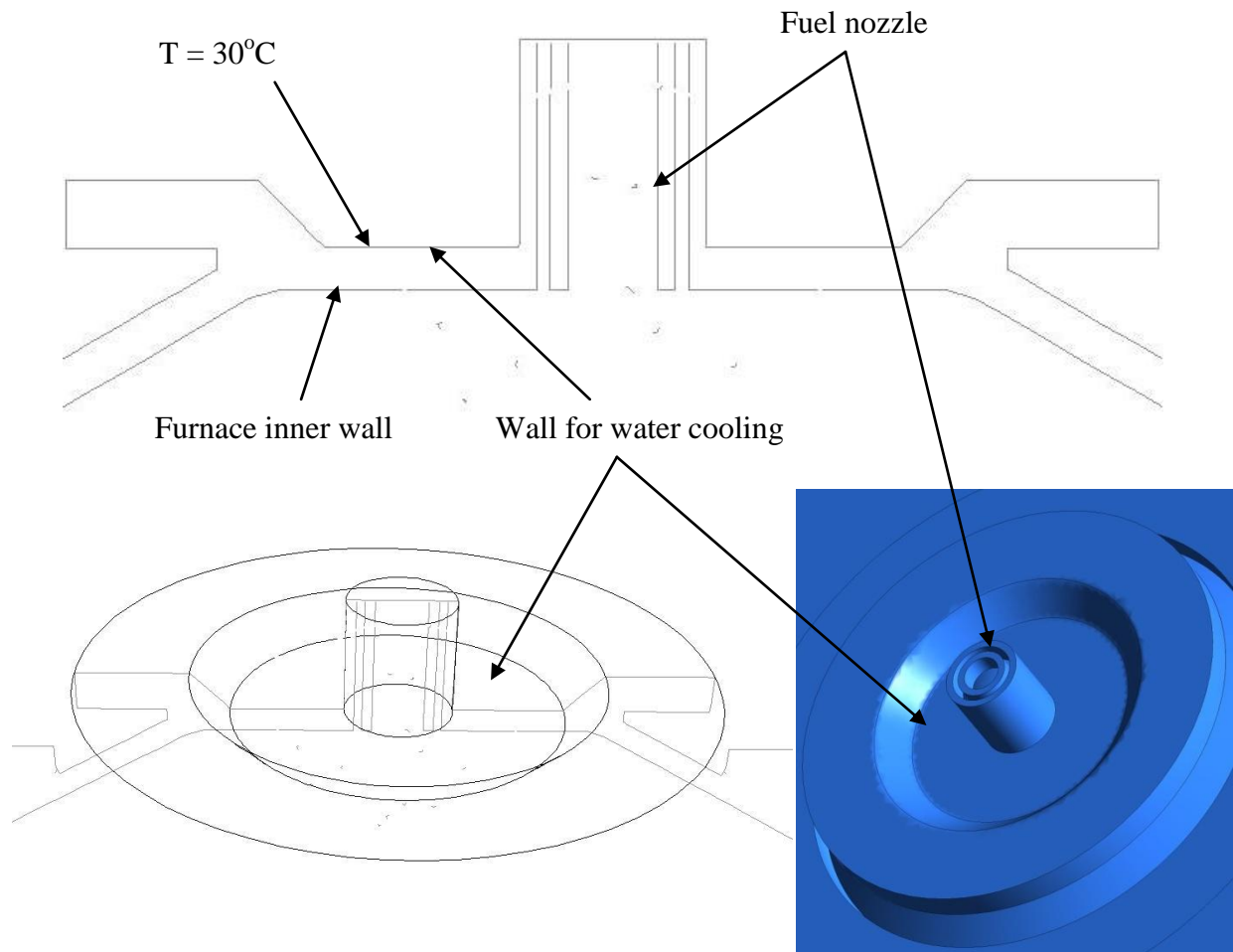


Fig. 4.9: Wall for water cooling

4.4.3 Operating conditions

Multiphase CFD simulations are conducted with the specified models and parameters (Section 4.4.1, Table 4.2). Fuel is injected with a mass flow rate of 20 kg h^{-1} and an inlet temperature of 25°C . Nozzle air is provided into two nozzle pipes, i.e. inner and outer section (Fig. 4.6). Fuel transport air (FTA) is supplied in the inner section with a flow rate of $12 \text{ m}^3 \text{ h}^{-1}$ while cooling air (CA) is injected at a flow rate of $11 \text{ m}^3 \text{ h}^{-1}$. The inlet temperature of the nozzle air fed into both nozzle sections is set to 25°C . Primary air is supplied through the primary air inlets available at the top of the furnace. The flow rate of primary air is given as $40 \text{ m}^3 \text{ h}^{-1}$, $53 \text{ m}^3 \text{ h}^{-1}$ and $67 \text{ m}^3 \text{ h}^{-1}$ for all four inner, middle and outer primary inlets (mounted as a ring), respectively. Due to several advantages of preheating of (primary) air supplied to the combustion chamber, the primary air is provided with a preheat temperature of 300°C [89]. Secondary air is supplied at a flow rate of $50 \text{ m}^3 \text{ h}^{-1}$ and at a temperature of 300°C , in order to achieve better combustion conditions.

4.5 Results and discussion

Steady state CFD simulations are conducted with the stated modeling and operating conditions (as a base case). Double precision is used in order to ensure the accuracy of the solution. Discretization of energy and momentum equations is performed with the SIMPLE scheme of pressure-velocity coupling. First order upwind scheme is used for momentum, turbulent kinetic energy, specific dissipation rate, species, energy and discrete ordinates. Report type “area-weighted-average” of static temperature on pressure outlet is used as surface monitor. Hybrid initialization is used for initiation of solution. The simulations are run with a processor of Intel Core i5-6600 CPU 3.30 GHz and an operating system of Win. 7, 64 Bit. The solution is run for 10000 iterations and solution is assumed to be converged when outflow temperature becomes constant during the iterations. The average computational time was observed to be approximately 30 h for all 3-D cases.

4.5.1 Mesh sensitivity analysis

A mesh sensitivity analysis has been conducted in order to check the influence of mesh cells on the computational results. For this purpose, two different mesh sizes were used, i.e. coarse mesh and fine mesh. As described before, a tetrahedral mesh is formed by the meshing tool (ANSYS Workbench) and then converted into a polyhedral structure in order to increase the mesh quality, after importing into Fluent.

Figure 4.10 illustrates the tetrahedral mesh structure of both the coarse and the fine mesh of the combustion furnace. It should be noted that the regions near the nozzle are refined to smaller sizes in case of the fine mesh which increases the overall elements number. The coarse (tetrahedral) mesh has approximately 1.2 million elements while the fine mesh is formulated with approximately 2.0 million tetrahedral elements. After conversion to polyhedral mesh, the number of elements decreases to 350,000 cells in the coarse mesh and to 550,000 in case of the fine mesh. The simulations were conducted with the stated operating and boundary conditions (Section 4.4). It was concluded from the analysis that there is a difference of 7 K in the nozzle temperature between the two cases (Appendix B, Fig. B9 and B10). Hence, it was found necessary to increase the grid density near the nozzle injection plane. Therefore, the fine mesh (with average number of polyhedral cells of 550,000) has been used in all simulations in this work to make comparatively reliable predictions.

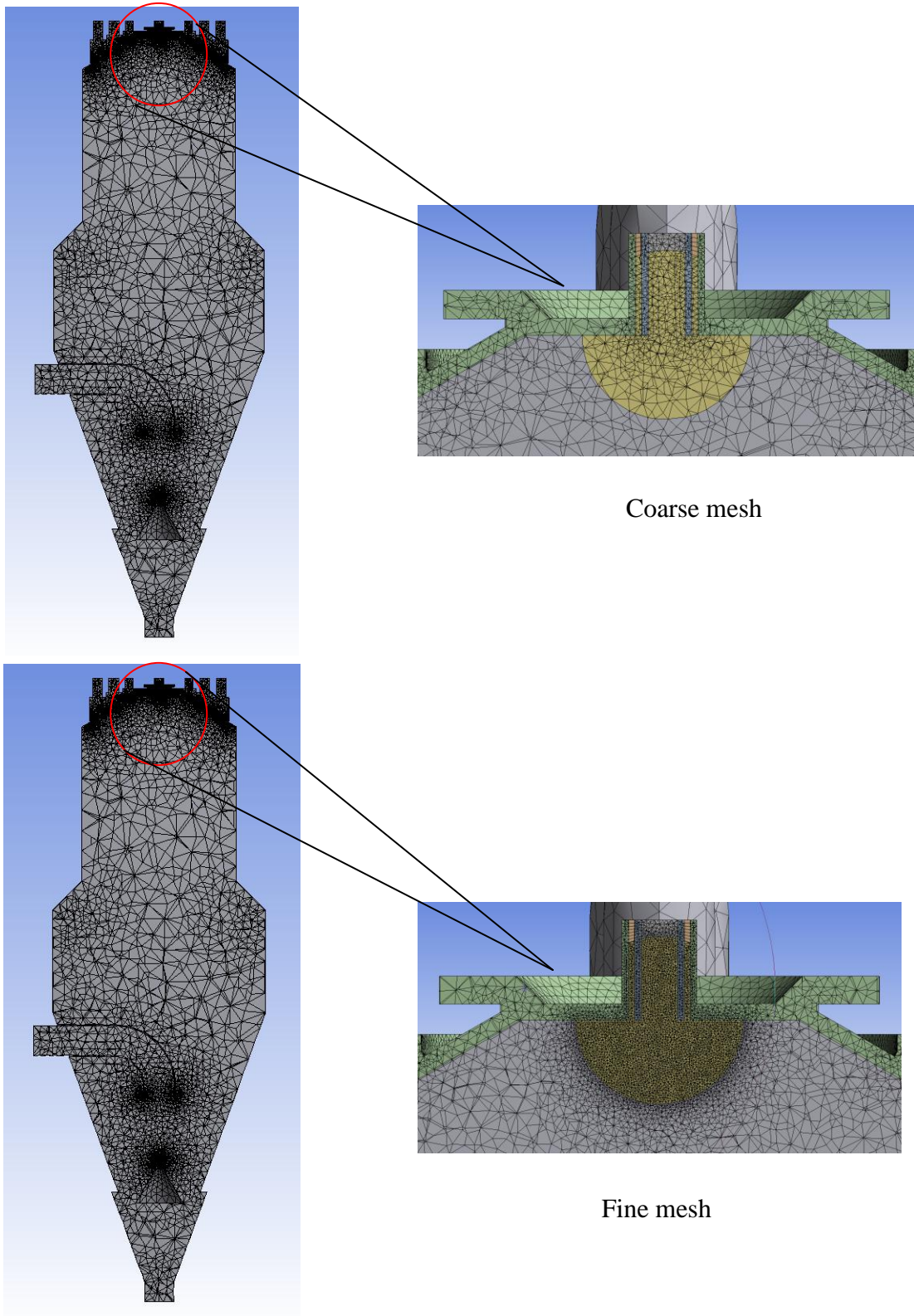


Fig. 4.10: Mesh sensitivity analysis

4.5.2 Temperature distribution in the furnace

Due to high combustion temperature generated in the combustion zone, temperature is shifted towards the nozzle and other parts of the furnace by heat transfer mechanisms. However, heat transfer through radiation is the dominant heat transfer mechanism in combustion processes. The most dominant mode of heat transfer in a combustion plant is radiation as it accounts for 96% of the total heat transfer [120][136-138]. In the present study, this effect has been modeled by the discrete ordinates model (Section 4.4.1). Temperature distribution in the combustion furnace (with operating conditions as described in Section 4.4.3) is illustrated in Fig. 4.11. It can be noted that temperature firstly increases and then decreases along the furnace length. This is due to the burning of fuel particles, once the ignition temperature is achieved. When the fuel particles are injected into the furnace, they heat up rapidly due to the hot combustion environment provided by the mixing of primary air streams and hot combustion gases. As a result volatile gases are released, which are ignited to produce the flame-like hot combustion zone.

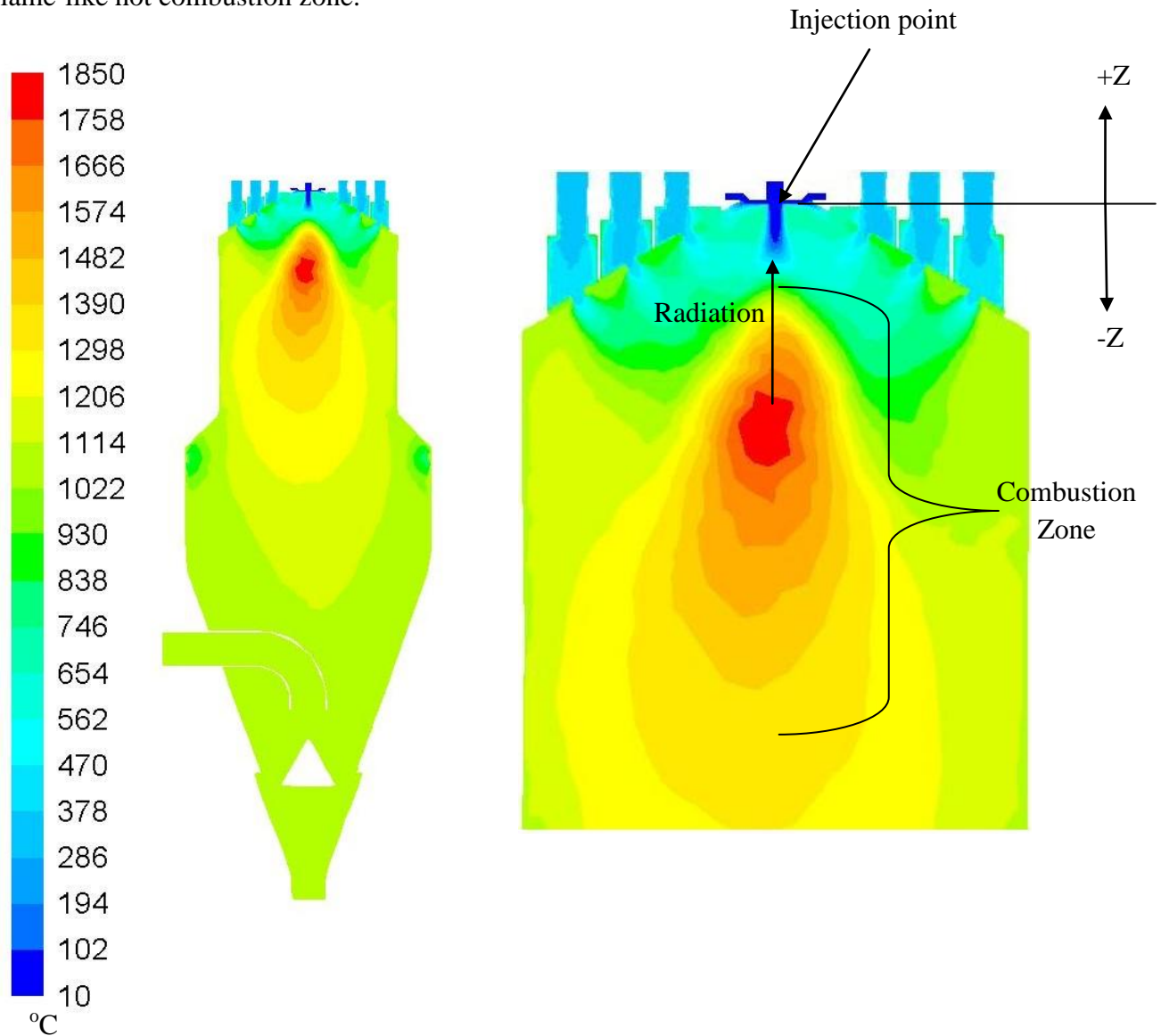


Fig. 4.11: Temperature distribution (°C) in combustion furnace

Though the high temperature generated is distributed to other parts of the combustion furnace, there is by far no perfect equilibrium, so that temperature decreases when moving away from the combustion zone, forming a heterogeneous temperature field (Fig. 4.11).

Figure 4.12 represents the axial temperature profile with respect to the position from the top of the nozzle. The current plot is made along the central line of the combustion furnace from top of the nozzle, i.e. +50 mm till -2000 mm inside the furnace. As described before (Table 4.3), the origin indicates the injection point, positive data points show the length of nozzle and negative points represent the distance inside the furnace from the injection point. Moreover, the current plot is made along the central line (starting from middle of nozzle inner section). It can be observed that temperature of the fuel particles is about 25°C (as initial temperature of the FTA is given as 25°C) during the distance +50 mm to 0 (injection point). After this point, the fuel particles undergo drying and devolatilization due to very hot combustion environment. As particles are injected with a high air flow rate, they push the combustion gases downwards making a stream of comparatively lower temperature until a distance of -35 mm inside the furnace (Fig. 4.12).

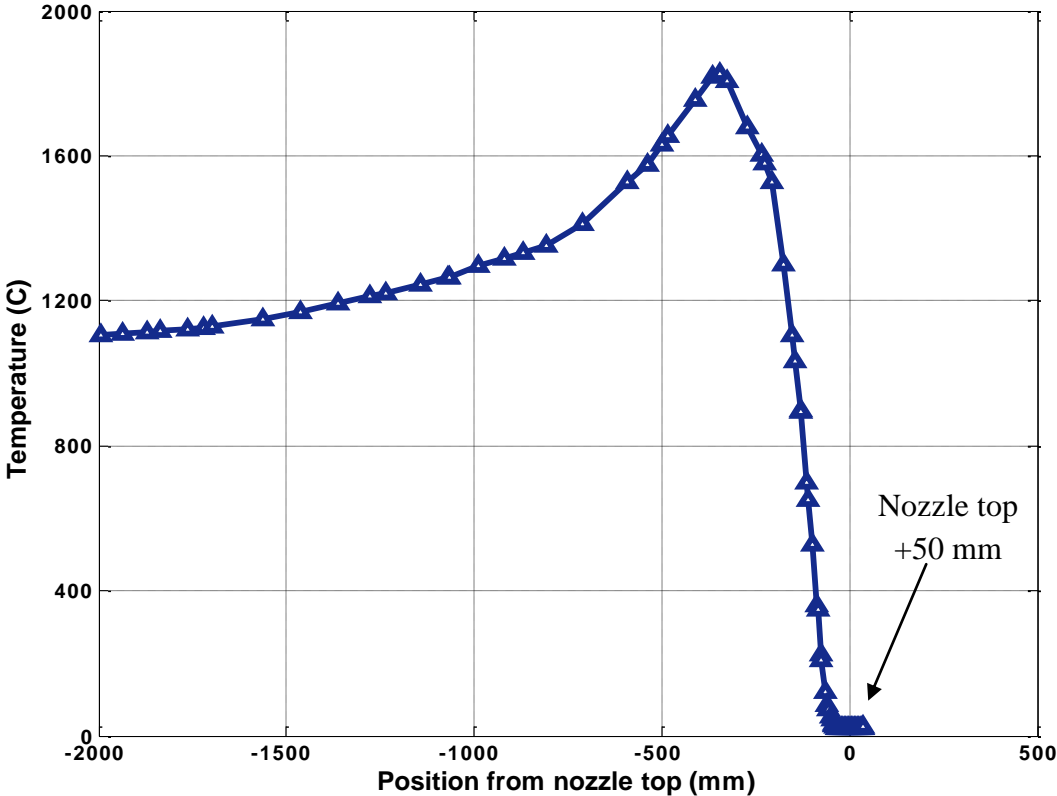


Fig. 4.12: Temperature profile (along central line) in the combustion furnace

After completing the drying and devolatilization, the temperature increases rapidly and reaches to a maximum value of 1830°C at a distance of -350 mm from the nozzle exit (injection point). The combustion temperature decreases significantly after this point due to less heat release by reactions in combination with heat transfer to the other parts of the combustion furnace. At a distance of about 2000 mm, the temperature is around 1100°C. The

temperature at the flue gas outlet has been noted to be at 1095°C (Figs. 4.11 and 4.12). The adiabatic temperature (neglecting heat losses to the ambient) is calculated as 1178°C with these operating conditions. However, in the present case, heat losses have been implemented from the top wall (water cooling wall) as described in previous section. Therefore, a lower outlet temperature is obtained as a result.

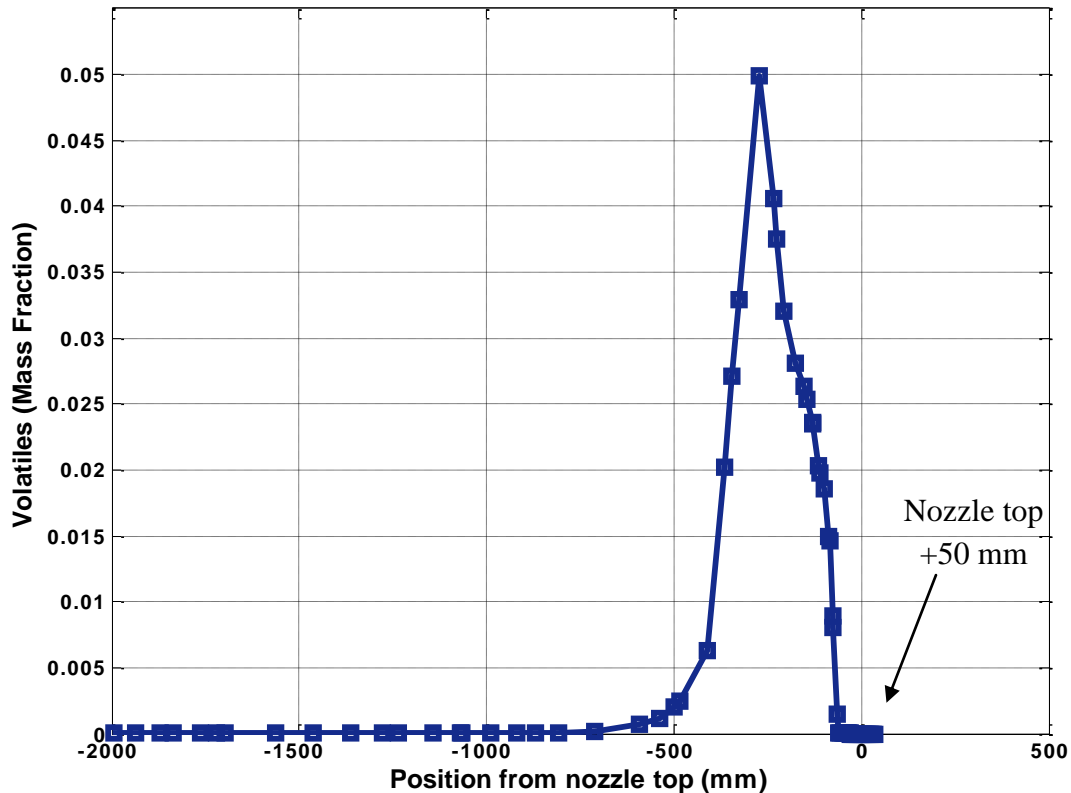


Fig. 4.13: Volatile release in combustion furnace

As described earlier, the combustion process is initialized after the release of volatiles from fuel particles. Releasing rate of volatiles depends on different factors, i.e. type of fuel, particle size, temperature exposure and the mixing ratios in the combustion chamber. However, the release of volatiles as well as volatile combustion occurs in a very short period of time. The axial profile of volatile mass fraction is shown in Fig. 4.13. It can be observed that volatile mass fraction is zero within the nozzle from top of nozzle (at a position of +50 mm till 0.0 mm). After feeding of the particles to the combustion chamber, the mass fraction of fuel volatiles increases rapidly and reaches its maximum value in close vicinity of the nozzle, e.g. at a distance of approximately -300 mm from the nozzle exit. After this point, volatile fraction starts decreasing and reaches a very low value at a position of -500 mm and then tends zero (Fig. 4.13). This is due to the fact that the volatile gases evolved during the devolatilization process are consumed by the combustion process. The reduction of volatile mass fraction to zero implies that the combustion process has been completed and there is no unburnt material left in the combustion furnace. A similar behavior of volatiles has also been described by previous studies [138-140].

4.5.3 Nozzle temperature

Figure 4.14 shows a close-up view of the fuel nozzle region. It can be observed that temperature of the inner and outer section is less than 60°C during the injection. However, the partition wall between inner and outer section has a significantly higher temperature. The top of the nozzle is observed to be at 75°C while the tip has a temperature of 92°C . The temperature of the partition wall of the nozzle gradually increases while moving from top of the nozzle to the nozzle exit.

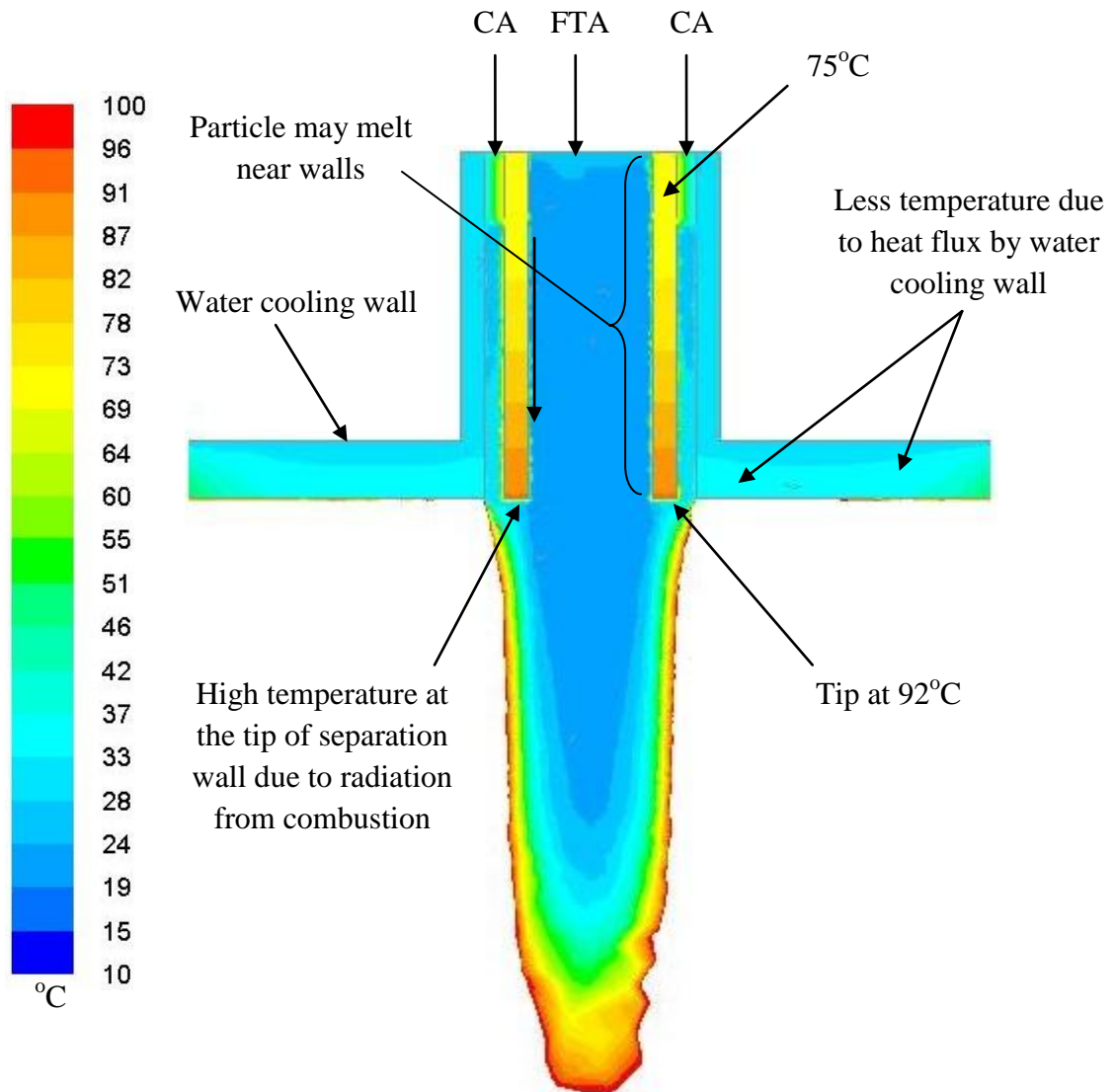


Fig. 4.14: Temperature distribution in fuel nozzle

This increase in temperature is because of the thermal radiation transmitted from the combustion zone, which is very hot and placed closely beyond the nozzle as presented in Figs. 4.12 and 4.13. However, the temperature of the adjoining furnace walls (on both sides of the nozzle, Fig. 4.8) is reduced by the heat flux to the water cooling wall. In this way, the temperature of nozzle outer wall is significantly reduced. However, the separation wall of the

nozzle sections is observed to be with significantly high temperature. As it is in direct contact with the incoming air/fuel streams, heat will also be transferred to these streams. As a result, fuel particles moving in the inner section may heat up and melt near the walls. This can make a sticky layer deposition on the inner pipe of the nozzle. Hence, the temperature at any point of the nozzle should be kept less than 60°C (< melting point of fuel particles) during fuel transportation/injection to the combustion furnace. Since, nozzle walls are observed to be at the highest temperature at the lower tip of the nozzle, it is concluded that measures should be taken for temperature reduction using this point as a (target) reference (Fig. 4.14).

4.6 Summary and outcomes

This chapter described the base case of CFD analysis. This case refers to a specific pulverized fuel combustion facility, the geometry and components of which have been explained. Moreover, it refers to paint residue generated from the metal coating industry as the fuel. It is concluded from analysis of this material that it contains constituents with relatively low melting point (around 60°C). In fact, this paint residue has the lowest melting point among all other considered solid waste materials, e.g. plastic wastes. On the other hand, it also possesses a significant energy content, i.e. 18.336 MJ kg⁻¹. Additionally, it is found in smaller size as a raw material as it is generated from the solidification of fine paint spray droplets. This makes its utilization by combustion economically more feasible, by eliminating the need of milling and grinding operations. In the base case, a simple geometry of fuel nozzle has been analyzed, made of two pipes that define an inner and an outer flow section. Fuel is transported in the inner section while the outer section is used for cooling air. Multiphase simulations have been conducted by means of computational fluid dynamics (CFD) for the base case with this simple nozzle. After an outline of theory and fundamentals, the sub-models and boundary conditions used in the CFD have been explained in details. Water cooling has been implemented by defining a water cooling wall on the upper boundary of the combustion furnace. Moreover, a grid independence analysis is also presented with two cases of mesh size. The results reflect the fact that combustion process starts after the devolatilization of fuel particles. It is observed that volatiles are released in close vicinity of the fuel nozzle. Hence, a high temperature is generated with radiative heat transfer to the fuel nozzle. As a result, the temperature of the partition wall of the nozzle sections increases significantly. The temperature of this nozzle wall is highest at the lower tip of the nozzle, where it reaches 92°C under base case simulation conditions. As this temperature is higher than the melting point of fuel particles, the current geometry and operating conditions are not suitable for the transportation of pulverized fuel to the combustion chamber, therefore, it is concluded that the effect of nozzle temperature, which is influenced by the temperature of the combustion zone, should be further investigated with different nozzle geometries. It has resulted from the base case simulations that the highest nozzle temperature is observed at the nozzle exit (i.e. lower tip of nozzle wall). Hence, further analysis should be made with reference to the lower tip of the fuel nozzle wall. Furthermore, it is theoretically expected that the combustion temperature

will decrease with an increase in excess air (Chapter 2). Therefore, the effect of different air supply levels should also be analyzed with the different geometries of fuel nozzle.

Optimization of Fuel Nozzle for PFC

The current chapter contains parts of a manuscript entitled “Study on nozzle design for combustion of solid materials with low melting points” published in Applied Thermal Engineering [116]. The goal is to optimize the nozzle design with respect to the problem stated, i.e. melting point around 60°C. Four different nozzle designs are evaluated by means of multiphase CFD simulations. Moreover, based on the base case, modifications are made in the operating conditions. In order to check the effect of fuel particle size, some simulations with different particle sizes are presented. Optimization of nozzle air flow rates is also presented, for the best fuel nozzle design obtained from the CFD simulation results. Moreover, the effect of excess air on combustion characteristics is discussed.

5.1 Overview and motivation

The fuel nozzle is the most important component of a PFC combustion plant. It has been reported earlier [118-120] that nozzle geometry and shape significantly influence the combustion characteristics in the combustion chamber. Inlet parameters have, in general, a strong influence on the combustion process. Based on the results of Chapter 4, further investigations are conducted with different nozzle designs in order to find the most appropriate nozzle for the transportation of pulverized fuel to the hot combustion chamber. Starting with relatively simple design from Chapter 4, more complicated structures of the fuel nozzle are developed. Multiphase CFD simulations are conducted in total four different fuel nozzle structures by keeping all parameters (fuel mass flow rate, inlet temperature, fuel type and composition, primary air, secondary air) constant, except geometry of nozzle and nozzle air flow rates.

In the previous Chapter 4, it was concluded that the temperature of nozzle wall increases from top to bottom of the nozzle. Maximum nozzle temperature is noted at the lower tip of the nozzle which is most exposed to radiation from the hot combustion zone. As fuel particles exit from this point, this is the most critical point in the fuel nozzle. Too high temperature at this point may cause melting of fuel particles, which may then accumulate at the injection point in the form of sticky matter. Hence, investigations are mainly focused on the injection point. However, the patterns of temperature distribution in the complete nozzle structure as well as in the whole combustion chamber are also presented.

5.2 Fuel nozzle designs

Four different fuel nozzle designs are formulated as shown in Fig. 5.1. All nozzles have an inner and an outer section, and Nozzle 4 has also a middle section in it. The inner section is used to transport fuel by means of fuel transport air (FTA) while cooling air (CA) is supplied via the outer section. However, in Nozzle 4, fuel is injected through the middle section, while the other two sections are used for cooling air. Nozzle 1 is exactly the same as in the base case of Chapter 4 (compare with Fig. 4.6). Nozzle 2 is an improved design of Nozzle 1 (Fig. 5.1). The diameter of the inner section of Nozzle 2 is the same as in Nozzle 1, i.e. 13 mm, while the diameter of the outer section varies gradually from 22 mm at the bottom to 30 mm at the top. In this way, the outer section has the form of a channel with changing cross-sectional area and a width of only 1.5 mm at the narrowest place (Fig. 5.2). The edge of the partition wall between inner and outer section is made quite narrow at the injection place, with an outer diameter of 17 mm and an inner diameter of 14 mm (Fig. 5.2). The wall between outer and inner section was modified to a zigzag pattern to increase surface area and therefore the cooling effect (Fig. 5.3).

Nozzle 3 has a different structure than the earlier nozzles. Fuel is injected from the top of the nozzle and moves along its outer section around a central pipe which carries the cooling air (as shown in Fig. 5.1). Cooling air (CA) is supplied from the side openings around the fuel nozzle into the inner section of the nozzle. Nozzle 4 is a combination of Nozzle 2 and Nozzle 3. The previous patterns are used, but Nozzle 4 has an additional middle section through which fuel is transported along with fuel transport air (FTA). The other two sections are used for air transportation. The inner diameters of the inner, middle and outer section are 14 mm, 34 mm and 40 mm, respectively, with two partition walls with a thickness of 2 mm each (Fig. 5.2).

It should be noted that the areas around the injection of fuel particles are of main concern in the present study. Moreover, temperature of the nozzle partition wall increases from top to bottom and maximum temperature is found at the lower tip of the nozzle (Chapter 4). Therefore, the heat flux and conduction have been studied in the highlighted parts of Fig. 5.1. The other parts represent the fluid domains of the nozzle sections separated by walls (without heat transfer). Similar boundary conditions have been used in all four cases as described in base case (Chapter 4). Computational domain of Nozzle 1 has already been presented in Chapter 4 while the computational domains of Nozzle 2, Nozzle 3 and Nozzle 4 are given in Appendix B (Table B1, Figs. B1-B5).

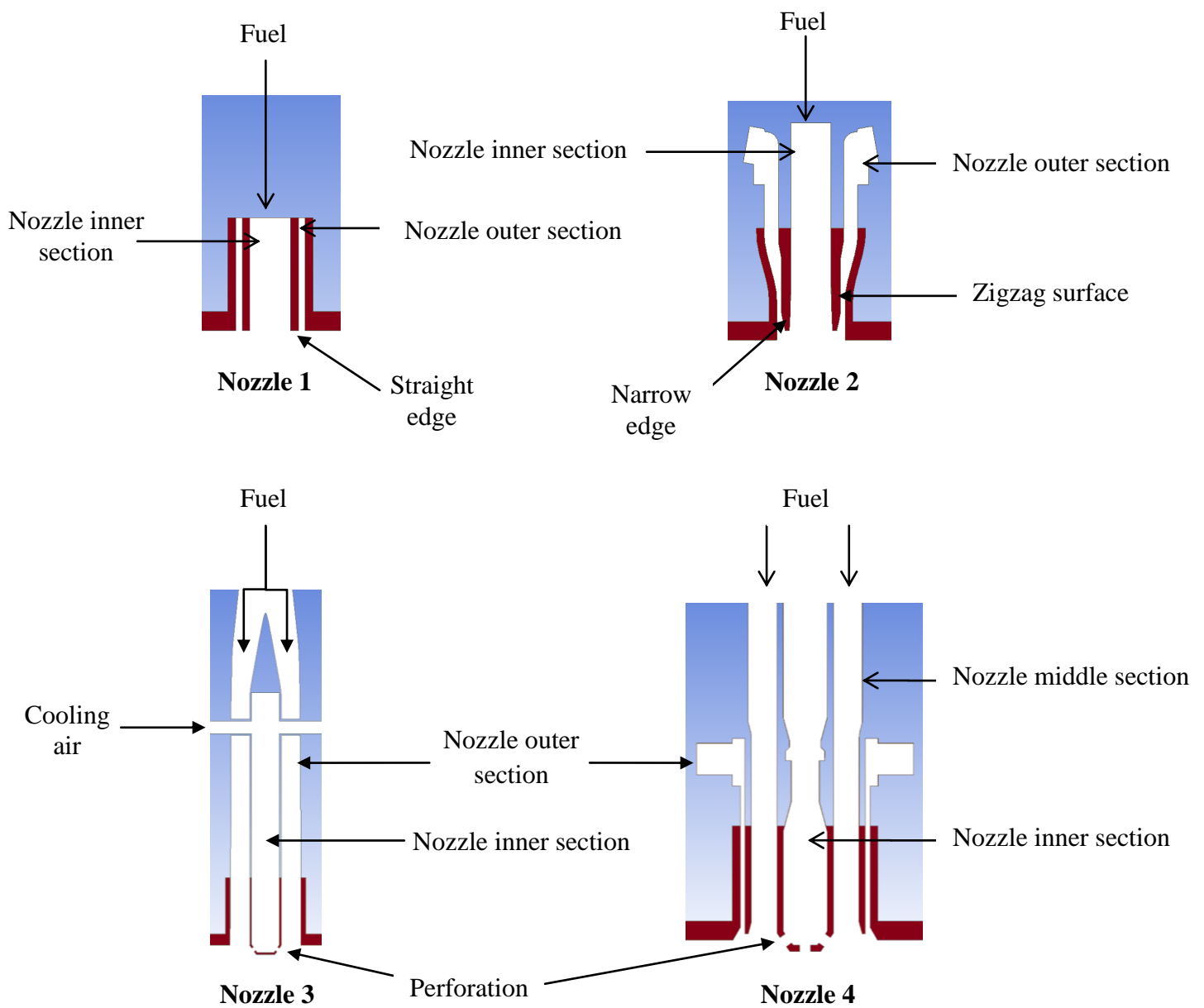


Fig. 5.1: Studied fuel nozzle designs

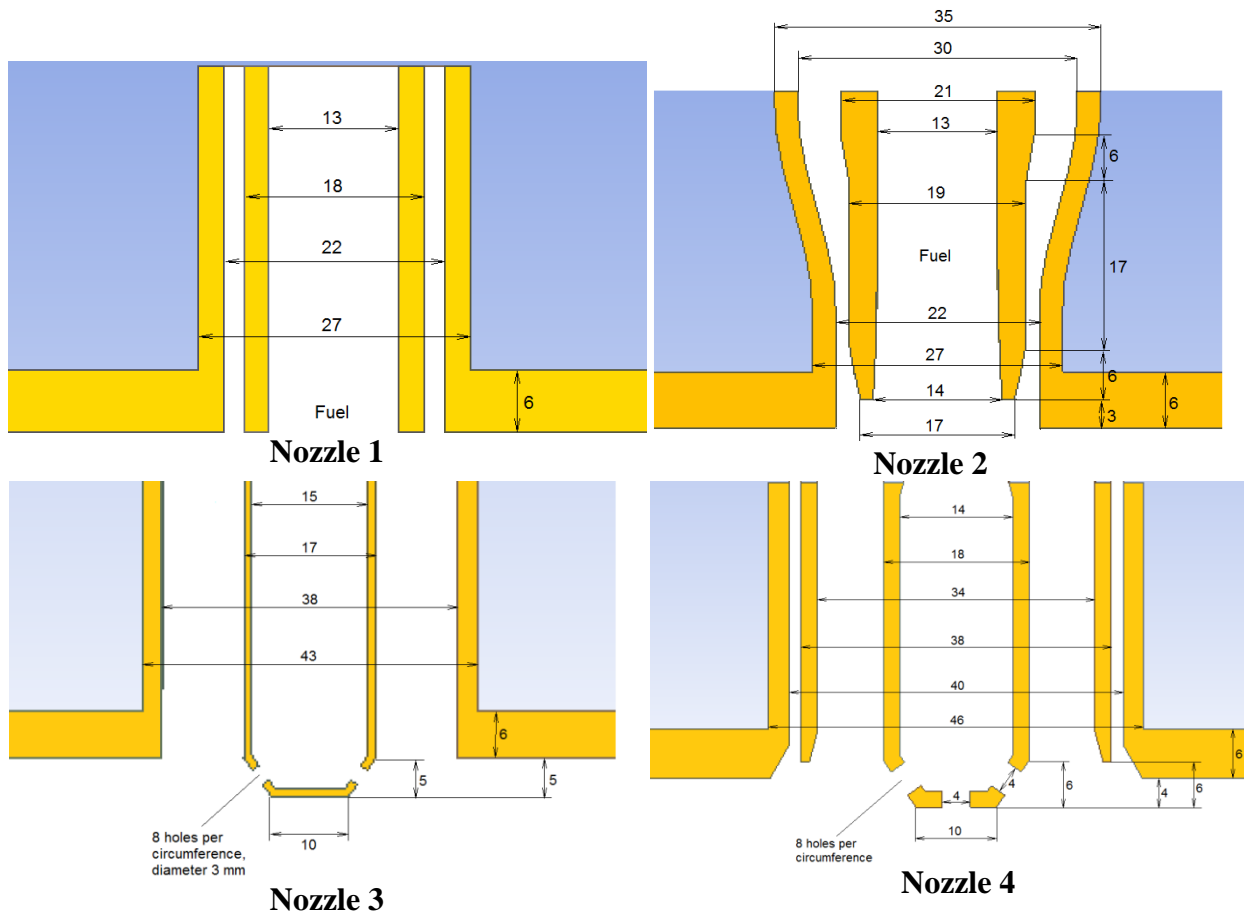


Fig. 5.2: Nozzle dimensions (mm)

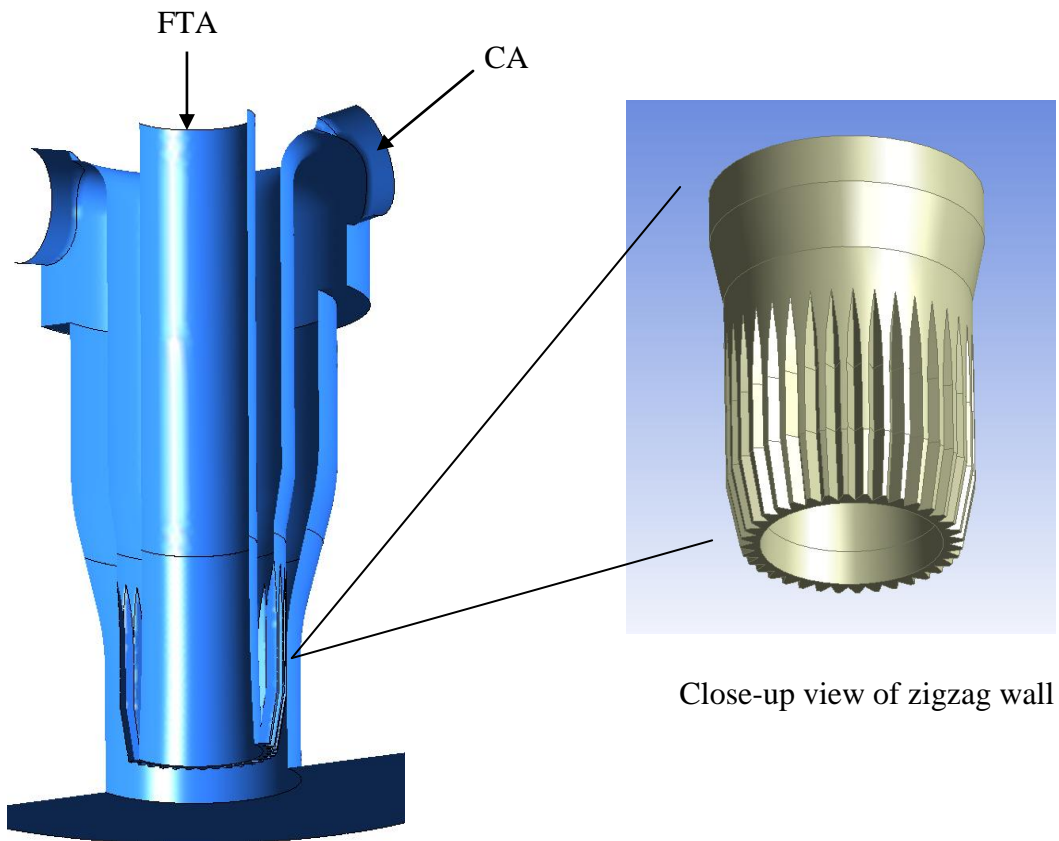


Fig. 5.3: Zigzag pattern of wall in Nozzle 2

5.3 Operating conditions

Two sets of boundary conditions (in nozzle air) are used in the CFD simulations. In the first case different flow rates are used in all the nozzles. However, in the second case, an equal total flow rate is used in all four nozzles.

5.3.1 Nozzle air

As described before, the nozzles are subdivided into sections denoted by nozzle inner section, nozzle outer section and nozzle middle section (only in case of Nozzle 4). Table 5.1 shows air flow rates provided in the different sections of the fuel nozzles. It should be noted that FTA is the fuel transport air used in the fuel nozzle. In Nozzles 1 and 2 the fuel and fuel transport air (FTA) move in the nozzle inner section, in Nozzle 3 in the outer section (as described in Fig. 5.1); In Nozzle 4, fuel and fuel transport air (FTA) are transported through the middle section. The other sections of the nozzles are used to transport the nozzle air (i.e. cooling air) at specified flow rate. Both, fuel transport air and cooling air are provided with an inlet temperature of 25°C (Table. 5.1).

Table 5.1: Nozzle air flow rates (Data Set 1)

Nozzle section	Nozzle 1	Nozzle 2	Nozzle 3	Nozzle 4	Temperature
Nozzle inner section	12 m ³ h ⁻¹ (FTA)	12 m ³ h ⁻¹ (FTA)	2 m ³ h ⁻¹	10 m ³ h ⁻¹	25°C
Nozzle middle section	-	-	-	25 m ³ h ⁻¹ (FTA)	25°C
Nozzle outer section	11 m ³ h ⁻¹	11 m ³ h ⁻¹	25 m ³ h ⁻¹ (FTA)	7 m ³ h ⁻¹	25°C
Total	23 m ³ h ⁻¹	23 m ³ h ⁻¹	27 m ³ h ⁻¹	42 m ³ h ⁻¹	25°C

5.3.2 Primary air

As explained in Chapter 4, primary air inlets are placed at the roof of the combustor in three coaxial rings: inner, middle and outer. Primary air is supplied at a temperature of 300°C [89] through these inlets at the specified flow rate, same, irrespectively of the nozzle used. Flow rates in primary air inlets (supplied to all four inlets of an inlet ring) are given in Table 5.2.

Table 5.2: Primary air conditions

Primary air inlet	Flow rate	Inlet temperature
Inner	40 m ³ h ⁻¹	300°C
Middle	53 m ³ h ⁻¹	300°C
Outer	67 m ³ h ⁻¹	300°C
Total	160 m ³ h ⁻¹	300°C

5.3.3 Secondary air

Secondary air is supplied through the secondary air inlets present on the periphery of the combustion furnace. Secondary air is injected with a total flow rate of $50 \text{ m}^3 \text{ h}^{-1}$ and at a temperature of 300°C in case of all four fuel nozzles.

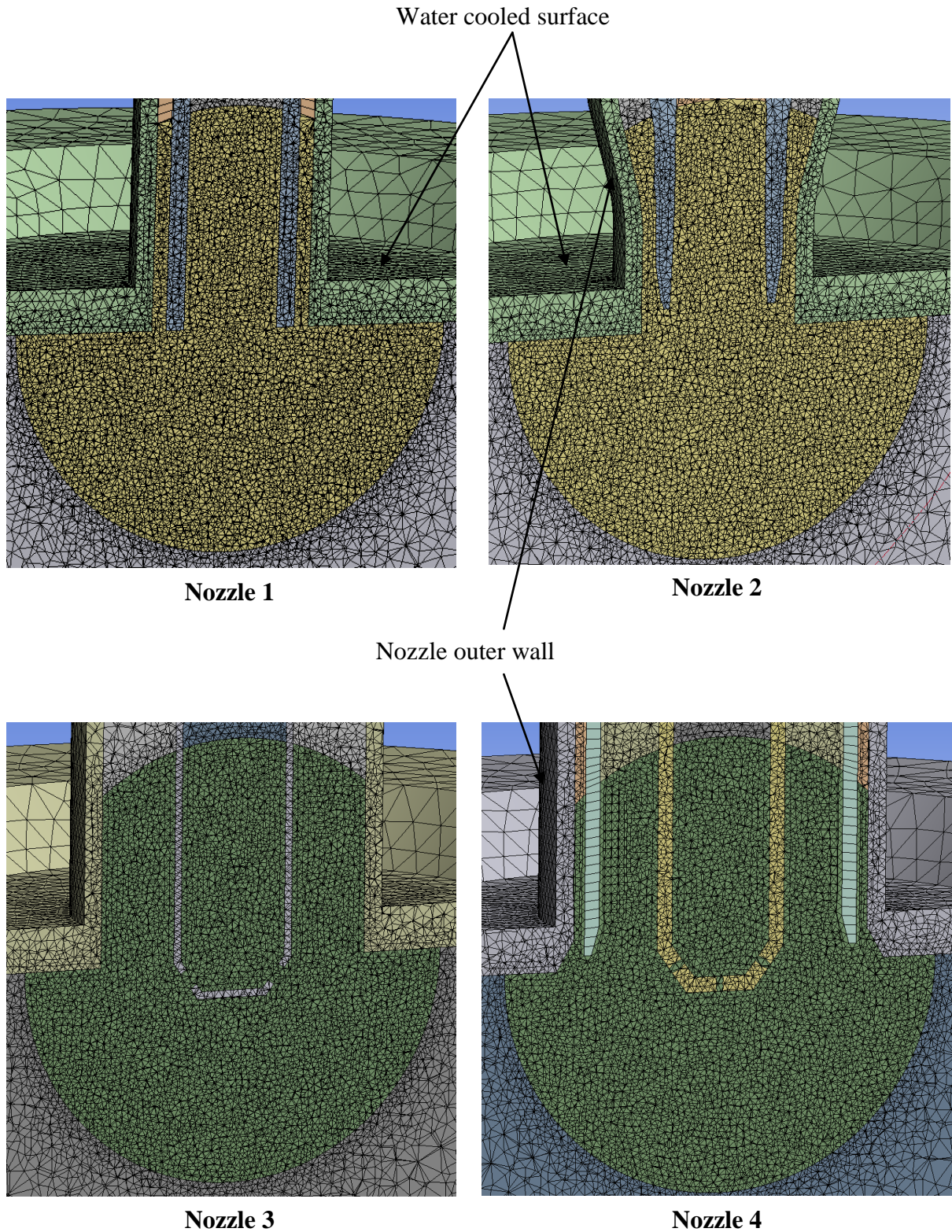


Fig. 5.4: Zoom in view of mesh of different nozzles

5.4 CFD modeling approach

Computational fluid dynamics (CFD) modeling methodology (i.e. discrete phase modeling) and the physical models prescribed in Chapter 4 are applied to the current operating conditions and nozzle designs. Based on the findings of mesh analysis (given in Chapter 4), fine mesh with around 550,000 polyhedral cells is used in all simulation cases. Mesh characteristics of furnace with Nozzle 1 have already been discussed there, while meshes of the combustor with Nozzle 2, Nozzle 3 and Nozzle 4 are given in Appendix B, Figs. B6-B8. Figure 5.4 shows the computational grid (close view of nozzle) for all four cases. The outer surface of the roof of the furnace is assumed to be cooled by water (Chapter 4) in all four cases.

5.5 Results with Data Set 1: Study of different nozzle geometries

Similar to the base case simulations, it is observed that radiation is responsible for heat transfer to the walls of the combustion plant. High temperature is shifted by conduction from insulated inner walls to water cooled surface. Water cooling reduces the temperature of the roof of the furnace. However, the partition wall of the nozzle section is directly exposed to the hot combustion zone which increases the nozzle tip temperature. The simulation results obtained from nozzle air flow rates provided in Data Set 1 are discussed in the following.

5.5.1 Temperature distribution

Depending upon the nozzle design and cross sectional area, all nozzles have different injection and flow patterns of fuel moving through them. These differences lead to a significant variation in mixing as well as temperature distributions in the combustion chamber.

Figure 5.5a illustrates the temperature fields (with Data Set 1) in the combustion zone of the pulverized fuel combustion plant with Nozzle 1 to Nozzle 4. Among others, a variation in the maximum combustion temperature is found in the combustion zone. Table 5.3 shows the maximum temperature, distance of maximum temperature from the injection plane and outlet temperature of the four cases of nozzle geometry (see also Appendix B, Fig. B11). Geometric dimensions, specifically the cross sectional area of the air inlet, are known to have a strong influence on combustion temperature [114].

Table 5.3: Temperature results with Data Set 1

Nozzle	Max. temperature	Distance from injection	Outlet temperature
Nozzle 1	1834°C	350 mm	1092°C
Nozzle 2	1812°C	377 mm	1094°C
Nozzle 3	1775°C	360 mm	1077°C
Nozzle 4	1837°C	382 mm	1035°C

Nozzle 1 and Nozzle 2 have nearly the same diameters of inner section and outer section near the injection plane, hence in both cases nearly the same pattern of combustion temperatures is

found. Quite similar combustion patterns are also found in case of Nozzle 3 and Nozzle 4. As both nozzles spread fuel or cooling air jets through cap holes present at the injection plane, they result in better mixing of fuel and air for the combustion process (Fig. 5.5a). It should also be noted that in both nozzles (Nozzle 3 and Nozzle 4), the perforated plane pushes the incoming fuel stream away from the straight path and hence, hot combustion gas is found further downstream in the combustion furnace. Moreover, recirculation of combustion gases in the chamber affects the combustion zone temperature.

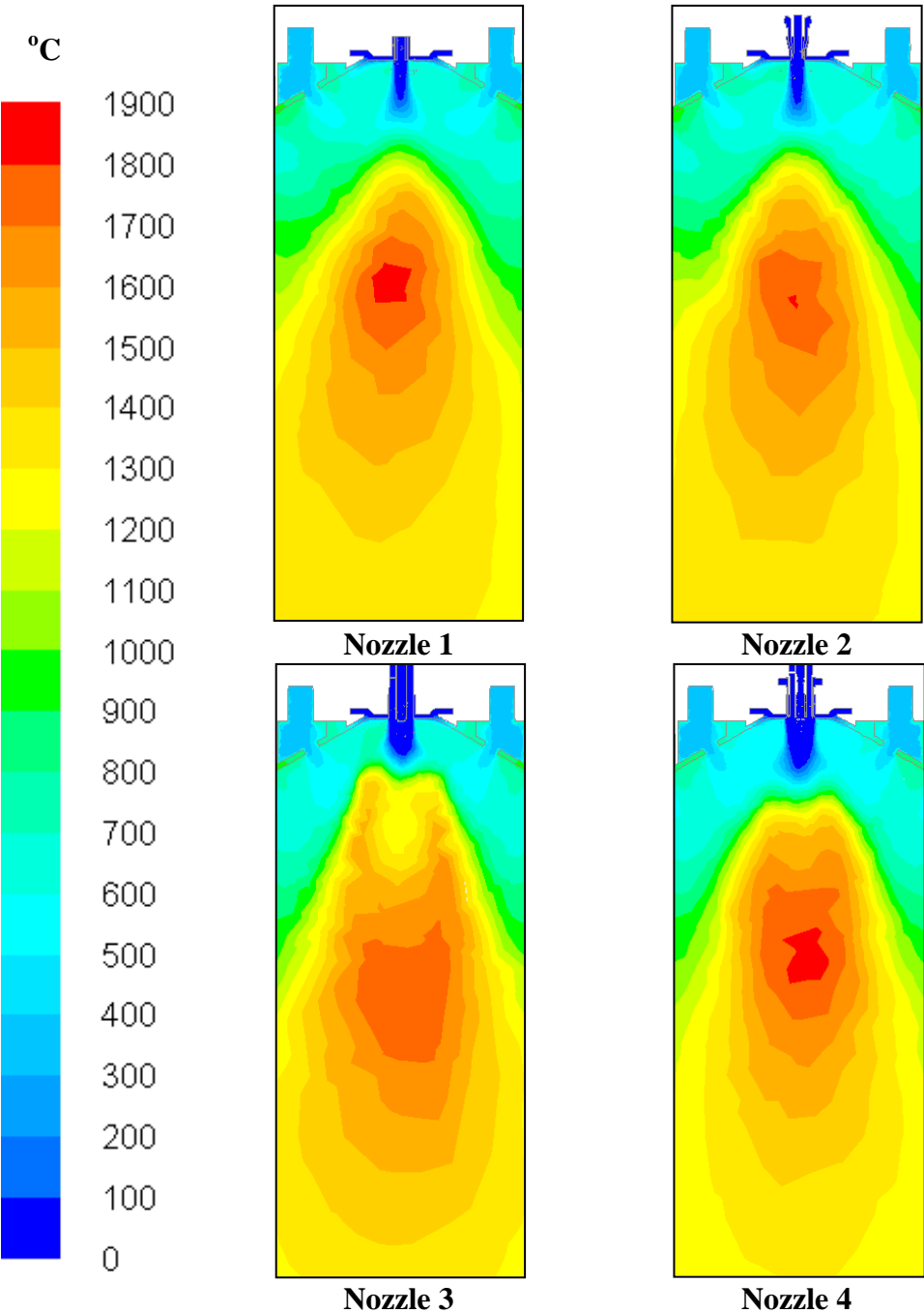


Fig. 5.5a: Contours of combustion temperature with Nozzles 1-4

Figure 5.5b shows the temperature profile along the radial direction in the furnace at an axial distance of 360 mm (-Z) from the injection point. It can be observed that temperature

increases when moving towards the centre of the combustion furnace (at 0 mm). However, the maximum temperature is found at various locations for the different nozzles, depending upon the injection and mixing patterns. Nozzle 1 and Nozzle 2 show similar profiles, as well as Nozzle 3 and Nozzle 4.

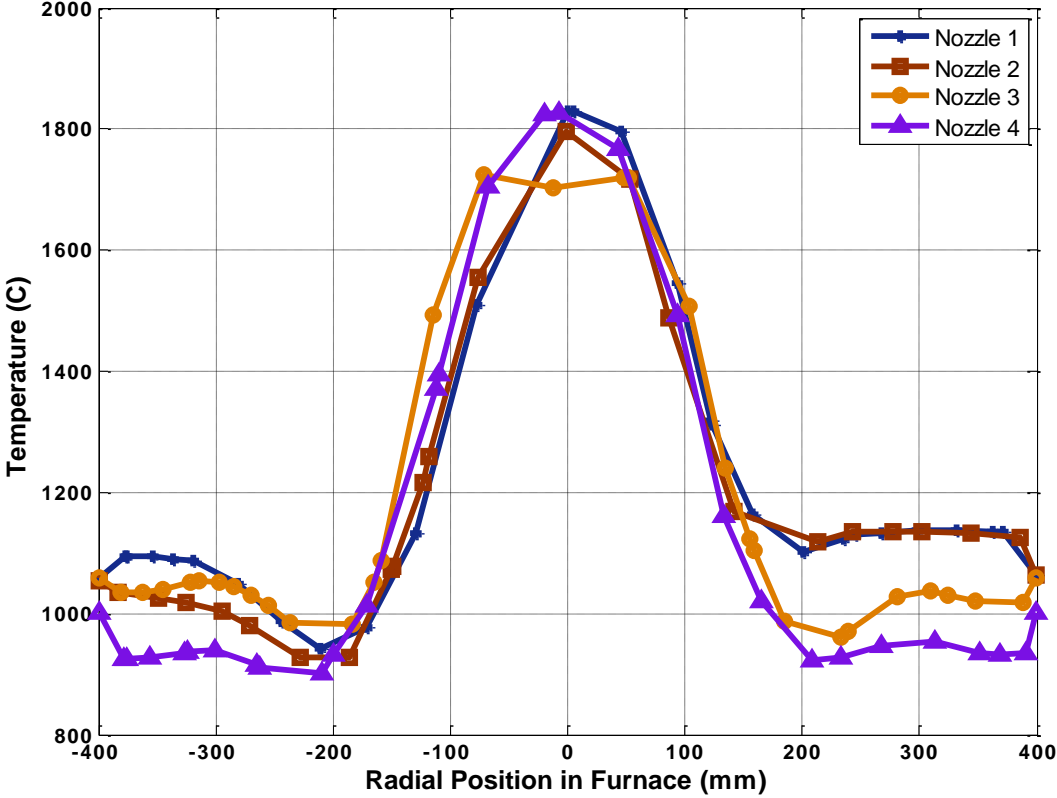


Fig. 5.5b: Radial temperature profiles in the furnace with Nozzles 1 to 4 (at Z = -360 mm)

5.5.2 Nozzle 1

A high combustion temperature at the combustion zone (1834°C) is responsible for high heat transfer by radiation in the combustion plant, especially to the fuel nozzle. A close up view of the nozzle (Fig. 5.6) shows the temperature distribution in both sections of this fuel nozzle. The temperature of the fluid (air and fuel) in the inner section of the nozzle is observed to be about 25°C, i.e. close to the inlet fuel temperature. However, the temperature of the partition wall between inner and outer section is observed to be quite high, ranging from 60-90°C. This wall of the nozzle even showed higher temperature than 90°C at the fuel injection plane (Fig. 5.6). As described previously, this high temperature is the result of direct radiation from the combustion zone. As the fuel has a melting point of around 60°C, the fuel can start melting and convert into agglomerates at over 90°C. Such sticky material can block the fuel nozzle sections and cause a break-down of operation and damage in the combustion plant.

5.5.3 Nozzle 2

The temperature distribution in the close up view of Nozzle 2 shows that the temperature of fluid in the inner section of the nozzle is similar as in Nozzle 1, i.e. around 25°C. However,

the partition wall between inner and outer section is observed to be at 50-65°C. The significant reduction in temperature is due to better design of Nozzle 2 than Nozzle 1, i.e. the lower part of Nozzle 2 is thinner and less exposed to the incoming radiation as compared to Nozzle 1 (Fig. 5.2).

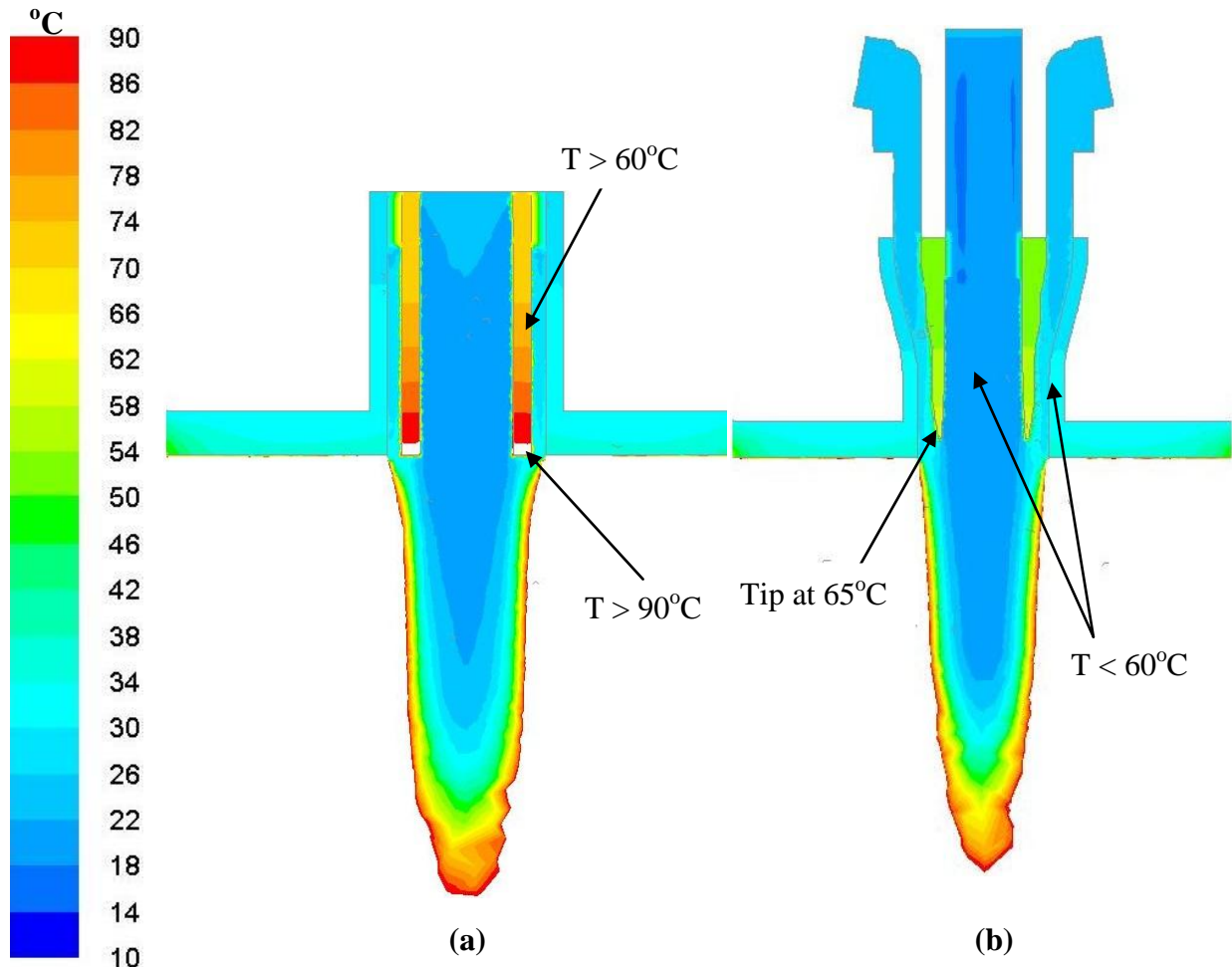


Fig. 5.6: Temperature profiles through Nozzle 1 (a) and Nozzle 2 (b)

Moreover, the zigzag shape at the partition wall between inner and outer section (as shown in Fig. 5.3) increases the surface area and hence, the heat dissipation. As described before, the temperature of nozzle increases from top to the bottom (tip) of nozzle and maximum temperature of nozzle partition wall is found at this tip. Therefore, heat conduction is studied only at the highlighted areas of Fig. 5.1 with the aim to reduce the lower tip temperature to less than 60°C. Further up in the partition wall, this has a temperature of 55°C which is lower than the permissible limit (i.e. melting point of fuel) but very close to it. This temperature increases gradually while moving downwards. The tip of partition wall at the injection plane, therefore, also in case of Nozzle 2 is still at a temperature higher than the allowable limit, i.e. at 65°C (Fig. 5.6). Being directly in contact with the incoming fuel, this may locally cause melting of the fuel.

5.5.4 Nozzle 3

Due to a quite different geometrical design, temperature investigations for the case of Nozzle 3 show different results than for the previous two nozzles. Nozzle 3 has a larger diameter than Nozzle 1 and Nozzle 2. Moreover, it has a perforated cap at the injection plane, which spreads the fuel when entering the combustion chamber. This leads to the generation of a wider flame with a maximum temperature in the combustion zone around 1775°C (Fig. 5.5a). The temperature within the nozzle remains quite low and within the permissible limit (i.e. under 60°C). During the fuel transport, the temperature is noted to be at 29°C in both sections of the nozzle; however, temperature rises to 64°C near the injection plane. In the thin wall around the cap of the fuel nozzle a very high temperature, i.e. 195°C is observed, which implies that the fuel might be heated up well above its melting point there (Fig. 5.7).

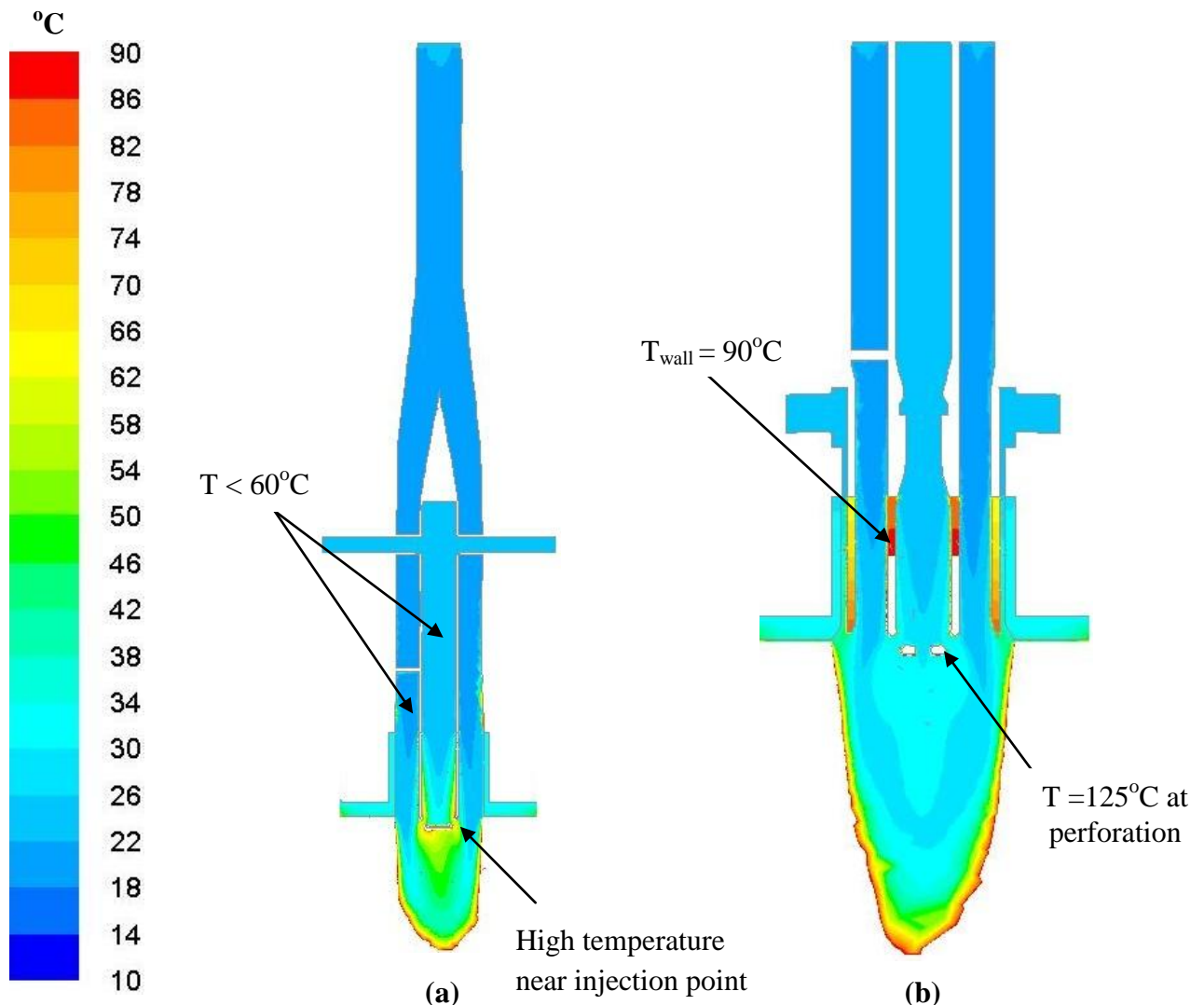


Fig. 5.7: Temperature profiles through Nozzle 3 (a) and Nozzle 4 (b)

5.5.5 Nozzle 4

Nozzle 4 is designed with an additional inner section. Simulation results reveal that the temperature in the combustion zone is 1837°C (Fig. 5.5a). A close up view (Fig. 5.7) shows that the temperature in all three sections of the nozzle is at 25-27°C in the upper part of the nozzle, however, there is a high temperature just near the injection point which is basically a critical point for fuel transportation into the furnace. The wall between middle and outer section has high temperatures in the range of 70 to 90°C, whereas the temperature of the wall between inner and middle section and of the inner section cap can be noted to be even much more than 90°C (i.e. 125°C). This may increase the temperature of incoming fuel and form a semi-molten material. This material can stick near the holes of the perforated cap (Fig. 5.2) and cause clogging of these holes.

5.6 Modifications in nozzle air

The simulation results with inlet conditions defined in previous section (Data Set 1) show a very significant variation of temperature profiles depending upon the nozzle geometries and injection patterns. However, there is still a risk in all the nozzle designs to melt the fuel before entering to the combustion chamber, as the temperature of nozzle walls is noted to be greater than 60°C. In order to bring the nozzle temperature below the melting point of the incoming fuel, a modification in the boundary conditions (nozzle air) is made. However, the mass flow of pulverized fuel is kept same, i.e. at 20 kg h⁻¹. The nozzle air is increased in such a way that the total air flow rate is equal (40 m³ h⁻¹) in all four cases (Table 5.4). All other boundary conditions and modeling parameters are kept unchanged.

Table 5.4: Modified nozzle air flow rates (Data Set 2)

Nozzle section	Nozzle 1	Nozzle 2	Nozzle 3	Nozzle 4	Temperature
Nozzle inner section	20 m ³ h ⁻¹ (FTA)	20 m ³ h ⁻¹ (FTA)	10 m ³ h ⁻¹	15 m ³ h ⁻¹	25°C
Nozzle middle section	-	-	-	20 m ³ h ⁻¹ (FTA)	25°C
Nozzle outer section	20 m ³ h ⁻¹	20 m ³ h ⁻¹	30 m ³ h ⁻¹ (FTA)	5 m ³ h ⁻¹	25°C
Total	40 m ³ h ⁻¹	25°C			

5.7 Results with Data Set 2: Study with modified nozzle air flow rates

Similar modeling approach is applied to the new operating conditions (Table 5.4). Simulation results with modified air flow rates given by Data Set 2 are discussed in the following.

5.7.1 Temperature distribution

Similar to the previous results, a different temperature distribution is obtained for each of the four nozzle designs, depending upon the nozzle cross section area and different air flow injection patterns.

Table 5.5: Temperature results with Data Set 2

Nozzle	Max. temperature	Distance from injection	Outlet temperature
Nozzle 1	1465°C	389 mm	1042°C
Nozzle 2	1505°C	380 mm	1043°C
Nozzle 3	1842°C	384 mm	1042°C
Nozzle 4	1833°C	380 mm	1040°C

A significant difference is found in the temperature profiles also because of the modification of the air flow rates. However, a similar outlet temperature is observed in all cases because of the same total air flow rate and hence, the excess air ratio. On the other hand, the outlet temperature decreases to 1042°C from 1092°C by increasing the nozzle air flow rate from 23 m³ h⁻¹ to 40 m³ h⁻¹ (in case of Nozzle 1). This is due to the presence of more air for the combustion of the same amount of solid fuel and, hence, resulting lean conditions. In case of Nozzle 4, the outlet temperature increases slightly, i.e. from 1035°C to 1040°C which is because of decreasing the total nozzle air flow rate from 42 m³ h⁻¹ to 40 m³ h⁻¹ to make an equal air flow rate. The combustion zone also shifts slightly downwards due to increasing the air supply for Nozzles 1 to 3. Maximum temperature is observed at a position of around 380 mm in the furnace from the injection plane (Table 5.5).

Figure 5.8a shows the temperature fields in the combustion zone for all four nozzles. It is interesting to note that a significant reduction in maximum temperature is revealed in the cases of Nozzle 1 and Nozzle 2 (Fig. 5.8), as nozzle air is significantly increased in these cases (Appendix B, Fig. B13). Radial profiles of temperature in the combustion zone are illustrated in Fig. 5.8b at a vertical (axial) position of 380 mm from the injection plane. Nozzle 1 and Nozzle 2 have similar profiles, and the same holds for Nozzle 3 and Nozzle 4. As described before, this is due to similar geometries of the nozzles. The temperature near the furnace walls is observed to be very high, i.e. around 1000°C. This temperature increases gradually while moving towards the centre of the furnace and reaches to its maximum value at the centre of the furnace. It should be noted that maximum temperature in the combustion zone also depends upon the mixing patterns of air and solid fuel particles.

It has been reported previously by Galletti et al. [114] that air excess has a great influence on the combustion temperatures. They found in their studies that with the same inlet cross sectional area, combustion temperature decreased from 2265 K to 2080 K by increasing the air excess from 16% to 46%.

The maximum combustion temperature in case of Nozzle 2 is predicted as 1505°C (with modified nozzle air flow rate, i.e. 40 m³ h⁻¹) which also agrees well (qualitatively) with the previous studies conducted by Stroh et al. [106] where a maximum gas temperature was achieved at 1500°C with transport air of 0.01257 kg s⁻¹ (35 m³ h⁻¹). Comparing Data Sets 1 and 2, the combustion temperature difference in case of Nozzle 4 is not as prominent, because

there is not much difference in nozzle air flow rates through this nozzle between Data Set 1 and Data Set 2.

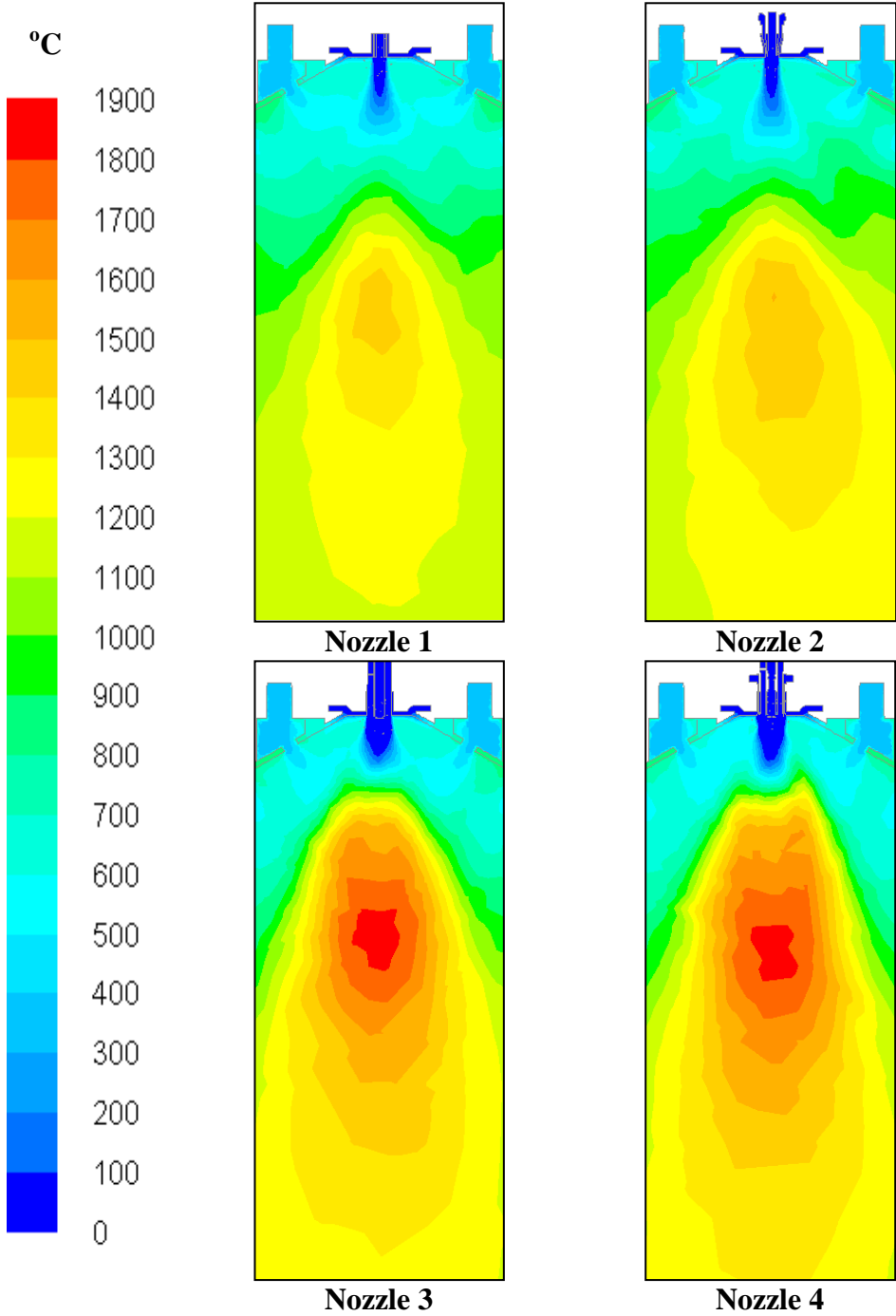


Fig. 5.8a: Contours of combustion temperature with modified nozzle air flow rates

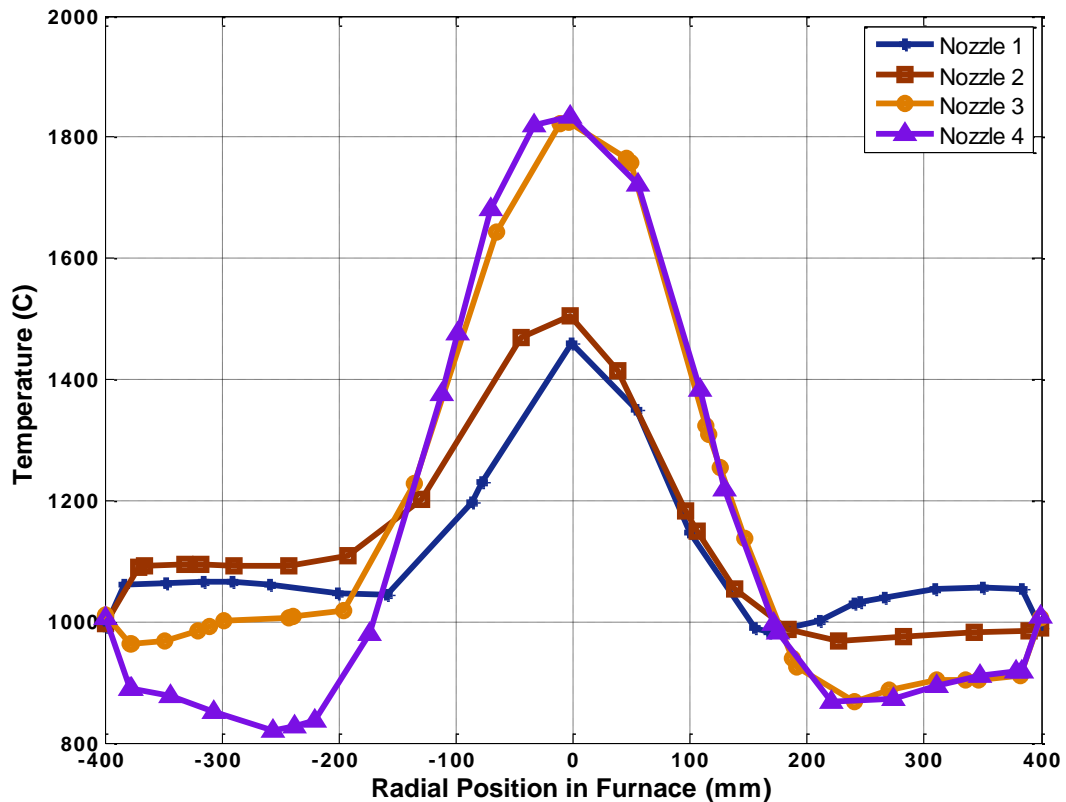


Fig. 5.8b: Radial temperature profiles in the furnace with Nozzles 1 to 4 (Data Set 2) (at Z = -380 mm)

A comparison of nozzle temperatures between the two cases (Data Set 1 and Data Set 2) is given in the following.

5.7.2 Nozzle 1

The simulation results indicate that with the modified nozzle air flow rates (Data Set 2), the temperature within the nozzle is also reduced significantly, i.e. a reduction of approximately 20 K is noted. Figure 5.9 shows the temperature profiles in Nozzle 1 with previous air flow rates (Data Set 1) and modified air flow rates (Data Set 2) as well.

It is interesting to note that the temperature at the partition wall between inner and outer section of the nozzle which was at 90°C with the previous nozzle air flow rates (Data Set 1) has been reduced to 65°C. This implies that there is a strong influence of nozzle air flow rate on the temperature profile in the nozzle during fuel transportation. A reduction in temperature of about 20 K is observed by increasing the nozzle air flow rate by a factor of 1.75. However, near the injection point the temperature is still higher than the melting point of the fuel. It is also noted that the temperature in both cases increases gradually while moving from top towards the furnace, which is due to the thermal exposure of the nozzle to the combustion chamber (Fig. 5.9).

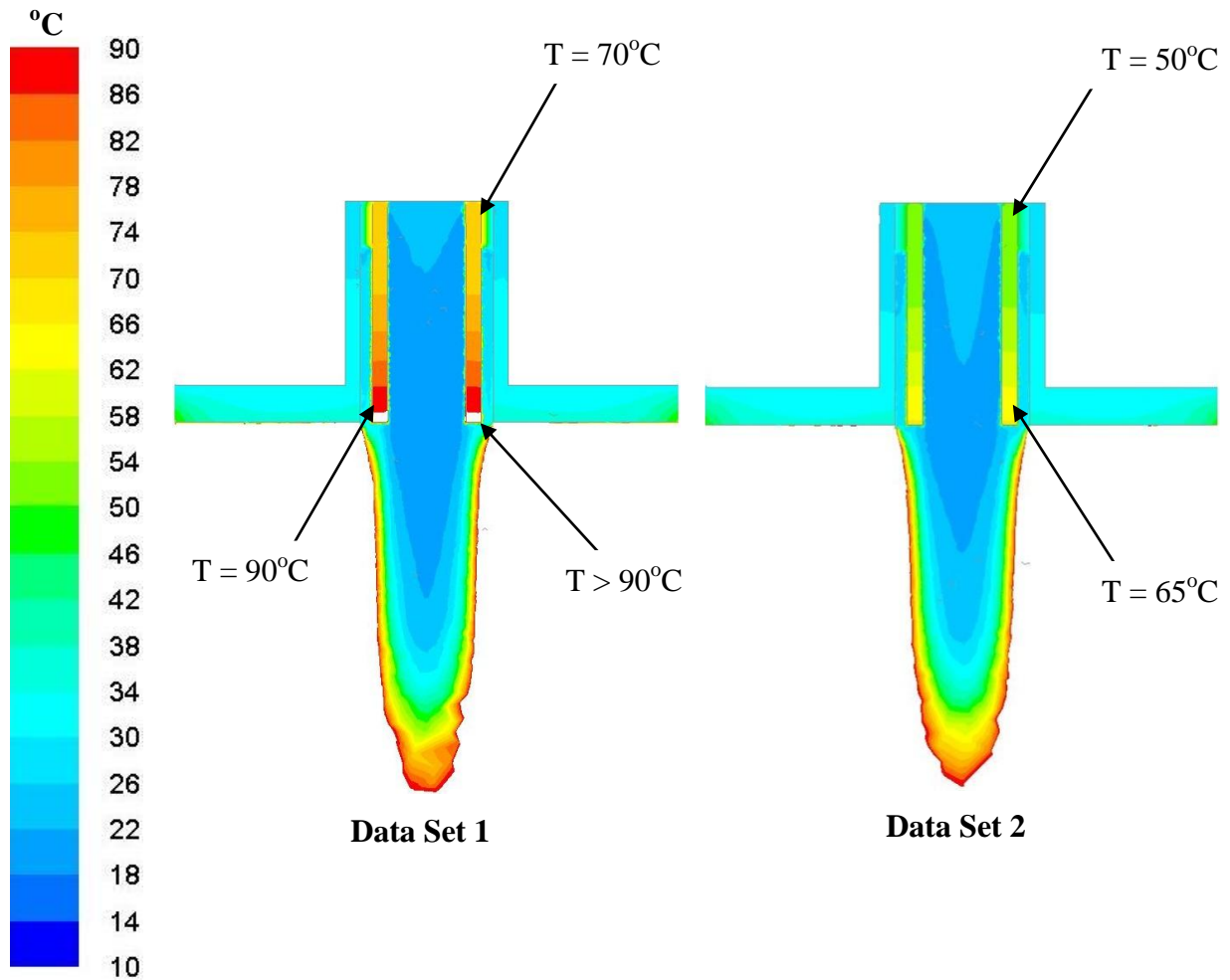


Fig. 5.9: Temperature profiles in Nozzle 1 with Data Set 1 and Data Set 2

5.7.3 Nozzle 2

Figure 5.10 represents the temperature profiles in Nozzle 2 for both cases, i.e. Data Set 1 and Data Set 2. In Nozzle 2, similarly to Nozzle 1, a significant reduction in temperature is observed with the modified air flow rates. By increasing total air flow rate from $23 \text{ m}^3 \text{ h}^{-1}$ to $40 \text{ m}^3 \text{ h}^{-1}$ (by a factor of 1.75) a reduction in the maximum temperature is noted from 65°C to 48°C . This shows that nozzle air has a strong influence on the temperature profile in the fuel nozzle. The temperature at the injection plane, i.e. at the tip of the wall between inner and outer section, is at 48°C , which is quite below the melting point of fuel.

Favorable behavior of Nozzle 2 is, as already mentioned, supported by the fact that the tip of the partition wall between inner and outer section is narrow (Fig. 5.1) and indented by 3 mm in respect to the roof (Fig. 5.2), so that it is less directly exposed to the radiation coming from the combustion zone.

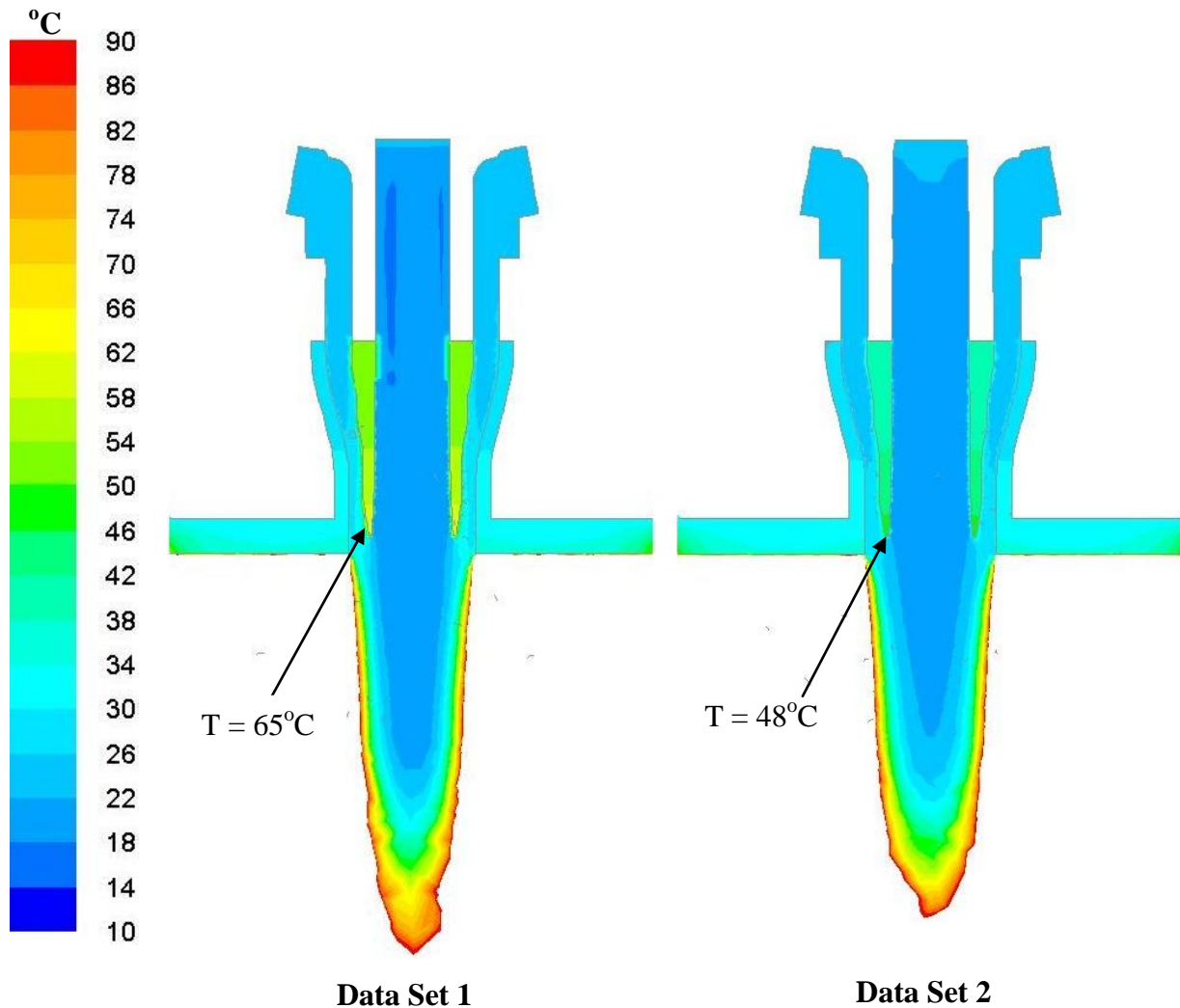


Fig. 5.10: Temperature profiles in Nozzle 2 with Data Set 1 and Data Set 2

Moreover, inflection of flow due to the shape of the walls and changing cross-sectional area of the outer section (down to very low value in the narrowest position) play an important role in better heat transfer to cooling air. The zigzag surface at the outer surface of the partition wall between inner and outer section (as shown in Fig. 5.3) increases the surface area and, hence, enhances the cooling effect. Therefore, the partition wall temperature, which was too high for the incoming fuel before, is reduced below the permissible limit with the modified flow rates.

5.7.4 Nozzle 3

In case of Nozzle 3, the air flow rate has been increased from $25 \text{ m}^3 \text{ h}^{-1}$ to $30 \text{ m}^3 \text{ h}^{-1}$ in the outer section (FTA) and from $2 \text{ m}^3 \text{ h}^{-1}$ to $10 \text{ m}^3 \text{ h}^{-1}$ in the inner section (CA) of the nozzle to make a total air flow rate of $40 \text{ m}^3 \text{ h}^{-1}$. Simulation results with modified flow rates show the temperature in both sections of the nozzle to be approximately the same as before (i.e. 27°C). However, with the increase in air flow rate in both sections, the temperature near the injection point is reduced significantly (Fig. 5.11).

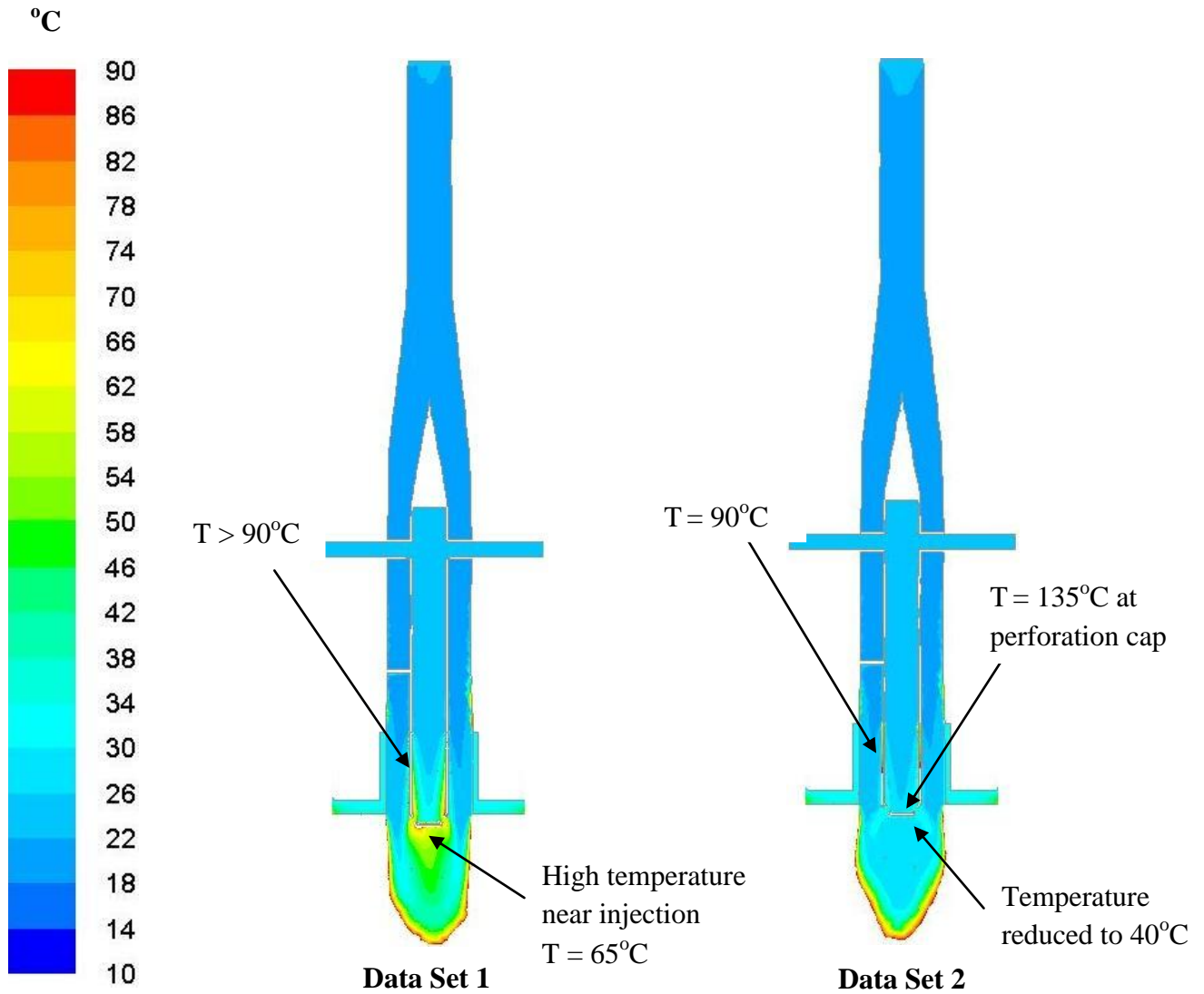


Fig. 5.11: Temperature profiles in Nozzle 3 with Data Set 1 and Data Set 2

With the nozzle air flow rates given in Data Set 1 (Table 5.1), the temperature below the perforated injection cap can be observed to be about 64°C which is reduced to 40°C with the modified flow rates in Data Set 2 (Table 5.4). However, the thin partition wall between inner and outer section and its perforated cap are still at a temperature of more than 90°C , which may become responsible for the melting of incoming fuel. It is also interesting to note that the temperature of the perforated cap is reduced to 135°C by increasing the nozzle air flow rate from Data Set 1 to Data Set 2.

5.7.5 Nozzle 4

In Nozzle 4, there is a minor difference in the flow rates between Data Set 1 and Data Set 2. The nozzle air flow rate in the inner section has been increased from $10\text{ m}^3\text{ h}^{-1}$ to $15\text{ m}^3\text{ h}^{-1}$, while in the middle section it is reduced from $25\text{ m}^3\text{ h}^{-1}$ to $20\text{ m}^3\text{ h}^{-1}$ and in the outer section it is reduced from $7\text{ m}^3\text{ h}^{-1}$ to $5\text{ m}^3\text{ h}^{-1}$ in order to make a total nozzle air flow rate equal to $40\text{ m}^3\text{ h}^{-1}$. A further increase in nozzle air flow rate may reduce the combustion temperature too much, extinct the flame or prevent ignition. Moreover, a too high flow rate in the inner section may spread the fuel towards the furnace side walls. Having a low difference in nozzle air flow

rate there is no much difference between the two cases (Fig. 5.12). However, it can be noted that the temperature at the partition wall between inner and middle section of the nozzle is reduced in case of Data Set 2. Parts of this wall, which were at 90°C with Data Set 1, are reduced to 80°C with the modified flow rates. But still the temperature at the critical position, i.e. injection plane, is around 120°C. As stated before, the high temperature just near the injection point (critical point) creates a very sensitive situation for the incoming fuel and hence there remains a high risk of clogging the nozzle with melted fuel.

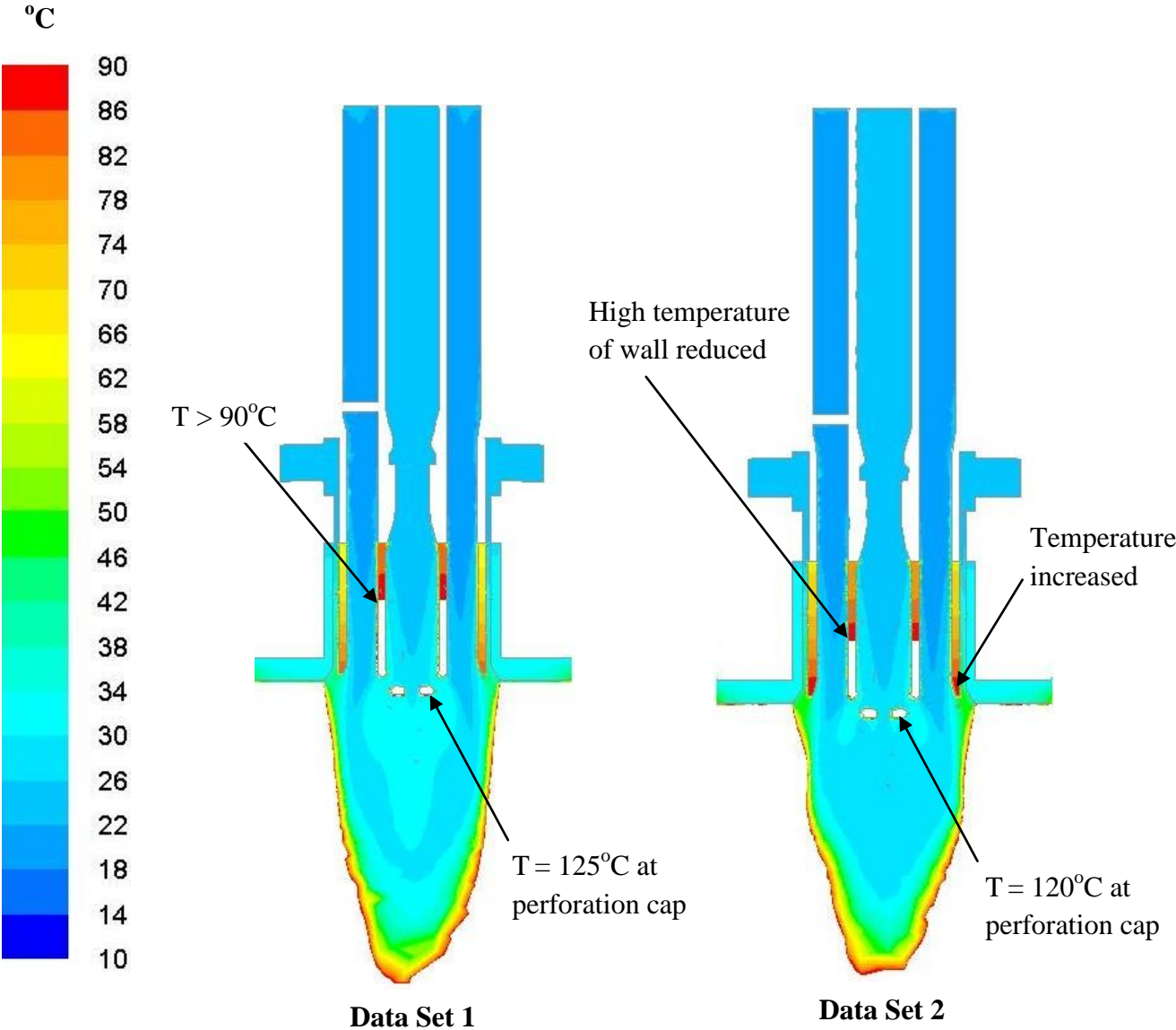


Fig. 5.12: Temperature profiles in Nozzle 4 with Data Set 1 and Data Set 2

5.8 Study of different fuel particle sizes

The investigations conducted with different nozzle air flow rates (Section 5.7) revealed that there is a significant effect of nozzle air flow on temperature profiles within the nozzle sections. The results have shown a significant reduction of tip temperature, and Nozzle 2 is found to have nozzle (tip) temperature under the permissible limit, i.e. less than 60°C, during the transportation of pulverized fuel with average particle size of 10 µm.

In order to check the effect of different fuel particle sizes on the combustion behavior and the resulting temperature of the fuel nozzle, a further investigation is carried out with different fuel particle sizes. Three different classes of fuel particle size, i.e. 2 µm, 10 µm and 20 µm, are analyzed in this study. The selection of fuel particle size is based on the particle size distribution described earlier in Section 4.2.

The current investigations are conducted for the nozzle geometries 2 and 3. Nozzle 2 is the only one to have shown the permissible temperature so far among all the nozzles while Nozzle 3 is selected in order to check the further effect on the extension of the region with too high temperature in the partition wall. Nozzle air flow rates are provided as given in Data Set 2 (Table 5.4). Numerical simulations are conducted with the same modeling approach and ANSYS (Fluent) settings as described in Chapter 4.

According to literature, pulverized solid fuels of different particle sizes behave in a very diverse way. Aerodynamics and mixing patterns at the combustion are significantly affected, if particle size is altered. Particle size of solid fuel also influences the heat and mass transfer mechanisms in several ways. For example, Sun et al. [141] presented a study about the effect of different particle size on the combustion process and reported that the combustion process is affected by fuel particle size by different means. Two-phase heat and mass transfer between solid and gas is influenced by particle size. The smaller the fuel particle size, the higher is the char burning rate. Moreover, a decrease in particle size reduces the temperature difference between solid and gas. Small fuel particles have a greater capability to absorb radiation; hence they increase heat propagation by means of radiation. A high burning rate of volatiles is found with smaller particles; therefore, with a smaller particle size combustion takes place earlier and faster as well. However, large fuel particles have higher temperature than the smaller ones [141].

Results of temperature distribution with smaller and larger particle size than the reference case (10 µm) are discussed in the following.

5.8.1 Temperature distribution with small fuel particle size

The study conducted with average fuel particle size of 2 μm shows that finer fuel particles result in shorter but wider combustion zones (Fig. 5.13). The main reason for this wider combustion zone is faster volatile release and rapid combustion of finer particles close to the nozzle outlet. In other words, when particles are injected into the combustion chamber, they undergo a devolatilization process (Chapter 3). This process is observed to be faster for smaller particle size. As described before, small particles have more capability to absorb heat (radiation) responsible for the larger volume of the high temperature zone. Being smaller in size, there is very small temperature difference between solid particles and air [141]. Due to the wider combustion zone, the thermal effect (heat transfer) is high. As a result, the lower section of the fuel nozzle faces more radiation from the combustion chamber.

Figure 5.14 shows the temperature distribution in Nozzle 2 with different particle sizes, i.e. 2 μm , 10 μm and 20 μm . A wider combustion zone can be observed in case of smaller particle size, i.e. 2 μm . As volatiles are released near the nozzle exit, the maximum temperature zone is observed to be very close to the nozzle. As a result, the nozzle walls face very high radiation from the combustion zone, which increases the temperature of the nozzle tip. In this way, smaller particle sizes result in a comparatively high temperature as compared to the larger particles. The temperature in the lower part of nozzle wall is noted to be at 50°C for Nozzle 2 (Fig. 5.14).

Similarly, as Nozzle 3 creates a good spray of fuel and nozzle air through the openings present in the injection cap resulting in better mixing of fuel and air for the combustion process, a wider region of high temperature (combustion zone) in case of small particle size is observed (Fig. 5.15). Being directly faced to the radiation (from the wider combustion zone), a very high temperature is observed near the injection point of Nozzle 3 (Fig. 5.16) with smaller particle size.

5.8.2 Temperature distribution with large fuel particle size

The simulation conducted with larger particle size reveals that combustion characteristics are significantly influenced by the increase in fuel particle size. Shape and extent of the flame and the combustion zone are transformed to longer from wider by increasing the particle size. This implies that the length of the combustion zone increases, and the volume of the high temperature (wider) region is reduced with an increase in particle size (Figs. 5.13 and 5.15). This is due to slow devolatilization of larger particle further away from the nozzle exit. Other reasons may in practice be the reduction in bulk density, increase in porosity of the fuel (material) and more amount of air surrounding the fuel particles as well. Moreover, being less influenced by gravity, smaller particles spread in the combustion zone, while larger particles tend to fall down making a longer combustion (high temperature) zone [139] [141].

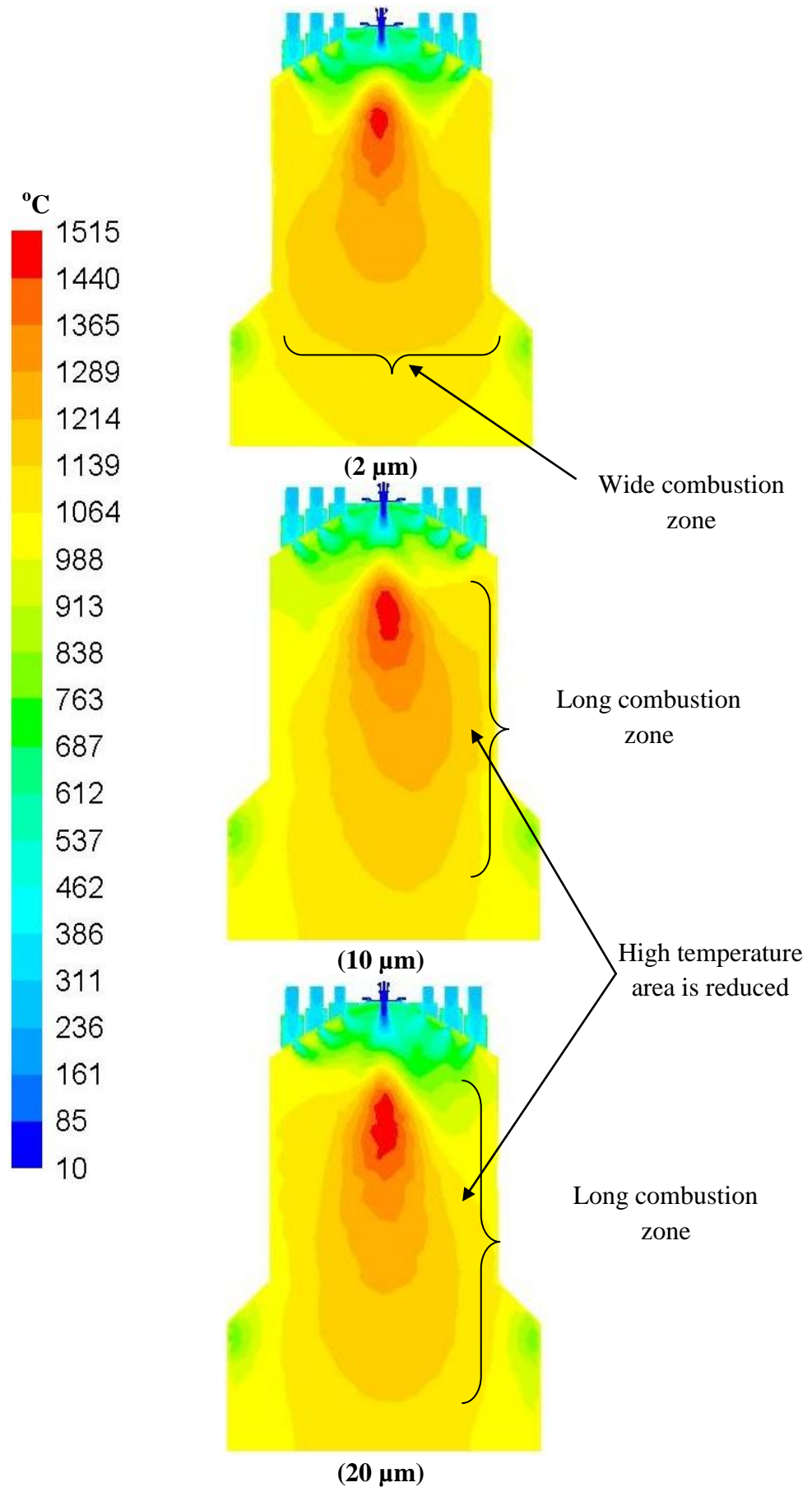


Fig. 5.13: Combustion temperatures with different particle sizes (Nozzle 2)

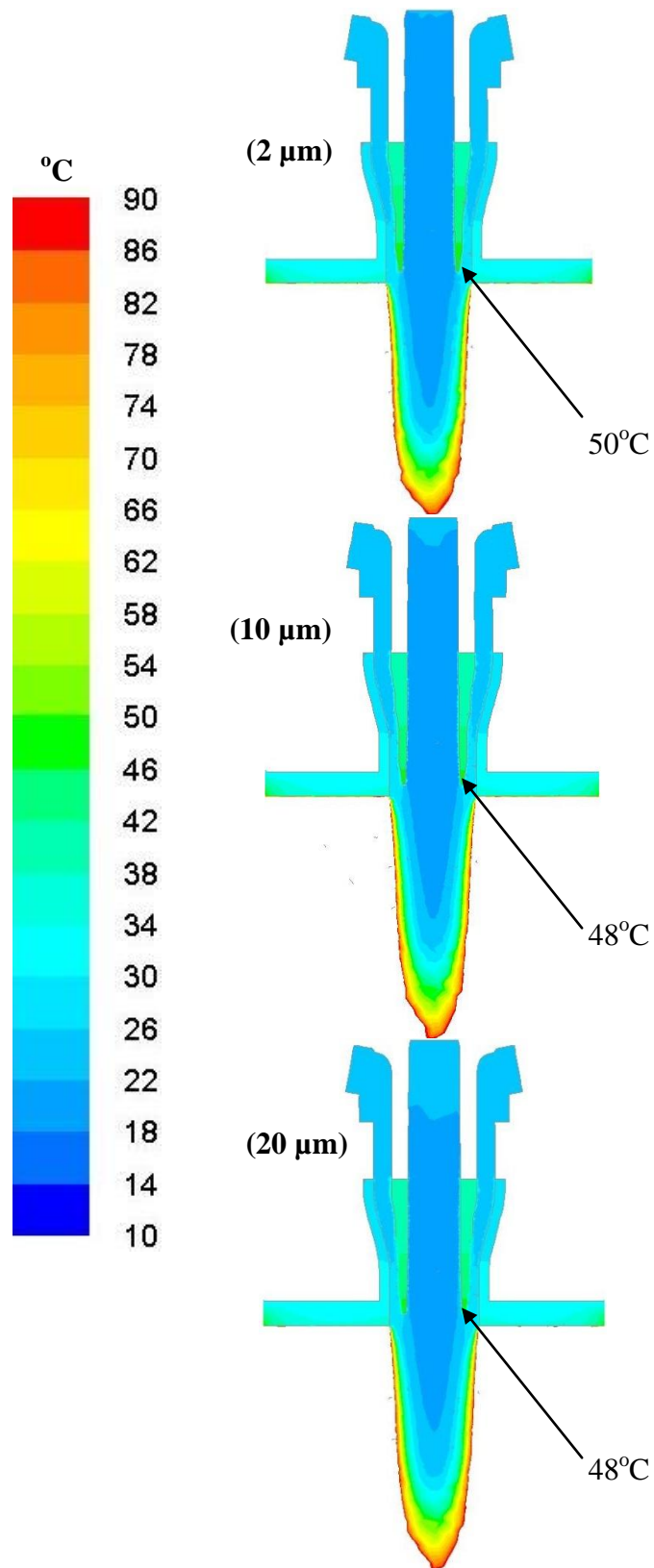


Fig. 5.14: Temperature distribution in Nozzle 2 with different particle sizes

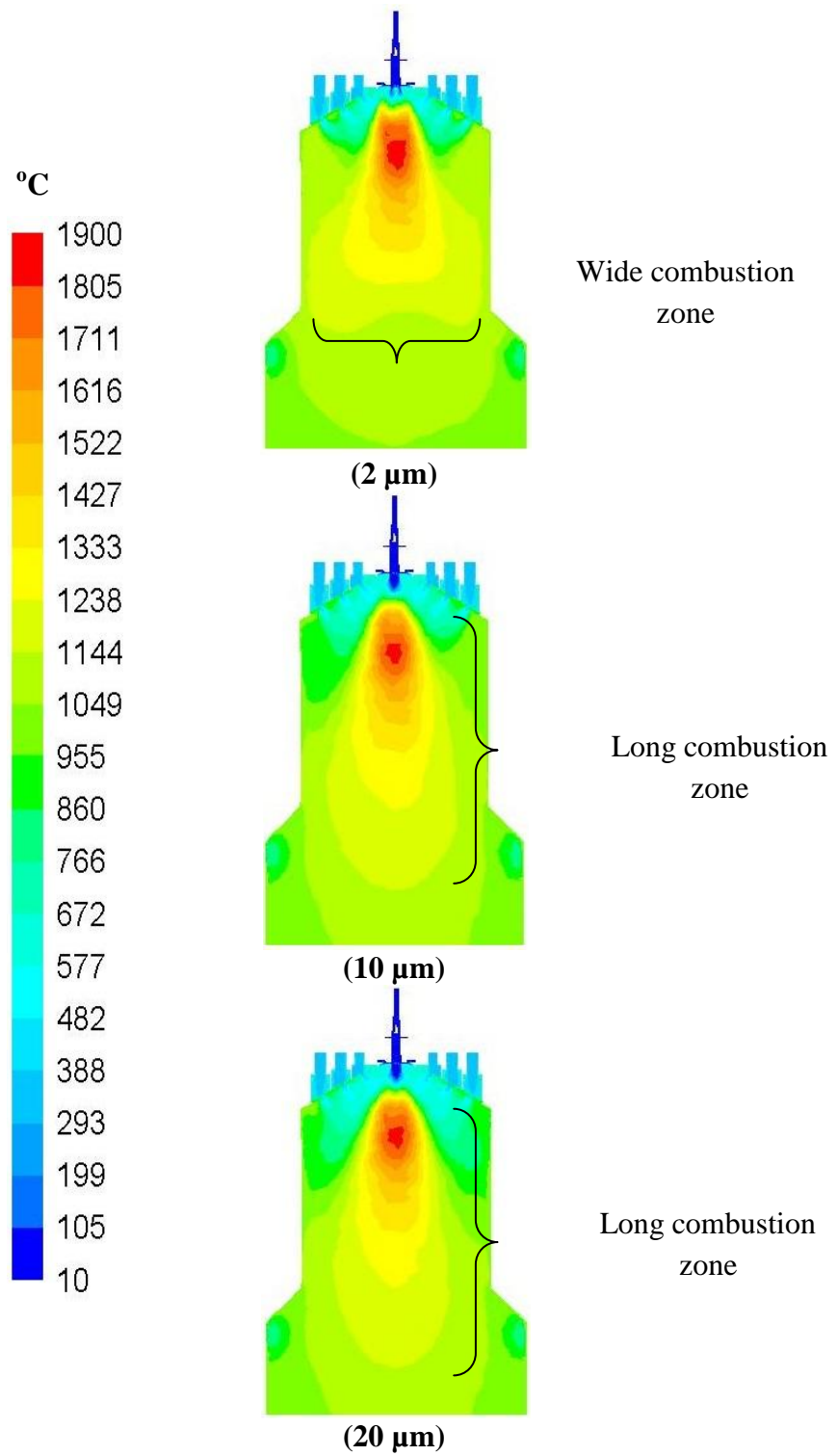


Fig. 5.15: Combustion temperature with different particle sizes (Nozzle 3)

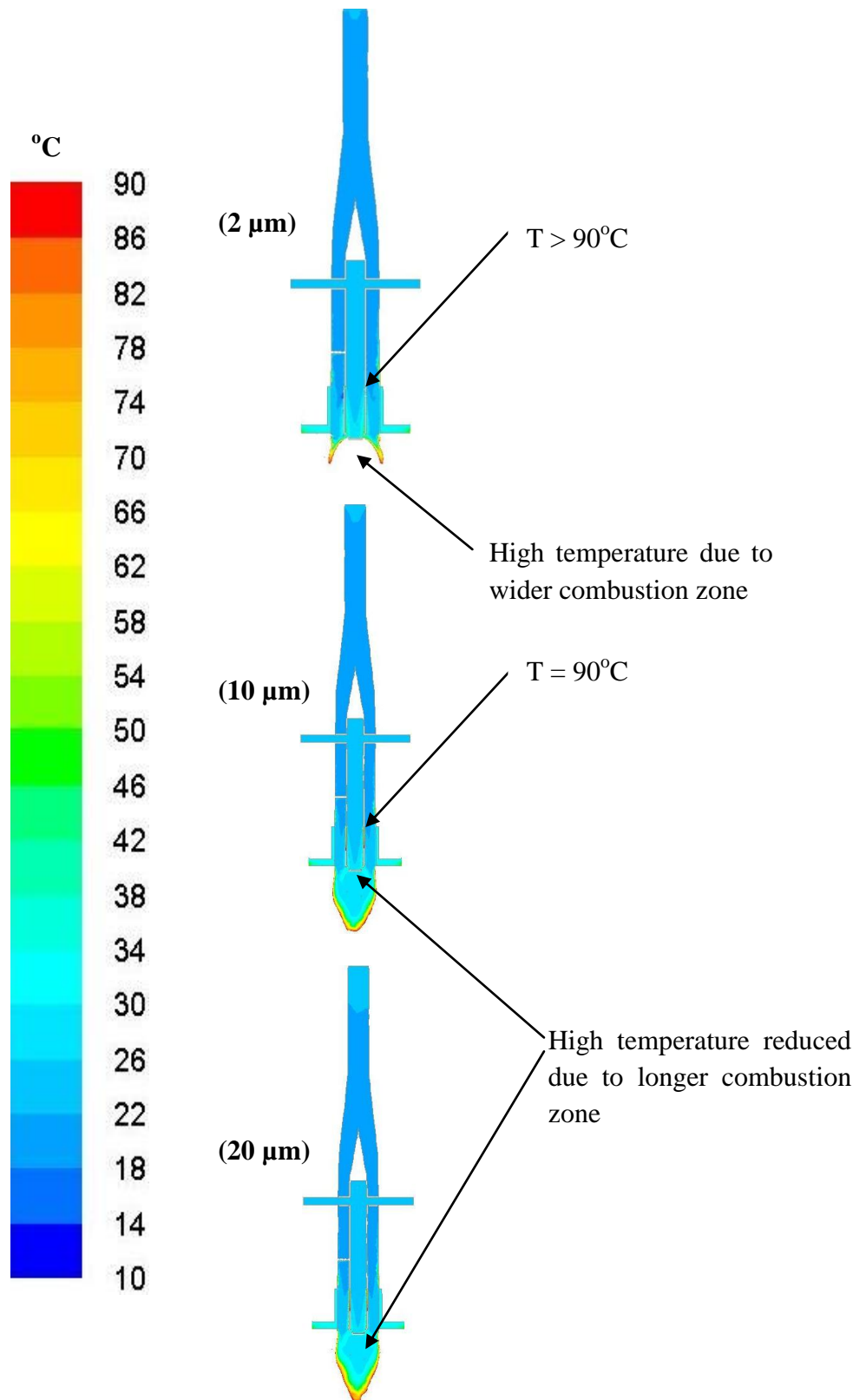


Fig. 5.16: Temperature distribution in Nozzle 3 with different particle sizes

The close-up view of both nozzles shows that the temperature of nozzle wall is reduced by increasing the fuel particle size (Figs. 5.14 and 5.16). The reduction in nozzle wall temperature is due to the poor convective heat transfer of larger sized fuel particles and lower intensity of radiation. For example in case of Nozzle 2, the temperature of nozzle wall (between inner and outer section), which is observed to be at 50°C with smaller particle size (2 μm), decreases to 48°C by increasing the fuel particle size (Fig. 5.14). Similarly, in case of Nozzle 3, a very high temperature is observed at the injection point with the smaller fuel particles, which significantly decreases with the larger fuel particle size (Fig. 5.16).

Ariyaratne et al. [139] also presented a study about the combustion of fuel with different particle size and fuel feeding. They stated that a larger mean particle size of fuel may lead to lower char burnout and incomplete burning. This effect is more prominent for fuels with high carbon content [141]. Fine grinding of fuel is recommended to overcome these issues. However, a decrease in particle size of fuel results in a wider combustion zone close to the burner (Figs. 5.13 and 5.15). It has also been reported earlier [88] that volatile release is initialized in close proximity of the injection nozzle in case of small particle size, while for larger particles volatiles are released further downstream. As a result, volatiles released from small particles react earlier than that of larger particles. Because of intensive volatile burning, high temperature is observed near the nozzle exit in case of small particles.

In the present study, three different particle sizes (2 μm , 10 μm and 20 μm) have been analyzed with Nozzle 2 and Nozzle 3. It can be concluded that too small particle sizes (2 μm) can lead to high nozzle temperature due to increase in thermal effect caused by radiation. While on the other hand a larger particle size (20 μm) shows better results in terms of temperature distribution in the nozzle (as per problem of fuel melting). Figure 5.17 shows the mass fraction of volatiles in the combustion furnace. It can be observed that there is an increase in volatiles mass fraction in the combustion chamber after the injection of fuel. This mass fraction of volatiles is the net result of volatiles production and consumption due to combustion of particles. The increment in volatiles mass fraction is faster in case of small particle size than that of larger size. This is because of faster devolatilization of smaller fuel particles than the larger ones at the combustion zone. Furthermore, complete combustion is observed in all cases of particle sizes in the present study. It can be observed that devolatilization occurs more closer to the nozzle exit in case of smaller particle size of 2 μm as compared to the fuel particle size of 20 μm (Fig. 5.17).

Moreover, it is noted that there is no combustible fraction found at the flue gas outlet which implies that all the combustible species have been completely burnt, i.e. combustion is complete. It is concluded that a comparatively large particle size, i.e. 10-20 μm , can be used for the combustion of pulverized material with low melting point. As described before, too large particles have slower char burning. The slower char burning in case of larger particle size is because of lower particle temperature and poor mixing of the fuel and oxidant in the post combustion zone.

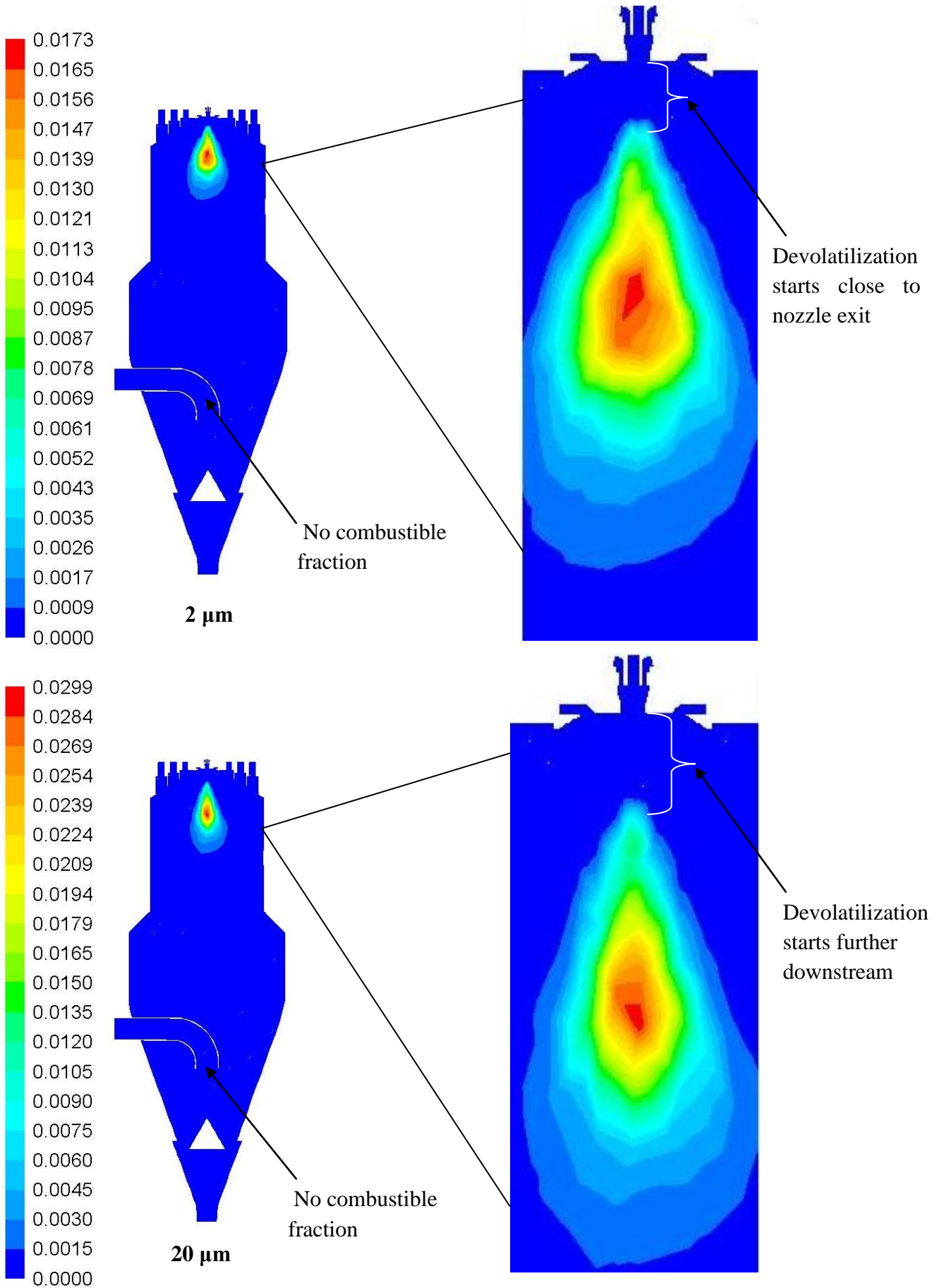


Fig. 5.17: Mass fraction of volatiles with particle size 2 μm and 20 μm (Nozzle 2)

Figure 5.18 illustrates the plot of temperature distribution in case of Nozzle 2 along the central line in the combustion chamber with different fuel particle sizes, i.e. 2 μm , 10 μm and 20 μm . The graphical representation shows the temperature distribution from the top of nozzle (+70 mm) to a distance of 2000 mm inside the combustion plant. It should be noted that the coordinate origin (Chapter 4, see also Appendix B and Table B1) is located at the injection point, i.e. end of the lower part of the nozzle.

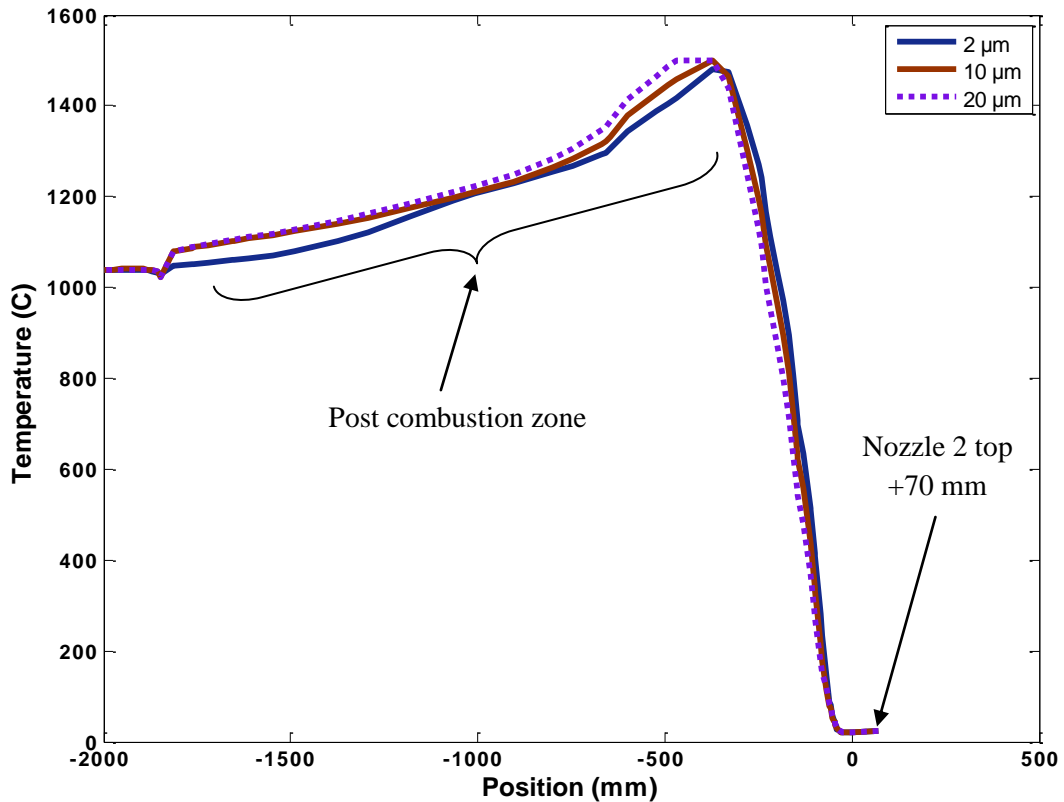


Fig. 5.18: Plot of combustion temperature distribution with Nozzle 2

It can be observed that fuel with a particle size of 2 μm results in a slightly higher temperature than the other two cases until it reaches to its maximum value. After this point, the temperature is observed to be significantly lower as compared to the cases of fuel particle size 10 μm and 20 μm . This implies that small particle size has a combustion zone, or in other words, maximum temperature zone closer to the burner. Contrary, the temperature is lower in case of particle size of 20 μm until the maximum temperature point but higher after the peak value, i.e. during post combustion zone (Fig. 5.18). This shows a longer combustion zone in case of larger particle size. It is also noted that all cases show a similar temperature at the end of the combustion zone (near outlet) due to the similar air and fuel ratios.

Similarly, the temperature distribution in case of Nozzle 3 with mean particle sizes of 2 μm , 10 μm and 20 μm is represented in Fig. 5.19. A similar behavior of combustion temperature can be observed as described above. However, a very high temperature is observed near at the perforated cap (Fig. 5.1) of Nozzle 3. This temperature is noted to be higher, i.e. 280°C, in case of small particle size while a temperature around 135°C is observed with the large particle size (Fig. 5.16). Moreover, a very high temperature, around 600°C is observed

beneath the perforated cap with some fluctuations caused by the injected air streams (Fig. 5.19). However, this temperature decreases with the larger particle sizes (10 μm and 20 μm) due to longer combustion zone found further downstream. Furthermore, a similar trend of temperature profile is obtained in post combustion zone as described before in case of Nozzle 2.

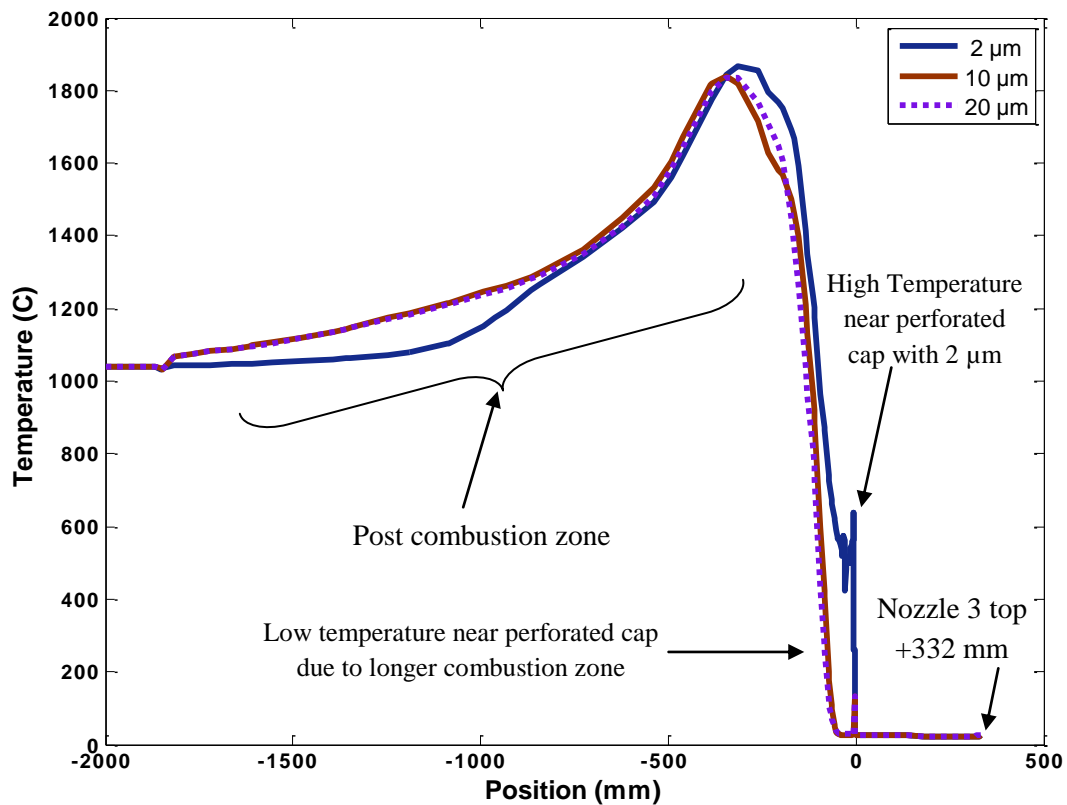


Fig. 5.19: Plot of combustion temperature distribution with Nozzle 3

5.9 Optimization of nozzle air with Nozzle 2

Based on the CFD simulation results obtained so far, it is revealed that the Nozzle 2 keeps the permissible limit of nozzle tip temperature ($< 60^{\circ}\text{C}$) during the transportation of fuel with nozzle air flow rate provided in Data Set 2. It is also concluded that nozzle air has a strong influence on temperature profiles (Section 5.7).

5.9.1 Variations in nozzle air

Based on these results, a further CFD study is conducted for the optimization of nozzle air flow rates with Nozzle 2 (Fig. 5.1). For this purpose, nozzle air flow rate is further varied in order to find optimized nozzle air flow rates and to check further the influence of nozzle air on nozzle temperature and combustion temperature as well. Based on previous air flow rates (Data Sets 1 and Data Set 2), five different levels of nozzle air flow rates are formulated. In each level, nozzle air is increased by a factor of 1.75. New nozzle air flow rates are evaluated for the same boundary conditions and process parameters as described before. Table 5.6 shows the five data sets of nozzle air used for the optimization of nozzle air flow rates for the

case of Nozzle 2. Similar to previous operating conditions, FTA (fuel transport air) is supplied in the inner section and outer section is used for cooling air (CA).

Table 5.6: Nozzle air flow rates in Nozzle 2

Nozzle section	Data Set 3	Data Set 1	Data Set 2	Data Set 4	Data Set 5
Nozzle inner section	6.5 m ³ h ⁻¹ (FTA)	12 m ³ h ⁻¹ (FTA)	20 m ³ h ⁻¹ (FTA)	35 m ³ h ⁻¹ (FTA)	61 m ³ h ⁻¹ (FTA)
Nozzle outer section	6.5 m ³ h ⁻¹	11 m ³ h ⁻¹	20 m ³ h ⁻¹	35 m ³ h ⁻¹	61 m ³ h ⁻¹
Total flow rate	13 m³ h⁻¹	23 m³ h⁻¹	40 m³ h⁻¹	70 m³ h⁻¹	122 m³ h⁻¹

Similar to the results of previous simulations, it is noted that maximum combustion temperature as well as nozzle tip temperature decreases significantly by increasing the nozzle air flow rate. Table 5.7 represents the results of temperature in the nozzle and the combustion zone in all cases of nozzle air flow rates.

Table 5.7: Temperature results with different nozzle air flow rates (Nozzle 2)

Nozzle air flow rate	Nozzle tip temperature	Max. combustion temperature
13 m ³ h ⁻¹	75°C	1863°C
23 m ³ h ⁻¹	65°C	1812°C
40 m ³ h ⁻¹	48°C	1505°C
70 m ³ h ⁻¹	38°C	1223°C
122 m ³ h ⁻¹	32°C	971°C

It can be observed that the maximum combustion temperature decreases by approximately 300°C by increasing the air flow rate by a factor of 1.75 in case of Data Sets 1, 2, 4 and 5. Combustion temperature with nozzle air flow rate of 23 m³ h⁻¹ was noted as 1812°C which decreases to 1505°C with air flow rate of 40 m³ h⁻¹ (nozzle air increased by a factor of 1.75). A further increase in nozzle air reduces the maximum combustion temperature to 1223°C and then to 971°C at a flow rate of 122 m³ h⁻¹. Therefore, it can be stated that there is a reduction of 300°C by each increment of nozzle air. However, it is also observed that there is minor difference in temperature when reducing the nozzle air from 23 m³ h⁻¹ to 13 m³ h⁻¹, which implies that there is no further (significant) effect of air flow rate on the combustion temperature (Fig. 5.20b, Appendix B, Fig. B15). This is because of rapid heating of incoming fuel particles and ignition of the fuel (combustible matter) at the lower flow rate, whereas the comparatively higher air flow rate imparts cooling effect on the combustion zone and significantly reduces the combustion zone temperature.

Similar phenomena are observed in case of nozzle tip temperature (Fig. 5.20a), i.e. the highest temperature of the nozzle wall decreases when increasing the nozzle air flow rate. In this case, the flow rate of cooling air provided in the outer section of the nozzle at a temperature of 25°C is also increased. It is also observed that the temperature drop at the lower tip of the nozzle wall is about 20 K by increasing the nozzle air flow rate (by a factor of 1.75) from 23

$\text{m}^3 \text{h}^{-1}$ to $40 \text{ m}^3 \text{h}^{-1}$, while there is a minor difference in temperature when nozzle air flow rate increases from $40 \text{ m}^3 \text{h}^{-1}$ to $70 \text{ m}^3 \text{h}^{-1}$.

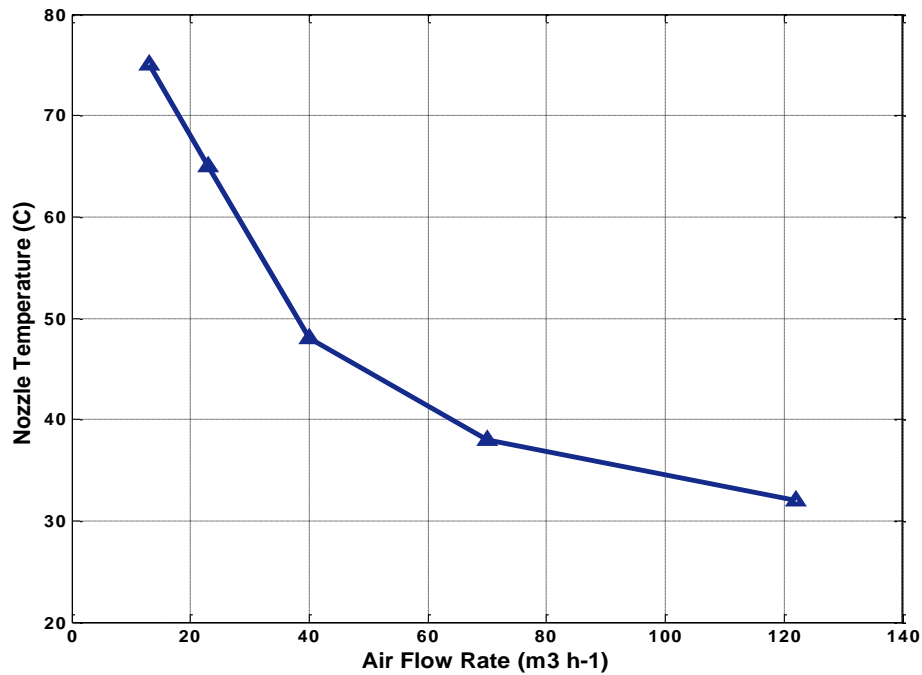


Fig. 5.20a: Effect of air flow rate on nozzle tip temperature

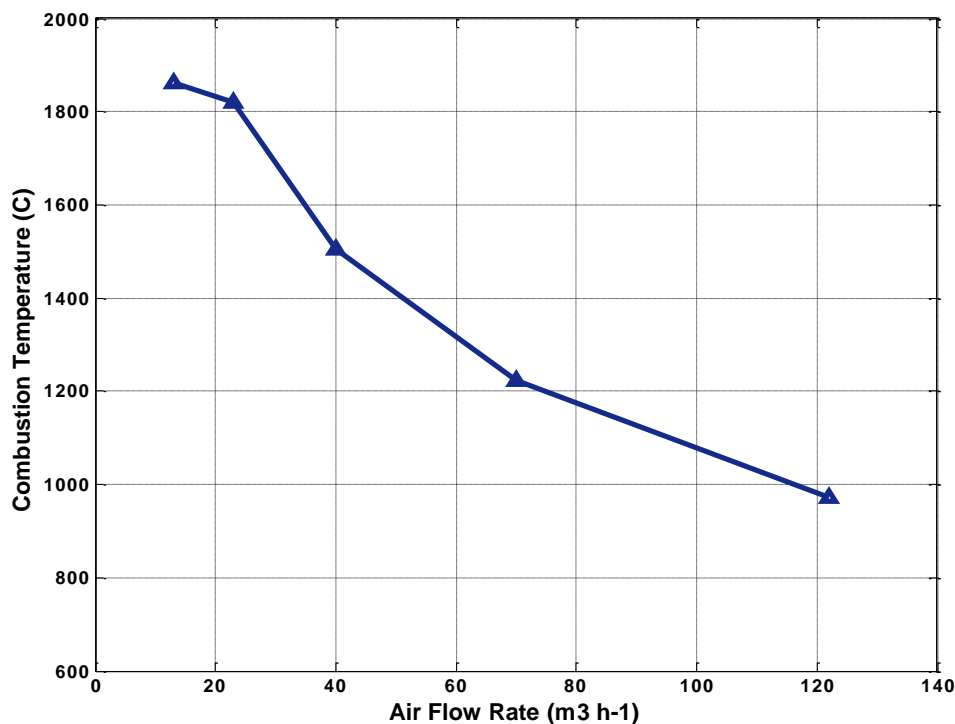


Fig. 5.20b: Effect of air flow rate on maximal combustion temperature

It can also be noted that there is no significant reduction of temperature when increasing the nozzle air flow rate from $70 \text{ m}^3 \text{h}^{-1}$ to $122 \text{ m}^3 \text{h}^{-1}$. This is due to less difference (gradient) in temperature between cooling air and temperature of nozzle which leads to lower heat exchange in both sections. Similarly, there is no significant increase in nozzle temperature when reducing the nozzle air flow rate from $23 \text{ m}^3 \text{h}^{-1}$ to $13 \text{ m}^3 \text{h}^{-1}$.

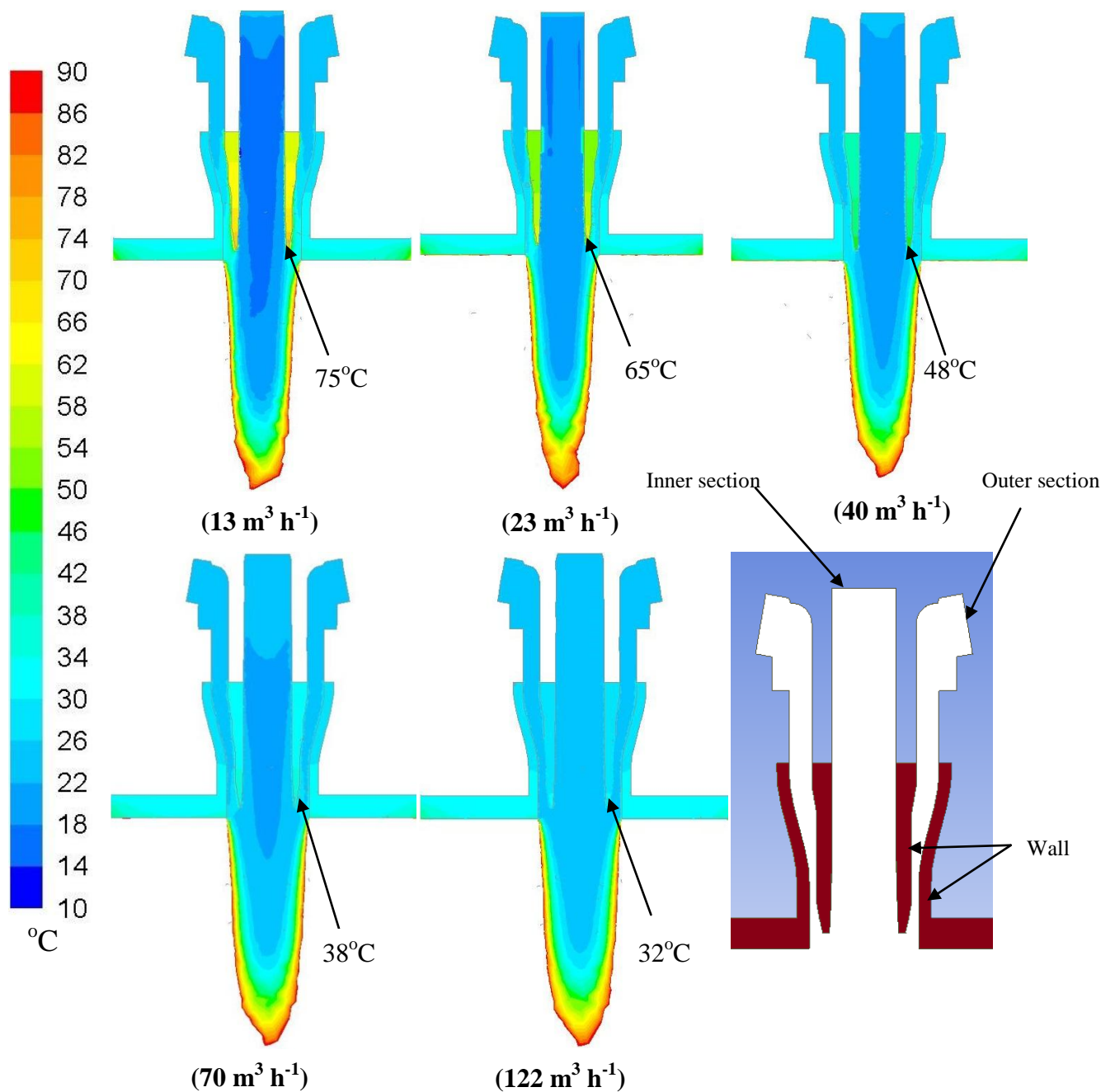


Fig. 5.21: Nozzle temperature (°C) with different nozzle air flow rates

Contours of temperature in the nozzle at different nozzle air flow rates are compared in Fig. 5.21. It can be concluded that larger nozzle air flow rate than 40 m³ h⁻¹ results in a minor temperature drop, however, on the other hand, it can also lead to high operational cost of the combustion plant. Moreover, a high air flow rate reduces the combustion temperatures significantly by imparting cooling effect (Fig. 5.20 b). The current work is focussed on the selection of fuel nozzle for the transportation of pulverized fuel material with low melting point. Therefore, it is necessary to discuss the favorable air flow rates. However, there are always limitations in using high nozzle air flow rate as it affects the combustion process significantly. For example, in Germany, combustion plants must fulfil the regulations given in

the “Siebzehnte Verordnung zur Durchführung des Bundes-Immissionsschutzgesetzes (Verordnung über die Verbrennung und die Mitverbrennung von Abfällen - 17. BImSchV)” [142] in which §6 (1) states that after provision of last air supply, temperature in the furnace/combustion plant must exceed 850°C. In the present situation, temperature decreases by around 300°C when increasing air flow rate by a factor of 1.75. Combustion temperature with air flow rate 122 m³ h⁻¹ is noted as 971°C which is above the stated limit in the law. Further increase in nozzle air (by again, factor 1.75) would though result in temperature reduction to approximately 650°C, which is much below the limit set by the law.

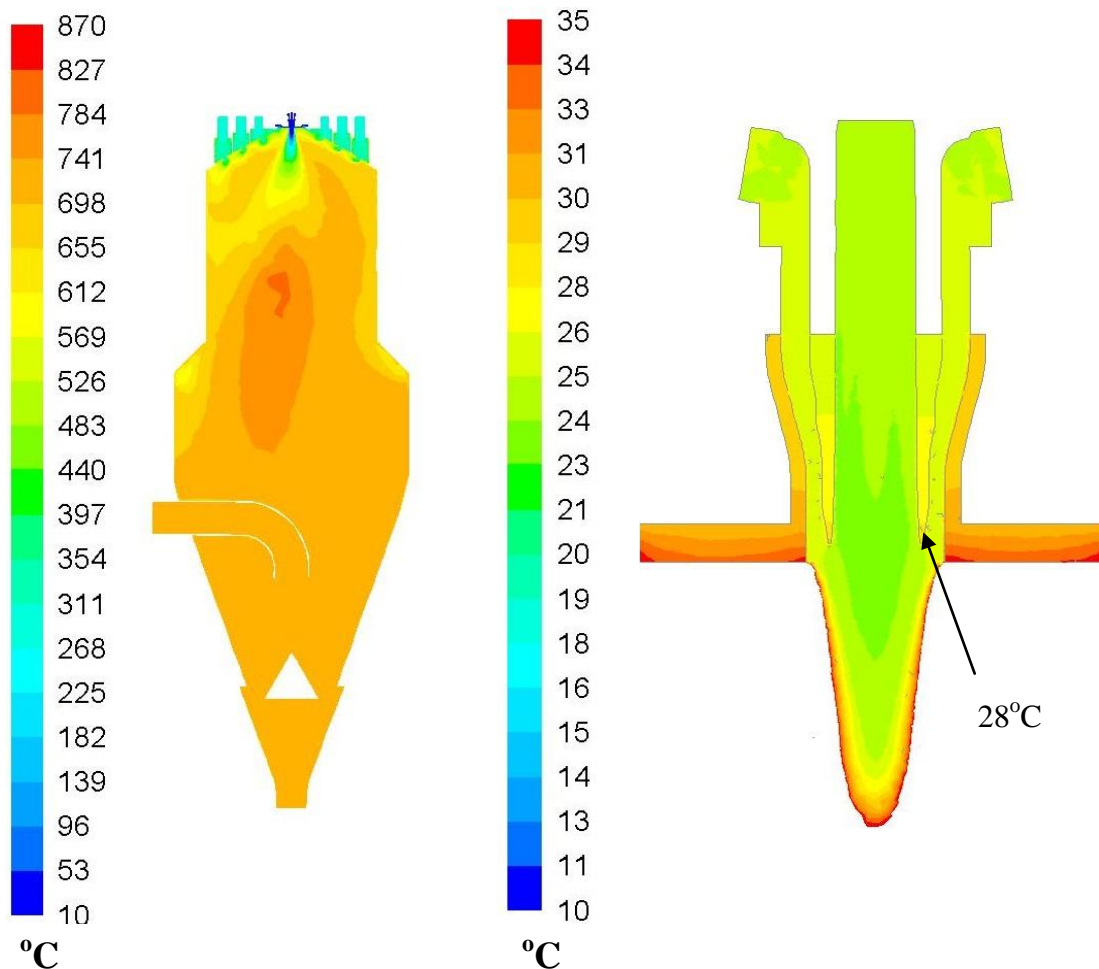


Fig. 5.22: Temperature profiles with Nozzle 2 with maximum allowable air flow rate

In order to suggest the maximum permissible nozzle air flow rate, further simulations have been conducted with Nozzle 2. It is concluded from the results that a flow rate of 194 m³ h⁻¹ (air in inner section at 97 m³ h⁻¹ and in outer section at 97 m³ h⁻¹) would be the maximum level of air flow which can be implemented under the current conditions and using Nozzle 2, as it results in maximum combustion temperature of 870°C in the furnace. Figure 5.22 shows the temperature fields in the combustion furnace and in Nozzle 2 at maximum nozzle air flow rate of 194 m³ h⁻¹. It can be seen that the very high nozzle air flow rate results in essentially flameless combustion (Fig. 5.22).

5.9.2 Sectional air flow rate increase

In case of Nozzle 2, nozzle air is provided in two sections of the nozzle, i.e. fuel transport air (FTA) is provided in the inner section while cooling air (CA) moves through the outer section of the nozzle (Fig. 5.1). To check the effect of different air flow rates through the sub-sections of the nozzle (i.e. inner section and outer section) on nozzle temperature, a variation is made (on the basis of flow rates given in Table 5.6) in the nozzle air to form two sub-data sets in such a way that in the first case FTA (fuel transport air) is kept same (as in original case) and cooling air is increased by a factor of 1.75, whereas in the second case cooling air is kept constant and FTA is increased by a factor of 1.75.

Table 5.8: Temperature results for different levels of air flow in the two sections of Nozzle 2

Nozzle air (Cases)	Inner section (FTA)	Outer section (CA)	Total air flow rate	Nozzle tip temperature	Combustion temperature	
1	Original	6.5 m³ h⁻¹	6.5 m³ h⁻¹	13 m³ h⁻¹	75°C	1863°C
	I	6.5 m ³ h ⁻¹	11 m ³ h ⁻¹	17.5 m ³ h ⁻¹	65°C	1863°C
	II	11 m ³ h ⁻¹	6.5 m ³ h ⁻¹	17.5 m ³ h ⁻¹	70°C	1880°C
2	Original	12 m³ h⁻¹	11 m³ h⁻¹	23 m³ h⁻¹	65°C	1812°C
	I	12 m ³ h ⁻¹	19 m ³ h ⁻¹	31 m ³ h ⁻¹	53°C	1719°C
	II	21 m ³ h ⁻¹	11 m ³ h ⁻¹	32 m ³ h ⁻¹	55°C	1789°C
3	Original	20 m³ h⁻¹	20 m³ h⁻¹	40 m³ h⁻¹	48°C	1505°C
	I	20 m ³ h ⁻¹	35 m ³ h ⁻¹	55 m ³ h ⁻¹	41°C	1364°C
	II	35 m ³ h ⁻¹	20 m ³ h ⁻¹	55 m ³ h ⁻¹	43°C	1333°C
4	Original	35 m³ h⁻¹	35 m³ h⁻¹	70 m³ h⁻¹	38°C	1223°C
	I	35 m ³ h ⁻¹	61 m ³ h ⁻¹	96 m ³ h ⁻¹	33°C	1072°C
	II	61 m ³ h ⁻¹	35 m ³ h ⁻¹	96 m ³ h ⁻¹	35°C	1065°C
5	Original	61 m³ h⁻¹	61 m³ h⁻¹	122 m³ h⁻¹	32°C	971°C

Table 5.8 shows the new data sets of nozzle air flow rate variation and the main results of respective CFD simulations. Similar to other cases, temperature at the lower tip of the nozzle is the main target of the analysis, i.e. reduction of nozzle tip temperature to a temperature less than 60°C. It is observed from the numerical simulations that there is always a reduction in nozzle temperature with increase in nozzle air flow rate. It is found that nozzle air flowing through the nozzle sections has a combined effect in reducing the nozzle temperature by heat exchange through the walls of the nozzle. Moreover, total nozzle air correlated with the (also shown) maximal combustion temperature and hence, with the intensity of heat transfer by radiation to the nozzle. The study on sectional changes of air flow rate shows that individual increment of cooling air (CA) or FTA also reduces the temperature of the nozzle. However, air flow increment in either one of the sections has less influence on temperature reduction as compared to the increment of air flow in both sections. It is also noted that air moving through the outer section (C A) has more influence on temperature reduction than air flowing

in the inner section (FTA). However, the difference between those cases is found to be very small. The contours of nozzle temperature at different levels of sectional nozzle air flow increment are illustrated in Fig. 5.23a, Fig. 5.23b, Fig. 5.23c and Fig. 5.23d.

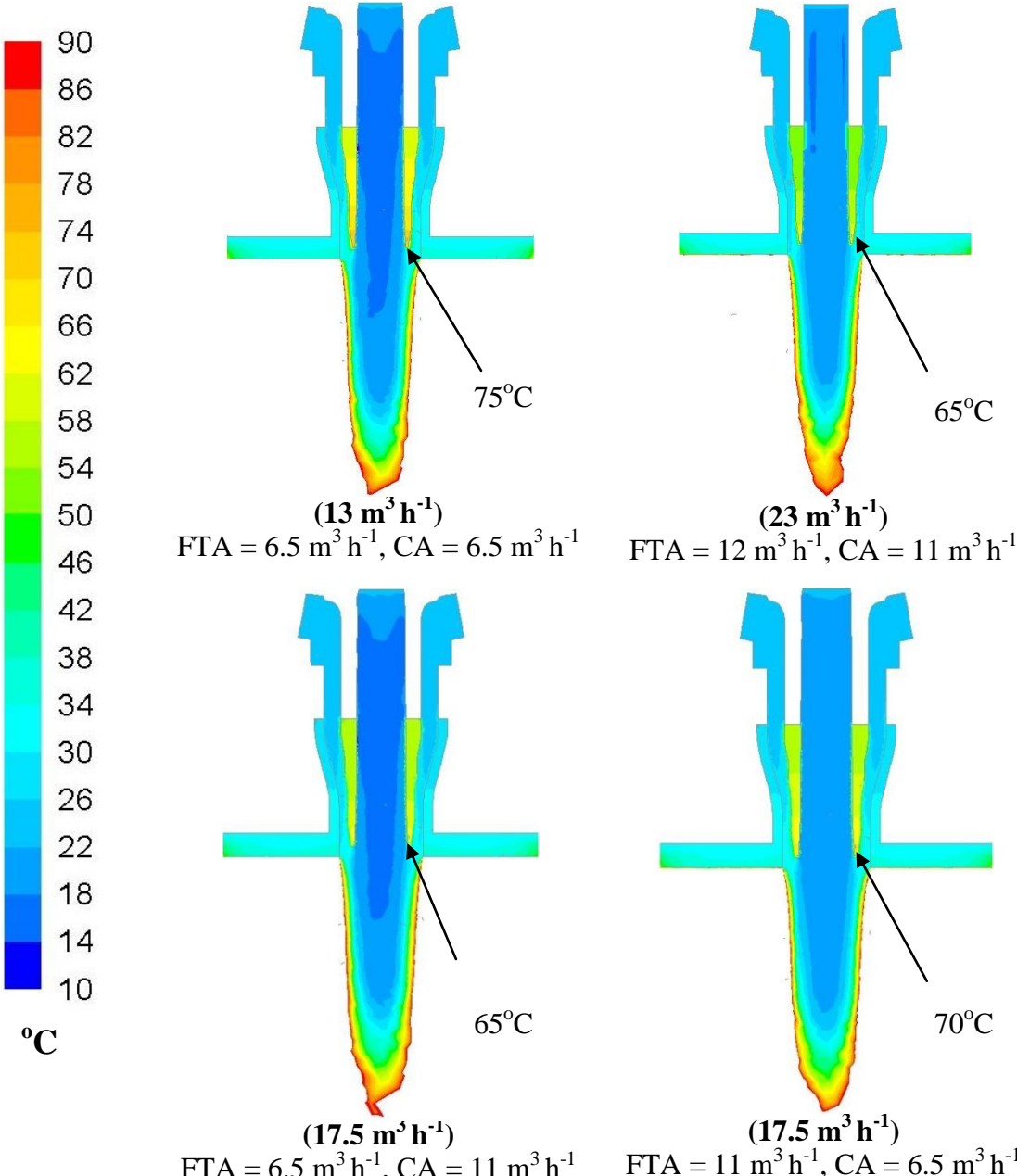


Fig. 5.23a: Nozzle temperature with different air flow rates (Case 1)

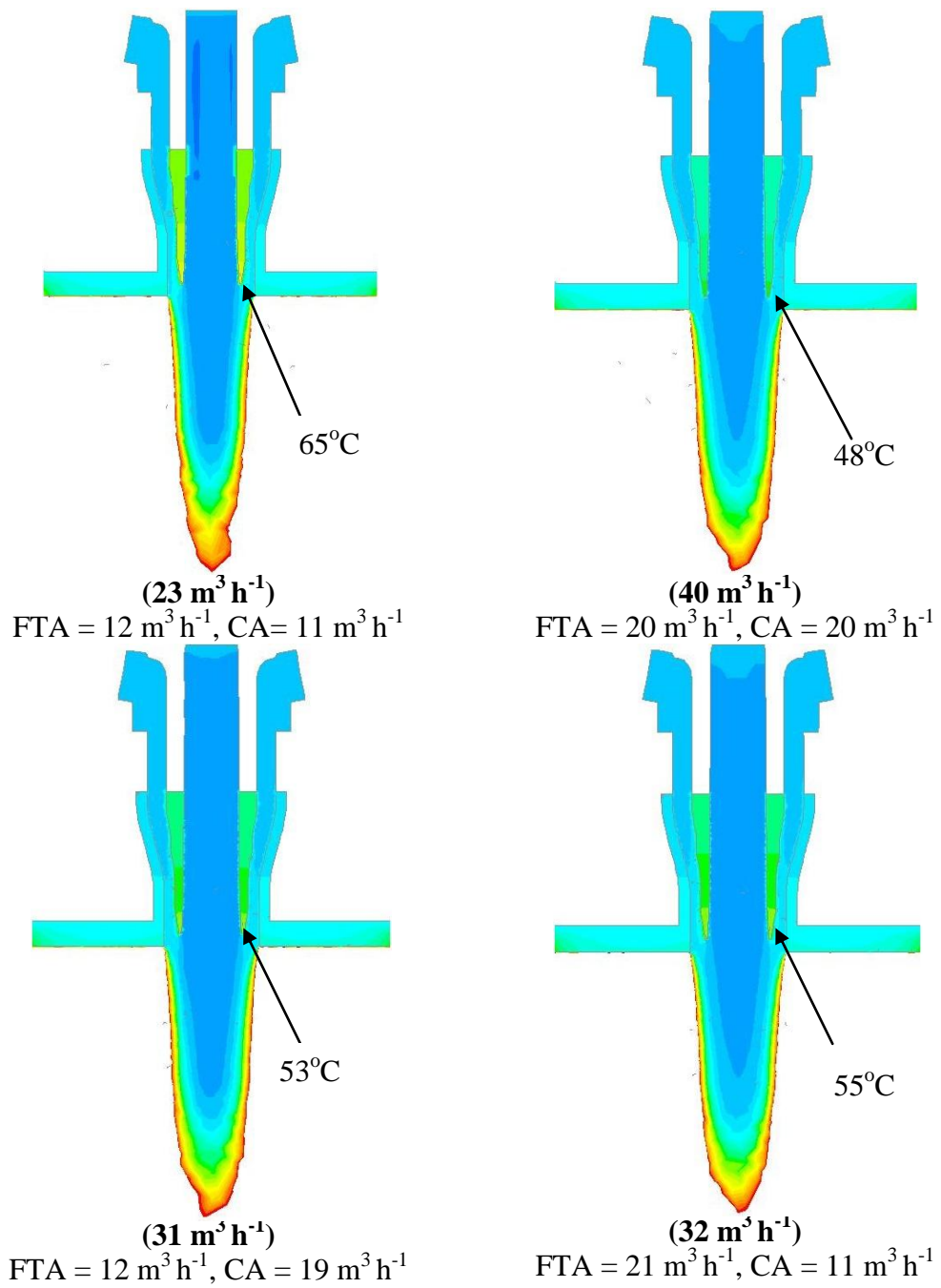
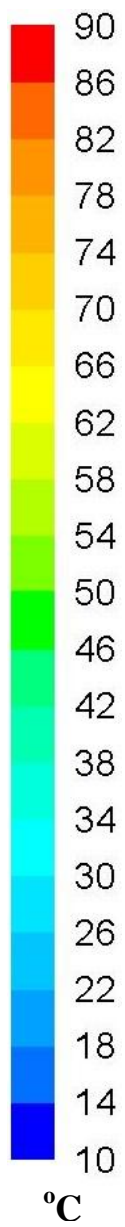


Fig. 5.23b: Nozzle temperature with different air flow rates (Case 2)

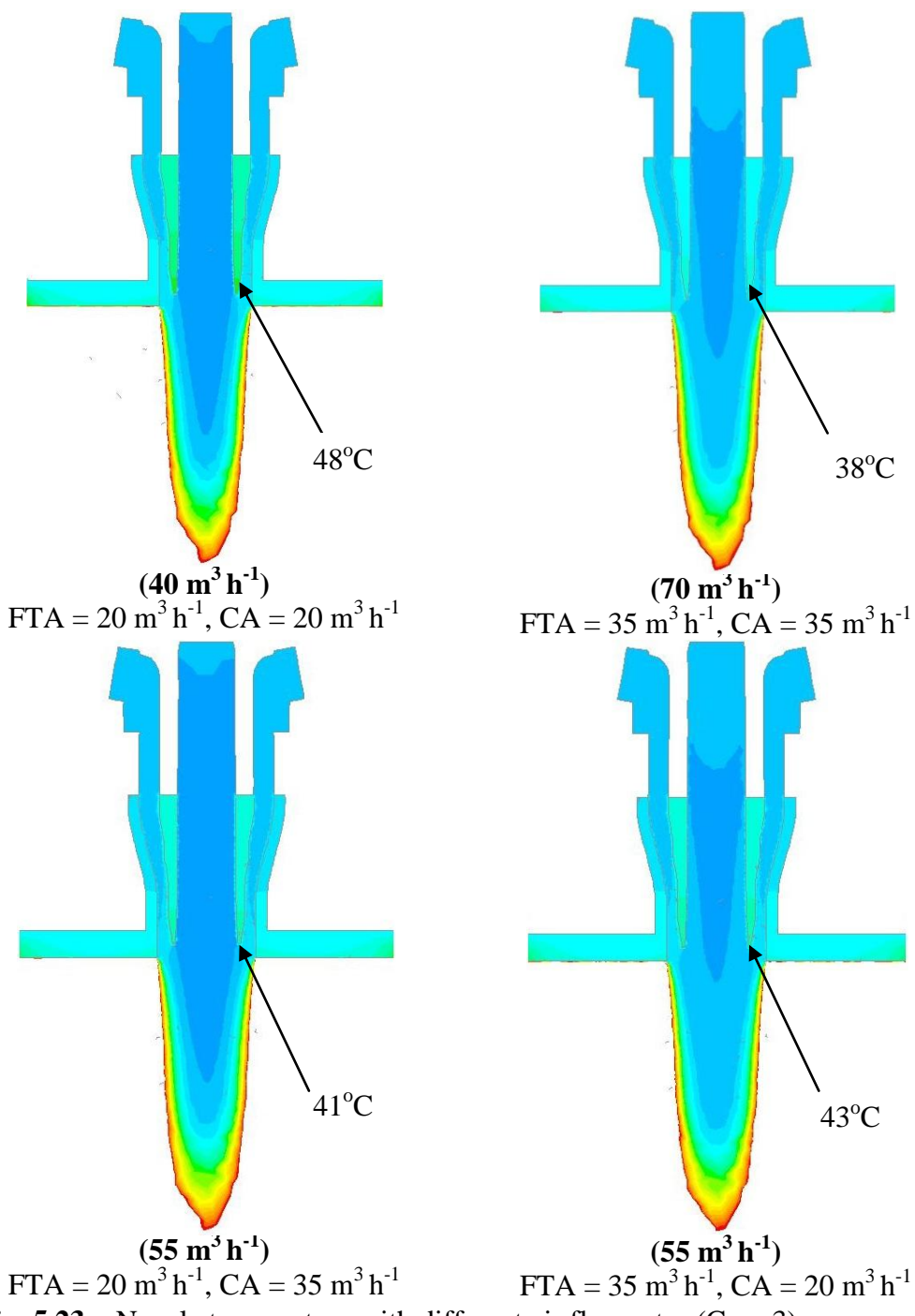
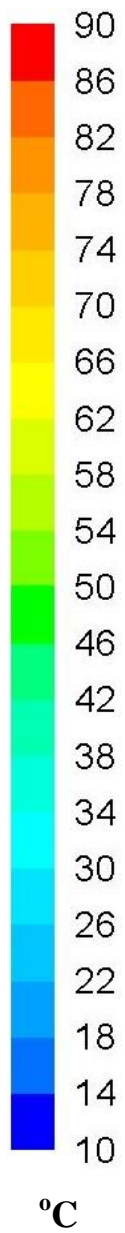


Fig. 5.23c: Nozzle temperature with different air flow rates (Case 3)

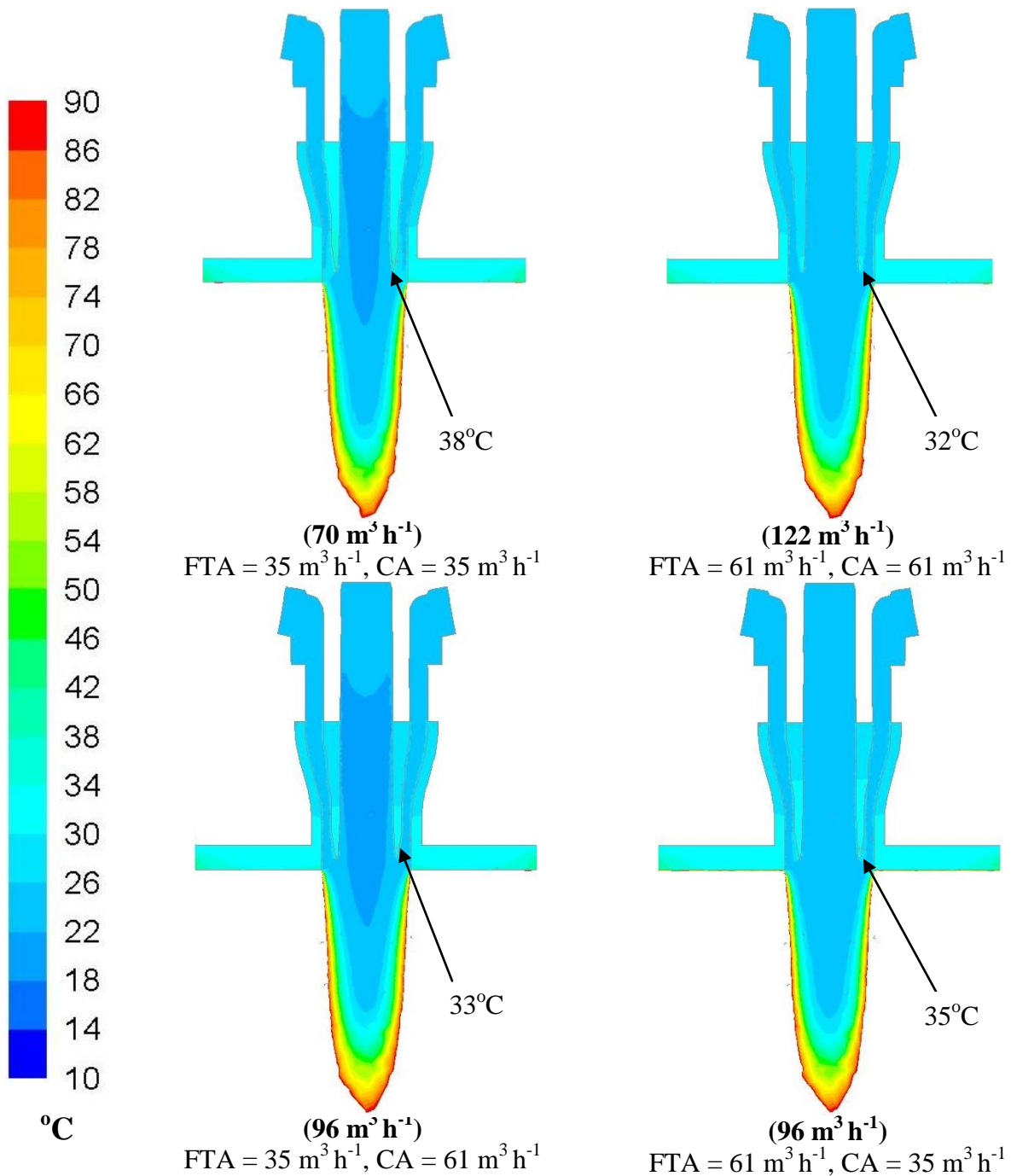


Fig. 5.23d: Nozzle temperature with different air flow rates (Case 4)

It can be observed that there is significant difference in nozzle temperature when moving from $23 \text{ m}^3 \text{ h}^{-1}$ to $40 \text{ m}^3 \text{ h}^{-1}$ while the temperature difference is smaller by increasing the air flow rate from this level on. This is because of less thermal gradient between air and wall temperature. On the other hand, the close views of the nozzle also show that nozzle air provided in the outer section results in more reduction in nozzle temperature than the fuel transport air. This is due to the zigzag surface of the wall between inner and outer section which is faced to the cooling air. The high surface area enhances the cooling effect (Fig. 5.3). It is concluded that effect of cooling air is more dominant than the nozzle air flow increment in inner section, i.e. fuel transport air. It is also interesting to note that the temperature

reduction is approximately similar in all three variations in the Case 4. This is because of less temperature gradient between cooling air and the hot wall (Fig. 5.23d).

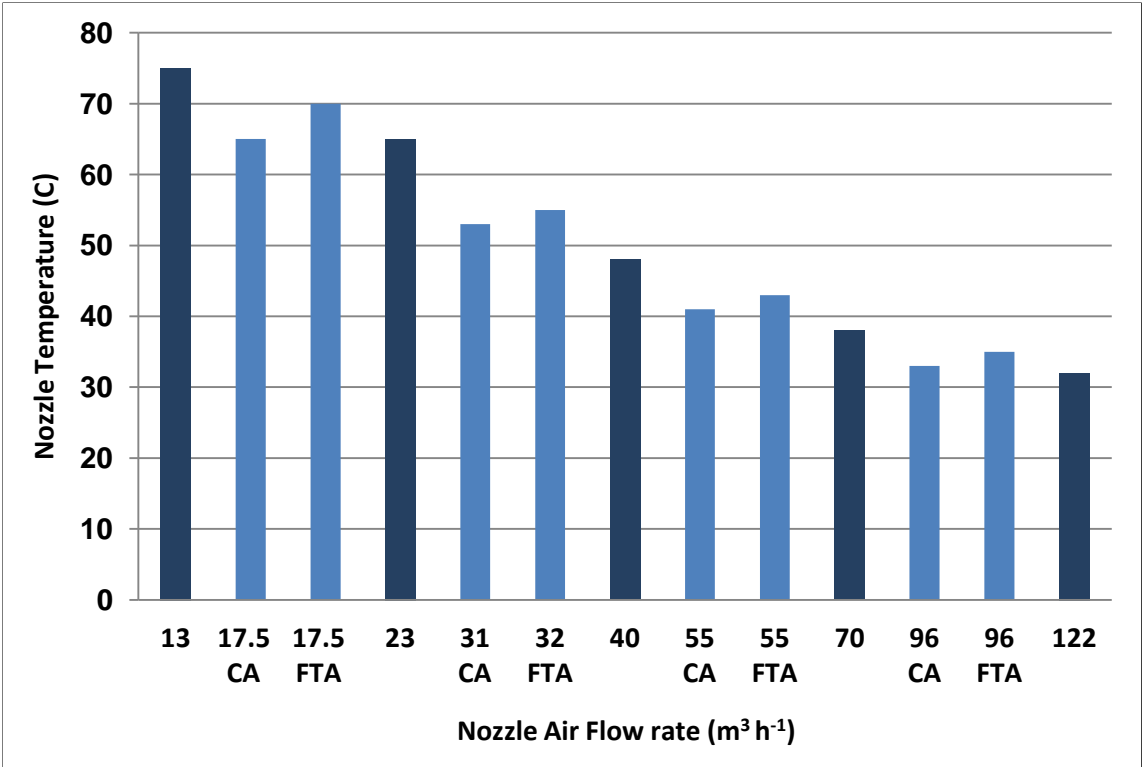


Fig. 5.24: Effect of different nozzle air flow rates on nozzle temperature

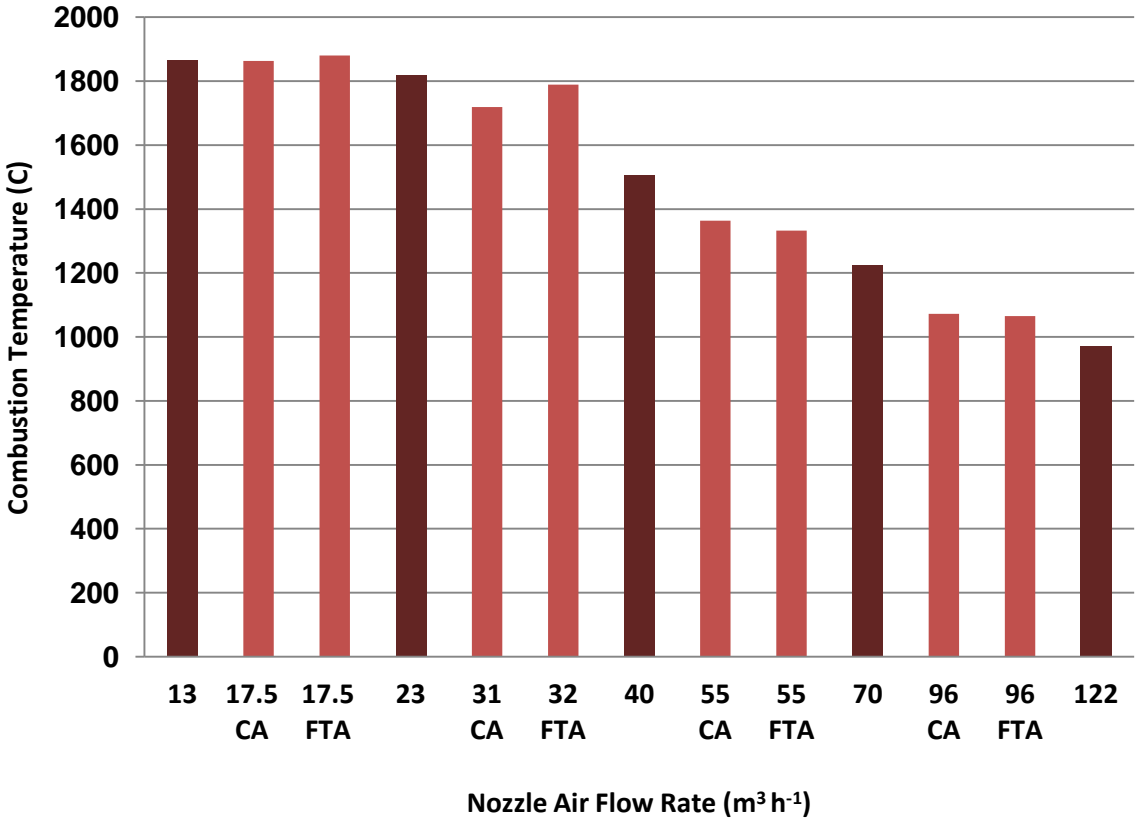


Fig. 5.25: Effect of different nozzle air flow rates on combustion temperature

A brief comparison between all the cases of nozzle air flow increment (i.e. total nozzle air as well as in individual nozzle sections) is represented in Fig. 5.24. The bold bars show the original (total increment in nozzle air by a factor of 1.75) while the light bars represent the cases of increment of either FTA (fuel transport air) or CA (cooling air) with a factor of 1.75. It can be observed that the reduction in nozzle temperature is more by increasing nozzle air flow rate in both sections (in total). However, it is revealed from the comparison between CA and FTA (Fig. 5.24) that cooling air (CA), as guessed from its name, has more cooling effect on nozzle wall than the fuel transport air (FTA).

Similarly, the effect of different nozzle air flow rates on maximal combustion temperature in the combustion zone is illustrated in Fig. 5.25. As described in the previous section, there is a reduction of 300°C by increasing total nozzle air flow rate from 23 m³ h⁻¹ to 40 m³ h⁻¹ and onwards with a factor of 1.75. On the other hand, there is no significant increment of combustion temperature by reducing the total air flow from 23 m³ h⁻¹ to 13 m³ h⁻¹ (Appendix B, Fig. B15). It is also noted that the individual increment of nozzle air in one of the two nozzle sections also affects the combustion temperature. However, the reduction in temperature is less as compared to the increment of nozzle air in both sections. This implies that the greater the nozzle air feeding is, the less is the maximal combustion temperature in the combustion zone.

5.10 Effect of excess air ratio (λ)

As described previously (Chapter 2) air and combustible should be in stoichiometric balance for complete combustion. Therefore, air provided for the combustion has a major influence on the combustion process. Increase excess air ratio reduces the combustion temperature significantly [143-146].

Table 5.9: Combustion temperature at different excess air ratio

Nozzle air flow rate (m ³ h ⁻¹)	Excess air ratio, λ	Maximum temperature (°C)	Outlet temperature (°C)	Adiabatic temperature (°C)
13	2.52	1863	1125	1221
17.5	2.57	1863	1110	1201
23	2.63	1812	1094	1178
31	2.72	1719	1068	1146
40	2.82	1505	1043	1112
55	2.99	1364	1000	1060
70	3.16	1223	962	1013
96	3.46	1072	898	941
122	3.75	971	845	879

In the present study, different nozzle air flow rates have been used while mass flow rate of the fuel and flow rates of primary and secondary air are kept constant (Section 5.3). Increase in air flow rate of nozzle results in more air in the furnace and, hence, increases the excess air ratio. Table 5.9 shows values of excess air ratio (λ) and respective temperature results with different levels of nozzle air flow rate (taken from Table 5.8). It should be noted that excess air ratio is calculated for the sum of air flow rates provided by nozzle air, primary air ($160 \text{ m}^3 \text{ h}^{-1}$) and secondary air ($50 \text{ m}^3 \text{ h}^{-1}$) from mass and energy balance (Appendix E, Table E1). It is observed that maximum temperature decreases significantly by increasing the excess air ratio. However, this factor is prominent at comparatively higher excess air numbers, i.e. above 2.5. Maximum temperature at the combustion zone is generated due to the ignition of combustible fraction of fuel particles. Mixing and surrounding of hot air environment are the key factors for this ignition (Chapter 3). At comparatively low air flow rate, i.e. $13 \text{ m}^3 \text{ h}^{-1}$, the particles are heated more rapidly and, hence, generate a combustion zone with comparatively higher temperature. On the other hand, high nozzle air flow rates dilute the combustion gas environment and impart a cooling effect which reduces the combustion temperature significantly (Table 5.9).

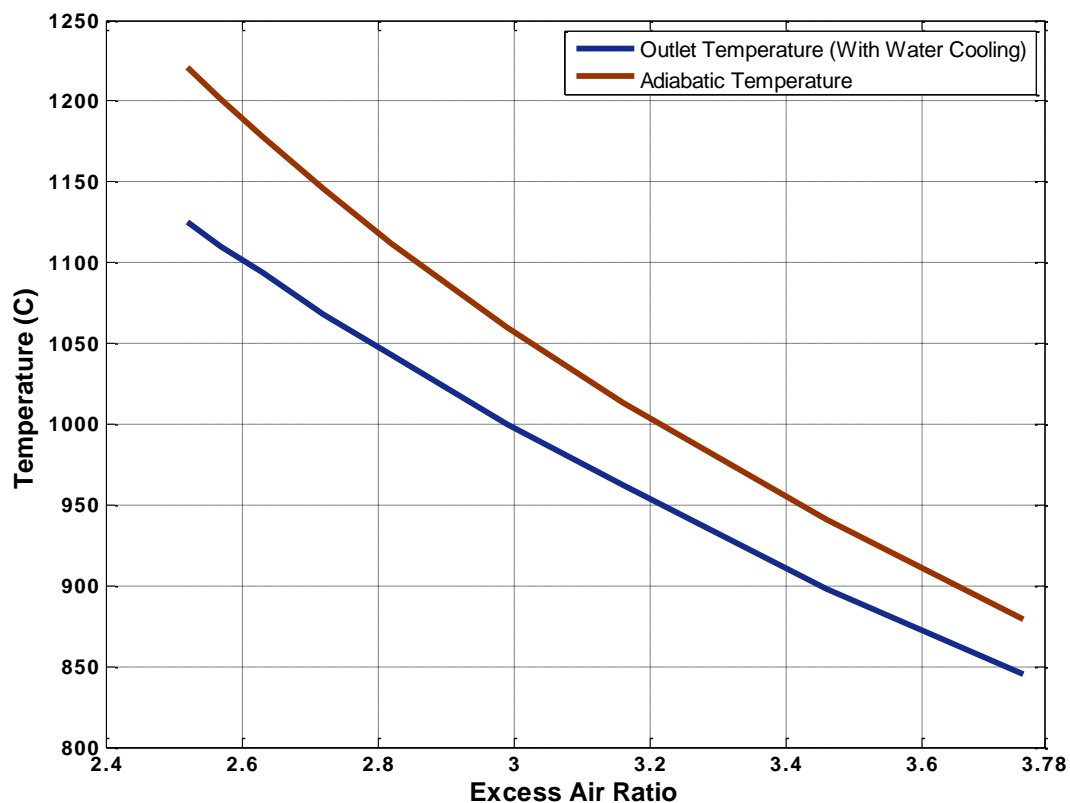


Fig. 5.26: Effect of excess air ratio on furnace outlet temperature

Figure 5.26 illustrates the effect of different excess air ratio on the furnace outlet temperature (with water cooling) and adiabatic temperature. It can be observed from the comparison of both temperatures that furnace outlet temperature is lower than the adiabatic temperature. For example, the outlet temperature is observed as 1094°C with nozzle air flow rate of $23 \text{ m}^3 \text{ h}^{-1}$ and excess air ratio of $\lambda = 2.63$ while the adiabatic temperature is calculated to be 1178°C at

this level. This difference is because of significant heat flux at the surface of the water cooling wall (Chapter 4) in the present simulations. It can also be observed that the outlet temperature of the furnace decreases significantly by increasing the nozzle air flow rate and, hence, the excess air ratio. It should be noted that a too high air flow rate imparts a cooling effect on the combustion chamber and, hence, reduces the thermal efficiency due to significant heat loss. On the other hand, less air supply may cause incomplete combustion. Hence, there are always certain limitations for using high excess air ratio (λ). Therefore, it is necessary to monitor and control the excess air ratio to achieve better combustion efficiency. An optimum value of excess air ratio should be implemented for the combustion process.

Based on the problem addressed in the present study, the best results have been found in case of nozzle air flow rate of $40 \text{ m}^3 \text{ h}^{-1}$ with Nozzle 2. At this nozzle air flow rate (along with primary and secondary air), excess air ratio is computed to be at $\lambda = 2.82$, resulting in maximal combustion temperature at 1505°C and an outlet temperature of 1043°C . A further increase in excess air ratio would result in too strong reduction in combustion temperature. Moreover, it would also be responsible for a significant increase in operational cost of the combustion plant.

5.11 Comparison of CFD results with the literature

The case of Nozzle 2 with nozzle air flow rate of $40 \text{ m}^3 \text{ h}^{-1}$ showed the best results with respect to the problem reported, i.e. the temperature at the nozzle should be less than 60°C during the transportation of fuel. The nozzle temperature in this case has been noted to be at 48°C and the maximum combustion temperature is 1505°C . In order to assess model performance, the simulation results were compared with the experimental study reported by Weidmann et al. [89]. In a series of experiments, similar burner geometry was used with a centralized fuel nozzle surrounded by primary air inlets. Measurements were taken with a (highly volatile) fuel with heating value of 26 MJ kg^{-1} injected with a mass flow rate of 32.4 kg h^{-1} . The fuel transport air was provided at a flow rate of $34.5 \text{ m}^3 \text{ h}^{-1}$ and preheated (around 150°C) primary/secondary air was supplied at $215.7 \text{ m}^3 \text{ h}^{-1}$ while in the present simulations primary and secondary air was supplied at a total air flow rate of $210 \text{ m}^3 \text{ h}^{-1}$ and a preheat temperature of 300°C . The experimental results of Weidmann et al. [89] showed quite similar temperature profile as compared to our simulation results within the furnace. The mixing zone starts near the exit of the burner due to the turbulent mixing of large volume of air jets and hot gases present in the furnace. With reference to the fuel nozzle, this section is found at a distance of 150 mm within the furnace in both studies. The temperature was observed to be in the range of $1000\text{-}1100^\circ\text{C}$ at this section. The experimental results also showed that the main combustion zone in the furnace is formed at a position of 450 mm from the injection point. The maximum combustion temperature was measured at 1250°C at this point. A very similar behavior has been predicted in the simulation results (as shown in Fig. 5.8, Fig. 5.18). The temperature of incoming jets of fuel and air increases gradually due to the mixing with hot gases. The main combustion zone is predicted to be at a position around 400 mm from the exit

of the nozzle. However, the maximum combustion temperature is predicted to be at 1500°C in the present simulation results. The difference in temperature is because of the type and composition of fuel used in the two studies. Moreover, a higher preheating temperature was used in the present simulations. Similar combustion behaviors have been reported by Stroh et al. [106], in which similar models have shown an adequate agreement with the experimental measurements. More studies have been reported by Saha et al. [88], Weber et al. [87], Schaffel et al. [111], Mei et al. [147], Suda et al. [148], He et al. [149] and Johansen et al. [150]. It should be noted that the comparison revealed a qualitative agreement of the temperature profiles in the furnace. The discrepancy in the predicted and experimental results is due to both the fuel used and the adoption of simplified models such as constant rate devolatilization and char combustion model (Chapter 4).

5.12 Summary

The current chapter was dedicated to the optimization of fuel nozzle design and operating conditions for the transportation of fuel particles with low melting point to the hot combustion chamber. Based on the findings of Chapter 4, four fuel nozzle geometries were prepared and evaluated through multiphase CFD simulations. The simulation results have revealed that nozzle shape and structure have a great impact on the fuel/air injection and mixing patterns in the combustion zone. The different injection patterns lead to a difference in temperature distribution in the combustion chamber as a result of burning of pulverized fuel particles. The comparison of the different nozzle geometries led to the result that Nozzle 2 has the lowest temperature at the nozzle walls during the transportation of solid fuel (Appendix B, Fig. B16). Moreover, the nozzle air flow rate significantly influences the temperature fields in the combustion chamber as well as in the nozzle partition wall (between inner and outer section). This is due to the cooling effect and temperature gradient between nozzle wall and nozzle air. The parametric study conducted with different fuel particle sizes has revealed that particle size also has a strong effect on the combustion behavior, especially in the combustion zone. Smaller particle size results in wider combustion zones while a rather long combustion (flame) area is obtained with larger particle size. Moreover, high nozzle tip temperature is obtained with smaller particles (due to the rapid devolatilization near the nozzle exit) as compared to larger fuel particles. It is concluded from the study presented for the optimization of nozzle air flow rate that nozzle temperature (at lower tip) significantly decreases by increasing the nozzle air flow rate. A reduction of approximately 20 K is observed at the nozzle tip by increasing nozzle air flow rate by a factor of 1.75. However, no prominent effect is found when increasing the nozzle air flow rate beyond 40 m³ h⁻¹. Moreover, it is concluded from the study conducted with increment of nozzle air flow rate in just one of the two sections (i.e. inner or outer) that the cooling air (CA) has a better cooling effect on the nozzle walls than the fuel transport air. It is concluded from the current findings that Nozzle 2 results in the most appropriate conditions (i.e. nozzle temperature < 60°C) with nozzle air flow rate of 40 m³ h⁻¹ and fuel particle size of 10 μm.

Simplification of the Fuel Transport Nozzle

This chapter is an outlook of Chapter 4 and Chapter 5. In this work, a simplified design of fuel transport nozzle is presented with efforts to reduce the nozzle temperature. The effect of nozzle air flow rate with the proposed nozzle is discussed along with its shortcomings. An alternative method for reduction of nozzle tip temperature is presented. The effect of water cooling as well as air cooling (heat losses to surrounding) is discussed.

6.1 Overview and motivation

In Chapter 5, the combustion behavior of pulverized paint residues (with low melting point) has been studied. Due to its low melting point, this kind of solid fuel tends to clog the fuel nozzle, when exposed to hot wall segments of the burner (Chapter 4). The geometry of the burner and the air flow therein is, therefore, a critical issue that needs particular attention. In Chapter 5, four nozzle designs have been investigated by multiphase CFD simulation. The influence of both nozzle geometry and nozzle air flow conditions onto the burner temperature has been evaluated. It has been revealed from the findings that a nozzle design with two pipes shows the best results for the transportation of solid fuel with low melting point among the four nozzle designs under consideration. However, it should also be noted that the suggested nozzle design has a zigzag wall between inner and outer pipe. Hence, the construction of this nozzle is relatively complicated and technically expensive. Similar to this nozzle, a rather simple fuel nozzle consisting of two concentric pipes turned out to perform near to the expected temperature (i.e. wall temperature $< 60^{\circ}\text{C}$). With the advantage of its simple construction, it is, therefore, decided to further optimize the concentric pipe fuel nozzle. The optimization process is carried out with respect to different parameters such as nozzle air flow rates, water cooling, primary air inlet position and heat flux (heat losses) from the furnace wall to the surroundings (termed as air cooling). The overall objective of this study is to suggest a simple and low-cost fuel nozzle for the transportation of pulverized fuel. Multiphase CFD simulations are conducted with different parametric investigations as described in the following.

6.2 Effect of nozzle air flow rate: A case of water cooling

In Chapter 5, it was found that the tip temperature of Nozzle 1 is around 65°C with a nozzle air flow rate of $40 \text{ m}^3 \text{ h}^{-1}$. Being very close to the melting point of the fuel, there are still chances of melting of fuel particles moving through this nozzle. In order to find the appropriate nozzle tip temperature, a further study is presented with different air flow rates. Similar to the previous simulations, fuel is transported through the inner section (Fig. 6.1) with the help of fuel transport air (FTA) while outer section is used for cooling air (CA) to cool down the nozzle to permissible temperature, i.e. 60°C .

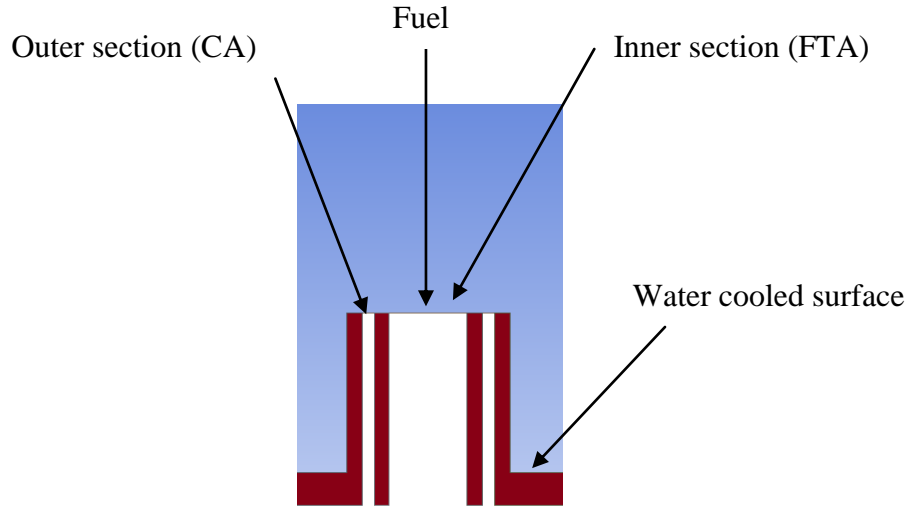


Fig. 6.1: Fuel transport nozzle

In order to find the similar effect (as of optimum nozzle, Nozzle 2 in Chapter 5) in the Nozzle 1, different air flow rates are applied through the nozzle sections. Nozzle air flow rates are selected on the base case of $40 \text{ m}^3 \text{ h}^{-1}$ (Chapter 5) and further variations are made with a factor of 1.5 in order to reach the expected nozzle tip temperature. Table 6.1 shows the four different cases of nozzle air flow rate to be investigated. Nozzle air is provided through the prescribed sections (Fig. 6.1) with an inlet temperature of 25°C .

Table 6.1: Nozzle air flow rates for Nozzle 1

Nozzle air flow (Cases)	Inner section (FTA)	Outer section (Cooling air)	Total (Nozzle air)
Case 1 (Base case)	$20 \text{ m}^3 \text{ h}^{-1}$	$20 \text{ m}^3 \text{ h}^{-1}$	$40 \text{ m}^3 \text{ h}^{-1}$
Case 2	$30 \text{ m}^3 \text{ h}^{-1}$	$30 \text{ m}^3 \text{ h}^{-1}$	$60 \text{ m}^3 \text{ h}^{-1}$
Case 3	$45 \text{ m}^3 \text{ h}^{-1}$	$45 \text{ m}^3 \text{ h}^{-1}$	$90 \text{ m}^3 \text{ h}^{-1}$
Case 4	$67.5 \text{ m}^3 \text{ h}^{-1}$	$67.5 \text{ m}^3 \text{ h}^{-1}$	$135 \text{ m}^3 \text{ h}^{-1}$

6.3 Primary and secondary air

As described in the previous Chapters 4 and 5, primary air is provided by a ring of three primary inlets, i.e. inner, middle and outer primary inlets. The primary air is supplied at a total flow rate of $40 \text{ m}^3 \text{ h}^{-1}$, $53 \text{ m}^3 \text{ h}^{-1}$ and $67 \text{ m}^3 \text{ h}^{-1}$, through all inner, middle and outer inlets respectively. The inlet temperature is set at 300°C to achieve optimum conditions for combustion. Primary air is kept unchanged in all four cases of nozzle air flow rate. Secondary air is provided at a flow rate of $50 \text{ m}^3 \text{ h}^{-1}$ and temperature of 300°C through secondary air inlets available around the combustion chamber (Chapter 4, Fig. 4.4). Mass flow rate of fuel is also kept same, i.e. 20 kg h^{-1} , as in previous investigations. Pulverized paint residue is used as solid fuel with a particle size of $10 \mu\text{m}$ (as suggested by the findings of Chapter 5). The composition of this type of fuel has been described in Chapter 4.

6.4 Simulation results with different nozzle air flow rates

Computational fluid dynamics (CFD) modeling approach as described in Chapter 4 is applied to the present operating conditions. Similar to the boundary conditions of previous investigations, water cooling is also adopted in the present simulations by setting the water cooling wall at a constant temperature of 30°C (Chapter 4, Section 4.4.2). From the simulations, it is resulted that the effect of nozzle air on temperature reduction is similar as described in case of Nozzle 2 (the optimum design of nozzle in Chapter 4). There is a significant reduction of temperature when increasing nozzle air flow rate from 40 m³ h⁻¹ to 60 m³ h⁻¹, i.e. a reduction in nozzle temperature of 15°C has been observed. After 60 m³ h⁻¹, a reduction of 12°C is observed by increasing nozzle air flow to 90 m³ h⁻¹. Increasing the nozzle air flow rate from Case 3 to Case 4, a reduction of 6°C is observed, which implies that further increment in nozzle air will only have a minor effect on nozzle temperature. A similar trend can be observed in case of maximum combustion temperatures (Appendix C, Fig. C1). Increasing the nozzle air with a factor of 1.5, a reduction of approximately 200°C has been observed (Fig. 6.2).

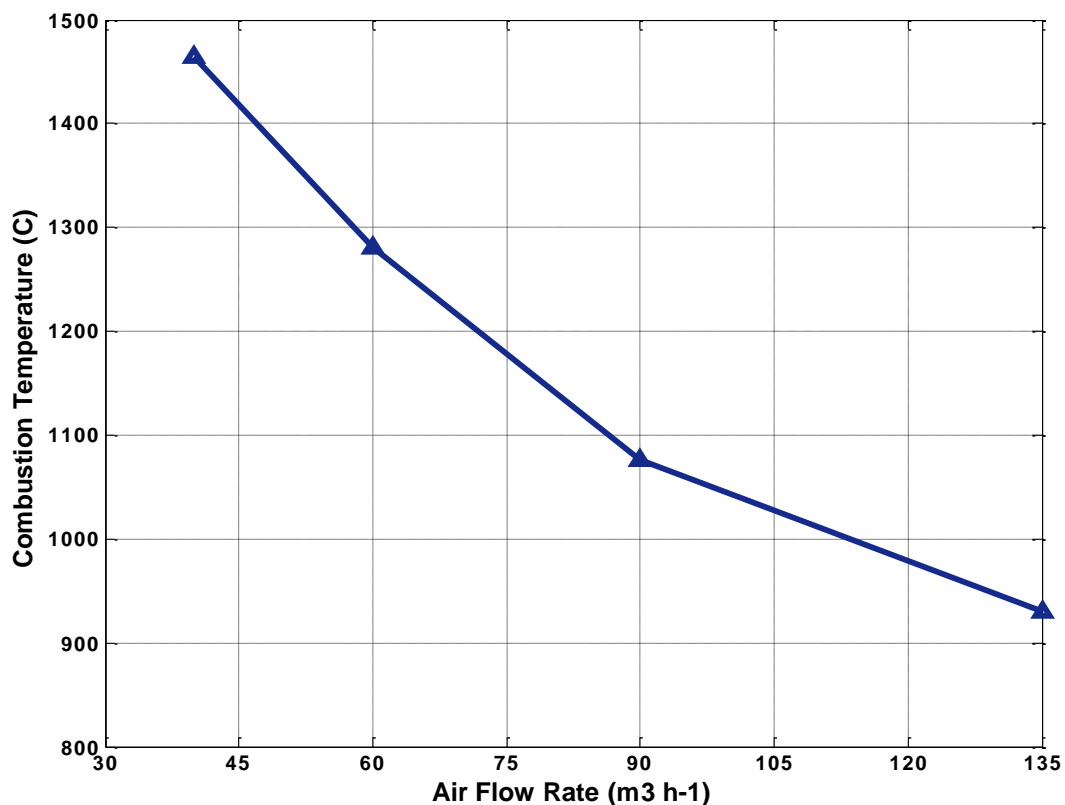


Fig. 6.2: Combustion temperature with different nozzle air flow rate in Nozzle 1

It is important to note that for reduction in temperature, a very high nozzle air flow rate is required in case of the considered (simpler) nozzle in order to reach the optimum value of nozzle temperature. A higher value (than the melting point of fuel) of tip temperature, i.e. 68°C, is obtained with a nozzle air flow rate of 40 m³ h⁻¹ with the present case of nozzle design, i.e. Nozzle 1 (Fig. 6.3). A nozzle air flow rate in the range of 60 m³ h⁻¹ is required to meet the required temperature with the simpler nozzle design (Nozzle 1). However, it should

be noted that the high air flow rate requirements lead to installments of very heavy apparatuses, i.e. fans, blowers, pipes etc., hence, increases the operational cost of the plant. On the other hand, combustion efficiency can also be affected due to the lower combustion temperature.

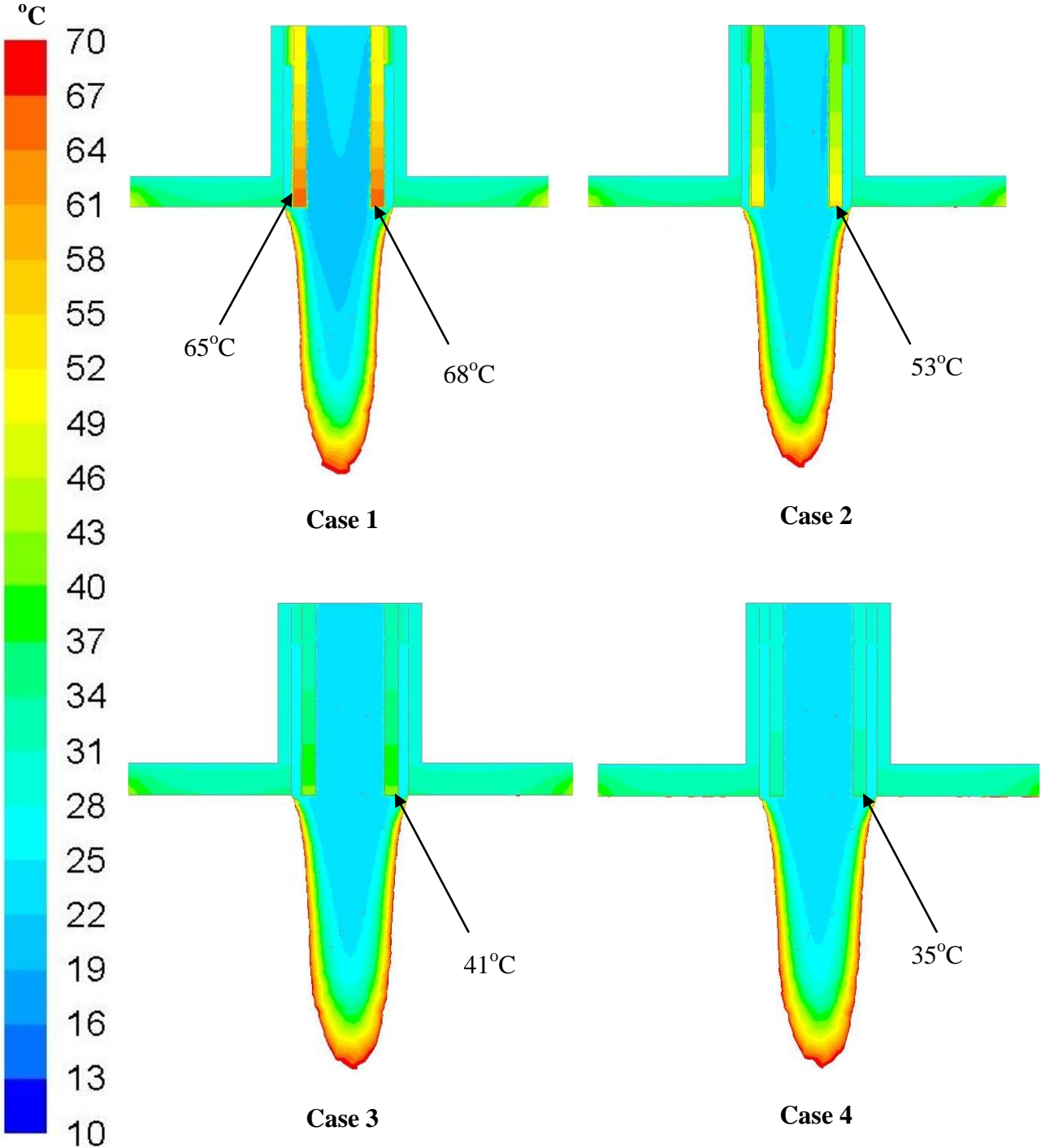


Fig. 6.3: Nozzle temperature with different cases of nozzle air

6.5 Effect of water cooling and primary air injection position

In the previous investigations, primary air was provided in ring shaped inner, middle and outer inlets. In order to check the effect of primary air injection (in only one of these rings) on nozzle temperature, a further study is presented. However, it should be noted that the present study is conducted at a smaller scale, i.e. with a thermal power capacity of 78 kW and an excess air number of $\lambda = 1.3$. Moreover, the effect of water cooling is studied along with three different positions of primary air. For this purpose, a parametric CFD simulation study has been planned with the operating conditions provided in Table. 6.2. In this case, nozzle air is provided with a mass flow rate of 19.29 kg h^{-1} in the inner section while in the outer section it is provided at a mass flow rate of 65.05 kg h^{-1} . Primary air is provided with a mass flow rate of 36.14 kg h^{-1} through only one inlet ring (Chapter 4) while other inlets are closed to check the influence of either primary air inlet (Fig. 6.4). Solid fuel is injected with a mass flow rate of 15.73 kg h^{-1} .

Table 6.2: Simulation operating conditions

Capacity	78 kW
Lambda (λ)	1.3
Nozzle air inner	19.29 kg h^{-1}
Nozzle air outer	65.05 kg h^{-1}
Primary air	36.14 kg h^{-1}
Fuel mass flow rate	15.73 kg h^{-1}
Fuel particle size	$12.4 \mu\text{m}$

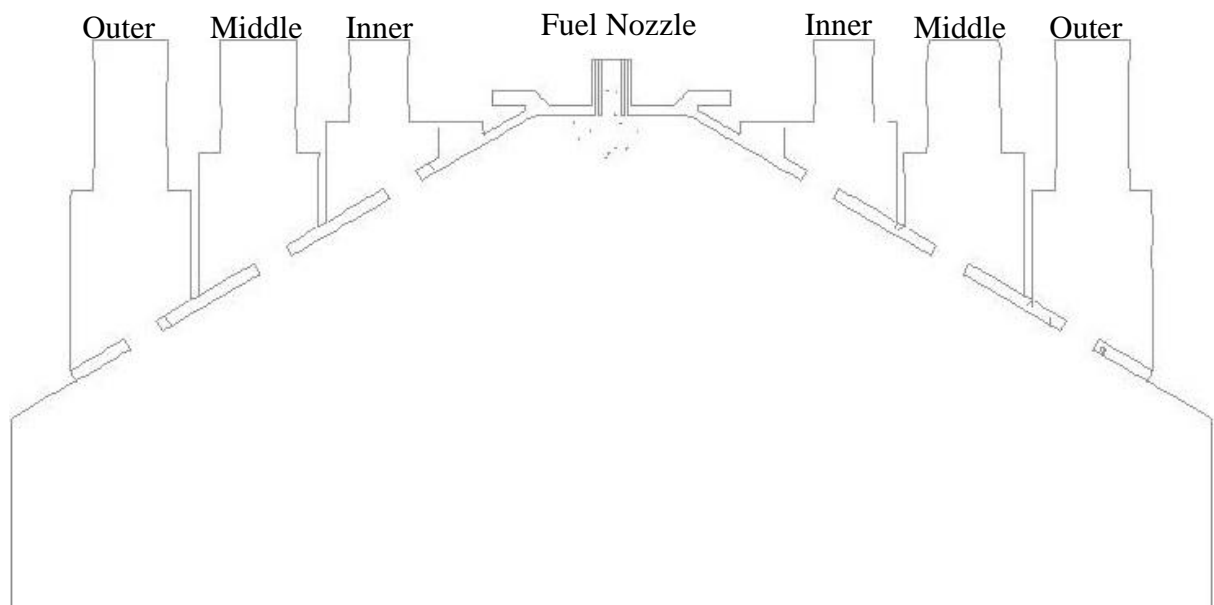


Fig. 6.4: Different positions of primary air inlets

The simulations with water cooling are conducted with similar computational domain of the combustion furnace (with Nozzle 1) and boundary conditions as described in Chapter 4.

Absence of water cooling (in the present simulations) implies that there is no heat flux from the top of the furnace to water cooling surface, i.e. heat flux from the surface of the water cooling wall is set to zero. However, heat transfer is still enabled at the walls near the burner (as in base case).

6.6 Simulation results

Three cases of primary air position are analyzed through operating parameters given by Table 6.2. It is observed that the maximum combustion temperature slightly changes by changing the primary air inlet position. For example, in case of primary air injection through inner inlet, the maximum temperature is 1474°C. The temperature slightly increases when changing the injection of primary air from inner to outer primary inlet (Appendix C). This is due to the mixing of primary air with the hot combustion gases. The temperature of combustion environment is higher in case of outer inlet. Therefore, a higher temperature is observed. However, the difference in temperature is very minor. Hence, it can be stated that the total temperature in the combustion zone is found to be approximately 1480°C. Table 6.3 represents the case of water cooling and temperature results with different positions of primary air. A similar temperature of the lower tip of the nozzle is observed all three cases (with water cooling).

Table 6.3: Temperatures for the case of water cooling

Primary air inlet	Max. temperature	Nozzle temperature	Outlet temperature
Inner	1474°C	107°C	1319°C
Middle	1487°C	107°C	1315°C
Outer	1491°C	107°C	1314°C

The comparison between the cases with and without water cooling of the top wall is illustrated in Fig. 6.5. A very high temperature is observed near the fuel nozzle in case of wall with no water cooling. The high temperature is due to the radiation from the combustion zone. As there is no heat transfer from the top wall, i.e. the system is assumed to be completely insulated, the wall temperature is very high. On the other hand, the temperature significantly decreases by enabling water cooling on the top wall. The reduction in temperature results because of the heat transfer from the furnace wall to the water cooled surface (Fig. 6.5). The heat flux is driven by the temperature gradient between the furnace wall and water. It is also observed that different positions of primary air injection led to a different heat flux from the water cooling wall. However, this difference is very small, i.e. the heat flow rate resulted as -15229 W, -15653 W and -15777 W in case of primary air injection at inner, middle and outer inlet respectively.

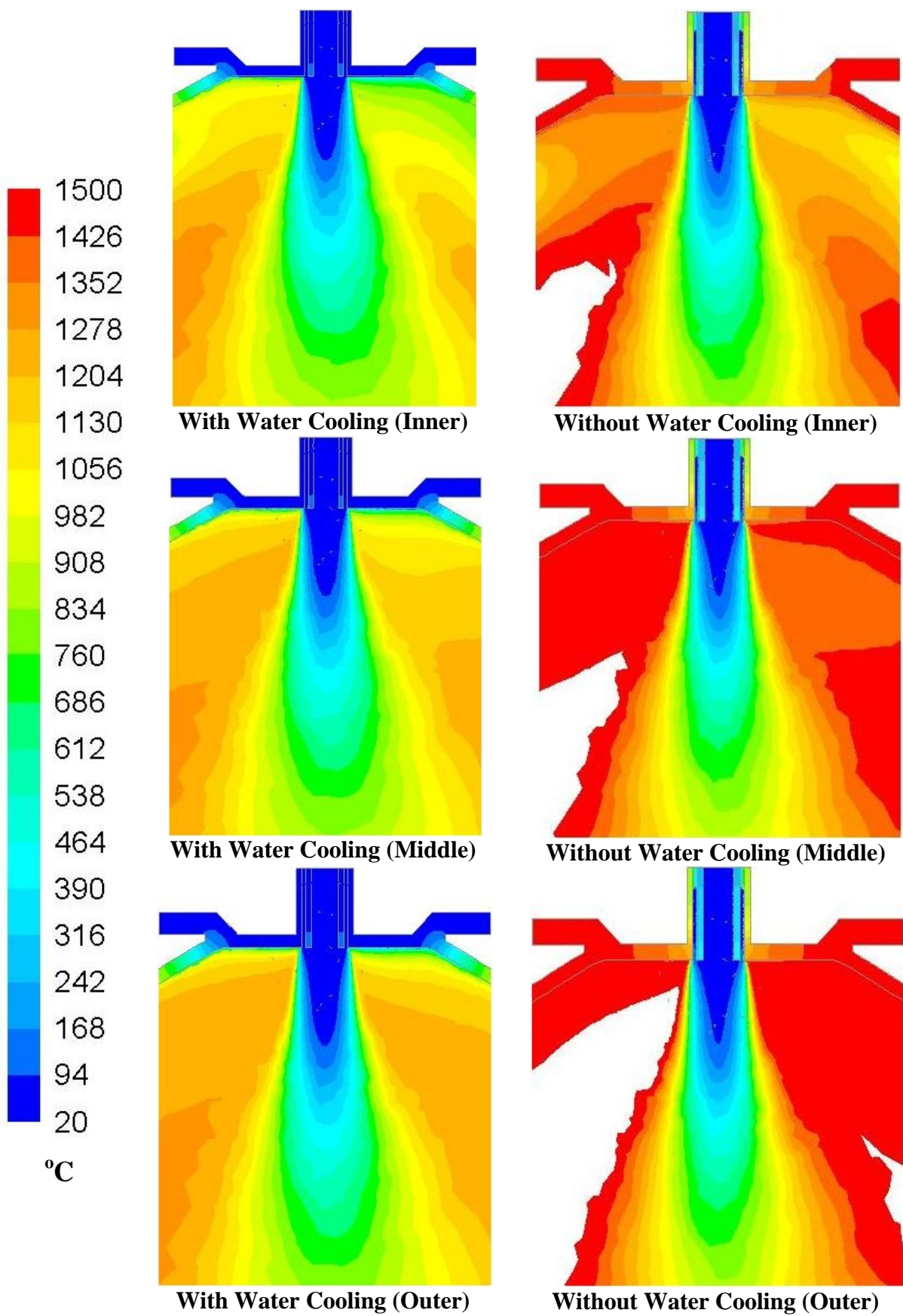


Fig. 6.5: Nozzle temperature with and without water cooling and positions of primary inlet

The comparison between different injection positions of primary air, i.e. providing primary air in only one of the primary inlet rings (Fig. 6.4), shows that the temperature near the nozzle exit increases when supplying the primary air away from the nozzle. This is because of the hot combustion zone which mixes the incoming primary air. It can be noted that the high temperature region (white area in Fig. 6.5) increases gradually with primary air supplying through inner, middle and outer inlet respectively (Appendix C, Fig. C3). A similar pattern has been observed for the case of water cooling. However, in this case the temperature is lower. Moreover, the temperature of the nozzle is less due to the cooling effect of the wall (water). In case without water cooling, the high temperature approaches to the nozzle exit and in this way increases the temperature of the nozzle walls. Therefore, the comparison has revealed a high temperature in case of outer position. The lowest temperature is obtained in the case of primary air injection from inner inlet. Table 6.4 represents the temperature results in the case without water cooling. The maximum temperature has been found in case of outer inlet, i.e. 1678°C, while in case of inner and middle inlet, the maximum combustion temperature is found as 1660°C and 1672°C, respectively (Appendix C, Fig. C2). However, the difference between maximum temperatures is minor, which results in similar outlet temperature, i.e. 1544°C.

Table 6.4: Temperatures for the case without water cooling

Primary air inlet	Max. temperature	Nozzle temperature	Outlet temperature
Inner	1660°C	405°C	1544°C
Middle	1672°C	414°C	1543°C
Outer	1678°C	418°C	1544°C

It is concluded from the analysis that water cooling has a strong effect (by heat flux) on the reduction of nozzle temperature. Hence, water cooling should be adopted in order to achieve better outcomes, i.e. optimum temperature at the nozzle walls, for the combustion of solid material which tends to transform to a sticky matter at high temperatures. However, implementation of such mechanism is, sometimes, difficult in large scale combustion systems. Moreover, it also increases the operational and maintenance costs.

6.7 Effect of heat losses through furnace walls: A case of air cooling

In the previous simulations, nozzle air flow rates have been studied by enabling water cooling at the top of the furnace (water cooling wall, Chapter 4). Heat losses (cooling effect) were implemented on this wall only, while side walls of the furnace have been assumed to be completely insulated. It was also concluded that water cooling significantly reduces the temperature of the nozzle wall (Section 6.6). Therefore, a water cooling apparatus should be installed along with the burner to cool down the nozzle temperature. However, this may increase the cost of overall furnace operations and maintenance by installing large pumps and water cooling fins. In order to find an alternative way to reduce the temperature of the nozzle,

the present study is taken up by enabling heat losses from the furnace walls. The heat flux from the top of the furnace is implemented with respect to the surrounding air temperature.

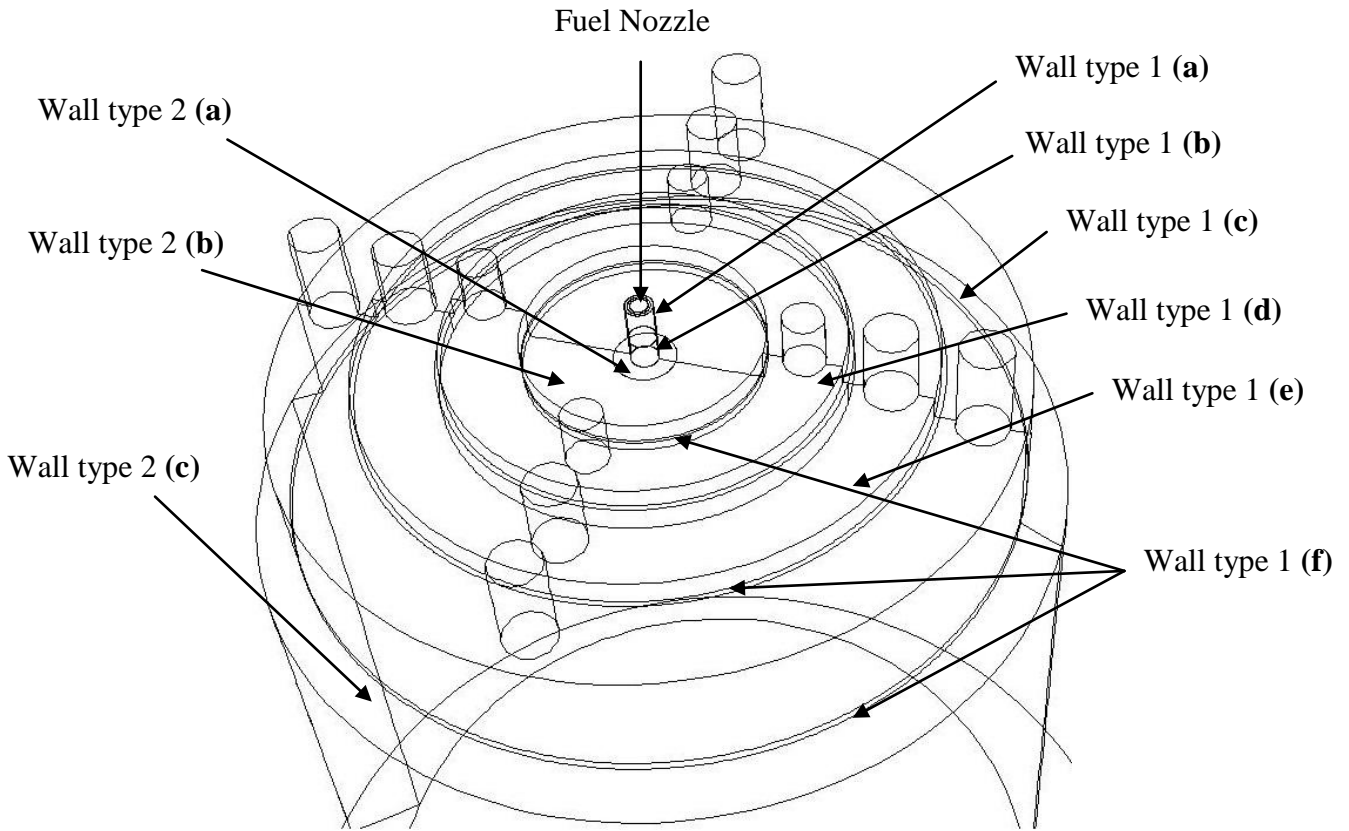


Fig. 6.6: Top of the combustion plant

For this purpose, the top of the combustion furnace has been divided into two types of wall (steel alloy) depending upon the thickness, i.e. wall type 1 and wall type 2. Wall type 1 has a thickness of 3 mm while wall type 2 has 8 mm thickness (Fig. 6.6). Moreover, both wall types are further classified (during geometry design) into different layers as a, b, c etc. in order to spot the heat flux from a specific location (wall) of the burner (Fig. 6.6). The external surface of the combustion chamber has been insulated with the help of rock wool and steel alloy. Three layers are deployed for the insulation purposes, i.e. steel alloy, rock wool and unalloyed steel. Similar material is used for insulation of the outlet pipe and sealings. However, heat flux due to ambient air temperature is also studied through these layers. Shell conduction is implemented in all types of wall, which enables the calculation of heat transfer in the normal direction as well as in wall planar direction [123]. The heat transfer coefficient is set as $13.9 \text{ W m}^{-2} \text{ K}^{-1}$ for all types of furnace walls based on the ambient air conditions. Similar to the previous analysis, simulations are conducted with three different positions of primary air such as inner, middle and outer inlet (Fig. 6.4). The analysis is conducted with the operating conditions given in Table 6.2 to check the effect of heat losses on nozzle tip temperature.

6.8 Simulation results with heat flux through walls: Heat losses to ambient air

Simulations are run with the process parameters provided in Table 6.2 and the same modeling approach. Similar to the previous investigations (Section 6.6), the effect of primary air inlet position is again investigated with the present process and wall specifications. It is observed that the maximum combustion temperature significantly decreases by enabling heat transfer through the top of the furnace. A heat flow rate of approximately -5000 W resulted from the wall type 1 while wall type 2 had a heat flow rate of approximately -1500 W to the surrounding. Similar to the previous results (Tables 6.3 and 6.4), a difference in combustion temperature is observed by changing the primary air injection position in one of the three inlet rings, i.e. inner, middle and outer. However, the temperature is observed to be less than in the simulation case without heat losses (Table 6.4). In case of primary air provided in the inner inlet, the maximum combustion temperature is observed to be 1583°C in contrast to 1660°C in the case without water cooling (i.e. completely insulated system). The significant reduction is because of heat loss from the top of the furnace through walls (Fig. 6.6). Similarly, the temperature decreases to 1593°C (Table 6.5) with primary air supply through the middle inlet in contrast to a maximum temperature of 1672°C in the fully insulated system (Table 6.4). In case of primary air provided in only the outer ring of primary inlets, the maximum temperature in the combustion zone is 1595°C (Appendix C, Fig. C4).

Table 6.5: Temperature results with heat flux through the furnace walls

Primary air inlet	Max. temperature	Tip temperature	Outlet temperature
Inner	1583°C	143°C	1208°C
Middle	1593°C	144°C	1211°C
Outer	1595°C	144°C	1213°C

It can also be noted that a similar trend has been found in the increment of maximum temperature, i.e. the combustion temperature increases when changing the position from the inner ring to the outer one. As described before, this is due to the mixing of incoming primary air with the hot combustion gases.

Figure 6.7 illustrates the nozzle temperature with different positions of primary air and heat flux through the walls (the case of air cooling, i.e. heat losses to ambient). It can be observed from the close-up view of the nozzle that there is a significant reduction of nozzle temperature by enabling the heat flux through the walls, especially from the top of the furnace. The nozzle tip is observed to be at a temperature of 143°C in case of primary air position at inner ring, while in case of middle ring the nozzle partition wall is at a temperature of 144°C. It is interesting to note that the case of completely insulated furnace, i.e. no losses from walls (Fig. 6.5, Table 6.4) resulted in nozzle tip temperature of approximately 400°C. The significant reduction in nozzle temperature in the present case (Fig. 6.7) is due to the heat transfer from nozzle/furnace walls to the surroundings.

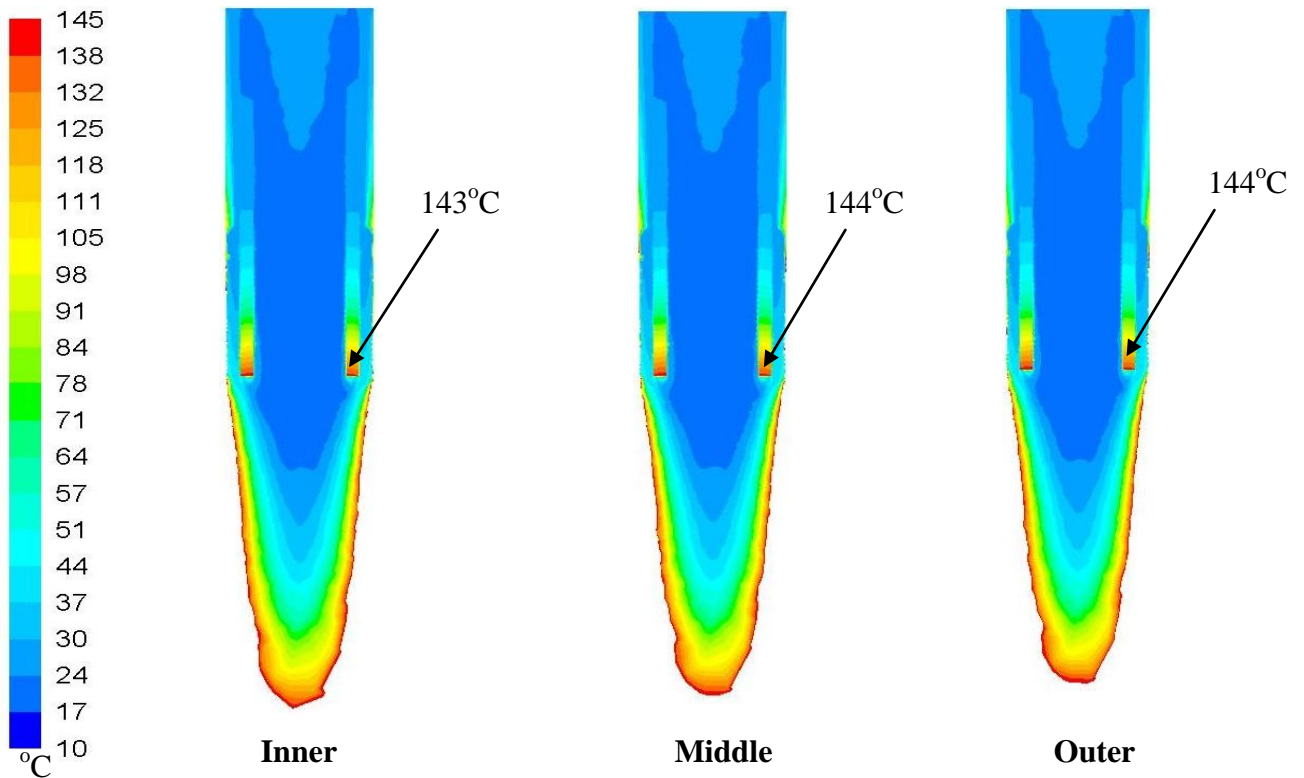


Fig. 6.7: Nozzle temperature for different positions of primary air inlet (air cooling)

The continuous heat flux from the nozzle walls results in a decrease in temperature at the nozzle. In case of primary air inlet position at the outer ring, the temperature has been noted to be at 144°C instead of 418°C for the insulated furnace (Fig. 6.5). Furthermore, it is also observed that the temperature of nozzle tip increases when injecting primary air away from the nozzle. A similar trend was found in the previous simulations (Fig. 6.5). It should also be noted that the temperature at the upper and middle part of the nozzle is less than the melting point of paint residue, i.e. less than 60°C. However, a high temperature is observed at the nozzle exit. The simulations with similar operating conditions (fuel and air quantities) conducted for the case of water cooling resulted in significantly less nozzle tip temperature, i.e. around 107°C (Table 6.3). This implies that the water cooling gives more feasible results than the air cooling method as the heat flux to the water cooling wall is greater than in the present case.

Moreover, it is also concluded from the results (Fig. 6.7) that the current operating conditions of walls and air supply are suitable for the combustion of those solid materials which have constituents with melting point around 145°C. For example plastics, e.g. polypropylene (PP) and polyethylene terephthalate (PET), have a melting point of 183°C and 265°C, respectively. Solid wastes containing such materials can be transported to PFC furnaces using the current nozzle design and operating conditions.

6.9 A case of materials with melting point at 60°C

The simulations conducted by enabling heat losses to the ambient resulted that there is a significant influence of heat flux from the top of the furnace. A significant reduction in nozzle

tip temperature is observed (Figs. 6.5 and 6.7). However, it is observed from the results that nozzle temperature is reduced to approximately 140°C which is suitable for those materials which have melting point greater than or equal to 140°C, e.g. plastics. In order to reduce nozzle tip temperature to a further lower level, i.e. less than 60°C, the present study is conducted by applying different nozzle air flow rates to the case of air cooling. For this purpose, nozzle air flow rates are adopted from Table 6.1. Primary air is injected in all three inlets rings, i.e. inner, middle and outer. The primary air flow rate is supplied at flow rates of 40 m³ h⁻¹, 53 m³ h⁻¹ and 67 m³ h⁻¹ through inner, middle and outer inlets respectively (as described in Section 6.3). However, secondary air is omitted in the present simulations. It is observed that the maximum combustion temperature decreases significantly (as expected) by implementing heat flux from the furnace walls and by increasing the nozzle air flow rates as also happens in the case of water cooling (Section 6.4). However, it is important to note that the reduction in temperature at the lower tip of the fuel nozzle is more by supplying primary air in all three rings, i.e. inner, middle and outer. However, the reduction in temperature is less as compared to the case of water cooling (Fig. 6.3). Table 6.6 shows the predicted temperatures for different nozzle air flow rates.

Table 6.6: CFD simulation results with different nozzle air flow rates (case of air cooling)

Case	Nozzle air flow rate	Nozzle temperature	Combustion temperature
Case 1	40 m ³ h ⁻¹	108°C	1896°C
Case 2	60 m ³ h ⁻¹	80°C	1608°C
Case 3	90 m ³ h ⁻¹	58°C	1344°C
Case 4	135 m ³ h ⁻¹	43°C	1055°C

A maximum temperature of 1896°C is achieved in Case 1, which is predicted as 1537°C in case of water cooling (Fig. 6.2). A decrease in maximum combustion temperature to 1608°C is observed when altering nozzle air from Case 1 to Case 2 (Appendix C, Fig. C5). The maximum temperature in the combustion zone is observed to be 1344°C and 1055°C in Case 3 and Case 4, respectively, which is noted as 1076°C and 930°C in case of water cooling (Fig. 6.2, Appendix C, Fig. C1). This implies that nozzle air has a similar effect of temperature reduction as in the previous case (i.e. case of water cooling). However, the reduction in temperature is more prominent in case of water cooling as compared to the air cooling case due to the greater cooling effect and heat flux from the surface of water cooling wall.

The close-up view (Fig. 6.8) of the nozzle shows that temperature at the lower tip decreases significantly by increasing the nozzle air flow rate with a factor of 1.5 (similar to the case of water cooling). However, the reduction in the temperature of the lower tip of the nozzle is less as compared to the case of water cooling. The nozzle temperature is observed to be 108°C (Fig. 6.8) instead of 68°C for water cooling (Fig. 6.3). The nozzle temperature decreases to 80°C by increasing the nozzle air flow rate from 40 m³ h⁻¹ with a factor of 1.5, i.e. 60 m³ h⁻¹. Similarly, the nozzle temperature is obtained as 58°C with a nozzle air flow rate of 90 m³ h⁻¹.

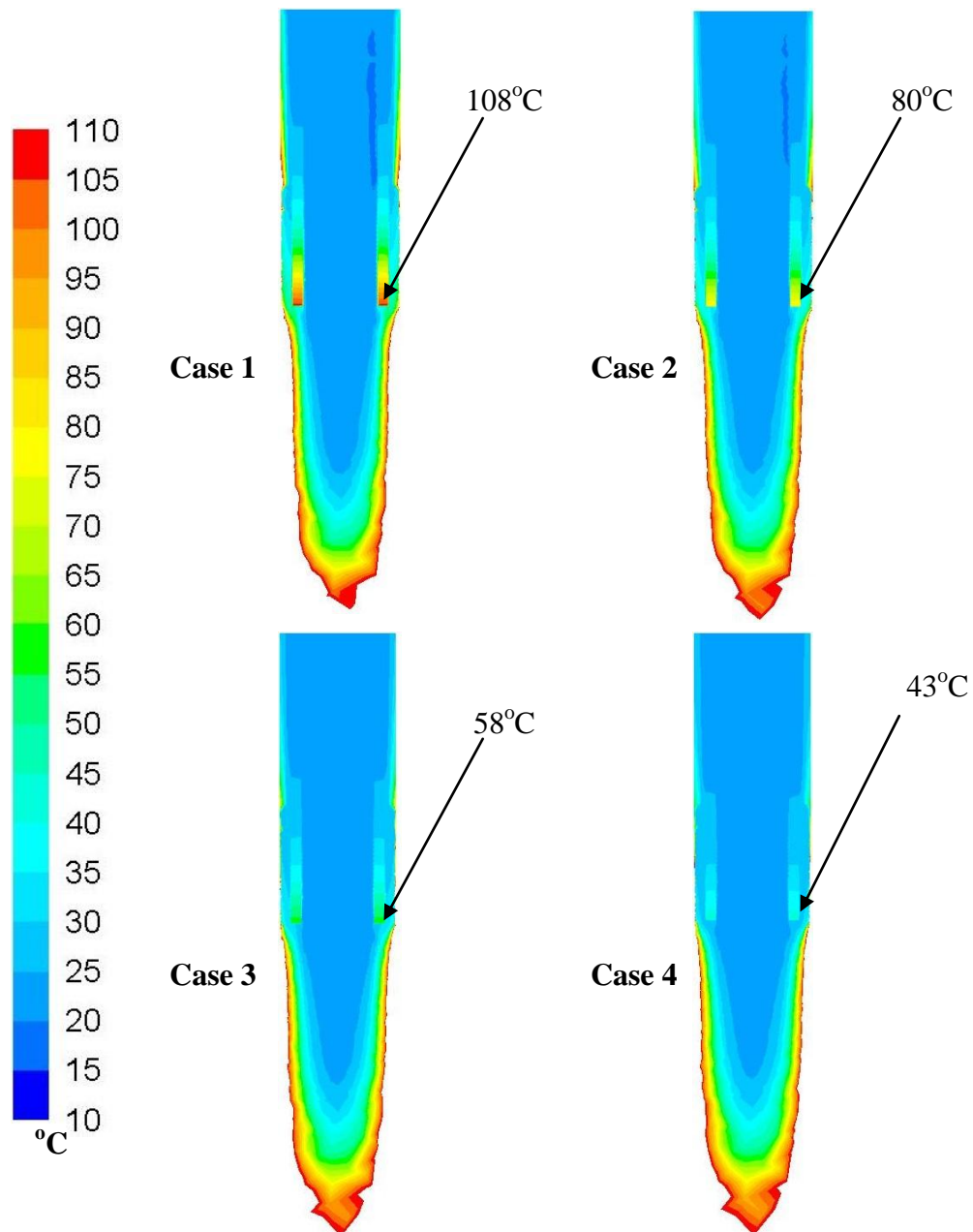


Fig. 6.8: Nozzle temperature with different levels of nozzle air (case of air cooling)

It is important to note that this level (Case 3) of air flow rate, i.e. $90 \text{ m}^3 \text{ h}^{-1}$, results in a nozzle tip temperature below the melting point of paint residue ($< 60^\circ\text{C}$). Hence, under such heat flux and operating conditions proposed by Case 3 the simpler design of fuel nozzle (Nozzle 1) can be used for the combustion of materials having melting point around 60°C . However, it should also be noted that the required limit of nozzle tip temperature is achieved with a nozzle air flow rate of $60 \text{ m}^3 \text{ h}^{-1}$ with water cooling while in case of air cooling, the required limit is obtained with a larger air flow rate, i.e. $90 \text{ m}^3 \text{ h}^{-1}$. The choice of either level of nozzle air flow rate depends upon the available resource, i.e. cooling system etc.

6.10 Summary

The current chapter presented the efforts made for the simplification of fuel nozzle and burner setup for transportation of pulverized fuel with low melting point. Pros and contras of the simplified nozzle are discussed in comparison with the optimized fuel nozzle (as described in Chapter 5). A parametric study with the simplified version of the nozzle (Nozzle 1) has been conducted with different nozzle air flow rates, primary air inlet positions, water cooling, air cooling and heat flux through the furnace walls. It is concluded from the CFD simulation results that the nozzle air flow rate still has a great influence on the nozzle tip temperature. The comparison between different positions of primary air inlet has revealed that the temperature at the nozzle tip increases by supplying the primary air away from the nozzle. Furthermore, water cooling has more significant effect on the nozzle temperature reduction than the air cooling. With air cooling, the temperature at the top of the nozzle has been observed to be less than 60°C while at the bottom of the nozzle the temperature is still high, e.g. 143°C. In this case, the suggested operating conditions are suitable for the combustion of solid materials with melting point of 145°C or more, such as plastics. Moreover, efforts made for lowering the nozzle tip temperature to less than 60°C revealed that the required limit can be obtained by providing primary air in all primary air inlets, which reduces the temperature near the nozzle exit. The study concluded that a nozzle air flow rate of 60 m³ h⁻¹ can be used with water cooling, while in case of air cooling an air flow rate of 90 m³ h⁻¹ should be used to achieve appropriate temperature at the fuel nozzle during the transportation of solid fuel with melting point around 60°C.

Partial Validation of CFD Model for PFC

This chapter is dedicated to a partial validation and comparison of simulation results of the proposed comprehensive computational fluid dynamics (CFD) model for the combustion of pulverized fuel with low melting point with a pilot plant combustion facility. For this purpose the CFD simulations are conducted with the operating conditions of an operating pulverized fuel combustion plant. The experimental measurements generated from the plant are compared with the simulation results. The case of optimum nozzle design and operating conditions has also been compared with mass and energy balance results. The outcomes from both investigations are discussed.

7.1 Overview

In the previous Chapters (Chapters 4, 5 and 6), different strategies have been presented for the combustion process of solid (pulverized) materials with low melting point. Different nozzle designs have been evaluated with different operating conditions. As an outlook of the parametric study, the present study has been conducted in order to compare the simulation results with experimental measurements in a pilot scale combustion plant. The emphasis in this work has been on the temperature results at different positions in the furnace. Moreover, the factors affecting the decrease in temperature in actual conditions are also presented.

7.2 Experimental investigations

The experimental investigations have been conducted at the pilot plant combustion facility of Fraunhofer Institute for Factory Operation and Automation (IFF), Magdeburg, Germany (Fig. 7.1). A series of experimental studies have been conducted at the combustion plant, however a selected operational case is discussed here (as given by Table 7.1).

Table 7.1: Operating conditions for experiments

Parameter	Quantity	Inlet Temperature
Fuel mass flow rate	29 kg h ⁻¹	10.4°C
Fuel transport air	20 m ³ h ⁻¹	10.4°C
Nozzle air (outer section)	72 m ³ h ⁻¹	4.1°C
Primary air	79 m ³ h ⁻¹	4.1°C
Fuel particle size (average)	12.4 μm	
Heating value	17835000 J kg ⁻¹	

It has been concluded from the previous findings (CFD modeling investigations) that the concentric pipe nozzle (Nozzle 1 in the present study) with two sections, i.e. inner and outer section provides satisfactory results and is comparatively easy to construct. Therefore, in order to take this advantage, i.e. simple construction and implementation in the furnace, the

experimental analysis has been conducted with this nozzle. The operating conditions for the experimental investigations are listed in Table 7.1. It should be noted that slightly different operating conditions and burner configuration (as compared to that used in Chapter 4) were used in the experimental investigations. The plant was run with a total thermal power capacity of 148 kW. The fuel is injected into the combustion furnace with a mass flow rate of 29 kg h^{-1} . The fuel is transported by a stream of air with flow rate of $20 \text{ m}^3 \text{ h}^{-1}$ in the inner pipe of the nozzle at an inlet temperature of 10.4°C . The cooling air is provided in the outer pipe (concentric) of the nozzle at a flow rate of $(10 \text{ m}^3 \text{ h}^{-1} + 62 \text{ m}^3 \text{ h}^{-1}) 72 \text{ m}^3 \text{ h}^{-1}$. The primary air is provided in only one ring (outer) of the primary air inlets with a flow rate of $79 \text{ m}^3 \text{ h}^{-1}$. As described in Chapter 4, spray paint residue has a different composition and a different particle size depending upon the type of paint and spraying mechanism. Hence, a paint residue with an average particle size of $12.4 \mu\text{m}$ and a heating value of $17835000 \text{ J kg}^{-1}$ was used in the experimental investigations.



Fig. 7.1: Combustion plant for pulverized materials (Fraunhofer IFF, Magdeburg-Germany)

The measurements have been recorded for one hour duration of the experiment. Thermocouple devices were installed at different locations in the combustion furnace, but near the furnace walls. Figure 7.2 illustrates the different positions of temperature measurements in the furnace. In the present work, temperature recorded at three different locations is discussed. Thermocouples have been allotted with different names for documentation purposes. For example, thermocouples T1-T4 (Fig. 7.3) have been placed at a distance of 100 mm from the edge of the top plane (outer ring of the primary inlet). Position 2 indicates the location of thermo couples T5-T8 at distance of 700 mm from the furnace top

edge. The temperature of the flue gases is determined by the thermocouple 23T1 (Fig. 7.3) located at the flue gas outlet (Fig. 7.2, Position 3).

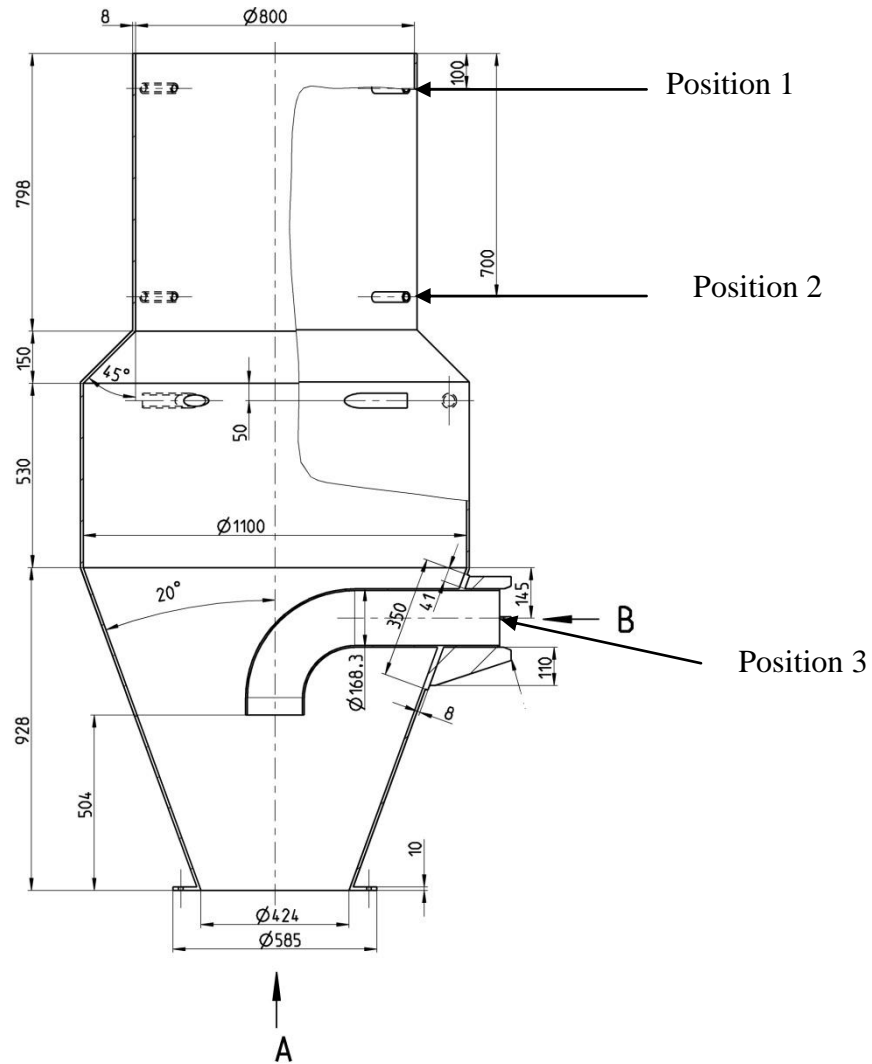


Fig. 7.2: Different positions for temperature measurements (Fraunhofer IFF, Magdeburg)

Figure 7.3 represents the data recording system for the combustion plant for pulverized material. The temperature results have been measured at different locations in the combustion apparatus (Fig. 7.3). However, three locations (as described earlier) are reported in the present study (Table 7.2). The average temperature at position 1, i.e. at a distance of 100 mm from the top edge of the furnace, has been observed at 487°C. The temperature increases gradually and reaches 611°C at a distance of 700 mm from the top edge. It is important to note that the temperature is recorded near the wall of the furnace as shown in Fig. 7.2. Difficulties are faced to measure the temperature at the centre of the furnace, i.e. the maximum combustion (flame) temperature. After reaching the maximum value of the combustion temperature, the temperature decreases significantly and is recorded to be at 805°C at the flue gas outlet (Table 7.2).

Table 7.2: Temperature at different locations in combustion plant

Position	Temperature (°C)
Position 1	487.49°C
Position 2	611.04°C
Position 3	805.49°C

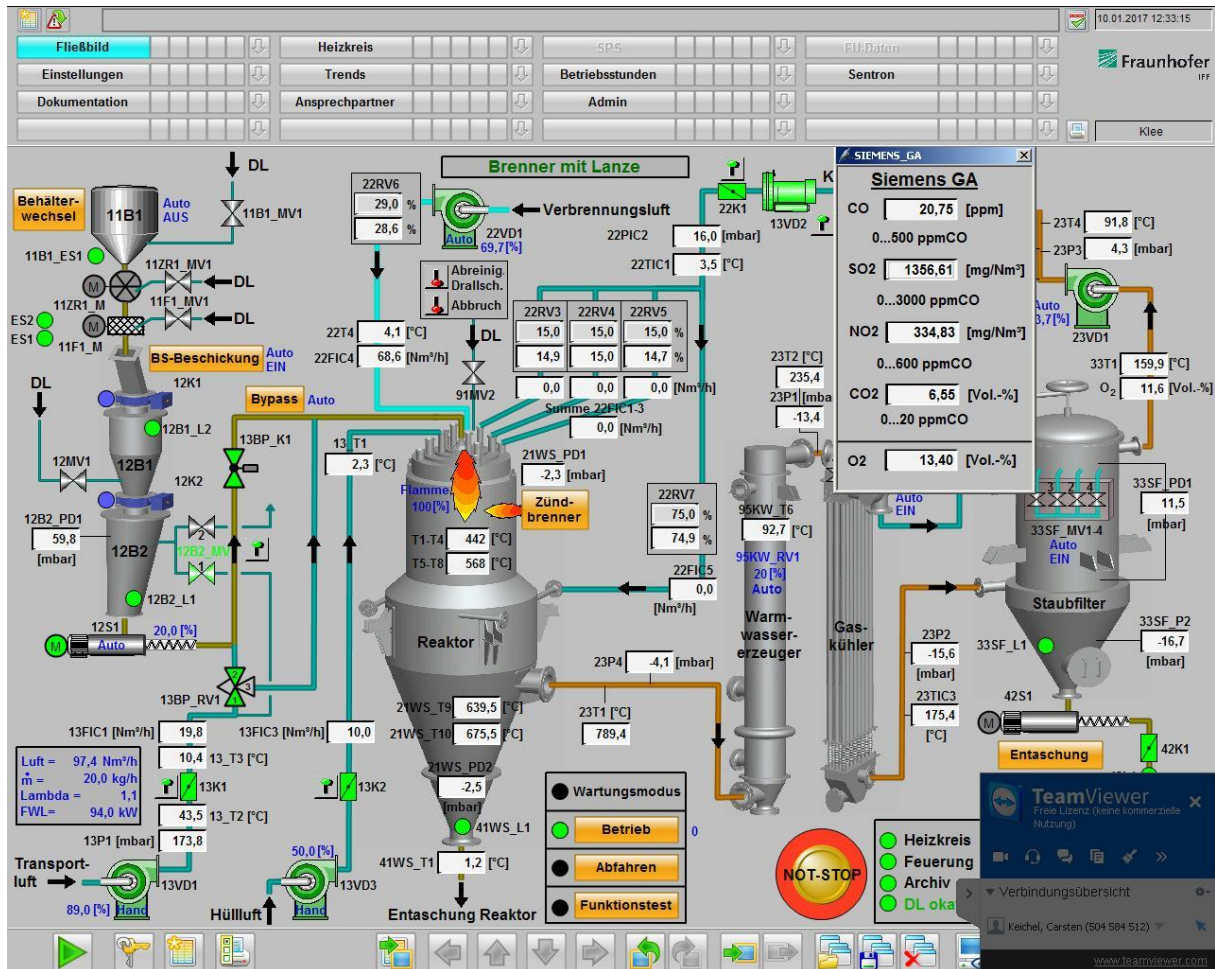


Fig. 7.3: Data recording system for combustion process (Fraunhofer IFF, Magdeburg)

7.3 CFD simulation results

Multiphase CFD simulations are conducted with the operating conditions of experimental analysis as provided in Table 7.1. The geometry of the furnace (with different initial/operating conditions of furnace walls) and simplified nozzle (Nozzle 1) presented in Chapter 6 is used in the present simulations. In the experimental investigations the primary air is fed through the outer ring of the furnace, therefore primary air is supplied through the same inlet (outer) in the numerical simulations. Moreover, the nozzle air flow rate as well as inlet temperature of all the reactants is also set according to the experimental operation (Table 7.1). The same modeling technique as in previous numerical investigations is applied with steady state

conditions. Heat losses are also implemented to the ambient by setting a heat transfer coefficient of $13.9 \text{ W m}^{-2} \text{ K}^{-1}$ (Chapter 6).

Figure 7.4 represents the simulation results (temperature field) with the stated operating conditions. The temperature of the injected streams of air and fuel increases due to the mixing with the hot combustion gas environment. The maximum combustion temperature is obtained as 1722°C in the combustion zone. After reaching the maximum value, the combustion temperature decreases significantly due to the transfer to walls of the furnace. The flue gases (combustion gases) also carry the heat of the combustion reaction to the outlet. The temperature of the flue gases at the furnace outlet is observed as 1364°C .

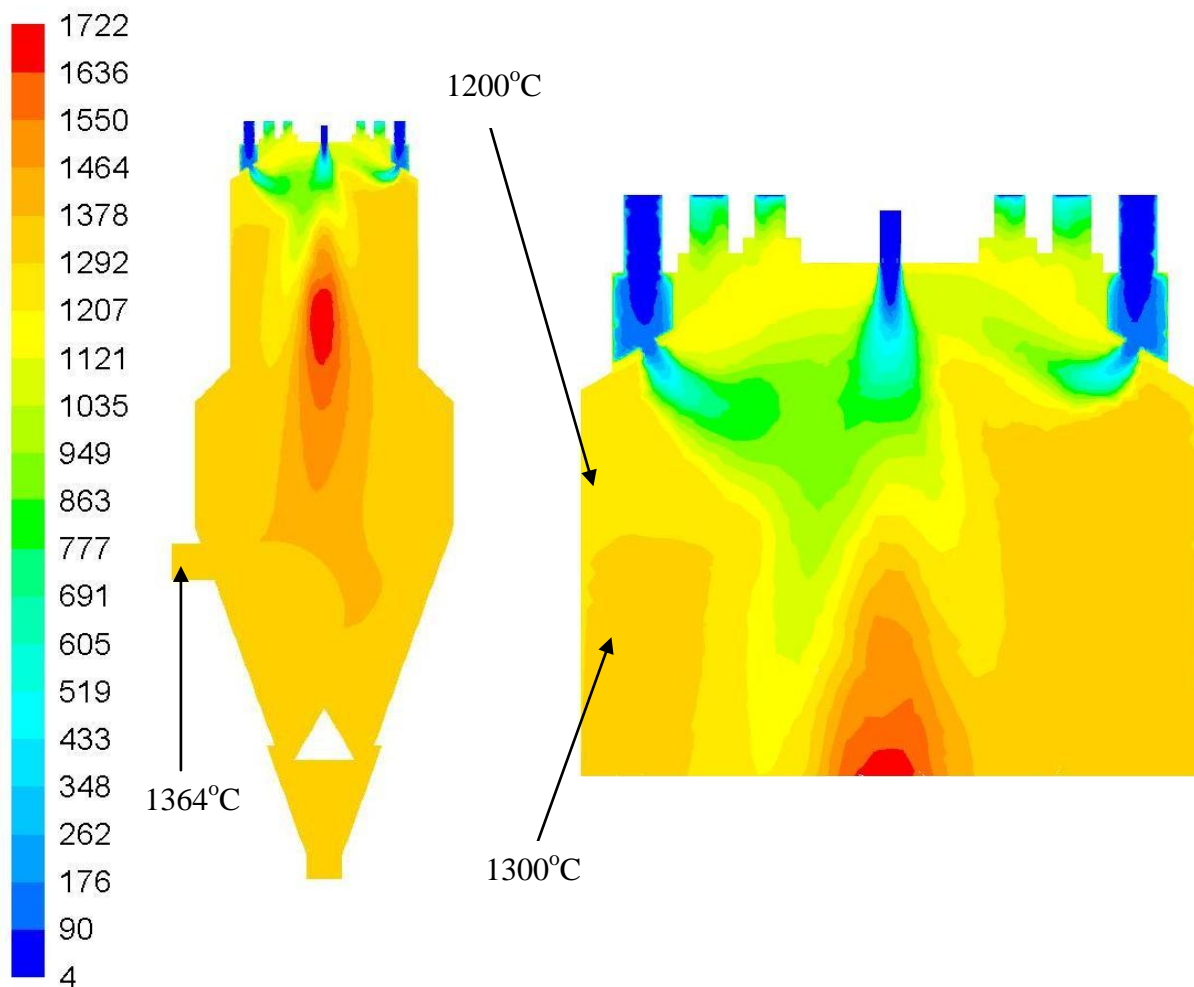


Fig. 7.4: Simulation results (temperature fields)

The temperature profile from the injection point to 1.5 m inside the furnace is illustrated in Fig. 7.5. It can be observed that the temperature increases gradually after the injection of pulverized material into the furnace. After reaching the maximum value, i.e. 1724°C , the temperature decreases to approximately 1400°C at a distance of 1.5 m from the injection point.

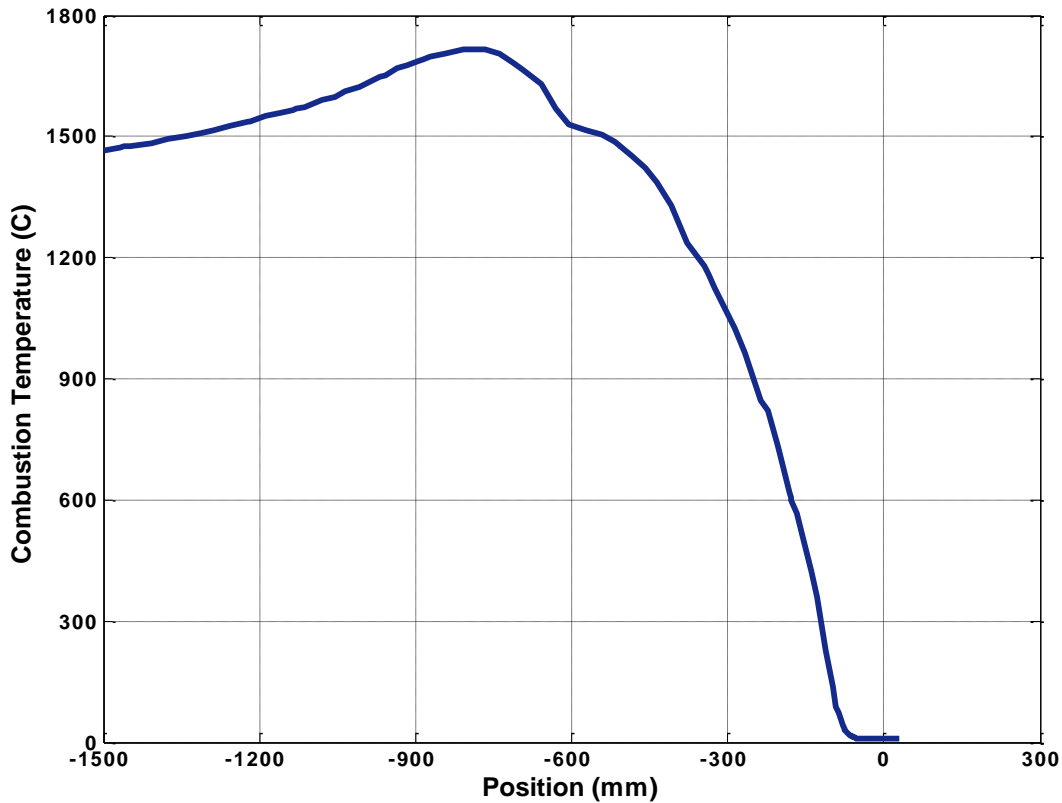


Fig. 7.5: Temperature profile along the furnace central line

7.4 Comparison between experimental and simulation results

The comparison between the experimental measurements and numerical simulation results has revealed that the predicted temperature is higher than the experimental values. For example, the average temperature at the position 1 has been predicted to be at approximately 1200°C while the temperature at this location has been observed to be at about 500°C in the experimental analysis. Similarly the temperature at the position 2, i.e. 700 mm from the furnace edge, has been observed at 611°C in the experimental measurements while simulation results have shown a higher temperature (around 1300°C) at this point. Similarly, the temperature of flue gases at the outlet has been predicted to be at about 1367°C, while in the experimental investigations the temperature of flue gases has been observed to be at 805°C. The major reason for this difference is the greater heat loss (heat flux) from the actual furnace. The significant heat flux from the furnace walls and top plates of the furnace imparts a cooling effect at the furnace and, hence, the temperature decreases significantly. Furthermore, a significant leakage of air has also been observed in the experimental investigations. This may also become a reason for a larger amount of heat loss from the furnace and, therefore, reduce the overall furnace temperature.

However, it should be noted that both analyses have resulted (qualitatively) in similar trends. Higher temperature has been obtained in position 2 as compared to position 1. Being further downstream than position 1, high temperature is observed at position 2 due to the hot combustion gases which are released as result of burning of combustible material. It can be

expected that measured temperature would be higher in the middle part of the furnace. A high temperature has been recorded at the flue gas outlet which is carried by the flue gases.

7.5 Outcomes and reasons for discrepancies

The comparison between experimental and simulation results shows similar trends qualitatively, however a deviation between predicted and measured temperatures is observed in the combustion furnace. Various factors are responsible for the lower values of temperature measured in the furnace. As described before, a major reason for the lower temperature near the walls and at the flue gas outlet is the greater heat loss from the top of the furnace and from the side walls. Simulations were conducted by implementing the heat losses to the ambient with a heat transfer coefficient of $13.9 \text{ W m}^{-2} \text{ K}^{-1}$. However, the temperature of the surroundings (in actual plant) also affects the heat flux from the walls. Moreover, a huge leakage of gases from the plant, especially at the inlets and outlet connections, and the bottom of the furnace, was also observed in the experiments, which may become a major cause for lowering the temperature. On the other hand, simulations are conducted by implementing heat flux from the top of the furnace; however, side walls and seals are insulated with rock wool and steel alloy (as described in Chapter 6). The bottom of the furnace is also closed with the insulation material. Moreover, simulations are based on the assumption of complete combustion; hence, production of secondary species is not considered which may also affect the temperature profiles. Based on current outcomes, further investigations are recommended with similar operational and geometrical configurations.

7.6 A case of optimized nozzle: Comparison with calculated results

Mass and energy balance indicate the correctness of the simulation results. In order to assess the proposed CFD model with the optimized nozzle design and operating conditions, the present study has been taken up with Nozzle 2 (the best case concluded in Chapter 5). A comparison is made between the simulation results, generated from the CFD modeling strategy, with the calculated results obtained from mass and energy balance (Appendix E, Table E1). Calculations are made with the operating conditions as described in Chapter 5. Nozzle air flow rate has been taken as $40 \text{ m}^3 \text{ h}^{-1}$ and at a temperature of 25°C . Primary air is supplied with air flow rates of $40 \text{ m}^3 \text{ h}^{-1}$, $53 \text{ m}^3 \text{ h}^{-1}$, $67 \text{ m}^3 \text{ h}^{-1}$ in the all inner, middle and outer primary air inlet rings, respectively, while the flow rate of secondary air has been set as $50 \text{ m}^3 \text{ h}^{-1}$ with a preheat temperature of 300°C . Fuel is injected with a mass flow rate of 20 kg h^{-1} . The mass and energy balance model has been applied to the current operating conditions (optimized operating conditions) to calculate different parameters. An excess air ratio of $\lambda = 2.82$ resulted with the current fuel and air quantities. The adiabatic temperature of the flue gases has been calculated to be 1112°C at this level of excess air number (λ). Moreover, the injection velocity of fuel is also calculated as 46.45 m s^{-1} depending upon the size and air flow rate of Nozzle 2.

The calculated results are compared with the simulation results with the optimized fuel nozzle and operating conditions. It should be noted that in the present case, the simulation results are obtained without implementing the water cooling effect, i.e. all walls are assumed to be insulated. Table 7.3 presents the values of different parameters with balance calculations and numerical simulations.

Table 7.3: Comparison between calculated and simulation results

Parameter	Calculated Results	Simulation Results
Injection velocity (m s^{-1})	46.45	47.55
Flue gas mass flow (kg s^{-1})	0.09334	0.09325
Flue gas temperature ($^{\circ}\text{C}$)	1112	1115

A very good agreement between the calculated and simulation results is revealed. For example, the adiabatic temperature of the flue gases is 1112°C from the balance and 1115°C from the CFD (Fig. 7.6).

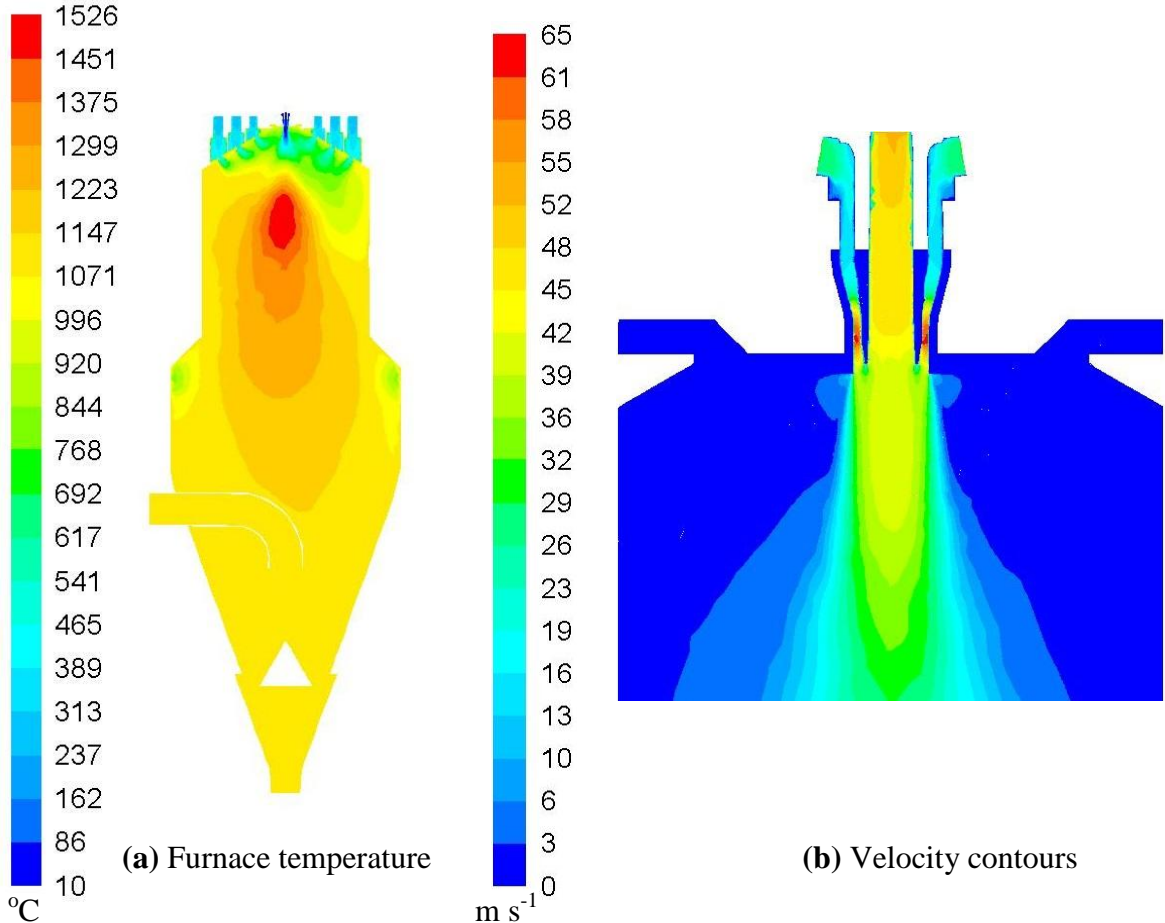


Fig. 7.6: Simulation results with optimized operating conditions (a) temperature (b) velocity

Table 7.4 represents the flue gases obtained from the combustion process with the stated operating conditions. It should be noted that the present work have been carried out with the assumption of complete combustion of all the combustible materials. This implies that all carbon present in the fuel is burnt to produce carbon dioxide (CO_2), hydrogen is oxidized to

H₂O and sulfur reacts with oxygen to produce sulfur dioxide (SO₂). Nitrogen, as present in air, does not take part in the combustion reaction. Hence, it leaves along with the mixture of flue gases with a relatively high quantity. It is interesting to note that the oxygen required for the complete combustion is consumed during the combustion process and the extra amount of oxygen is contained in the combustion gases leaving through the outlet (Chapter 2). However, efforts must be made in order to avoid favorable conditions for the production of nitrogen oxides (NO_x). The conditions and measures to reduce NO_x emissions have been presented in Chapter 2.

Balance results show that carbon dioxide is produced with a mass fraction of 0.0967. Mass fraction of water vapor is computed to be 0.0246 due to the oxidation of hydrogen. As sulfur is contained in a very minor quantity, sulfur dioxide is generated with the lowest mass fraction, i.e. 0.0016. As air is provided in excess, i.e. the excess air ratio is calculated as 2.82, oxygen is also contained in the flue gas mixture with a mass fraction of 0.1438. Nitrogen is contained in the flue gas mixture with a mass fraction of 0.7334, as air contains a major portion of nitrogen. Regarding flue gas comparison, a very good agreement has been found between calculated and CFD simulation results (Table 7.4, Appendix D, Fig. D1).

Table 7.4: Mass fractions of flue gases at furnace outlet

Flue Gases	Calculated Results	Simulation Results
CO ₂	0.0967	0.0965
H ₂ O	0.0246	0.0239
N ₂	0.7334	0.7348
O ₂	0.1438	0.1455
SO ₂	0.0016	0.0019

7.7 Summary

As an outcome of this chapter, it is concluded that both investigations (experimental and numerical) have resulted in similar trends qualitatively. Because of various factors (heat losses, air leakage from the furnace etc.) involved in the measurements of the actual combustion furnace, a significant difference is also found in the experimental measurements and simulation results. However, the CFD model has been revealed to not offend the mass and energy balances of the process. A similar trend of furnace outlet temperature against adiabatic temperature is also described in Chapter 5. Further experimental investigations should be conducted to fully validate the CFD simulation results for better exploitation of the proposed model.

Conclusions and Outlook

The present research work was carried out for the modeling of combustion process of solid materials with low melting point. Special focus has been made on apparatus design, i.e. fuel nozzles for such materials (with low melting point). The background of combustion process, in particular, pulverized fuel combustion has been discussed briefly. Type and constituents of the solid (fuel) material play a vital role in the PFC process. The special technical challenge of the fuel material considered in this study, however, is the significantly lower melting point as compared to other fuels, which may lead to blocking in the nozzle. Hence, the main objective of the investigations in this work was to minimize the temperature of the fuel nozzle walls. Different solid materials having low melting point were discussed briefly. However, an example of paint residue generated from metal/furniture coating industry has been taken, as it contains constituents with relatively low melting point, i.e. around 60°C. In this work, a unified modeling approach has been presented for the combustion of solid fuels. A mass and energy balance model has been presented to identify the basic parameters and to check their influence on the (stoichiometric) combustion process. A comprehensive CFD model has been presented for modeling the combustion process of solid materials with low melting point, i.e. around 60°C. Multiphase CFD simulations were conducted with the commercial software ANSYS (Fluent). Different fuel nozzle designs were evaluated in order to suggest the most appropriate fuel nozzle for the transportation of pulverized fuel (having melting point around 60°C) to the PFC furnace. The effect of nozzle air flow rates and fuel particle size on combustion process was also addressed with the proposed CFD modeling technique.

Major conclusions of the present work are summarized in the following:

1- Thermal characteristics and chemical composition of the solid materials play an important role in the combustion phenomena. For example, the lower the moisture content (MC), the higher the heating value of the solid fuel and vice versa. Similarly, solid fuels with high volatile matter (VM) have higher heating value. According to the elemental analysis, carbon and hydrogen are the main combustible constituents present in the solid fuel, which burn to release energy. Both constituents determine the oxidant requirements for complete combustion. The higher the carbon content present in the solid fuel, the higher is the oxygen demand (OD). Air demand (AD) also depends upon the type and composition of the constituents present in the solid fuel. It also slightly depends upon the concentration of oxygen present in the air supplied. The more the oxygen concentration in the air, the less will be the air demand (AD) and vice versa. The adiabatic temperature, generated as a result of burning of combustible matter, is mainly governed by three different parameters, i.e. heating value, air demand and excess air ratio. The higher the heating value, the higher is the adiabatic

temperature. The higher the air demand (AD), the lower is the adiabatic temperature. The adiabatic temperature decreases with an increase in excess air ratio. Moreover, it is also concluded that preheating of air entering to the combustion system increases the adiabatic combustion temperature.

2- The CFD modeling investigations conducted with four different nozzle designs revealed that the different nozzle designs resulted in significant variations regarding the flow patterns and temperature distributions in the PFC furnace depending upon their structure and cross sectional area. Devolatilization is greatly influenced by such flow patterns which control the maximum combustion temperature in the combustion zone. Nozzle 1 and Nozzle 2 showed similar flow patterns and combustion temperatures, while similar contours have been found in cases of Nozzle 3 and Nozzle 4. Moreover, it is also concluded that there is a strong influence of (nozzle) air flow rates on combustion temperature. The combustion temperature decreases significantly by increasing the air flow rates supplied to the PFC furnace. A reduction of approximately 300°C in combustion temperature was observed by increasing air flow rate with a factor of 1.75.

3- It is concluded from the CFD modeling investigations of the four studied nozzles that the temperature at the nozzle also depends on its shape and design. Although a more uniform and better mixing is obtained with the perforated (bottom) nozzle, such nozzles result in a very high temperature at the injection point due to direct exposure to the radiation from the combustion zone. An open end nozzle, on the other hand, showed comparatively better outcomes in this context. Nozzle 3 and Nozzle 4 resulted in a high wall temperature (> 100°C) at the injection plane (perforated plane). On the other hand, Nozzle 1 showed comparatively lower temperature than Nozzle 3 and Nozzle 4 but higher than the melting point of fuel particles. The best results were obtained in case of Nozzle 2 (with Data Set 2) as the temperature during the fuel transportation was lower than the maximum limit (60°C), i.e. the major finding of the current work. It is also concluded that there is a strong influence of nozzle air flow rates on the temperature of the partition wall between the nozzle sections. The nozzle tip temperature decreases by (approximately) 20 K by increasing the nozzle air flow rate with a factor of 1.75. Hence, Nozzle 2 is recommended with a nozzle air flow rate of 40 m³ h⁻¹ for the injection of pulverized fuel with low melting point.

4- An investigation conducted with different fuel particle sizes resulted that the fuel particle size has a significant influence on the formation of combustion zone. Volatiles are released closer to the nozzle exit resulting in a wider combustion zone in the case of small fuel particles. On the other hand, the combustion zone is prolonged with the large fuel particle size. A large fuel particle size results in less temperature at the nozzle while too small particles increase the temperature in the nozzle tip due to formation of a wider and closer combustion zone. An average fuel particle size of 10 µm is suggested for the combustion of pulverized paint waste material. Paint residue is formed by solidifying of spray droplets and, hence, composed of very fine particles, i.e. particle size in the range of 10-50 µm. However,

other solid fuels and waste materials, i.e. coal, biomass, plastics etc. should be ground and milled to a finer particle size to get optimum outcomes.

5- The study conducted for the optimization of nozzle air flow rate revealed that the nozzle temperature decreases significantly by increasing nozzle air flow rate from $13 \text{ m}^3 \text{ h}^{-1}$ to $40 \text{ m}^3 \text{ h}^{-1}$, however, after $40 \text{ m}^3 \text{ h}^{-1}$, the reduction in nozzle tip temperature is not very prominent. Moreover, excess air imparts a cooling effect on the combustion temperature, i.e. reduction of 300°C in combustion temperature was observed by increasing nozzle air flow rate (with a factor of 1.75). There are certain limitations for using high air flow rates for the combustion process (Chapter 5). Moreover, a high nozzle air flow rate also increases the operational cost of the combustion plant. In the findings of current work, an optimized nozzle air flow rate of $40 \text{ m}^3 \text{ h}^{-1}$ was proposed. It is concluded from the investigations conducted for the sectional increment of nozzle air flow rates that nozzle temperature reduction is a combined effect of the FTA and the CA. However, the CA has more significant cooling effect than the FTA.

6- Simplified design of nozzle (Nozzle 1) was found to be easier to construct, however, a high temperature may result at the nozzle lower tip with the air flow rate given by Data Set 2. Moreover, additional apparatus is required for the implementation of water cooling at the burner. The efforts made for reducing the nozzle tip temperature and simplification of burner structure (Chapter 6) resulted that heat flux from the top walls to the ambient (air cooling) also has a significant influence on the temperature reduction, however a higher nozzle air flow rate is required in this case. Moreover, it is also concluded that the injection of primary air near to the fuel nozzle contributes to lowering the nozzle tip temperature.

7- The proposed CFD model showed a very good agreement with the calculated results obtained from mass and energy balance. However, certain discrepancies were found in the comparison of experimental and simulation results. The main reasons for these differences are the slightly different operating conditions and escape of significant amount of heat from the combustion plant. However, similarities have been observed (qualitatively) in the trends of temperature profile along the furnace in both investigations.

The present work has been focused on the identification of the most appropriate fuel nozzle for the transportation of pulverized fuel material (with low melting point). Although significant outcomes have been revealed, many aspects remain un-excavated in the investigated field. As an outlook of the current work, further investigations are recommended for the exploitation of the proposed combustion technology to be carried out on following areas:

1- The proposed comprehensive CFD should be studied with different solid materials in order to justify the feasibility and application of the model. Moreover, the effect of co-firing with multiple fuel blends should also be investigated.

2- The current work has been focused on the temperature profiles in the furnace and at the nozzle in particular. Further investigations should be carried out with the suggested operating conditions and nozzle design for the evaluation of flue gas emission levels. Formation and

mitigation of NO_x should also be addressed in future work. The fate of ash formed in the combustion furnace should also be studied experimentally and numerically.

3- The latest advancements in pulverized fuel combustion (PFC) technology such as oxy-fuel combustion, flue gas recirculation, high preheating air combustion etc. should be studied with the proposed model.

4- The effect of water cooling should be further exploited with a volume flow device attached to the burner. The cooling effect can also be investigated at different levels of water (cooling) temperatures and volume flow rates.

5- The current work has been carried out for steady state conditions. The transient modeling approach should be applied in order to check the melting behavior of fuel particles at different time steps, especially within the fuel nozzle.

6- Further experimental studies are recommended with the optimized operating conditions and burner configuration for the validation of proposed comprehensive CFD model.

Bibliography

- [1] Christensen, T. H. 2011. Introduction: Introduction to waste management. In Christensen, T. H. (Eds.), Solid waste technology & management, Chapter 1.1. John Wiley & Sons Ltd., Chichester ISBN: 978-1-405-17517-3.
- [2] Song, Q., J. Li and X. Zeng. 2015. Minimizing the increasing solid waste through zero waste strategy. *Journal of Cleaner Production*. 104:199-210.
- [3] Ghinea, C., E. N. Dragoi, E. D. Comanita, M. Gavrilescu, T. Campean, S. Curteanu and M. Gavrilescu. 2016. Forecasting municipal solid waste generation using prognostic tools and regression analysis. *Journal of Environmental Management*. 182:80-93.
- [4] Persson, U. and M. Munster. 2016. Current and future prospects for heat recovery from waste in European district heating systems: A literature and data review. *Energy*. 110:116-128.
- [5] Moh, Y. C. and L. A. Manaf. 2017. Solid waste management transformation and future challenges of source separation and recycling practice in Malaysia. *Resource, Conservation and Recycling*. 116:1-14.
- [6] Fudala-Ksiazek, S., M. Pierpaoli, E. Kulbat and A. Luczkiewicz. 2016. A modern solid waste management strategy: The generation of new by-products. *Waste Management*. 49:516-529.
- [7] Vaajasaari, K., M. Kulovaara, A. Joutti, E. Schultz and K. Soljamo. 2004. Hazardous properties of paint residues from the furniture industry. *Journal of Hazardous Materials*. 106A:71-79.
- [8] Couto, N., V. Silva, E. Monteiro, S. Teixeira, R. Chacartegui, K. Bouziane, P. S. D. Brito and A. Rouboa. 2015. Numerical and experimental analysis of municipal solid wastes gasification process. *Applied Thermal Engineering*. 78:185-195.
- [9] Pan, S. Y., M. A. Du, I. T. Huang, I. H. Liu and E. E. Chang. 2015. Strategies on implementation of waste-to-energy (WTE) supply chain for circular economy system: A review. *Journal of Cleaner Production*. 108:409-421.
- [10] Huber, F., D. Blasenbauer, O. Mallow, J. Lederer, F. Winter and J. Fellner. 2016. Thermal co-treatment of combustible hazardous waste and waste incineration fly ash in a rotary kiln. *Waste Management*. 58:181-190.
- [11] Rao, M. N., R. Sultana and S. H. Kota. 2016. Solid and hazardous waste management science and engineering. BS publishers Ltd. ISBN: 978-0-12-809734-2.
- [12] Hussain, A., S. M. Arif and M. Aslam. 2017. Emerging renewable and sustainable energy technologies: State of the art. *Renewable and Sustainable Energy Reviews*. 71:12-28.
- [13] Cucchiella, F., I. D'Adamo and M. Gastaldi. 2017. Sustainable waste management: Waste to energy plant as an alternative to landfill. *Energy Conversion and Management*. 131:18-31.

- [14] Maria, F. D., S. Contini, G. Bidini, A. Boncompagni, M. Lasagni and F. Sisani. 2016. Energetic efficiency of an existing waste to energy power plant. *Energy Procedia*. 101:1175-1182.
- [15] Bujak, J. W. 2015. Thermal utilization (treatment) of plastic waste. *Energy*. 90:1468-1477.
- [16] Bujak, J. W. 2015. Heat recovery from thermal treatment of medical waste. *Energy*. 90:1721-1732.
- [17] Ohnishi, S., M. Fujii, M. Ohata, I. Rokuta and T. Fujita. 2016. Efficient energy recovery through a combination of waste-to-energy systems for a low carbon-city. <http://dx.doi.org/10.1016/j.resconrec.2016.11.018>.
- [18] Leckner, B. 2015. Process aspects in combustion and gasification Waste-to-Energy (WtE) units. *Waste Management*. 37:13-25.
- [19] Nasrullah, M., P. Vainikka, J. Hannula, M. Hurme and J. Karki. 2014. Mass, energy and material balance of SRF production process. Part 1: SRF produced from commercial and industrial waste. *Waste Management*. 34:1398-1407.
- [20] Nasrullah, M., P. Vainikka, J. Hannula and M. Hurme. 2015. Elemental balance of SRF production process: solid recovered fuel produced from commercial and industrial waste. *Fuel*. 145:1-11.
- [21] Garces, D., E. Diaz, H. Sastre, S. Ordonez and J. M. Gonzalez-Lafuente. 2016. Evaluation of the potential of different high calorific waste fraction for the preparation of solid recovered fuels. *Waste Management*. 47:164-173.
- [22] Arena, U. and F. D. Gregorio. 2016. Fluidized bed gasification of industrial solid recovered fuels. *Waste Management*. 50:86-92.
- [23] Maschowski, C., M. C. Zangna, G. Trouve and R. Giere. 2016. Bottom ash of trees from Cameroon as fertilizer. *Applied Geochemistry*. 72:88-96.
- [24] Herzel, H., O. Kruger, L. Hermann and C. Adam. 2016. Sewage sludge ash: A promising secondary phosphorous source for fertilizer production. *Science of the Total Environment*. 542:1136-1143.
- [25] Li, Y., L. Hao and X. Chen. 2016. Analysis of MSWI bottom ash reused as alternative material for cement production. *Procedia Environmental Sciences*. 31:549-553.
- [26] Eliche-Quesada, D. and J. Leite-Costa. 2016. Use of bottom ash from olive pomace combustion in the production of eco-friendly fired clay bricks. *Waste Management*. 48:323-333.
- [27] Souza, A. E., S. R. Teixeira, G. T. A. Santos, F. B. Costa and E. Longo. 2011. Reuse of sugarcane bagasse ash (SCBA) to produce ceramic materials. *Journal of Environmental Management*. 92:2774-2780.
- [28] Fellner, J., J. Lederer, A. Purgar, A. Winterstetter, H. Rechberger, F. Winter and D. Laner. 2015. Evaluation of resource recovery from waste incineration residues-the case of zinc. *Waste Management*. 37:95-103.

- [29] Sun, J., H. Peng, J. Chen, X. Wang, M. Wei, W. Li, L. Yang, Q. Zhang, W. Wang and A. Mellouki. 2016. An estimation of CO₂ emission via agricultural crop residue open field burning in China from 1996 to 2013. *Journal of Cleaner Production*. 112:2625-2631.
- [30] Wang, Y., K. Cheng, W. Wu, H. Tian, P. Yi, G. Zhi, J. Fan and S. Liu. 2017. Atmospheric emissions of typical toxic heavy metals from open burning of municipal solid waste in China. *Atmospheric Environment*. 152:6-15.
- [31] Montiano, M. G., A. M. Fernandez, E. Diaz-Faes and C. Barriocanal. 2015. Tar from biomass/coal-containing briquettes, evaluation of PAHs. *Fuel*. 154:261-267.
- [32] Zhang, X., Z. Cai, L. Chen and Y. Chen. 2014. Research on the processing methods and equipments for densified biomass fuel. *Advanced Materials Research*. 953-954:199-202.
- [33] Coal: American's energy future. 2006. The National Coal Council. Volume II. A technical overview. March 2006. Page 1-2.
- [34] Amoo, L. M. 2015. Computational fluid dynamics simulation of Lafia-Obi bituminous coal in a fluidized-bed chamber for air- and oxy-fuel combustion. *Fuel*. 140:178-191.
- [35] Jang, H. N., J. H. Kim, S. K. Back, J. H. Sung, H. M. Yoo, H. S. Choi and Y. C. Seo. 2016. Combustion characteristics of waste sludge at air and oxy-fuel combustion conditions in a circulating fluidized bed reactor. *Fuel*. 170:92-99.
- [36] Zou, C., L. Wen, S. Zhang, C. Bai and G. Yin. 2014. Evaluation of catalytic combustion of pulverized coal for use in pulverized coal injection (PCI) and its influence on properties of unburnt chars. *Fuel Processing Technology*. 119:136-145.
- [37] Barnes, D. I. 2015. Understanding pulverized coal, biomass and waste combustion: A brief review. *Applied Thermal Engineering*. 74:89-95.
- [38] Wu, H., P. Glarborg, F. J. Frandsen, K. D. Johansen, P. A. Jensen and B. Sander. 2011. Co-combustion of pulverized coal and solid recovered fuel in an entrained flow reactor-general combustion and ash behavior. *Fuel*. 90:1980-1991.
- [39] Elfasakhany, A., L. Tao, B. Espenas, J. Larfeldt and X. S. Bai. 2013. Pulverized wood combustion in a vertical furnace: Experimental and computational analyses. *Applied Energy*. 112:454-464.
- [40] Beer, J. M. 2000. Combustion technology developments in power generation in response to environmental challenges. *Progress in Energy and Combustion Science*. 26:301-327.
- [41] Warnatz, J., U. Mass and R. W. Dibble. 2006. Combustion, physical and chemical fundamentals, modeling and simulation, experiments, pollutant formation, 4th edition. Springer. ISBN: 13-978-3-540-25992-3.
- [42] Biarnes, M. Combustion. E instruments international LLC. www.E.Inst.com.
- [43] Syed Shabudeen, P.S. 2010. Fuels and combustion, Chapter 4. In book: *Engineering Chemistry II*. pp. 4.1-4.83.

- [44] Penninger, A., F. Lezsovits, J. Rohaly and V. Wolff. Combustion: Heat engines and boilers. Lecture Notes. Department of Energy Engineering, Faculty of Mechanical Engineering, Budapest University of Technology and Economics.
- [45] Bartok, W. and A. F. Sarofim. 1991. Fossil fuel combustion: A source book. John Wiley & Sons, Inc. ISBN: 0-471-84779-8.
- [46] Santoleri, J. J., J. Reynolds and L. Theodore. 2000. Introduction to hazardous waste incineration, 2nd edition. John Wiley & Sons, Inc. ISBN: 0-471-01790-6.
- [47] Caretto, L. 2010. Introduction to combustion analysis. Lecture Notes. Mechanical Engineering Department. California State University Northridge. Pages 1-10.
- [48] Lackner, M., F. Winter and A. K. Agarwal. 2010. Handbook of combustion volume 4: Solid fuels. Wiley-VCH Verlag GmbH & Co. KGaA. ISBN: 978-3-527-32449-1.
- [49] Mckendry, P. 2002. Energy production from biomass, Part 1: Overview of biomass. Bioresource Technology. 83:37-46.
- [50] Thunman, H. and B. Leckner. 2007. Thermo chemical conversion of biomass and wastes. Nordic Graduate School Biofuels GS-2 Chalmers, Goteborg, 19-23 November 2007.
- [51] Vassilev, S. V., D. Baxter, L. K. Andersen and C. G. Vassileva. 2010. An overview of the chemical composition of biomass. Fuel. 89:913-933.
- [52] Singh, H., P. K. Sapra and B. S. Sindhu. 2013. Evaluation and characterization of different biomass residues through proximate & ultimate analysis and heating value. Asian Journal of Engineering and Applied Technology. Vol.2:6-10.
- [53] Pavlova, A. I., D. S. Dobrev and P. G. Ivanova. 2009. Determination of total nitrogen content by different approaches in petroleum matrices. Fuel. 88:27-30.
- [54] Phyllis2, database for biomass and waste, <https://www.ecn.nl/phyllis2>. Energy Research Centre of the Netherlands. Accessed: 01.04.2017.
- [55] Kiep, B. 2012. Technische Entwicklung und wissenschaftliche Begleitung der Pilotanlagenrealisierung "Thermische Restpulververwertung". Internal Report. Fraunhofer Institut für Fabrikbetrieb und -automatisierung (IFF), Magdeburg-Germany.
- [56] Specht, E. Chapter 2, Combustion Engineering, Lecture Notes. 2014. Thermodynamic and Combustion. Otto von Guericke University, Magdeburg.
- [57] Jain, R. K. 2014. Experimentally investigated effect of flame temperature on performance of rotary furnace. IPASJ International Journal of Mechanical Engineering (IJME). 2:20-28.
- [58] Asl, Z. M. and A. Salem. 2010. Investigation of the flame temperature for some gaseous fuels using artificial neural network. International Journal of Energy and Environmental Engineering (IJEEE). 1:57-63.

- [59] Quaak, P., H. Knoef and H. Stassen. 1999. Energy from biomass, a review of combustion and gasification technologies. World Bank Technical Paper No. 422. Page 20.
- [60] Martinez, F. R., A. A. Rueda Martinez, M. T. Velazquez, P. Q. Diez, G. T. Eslava and J. A. Francis. 2011. Evaluation of the gas turbine inlet temperature with relation to the excess air. *Energy and Power Engineering*. 3:517-524.
- [61] Amini, A. H. and M. R. Samani. 2016. The flame temperature effect on the reduction of environmental pollutants in a thermal power plant. *Journal of Biodiversity and Environmental Sciences*. 8:293-297.
- [62] Energy tips-Process heating. November 2007. Industrial technologies program. Process heating tip sheet #1. *Energy Efficiency and Renewable Energy*. U.S. Department of Energy. EERE information centre. www.eere.energy.gov.
- [63] Hesselmann, G. and M. Rivas. What are the main NO_x formation processes in combustion plant? Combustion File No. 66. IFRF Online Combustion Book. ISSN: 1607-9116.
- [64] Agrawal, A. K., S. K. Singh, S. Sinha and M. K. Shukla. 2004. Effect of EGR on the exhaust gas temperature and exhaust opacity in compression ignition engines. *Sadhana*. 29:275-284.
- [65] Lee, H. and S. Choi. 2016. Motion of single pulverized coal particles in a hot gas flow field. *Combustion and Flame*. 169:63-71.
- [66] Williams, A., M. Pourkashanian and J. M. Jones. 2000. The combustion of coal and some other solid fuels. *Proceeding of the Combustion Institute*. 28:2141-2162.
- [67] Yin, C. and J. Yan. 2016. Oxy-fuel combustion of pulverized fuels: Combustion fundamentals and modeling. *Applied Energy*. 162:742-762.
- [68] Umair, S. M. and P. T. Borlepwar. 2014. A review of literature on flame intensity of pulverized coal combustion. *International Journal of Innovative Research in Science, Engineering and Technology*. 3 (special issue 4):1-5.
- [69] Williams, A., M. Pourkashanian and J. M. Jones. 2001. Combustion of pulverised coal and biomass. *Progress in Energy and Combustion Science*. 27:587-610.
- [70] Ma, L., J. M. Jones, M. Pourkashanian and A. Williams. 2007. Modeling the combustion of pulverized biomass in an industrial combustion test furnace. *Fuel*. 86:1959-1965.
- [71] Pereira, S. and M. Costa. 2017. Short rotation coppice for bioenergy: from biomass characterization to establishment: A review. *Renewable and Sustainable Energy Reviews*. 74:1170-1180.
- [72] McLennan, A. R., G. W. Bryant, B. R. Stanmore and T. F. Wall. 2000. Ash formation mechanisms during pf combustion in reducing conditions. *Energy & Fuels*. 14:150-159.

- [73] Lind, T. 1999. Ash formation in circulating fluidised bed combustion of coal and solid biomass. PhD Dissertation, VTT Chemical Technology. VTT Publication 378. Technical Research Centre of Finland Espoo.
- [74] Gou, Y. F., S. Wang, Y. He, T. Jiang, F. Chen and F. Q. Zheng. 2017. Deposit formation mechanisms in a pulverized coal fired grate for hematite pellet production. *Fuel Processing Technology*. 161:33-40.
- [75] Ciolkosz, D. 2010. Co-firing biomass with coal. Renewable and alternative energy fact sheet. College of Agricultural Sciences, The Pennsylvania State University. Page 1-4.
- [76] Lempp, P. 2013. Biomass co-firing in coal power plants. IEA-ESTSAP and IRENA Technology Policy Brief E21. www.irena.org.
- [77] Chaplin, R. A. 2009. Fossil fuel combustion systems. Thermal power plants Volume II. Encyclopedia of Life support Systems (EOLSS). ISBN: 978-1-905839-27-8.
- [78] Mullinger, P. and B. Jenkins. 2013. Chapter 5, Flames and burners for furnaces. *Industrial and Process Furnaces (2nd Edition)*. Pages: 139-207.
- [79] Katzer, C., K. Babul, M. Klatt and H. J. Kroutz. 2017. Quantitative and qualitative relationship between swirl burner operating conditions and pulverized coal flame length. *Fuel Processing Technology*. 156:138-155.
- [80] Sung, Y., M. Choi, S. Lee, G. Lee, M. Shin, G. Choi and D. Kim. 2017. Generation mechanisms of tube vortex in methane-assisted pulverized coal swirling flames. *Fuel Processing Technology*. 156:228-234.
- [81] Tamura, M., S. Watanabe, E. Oono, R. Itokazu and T. Kozaki. 2011. Advanced development of pulverized coal firing technologies. *IHI Engineering Review* vol. 44 no. 2.
- [82] Li, Z., S. Fan, Q. Zhu, W. Su, Z. Chen and Y. Qin. 2012. Influence of staged-air flow on flow characteristics in a scale model of a down-fired utility boiler with swirl burners: An experimental study. *Fuel*. 93:160-166.
- [83] Zhou, H., Y. Yang, H. Liu and Q. Hang. 2014. Numerical simulation of the combustion characteristics of a low NO_x swirl burner: Influence of the primary air pipe. *Fuel*. 130:168-176.
- [84] Katsuki, M. and T. Hasegawa. 1998. The science and technology of combustion in highly preheated air. Twenty-Seventh Symposium (International) on Combustion/The Combustion Institute. Page 3135-3146.
- [85] Cavaliere, A. and M. D. Jaonnon. Mild combustion. 2004. *Progress in Energy and Combustion Science*. 30:329-366.
- [86] Saha, M., A. Chinnici, B. B. Dally and P. R. Medwell. 2015. Numerical study of pulverized coal MILD combustion in a self-recuperative furnace. *Energy & Fuels*. 29:7650-7669.

- [87] Weber, R., J. P. Smart and W. vd Kamp. 2005. On the (MILD) combustion of gaseous, liquid, and solid fuels in high temperature preheated air. *Proceedings of the Combustion Institute*. 30:2623-2629.
- [88] Saha, M., B. B. Dally, P. R. Medwell and A. Chinnici. 2017. Effect of particle size on the MILD combustion characteristics of pulverised brown coal. *Fuel Processing Technology*. 155:74-87.
- [89] Weidmann, M., D. Honore, V. Verbaere, G. Boutin, S. Grathwohl, G. Godard, C. Gobin, R. Kneer and G. Scheffknecht. 2016. Experimental characterization of pulverized coal MILD flameless combustion from detailed measurements in a pilot-scale facility. *Combustion and Flame*. 168:365-377.
- [90] Khadilkar, A., P. L. Rozelle and S. V. Pisupati. 2014. Models of agglomerate growth in fluidized bed reactors: Critical review, status and applications. *Powder Technology*. 264:216-228.
- [91] Niu, Y., H. Tan and S. Hui. 2016. Ash-related issues during biomass combustion: Alkali-induced slagging, silicate melt-induced slagging (ash fusion), agglomeration, corrosion, ash utilization, and related countermeasures. *Progress in Energy and Combustion Science*. 52:1-61.
- [92] Febrero, L., E. Granada, D. Patino, P. Eguia and A. Regueiro. 2015. A comparative study of fouling and bottom ash from woody biomass combustion in a fixed-bed small-boiler and evaluation of the analytical techniques used. *Sustainability*. 7:5819-5837.
- [93] Melissari, B. 2014. Ash related problems with high alkali biomass and its mitigation-experimental evaluation. *Memoria Investigaciones en Ingenieria*. 12:31-44. ISSN: 2301-1092.
- [94] Li, G., S. Li, Q. Huang and Q. Yao. 2015. Fine particulate formation and ash deposition during pulverized coal combustion of high-sodium lignite in a down-fired furnace. *Fuel*. 143:430-437.
- [95] Naganuma, H., N. Ikeda, T. Ito, H. Satake, M. Matsuura, Y. Ueki, R. Yoshiie and I. Naruse. 2013. Control of ash deposition in solid fuel fired boiler. *Fuel Processing Technology*. 105:77-81.
- [96] Bartels, M., W. Lin, J. Nijenhuis, F. Kapteijn and J. R. V. Ommen. 2008. Agglomeration in fluidized beds at high temperatures: Mechanisms, detection and prevention. *Progress in Energy and Combustion Science*. 34:633-666.
- [97] Arena, U. and M. L. Mastellone. 2000. Defluidization phenomena during the pyrolysis of two plastic wastes. *Chemical Engineering Science*. 55:2849-2860.
- [98] Mastellone, M. L. and U. Arena. 2004. Bed defluidization during the fluidised bed pyrolysis of plastic waste mixtures. *Polymer Degradation and Stability*. 85:1051e-1058.

- [99] Pedersen, M. N., P. A. Jensen, K. Hjuler, M. Nielsen and K. D. Johansen. 2016. Agglomeration and deposition behavior of solid recovered fuel. *Energy and Fuels*. 30:7858-7866.
- [100] Venturini, P., D. Borello, C. Iossa, D. Lentini and F. Rispoli. 2010. Modeling of multiphase combustion and deposit formation in a biomass-fed furnace. *Energy*. 35:3008-3021.
- [101] Akiyama, K., H. Pak, Y. Takubo, T. Tada, Y. Ueki, R. Yoshiie and I. Naruse. 2011. Ash deposition behavior of upgraded brown coal in pulverized coal combustion boiler. *Fuel Processing Technology*. 92:1355-1361.
- [102] Liu, Z. S., T. H. Peng and C. L. Lin. 2014. Impact of CaO and CaCO₃ addition on agglomeration/defluidization and heavy metal emission during waste combustion in fluidized-bed. *Fuel Processing Technology*. 118:171-179.
- [103] Zhou, H., B. Zhou, L. Li and H. Zhang. 2014. Investigation of the influence of the furnace temperature on slagging deposit characteristics using a digital image technique. *Energy and Fuels*. 28:5756-5765.
- [104] Noor, M. M., A. P. Wandel and T. Yusaf. 2013. Detail guide for CFD on the simulation of biogas combustion in bluff-body MILD burner. ICMER July 1-3, 2013. Paper ID:P342.
- [105] Zahirovic, S., R. Scharler and I. Obernberger. 2004. Advanced CFD modelling of pulverised biomass combustion. International Conference on Science in Thermal and Chemical Conversion, Canada, 2004.
- [106] Stroh, A., F. Alobaid, J. P. Busch, J. Strohle and B. Epple. 2015. 3-D numerical simulation for co-firing of torrefied biomass in a pulverized-fired 1 MW_{th} combustion chamber. *Energy*. 85:105-116.
- [107] Silaen, A. and T. Wang. 2010. Effect of turbulence and devolatilization models on coal gasification simulation in an entrained-flow gasifier. *International Journal of Heat and Mass Transfer*. 53:2074-2091.
- [108] Jeldres, R. P., P. Cornejo, M. Flores and A. Gordon. 2017. A modeling approach to co-firing biomass/coal blends in pulverized coal utility boiler: Synergistic effects and emissions profiles. *Energy*. 120:663-674.
- [109] Yin, C. 2016. Effects of moisture release and radiation properties in pulverized fuel combustion: A CFD modelling study. *Fuel*. 165:252-259.
- [110] Kumar, M. and S. G. Sahu. 2007. Study on the effect of the operating condition on a pulverized coal-fired furnace using computational fluid dynamics commercial code. *Energy & Fuels*. 21:3189-3193.
- [111] Schaffel, N., M. Mancini, A. Szlek and R. Weber. 2009. Mathematical modeling of MILD combustion of pulverized coal. *Combustion and Flame*. 156:1771-1784.
- [112] Gubba, S. R., D. B. Ingham, K. J. Larsen, L. Ma, M. Pourkashanian, H. Z. Tan, A. Williams and H. Zhou. 2012. Numerical modelling of the co-firing of pulverised coal

- and straw in a 300 MWe tangentially fired boiler. *Fuel Processing Technology*. 104:181-188.
- [113] Perrone, D. and M. Amelio. 2016. Numerical investigation of oxy-mild combustion of pulverized coal in a pilot furnace. *Energy Procedia*. 101:1191-1198.
- [114] Galletti, C., A. Parente and L. Tognotti. 2007. Numerical and experimental investigation of a mild combustion burner. *Combustion and Flame*. 151:649-664.
- [115] Poulrud, S. and C. Nilsson. 2004. The effects of particle characteristics on emissions from burning wood fuel powder. *Fuel*. 83:813-821.
- [116] Farid, M. U., A. Bück, W. Heineken, M. Gohla and N. Zobel. 2017. Study on nozzle design for combustion of solid materials with low melting points. *Applied Thermal Engineering*. 115:832-859.
- [117] Massari, A., M. Beggio, S. Hreglich, R. Marin and S. Zuin. 2014. Behavior of TiO₂ nanoparticles during incineration of solid paint waste: A lab-scale test. 34:1897-1907.
- [118] Taskiran, O. O. and M. Ergeneman. 2014. Effect of nozzle dimensions and fuel type on flame lift-off length. *Fuel*. 115:833-840.
- [119] Zhang, Z., C. Zhao, Z. Xie, F. Zhang and Z. Zhao. 2014. Study on the effect of the nozzle diameter and swirl ratio on the combustion process for an opposed-piston two-stroke diesel engine. *Energy Procedia*. 61:542-546.
- [120] Law, W. P. and J. Gimbut. 2015. Influence of nozzle design on the performance of a partial combustion lance: A CFD study. *Chemical Engineering Research and Design*. 104:558-570.
- [121] Peric, M. and S. Ferguson. The advantage of polyhedral meshes. CD-adapco. www.cd-adapco.com.
- [122] Peric, M. 2004. Flow simulation using control volumes of arbitrary polyhedral shape. *ERCOFTAC Bulletin*. No. 62, September 2004.
- [123] ANSYS® Academic research, release 15.0, theory guide, help system, user guide, ANSYS, Inc. 2013.
- [124] Fidaros, D. K., C. A. Baxevanou, C. D. Dritselis and N. S. Vlachos. 2007. Modelling of combustion and calcination in a cement precalciner. *Proceedings of the European Combustion Meeting 2007*.
- [125] Chen, L. 2013. Computational fluid dynamics simulations of oxy-coal combustion for carbon capture at atmospheric and elevated pressures. PhD Thesis, Massachusetts Institute of Technology, USA.
- [126] Morsi, S. A. and A. J. Alexander. 1972. An investigation of particle trajectories in two-phase flow systems. *Journal of Fluid Mechanics*. 55:193-208.
- [127] Menter, F.R. 1994. Two-equation eddy-viscosity turbulence models for engineering applications. *AIAA Journal*. 32:1598-1605.
- [128] Menter, F. R., M. Kuntz and R. Langtry. 2003. Ten years of industrial experience with the SST Turbulence Model. *Turbulence, Heat and Mass Transfer 4*. Begell House Inc.

- [129] Murgia, S., M. Vascellari and G. Cau. 2012. Comprehensive CFD model for an air-blown coal-fired updraft gasifier. *Fuel*. 101:129-138.
- [130] Baum, M. M. and P. J. Street. 1971. Predicting the combustion behavior of coal particles. *Combustion Science Technology*. 3(5):231-243.
- [131] Khodabandeh, E., M. Pourramezan and M. H. Pakravan. 2016. Effects of excess air and preheating on the flow pattern and efficiency of the radiative section of a fired heater. *Applied Thermal Engineering*. 105:537-548.
- [132] Magnussen, B. F. and B. H. Hjertager. 1977. On mathematical modeling of turbulent combustion with special emphasis on soot formation and combustion. *Symposium (International) on Combustion*. 719-729.
- [133] Kassem, H. I., K. M. Saqr, H. S. Aly, M. M. Sies and M. A. Wahid. 2011. Implementation of the eddy dissipation model of turbulent non-premixed combustion in OpenFOAM. *International Communications in Heat and Mass Transfer*. 38:363-367.
- [134] Achim, D., J. Naser and Y. S. Morsi. 2009. Numerical investigation of full scale coal combustion model of tangentially fired boiler with the effect of mill ducting. *Heat Mass Transfer*. 46:1-13.
- [135] Saqr, K. M., H. S. Aly, M. M. Sies and M. A. Wahid. 2010. Effect of free stream turbulence on NO_x and soot formation in turbulence diffusion CH₄-air flame. *International Communications in Heat and Mass Transfer*. 37:611-617.
- [136] Gogoi, B. and D. C. Baruah. 2016. Steady state heat transfer modeling of solid fuel biomass stove: Part 1. *Energy*. 97:283-295.
- [137] Sieder, E. N. and G. E. Tate. 1936. Heat transfer and pressure drop of liquids in tubes. *Industrial and Engineering Chemistry*. 28:1429-1435.
- [138] Park, S., J. A. Kim, C. Ryu, T. Chae, W. Yang, Y. J. Kim, H. Y. Park and H. C. Lim. 2013. Combustion and heat transfer characteristics of oxy-coal combustion in a 100 MWe front-wall-fired furnace. *Fuel*. 106:718-729.
- [139] Ariyaratne, W. K. H., A. Malagalage, M. C. Melaen and L. A. Tokheim. 2015. CFD modelling of meat and bone meal combustion in a cement rotary kiln-investigation of fuel particle size and fuel feeding position impacts. *Chemical Engineering Science*. 123:596-608.
- [140] Mtui, P. 2013. CFD modeling of devolatilization and combustion of shredded tires and pine wood in rotary cement kilns. *American Journal of Energy Engineering*. 1:51-55.
- [141] Sun, R., T. M. Ismail, X. Ren and M. A. El-Salam. 2016. Influence of simulated MSW sizes on the combustion process in a fixed bed: CFD and experimental approaches. *Waste Management*. 49:272-286.
- [142] Siebzehnte Verordnung zur Durchführung des Bundes-Immissionsschutzgesetzes (Verordnung über die Verbrennung und die

- Mitverbrennung von Abfällen - 17. BImSchV). 2013. Section §6 (1), Page No. 8. https://www.gesetze-im-internet.de/bimschv_17_2013/BJNR104400013.html.
- [143] Hougou, O.A., K.M. Watson and R. A. Ragatz. 1976. Chemical process principles, Part-I, materials and energy balances. 1st Edition, Asia publishing house, Calcutta.
- [144] White Paper No. 15. 2004. Lambda calculation-The Brettschneider equation, general principles and methods. Bridge analyzers, inc. Rev. 030903. Page 1-3.
- [145] Wood for energy production, technology-environment-economy, 2nd edition. 2002. The centre of biomass technology. 6:30-33.
- [146] Varol, M., A. T. Atimtay, H. Olgun and H. Atakul. 2014. Emission characteristics of co-combustion of a low calorie and high sulfur-lignite coal and woodchips in a circulating fluidized bed combustor: Part 1. Effect of excess air ratio. Fuel. 117:792-800.
- [147] Mei, Z., P. Li, F. Wang, J. Zhang and J. Mi. 2014. Influences of reactant injection velocities on moderate or intense low-oxygen dilution coal combustion. Energy & Fuels. 28:369-384.
- [148] Suda, T., M. Takafuji, T. Hirata, M. Yoshino and J. Sato. 2002. A study of combustion behavior of pulverized coal in high-temperature air. Proceeding from the Combustion Institute. 29:503-509.
- [149] He, R., T. Suda, M. Takafuji, T. Hirata and J. Sato. 2004. Analysis of low NO emission in high temperature air combustion for pulverized coal. Fuel. 83:1133-1141.
- [150] Johansen, J. M., R. Gadsboll, J. Thomsen, P. A. Jensen, P. Glarborg, P. Ek, N. D. Martini, M. Mancini, R. Weber and R. E. Mitchell. 2016. Devolatilization kinetics of woody biomass at short residence times and high heating rates and peak temperatures. Applied Energy. 162:245-256.

Appendices

Appendix A: Tabulated data of SBM model and mass and energy balance model

Table A1: Oxygen demand (OD) for different solid fuels

Fuel	Oxygen demand (kg O₂/kg fuel)
Coal	
Brown coal	1.89
Bituminous coal	2.47
Anthracite	2.71
Biomass	
Spruce bark	1.42
Barley straw	1.35
Miscanthus	1.38
Municipal solid waste	
MSW	2.08
Sewage sludge	1.81
Sewage sludge dry	1.59
Industrial waste	
Waste tyres	2.93
Plastics (PE)	3.39
Paint residue	1.88

Table A2: Air demand (AD) for different solid fuels

Fuel	L waf	L raw
Coal		
Brown coal	8.23	7.01
Bituminous coal	10.75	9.84
Anthracite	11.77	11.21
Biomass		
Spruce bark	6.18	5.72
Barley straw	5.88	4.89
Miscanthus	5.98	5.33
Municipal solid waste		
MSW	9.04	7.06
Sewage sludge	7.87	4.09
Sewage sludge dry	6.93	4.63
Industrial waste		
Waste tyres	12.72	11.67
Plastics (PE)	14.76	14.72
Paint residue	8.18	5.79

Table A3: Adiabatic temperature of different solid fuels for base case of lambda (λ)

Fuel	Lambda (λ)	Temperature ($^{\circ}\text{C}$)
Coal		
Brown coal	1.3	1866
Bituminous coal	1.3	1887
Anthracite	1.3	1841
Biomass		
Spruce bark	1.3	1881
Barley straw	1.3	1897
Miscanthus	1.3	1884
Municipal solid waste		
MSW	1.3	1599
Sewage sludge	1.3	1640
Sewage sludge dry	1.3	1754
Industrial waste		
Waste tyres	1.3	2060
Plastics (PE)	1.3	1704
Paint residue	1.3	1817

Table A4: Adiabatic temperature of solid fuels at different excess air numbers (λ)

[Coal]				[Biomass]			
λ	Brown coal	Bitum. coal	Anthracite	λ	Spruce bark	Barley straw	Miscanthus
1.3	1866	1887	1841	1.3	1881	1897	1884
1.6	1549	1558	1519	1.6	1567	1586	1572
1.9	1325	1329	1293	1.9	1344	1364	1350
2.2	1158	1159	1127	2.2	1178	1197	1187
2.5	1030	1028	999	2.5	1048	1067	1054
2.8	927	924	898	2.8	945	963	951
3.1	844	840	816	3.1	861	877	866
3.4	775	770	748	3.4	791	807	796
3.7	716	711	691	3.7	731	746	736
[Municipal solid waste]				[Industrial waste]			
λ	MSW	S. sludge	S. sludge dry	λ	Waste tyres	Plastics	Paint residue
1.3	1599	1640	1754	1.3	2060	1704	1817
1.6	1328	1377	1468	1.6	1697	1402	1514
1.9	1136	1188	1263	1.9	1445	1192	1299
2.2	994	1045	1110	2.2	1258	1037	1137
2.5	884	934	990	2.5	1115	919	1013
2.8	796	844	894	2.8	1002	826	913
3.1	725	771	815	3.1	910	750	832
3.4	666	709	750	3.4	834	687	764
3.7	616	657	694	3.7	770	634	707

Table A5: Adiabatic temperature (base case for preheating study) with air at 25°C

Fuel	Lambda	Adiabatic temperature
Anthracite	2.5	999
Miscanthus	2.5	1054
Sewage sludge dry	2.5	990
Paint residue	2.5	1013

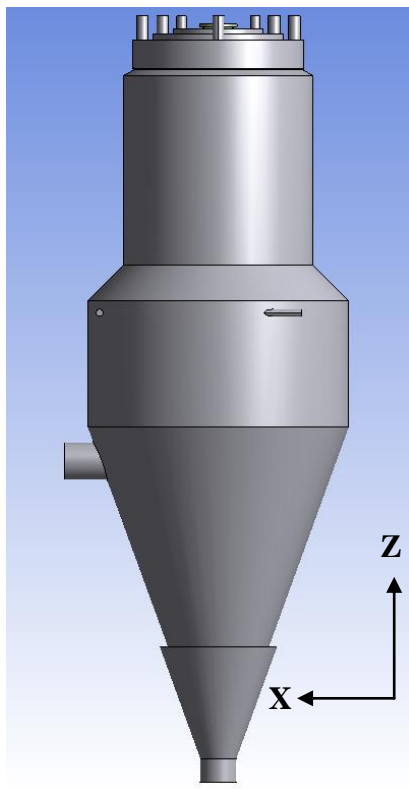
Table A6: Effect of preheating of air

Air temperature (°C)	Adiabatic temperature (°C)			
	Anthracite	Miscanthus	Sewage sludge dry	Paint residue
25	999	1054	990	1013
50	1024	1079	1015	1038
100	1074	1129	1065	1088
200	1174	1229	1165	1188
400	1374	1429	1365	1388

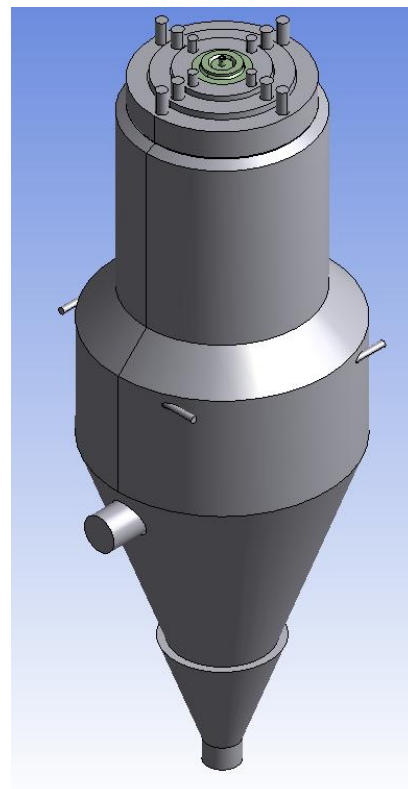
Appendix B: Domain of furnace with different nozzles and CFD simulation results

Table B1: Domain extents of combustion furnace with different nozzles

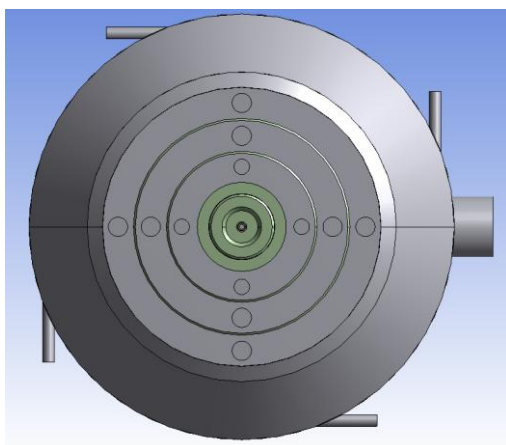
Nozzle	X min. (m)	X max. (m)	Y min. (m)	Y max. (m)	Z min. (m)	Z max. (m)
1	-0.549	0.65	-0.549	0.549	-3.176	0.05
2	-0.549	0.65	-0.549	0.549	-3.176	0.07
3	-0.549	0.65	-0.549	0.549	-3.176	0.332
4	-0.549	0.65	-0.549	0.549	-3.176	0.15



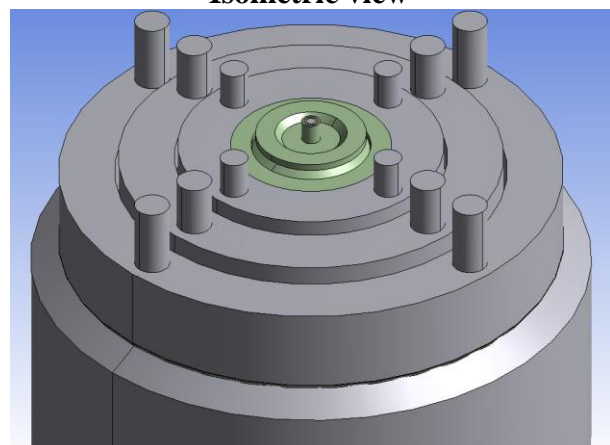
Side view



Isometric view



Top view



Isometric view (Zoom in)

Fig. B1: Difference views of furnace (with Nozzle 1)

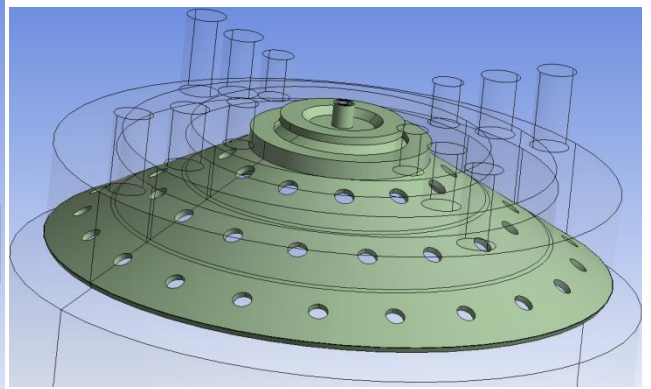
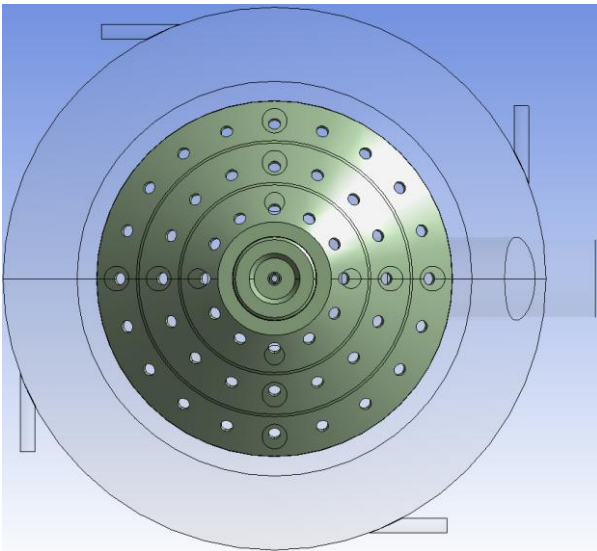
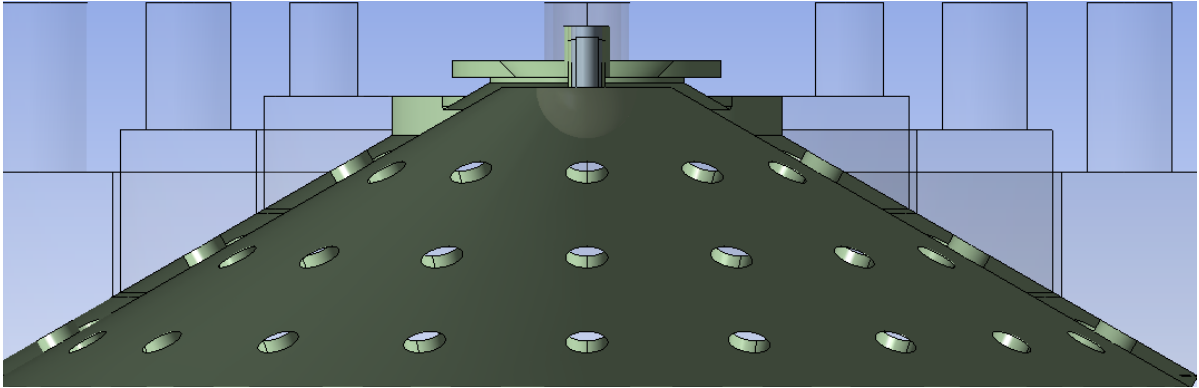


Fig. B2: Structure of furnace top with Nozzle 1

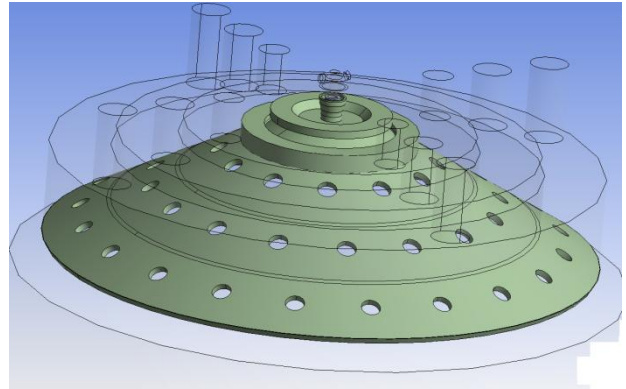
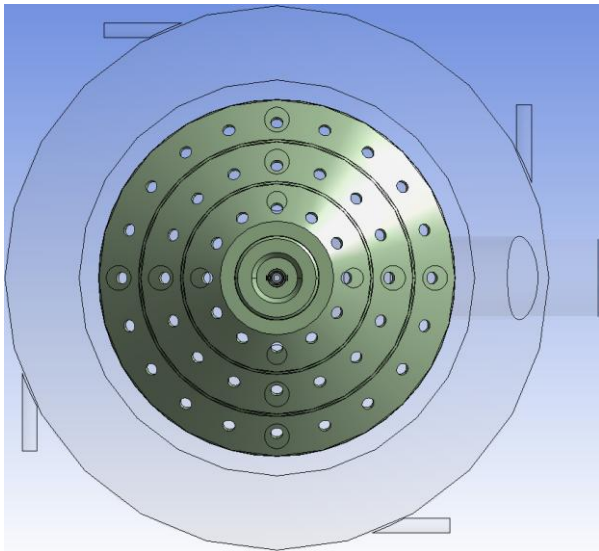
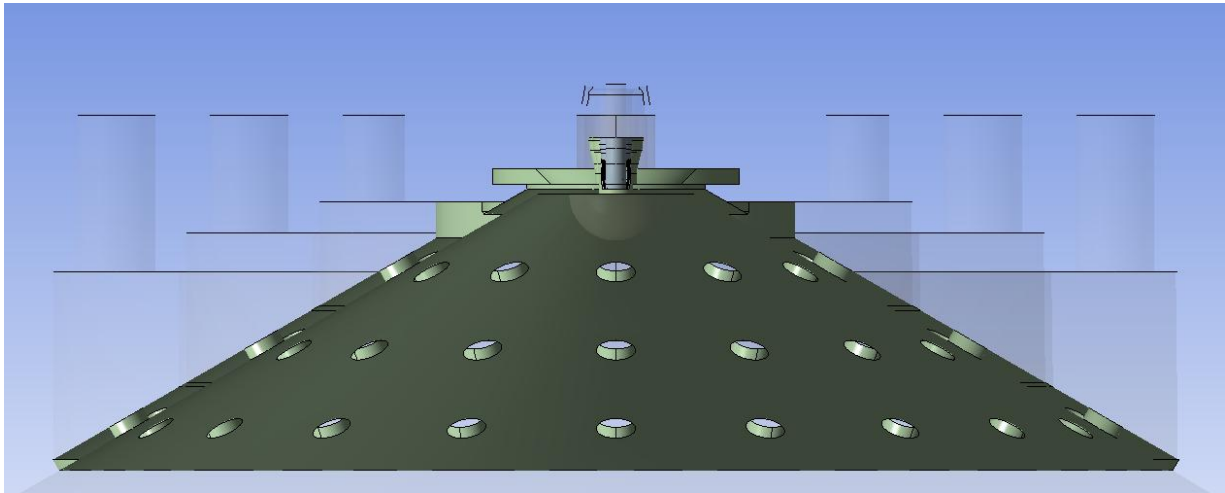


Fig. B3: Structure of furnace top with Nozzle 2

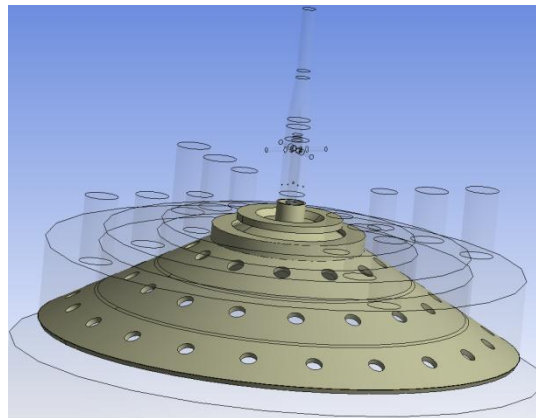
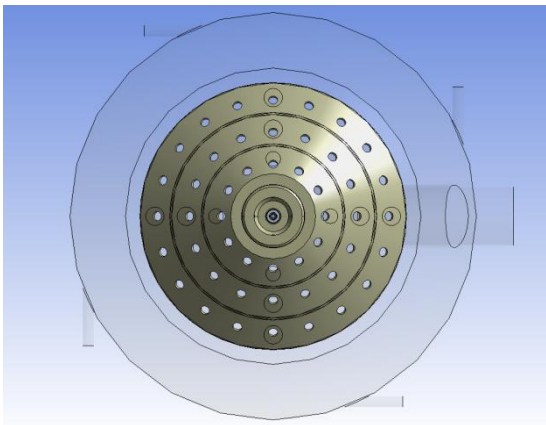
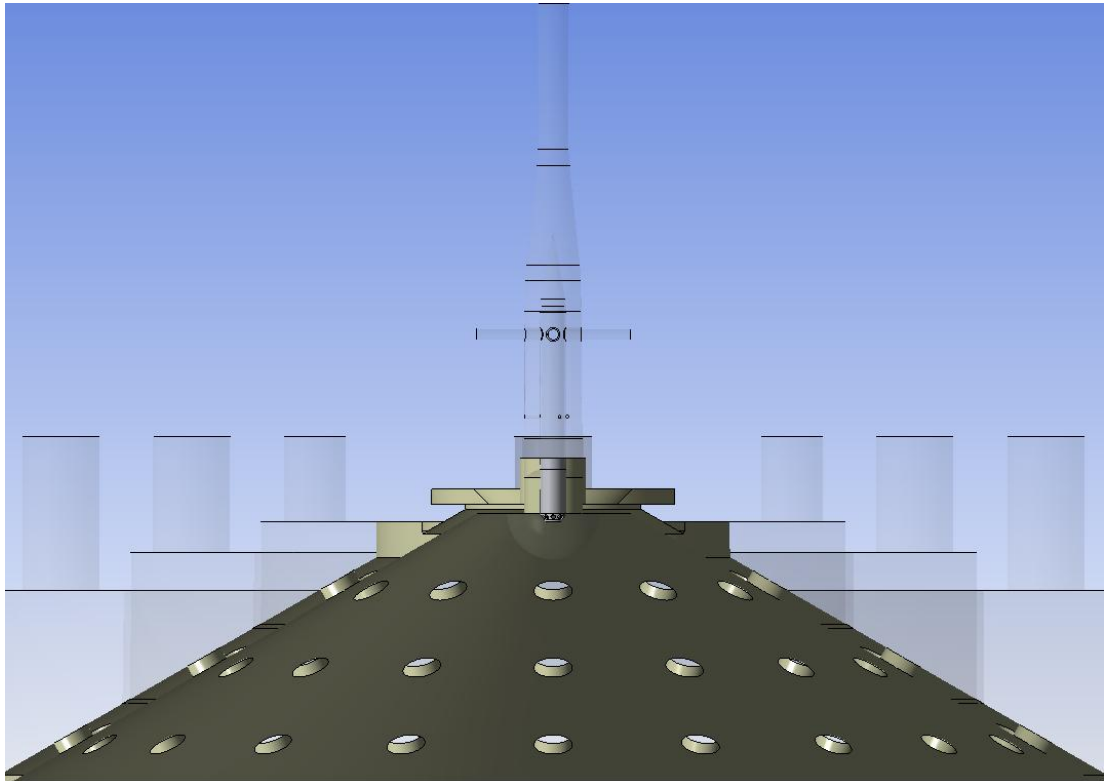


Fig. B4: Structure of furnace top with Nozzle 3

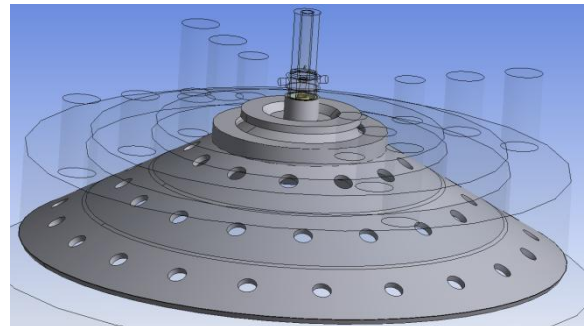
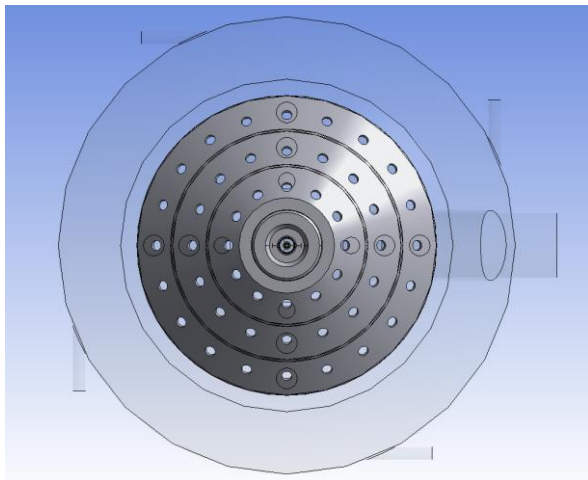
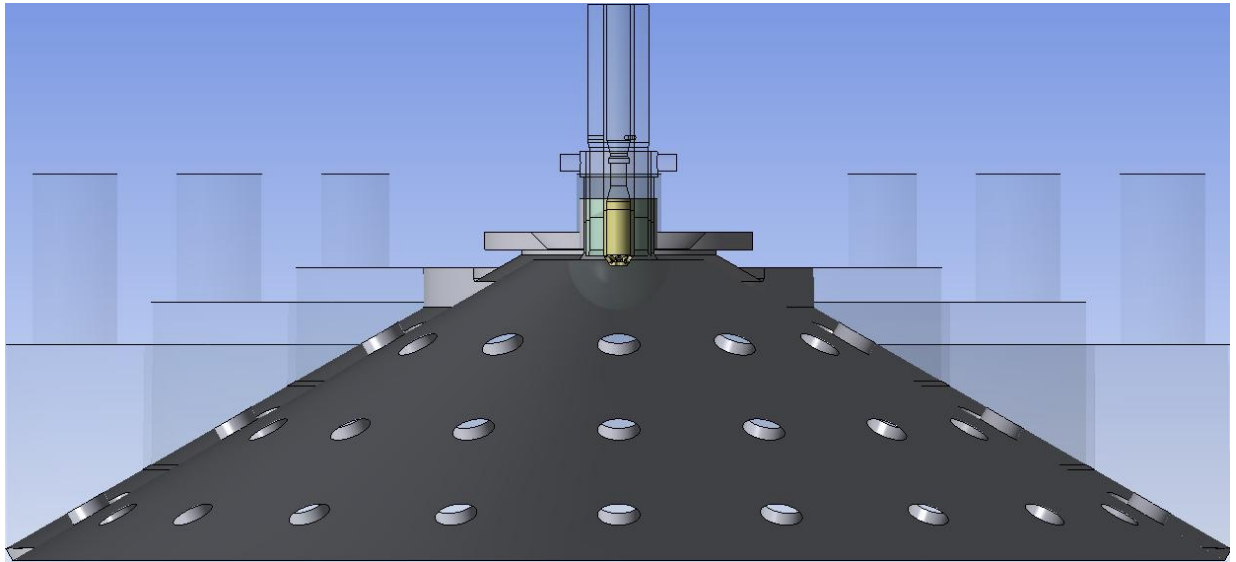
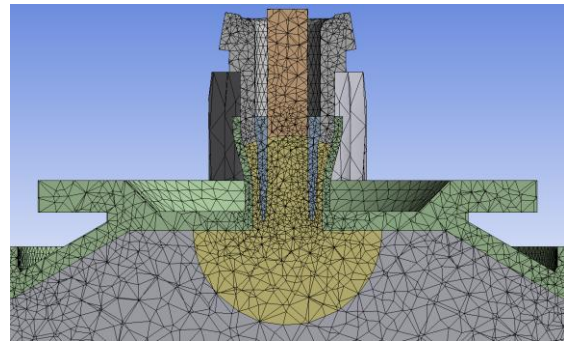
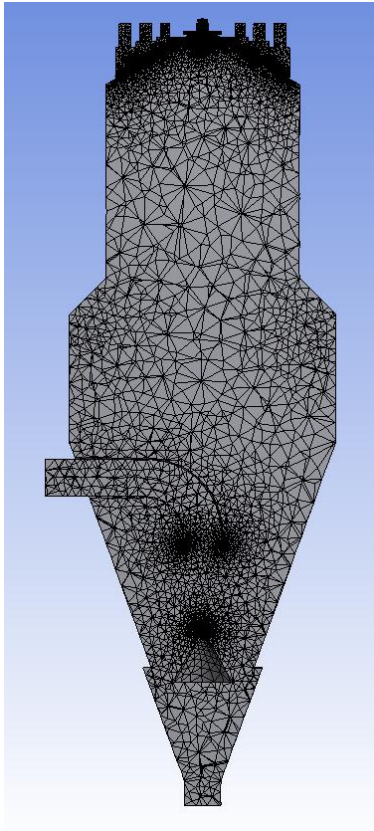
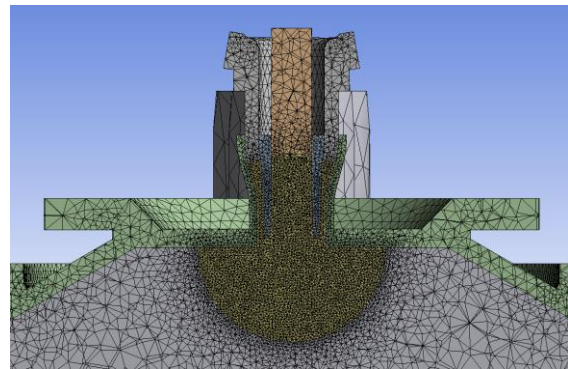


Fig. B5: Structure of furnace top with Nozzle 4

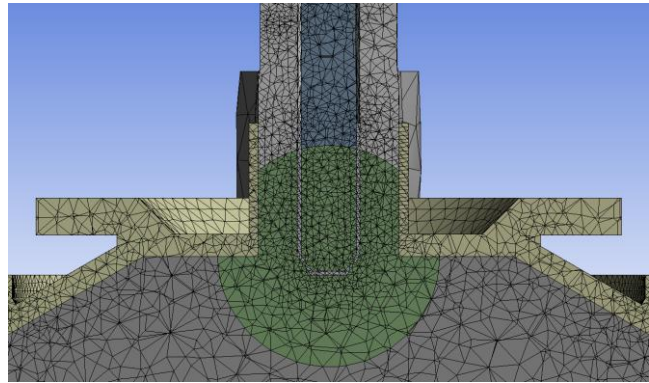
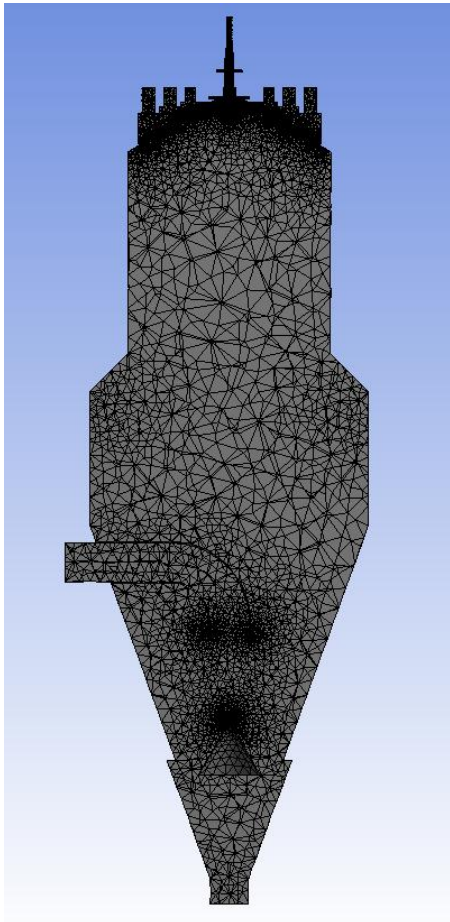


Coarse mesh

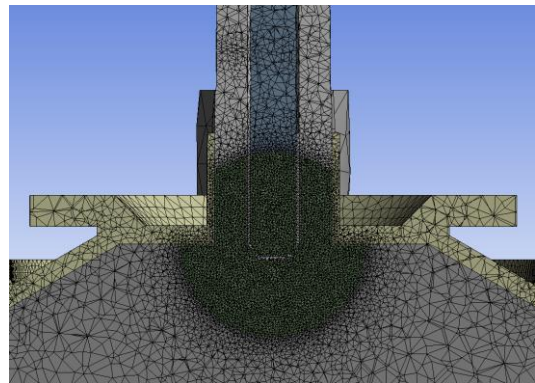


Fine mesh

Fig. B6: Computational domain of furnace with Nozzle 2

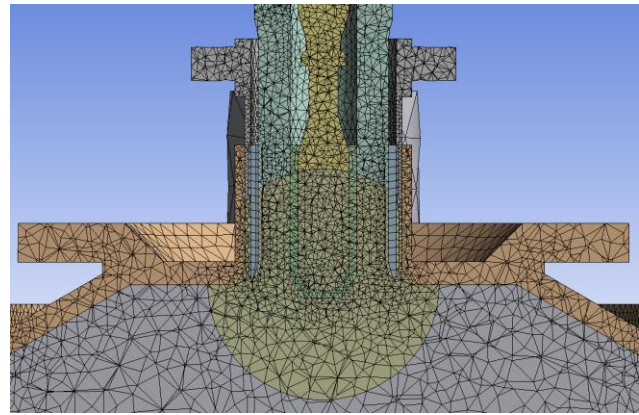
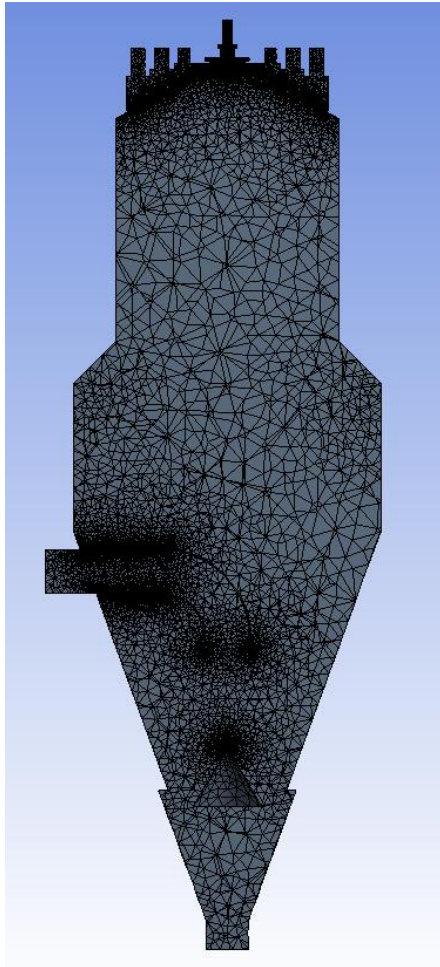


Coarse mesh

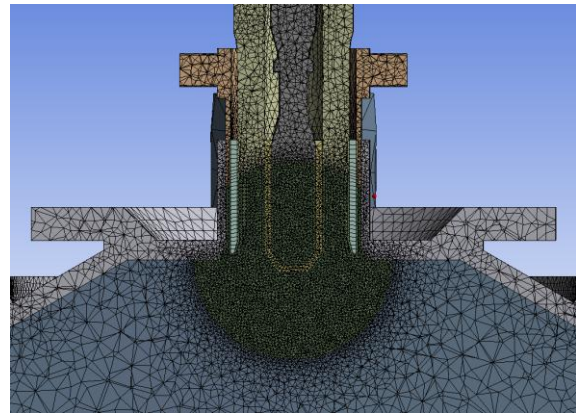


Fine mesh

Fig. B7: Computational domain of furnace with Nozzle 3



Coarse mesh



Fine mesh

Fig. B8: Computational domain of furnace with Nozzle 4

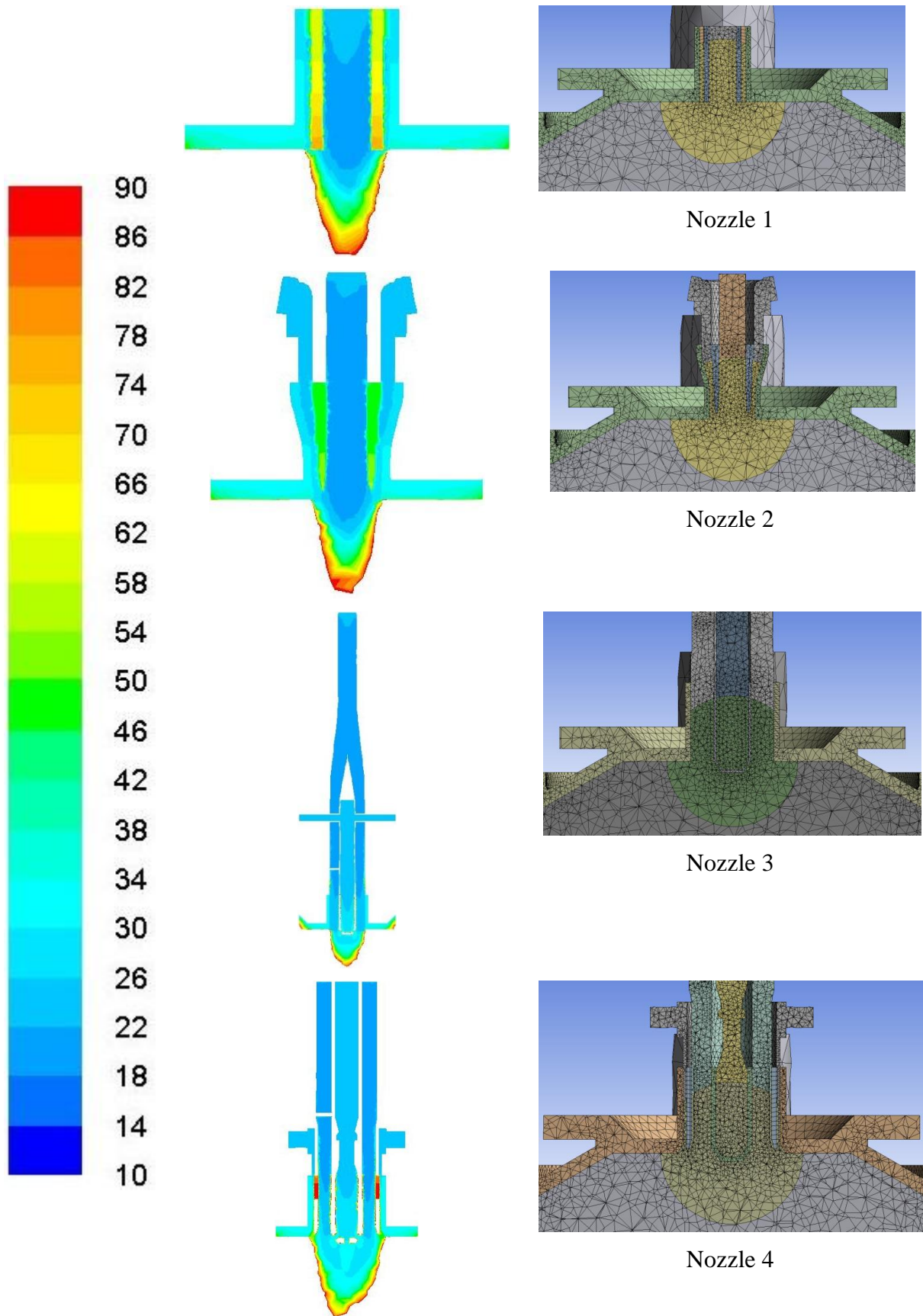


Fig. B9: Simulation results with coarse mesh

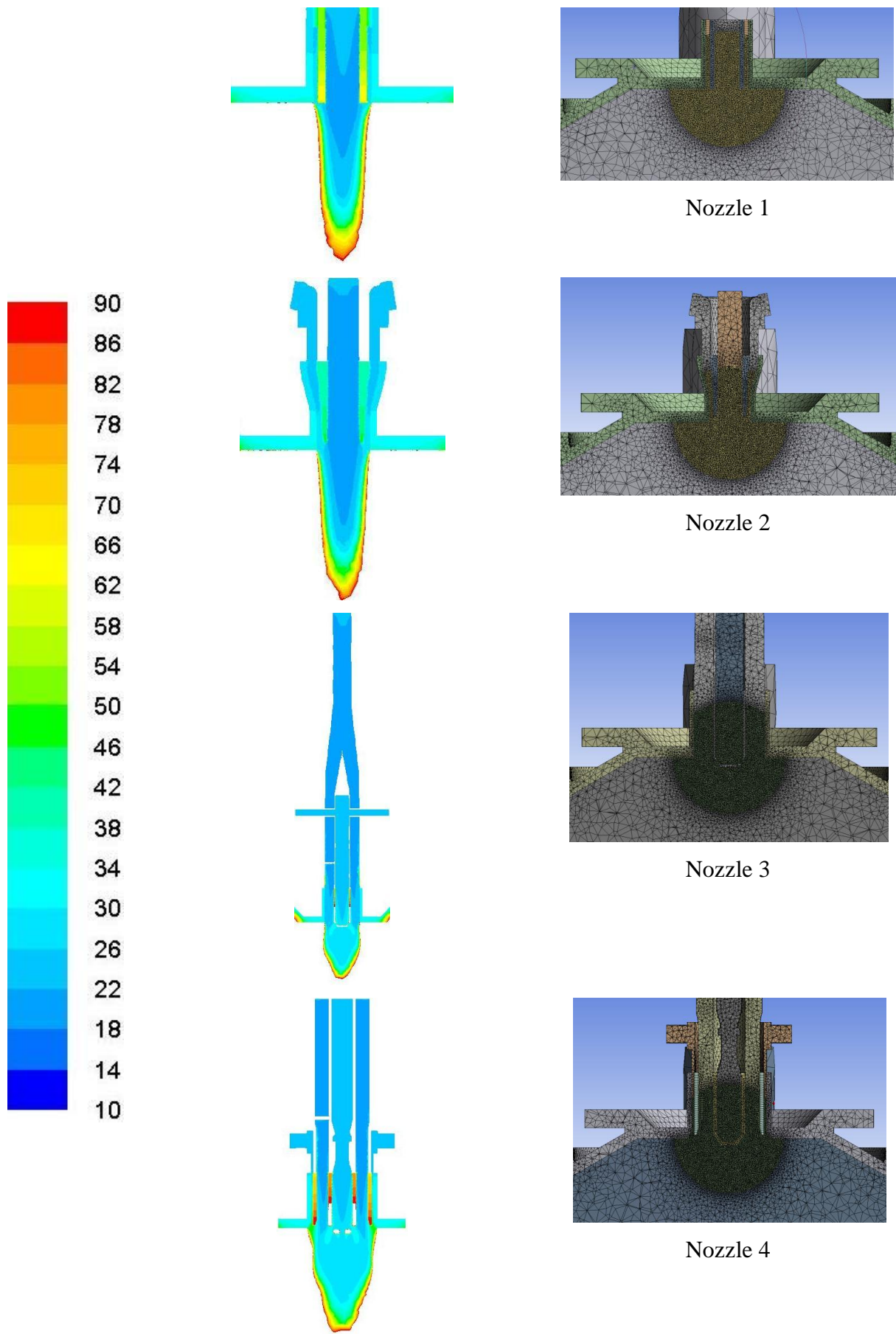


Fig. B10: Simulation results with fine mesh

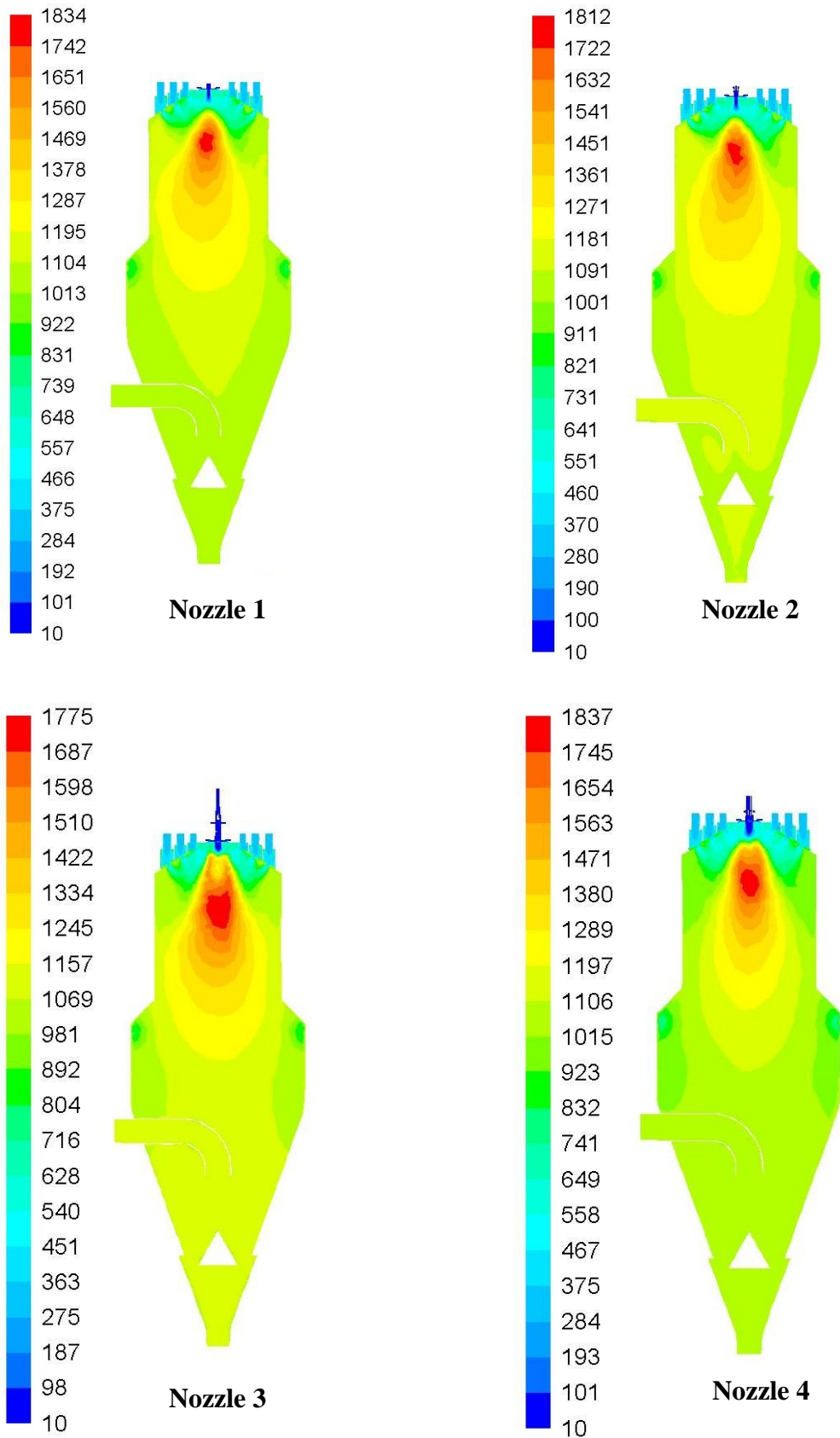


Fig. B11: Temperature profile with different nozzle designs (Data Set1)

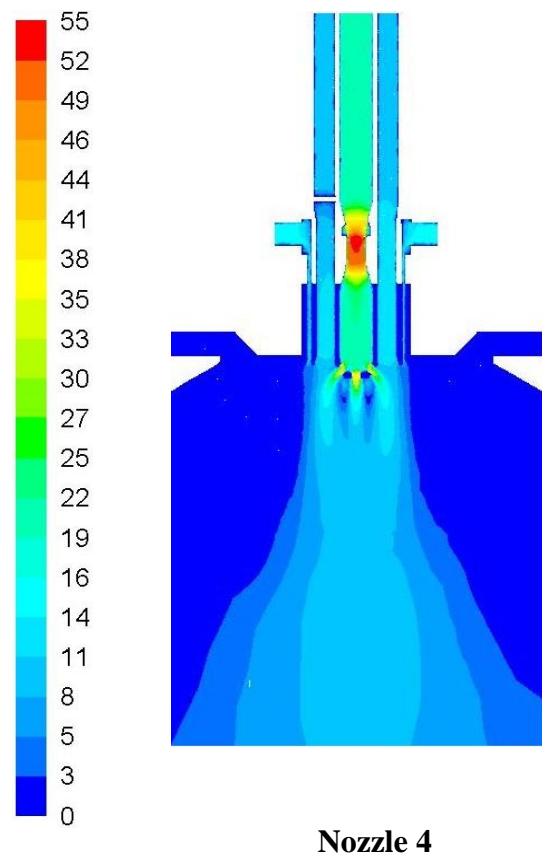
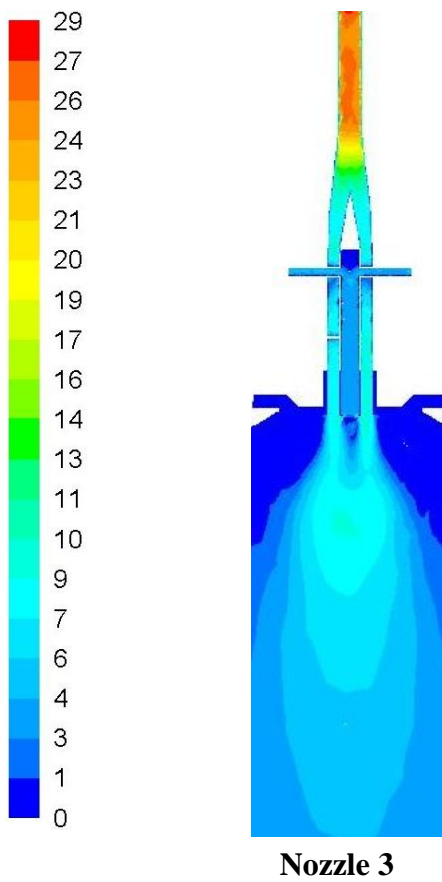
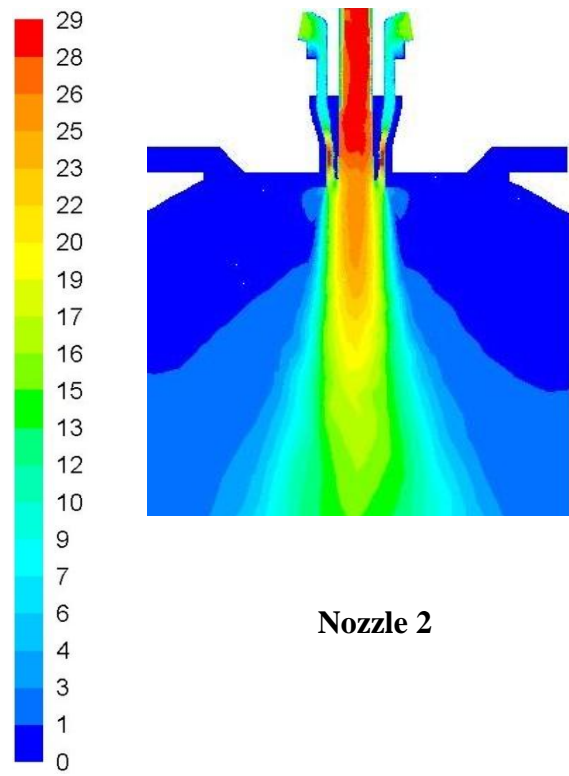
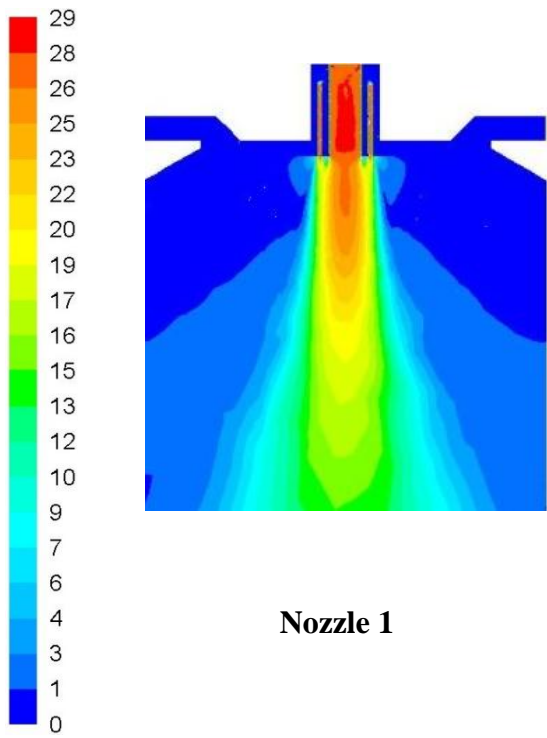


Fig. B12: Velocity profile (m s^{-1}) through different nozzles (Data Set 1)

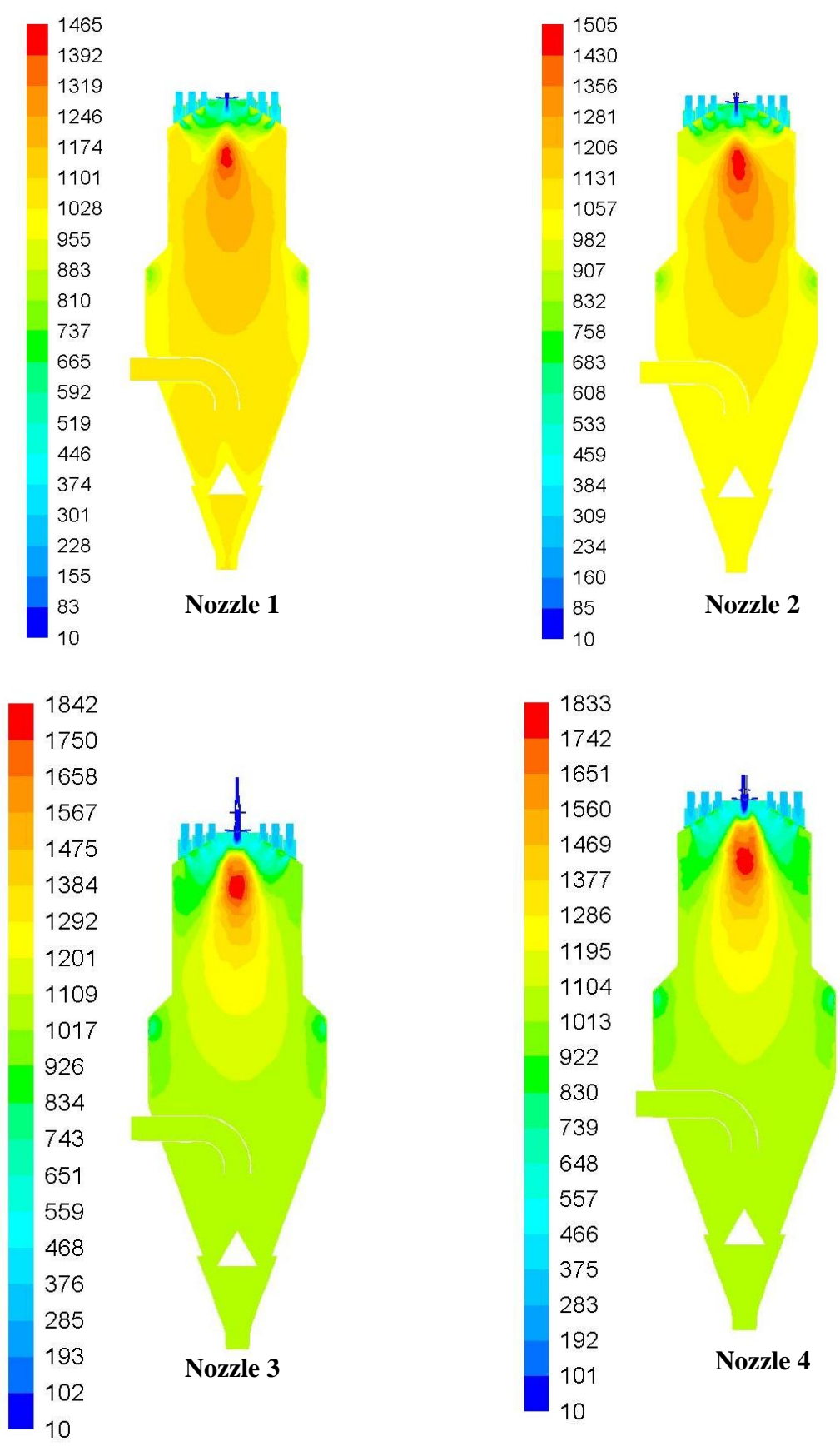
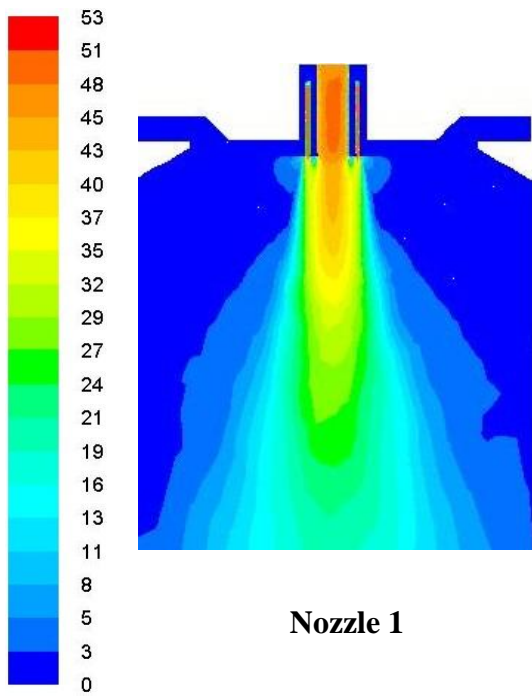
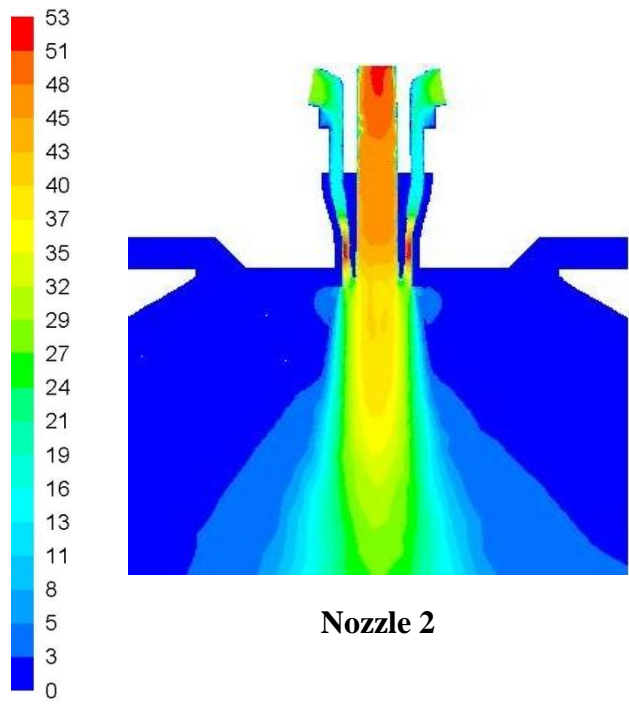


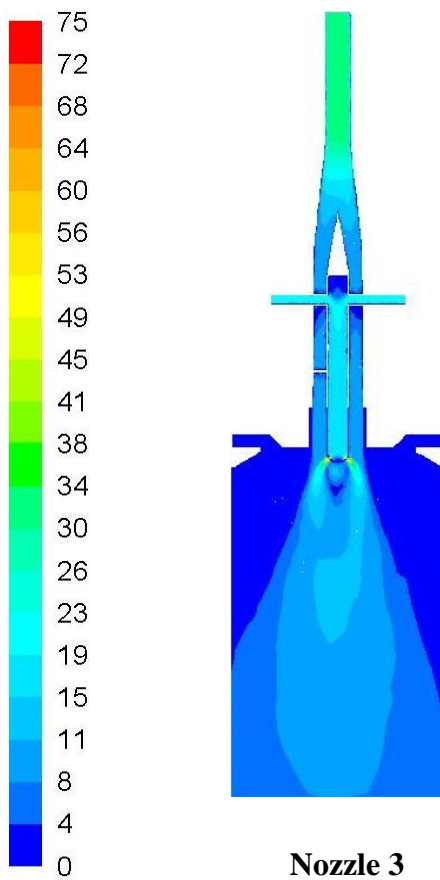
Fig. B13: Temperature profile in furnace with different nozzle designs (Data Set 2)



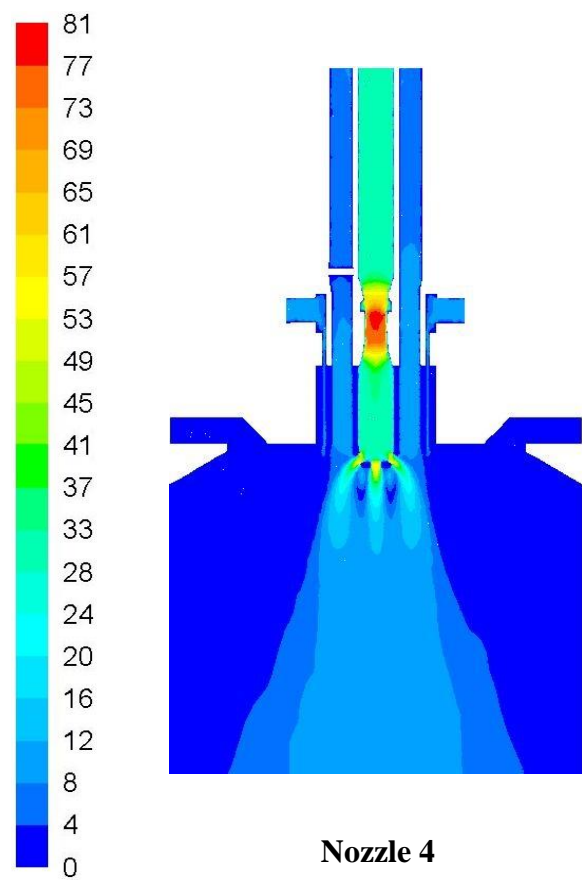
Nozzle 1



Nozzle 2



Nozzle 3



Nozzle 4

Fig. B14: Velocity profile (m s^{-1}) through different nozzles (Data Set 2)

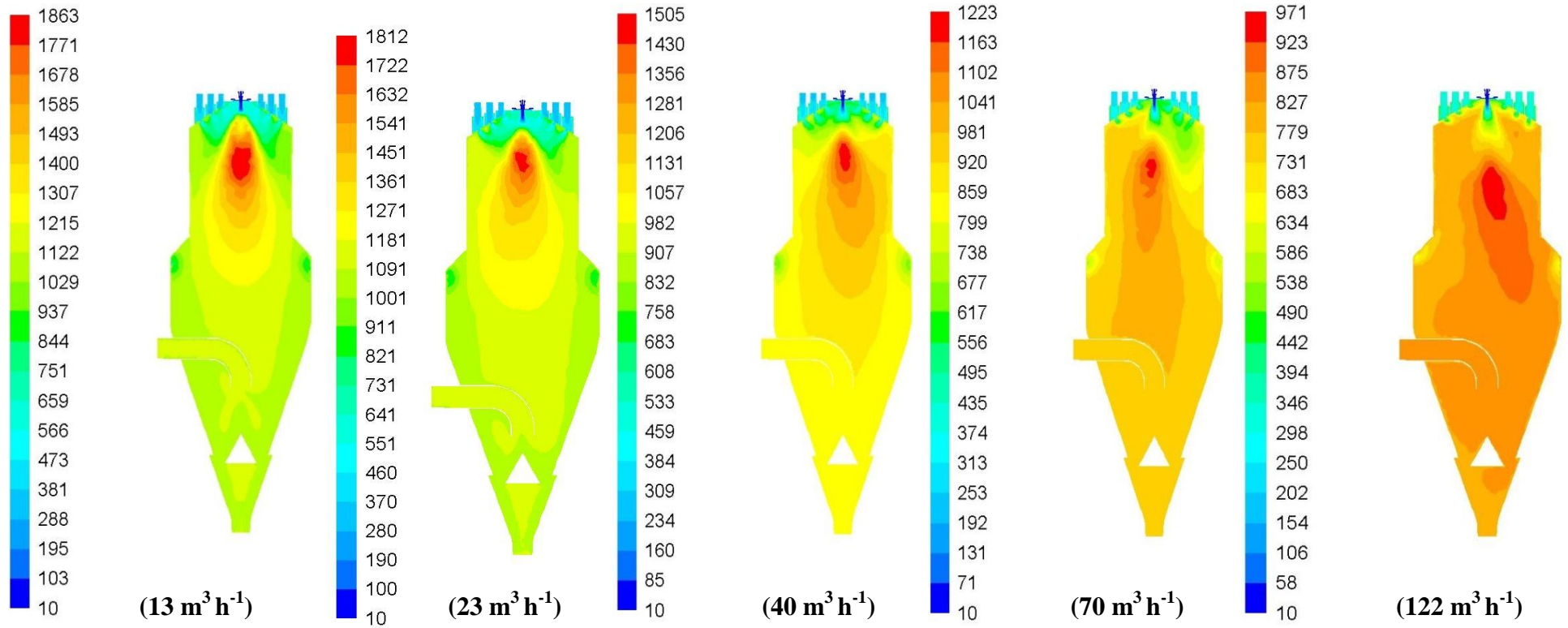


Fig. B15: Combustion temperature ($^{\circ}\text{C}$) with Nozzle 2 at different nozzle air flow rates (optimization study)

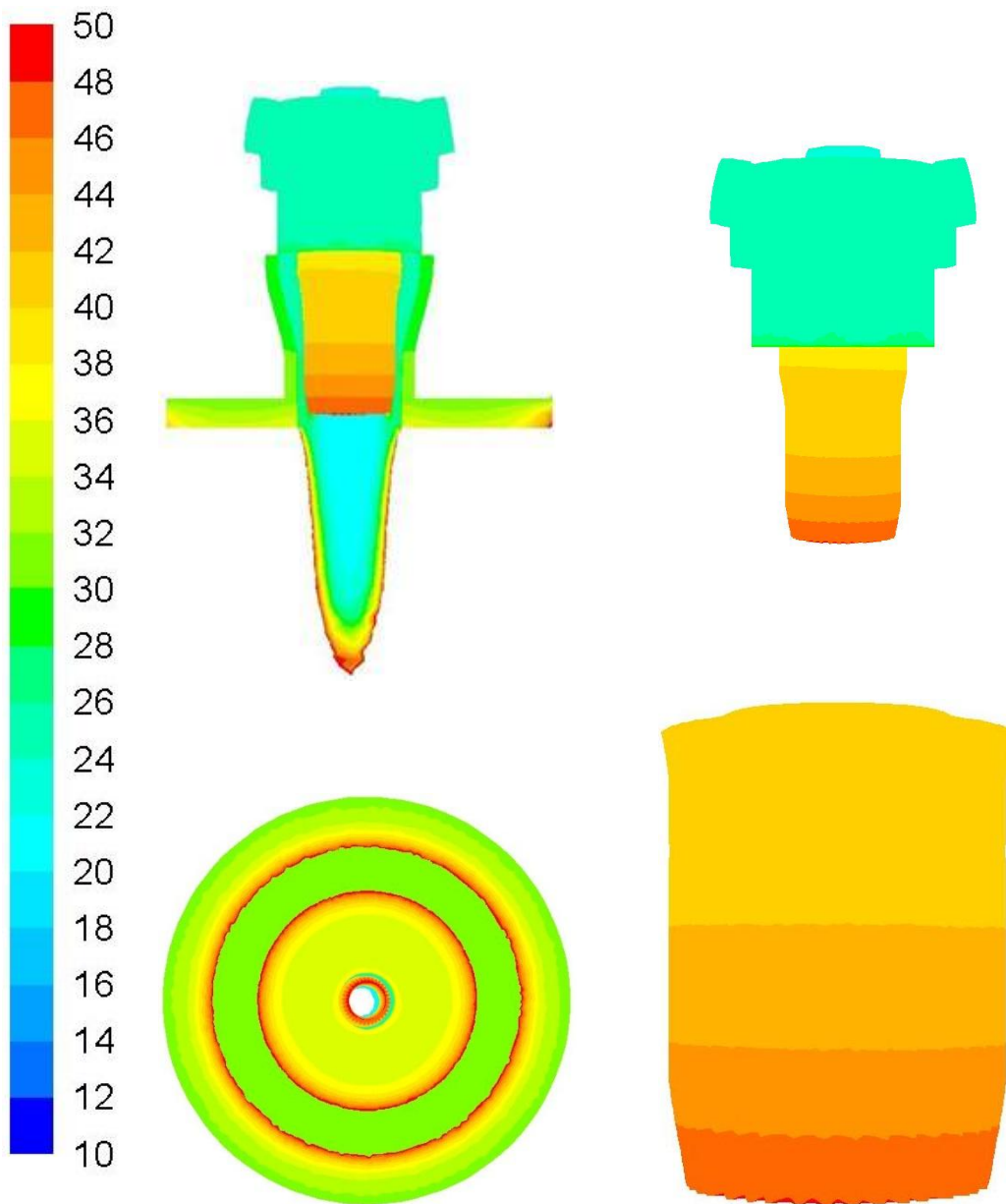


Fig. B16: Temperature of Nozzle 2 with optimized nozzle air flow rate ($40 \text{ m}^3 \text{ h}^{-1}$)

Appendix C: CFD Simulation results of simplified nozzle (Chapter 6)

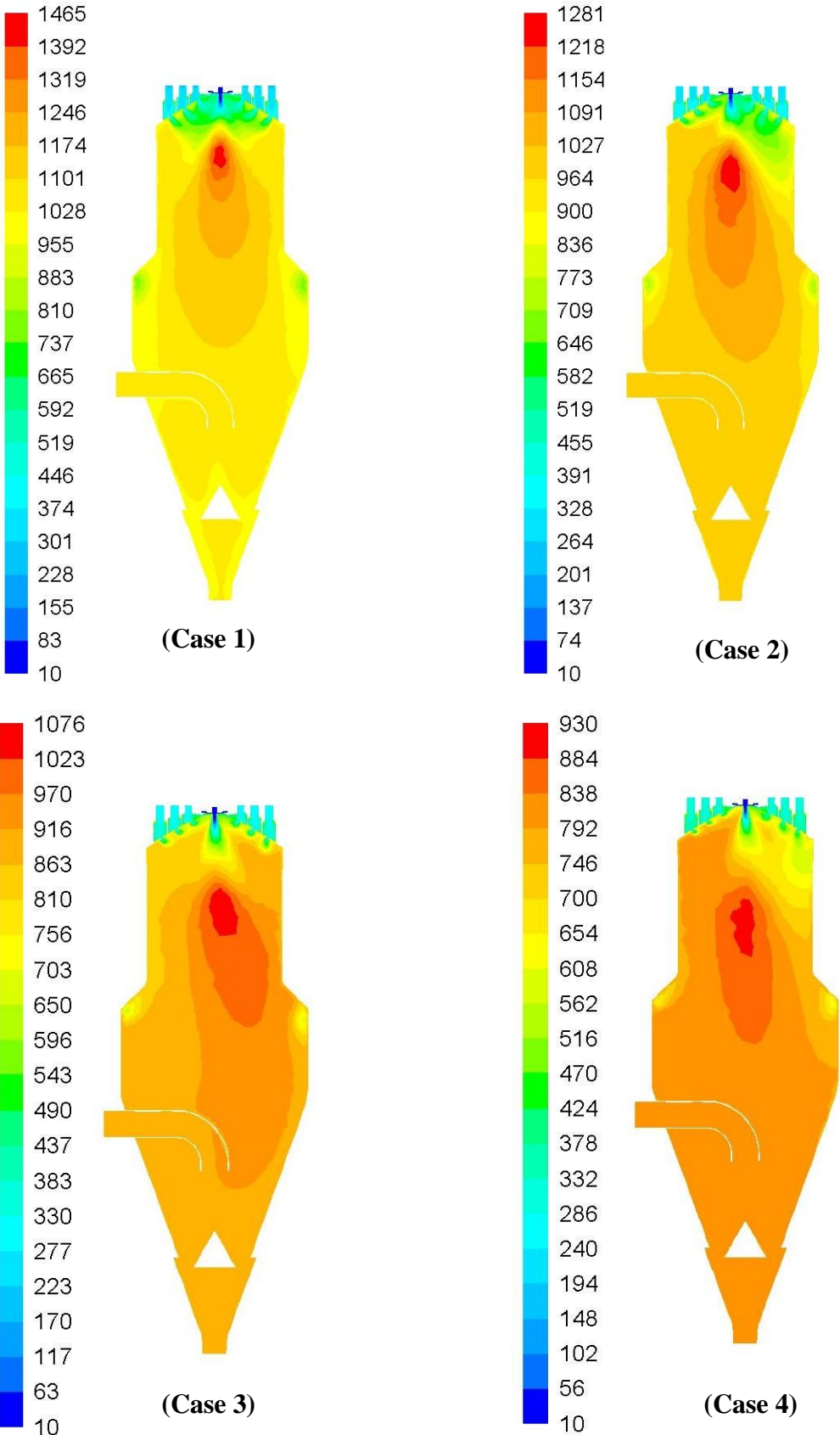
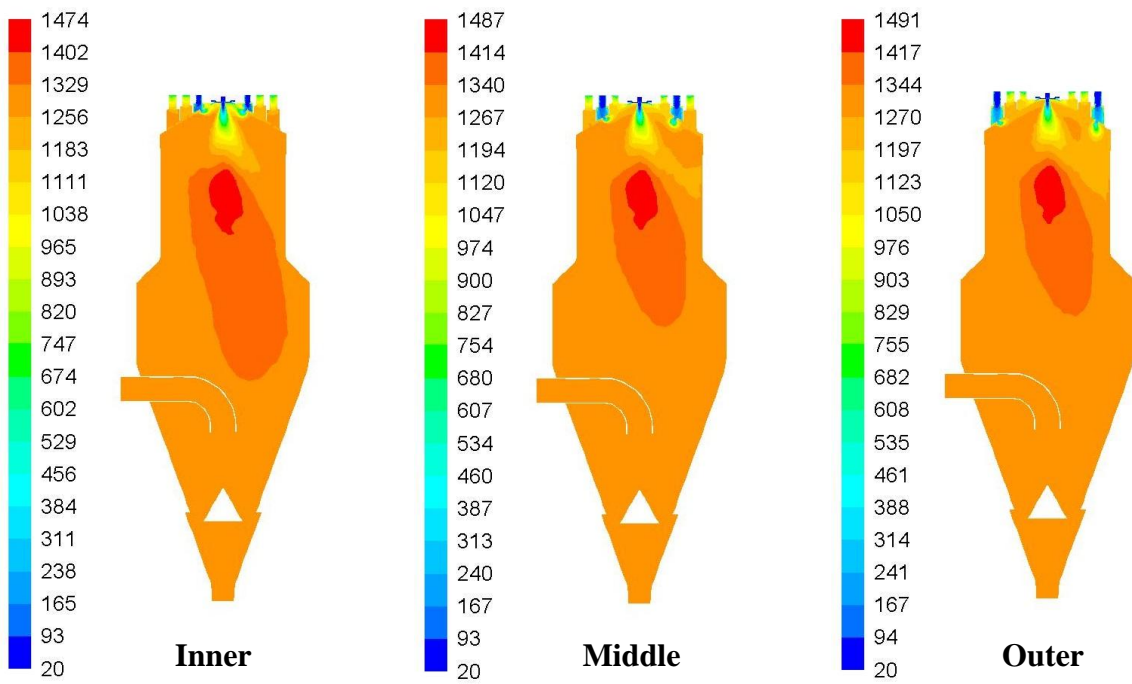
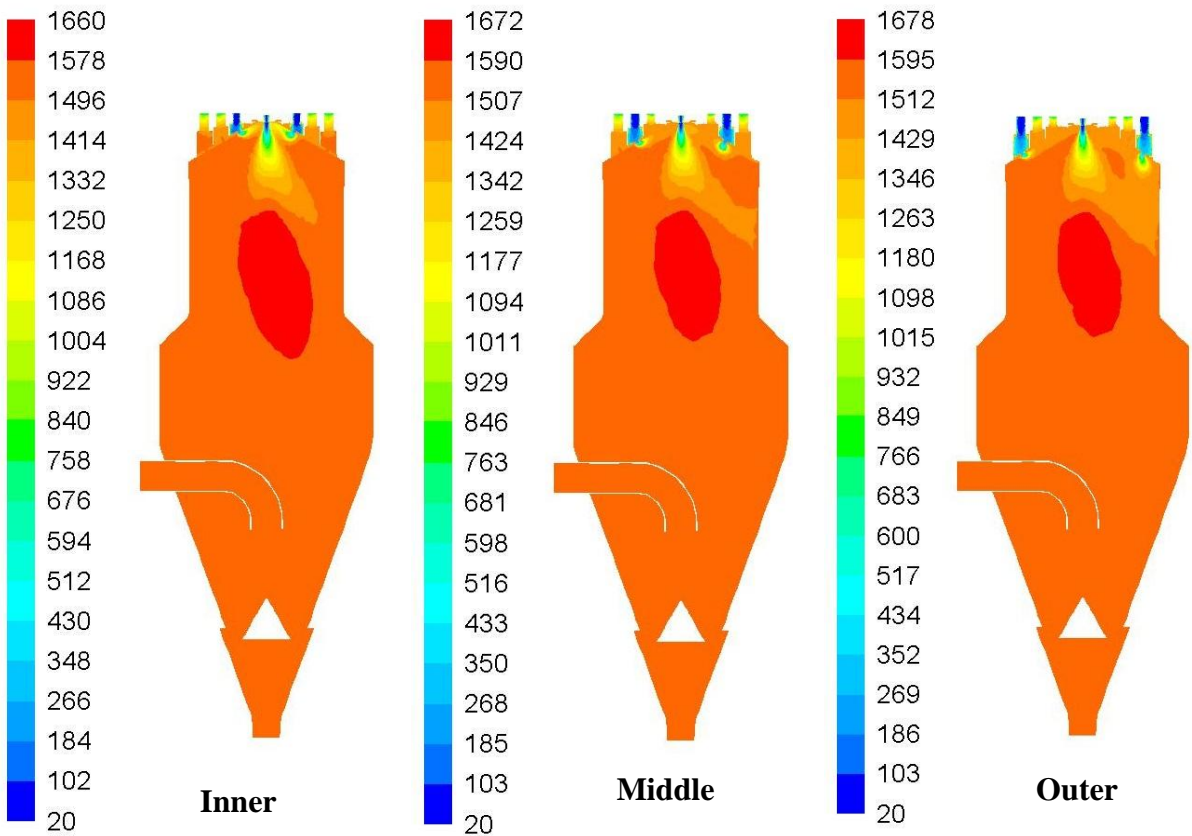


Fig. C1: Temperature profile for different cases of nozzle air flow rates (water cooling)



With water cooling



Without water cooling

Fig. C2: Temperature profile with different injection locations of primary air

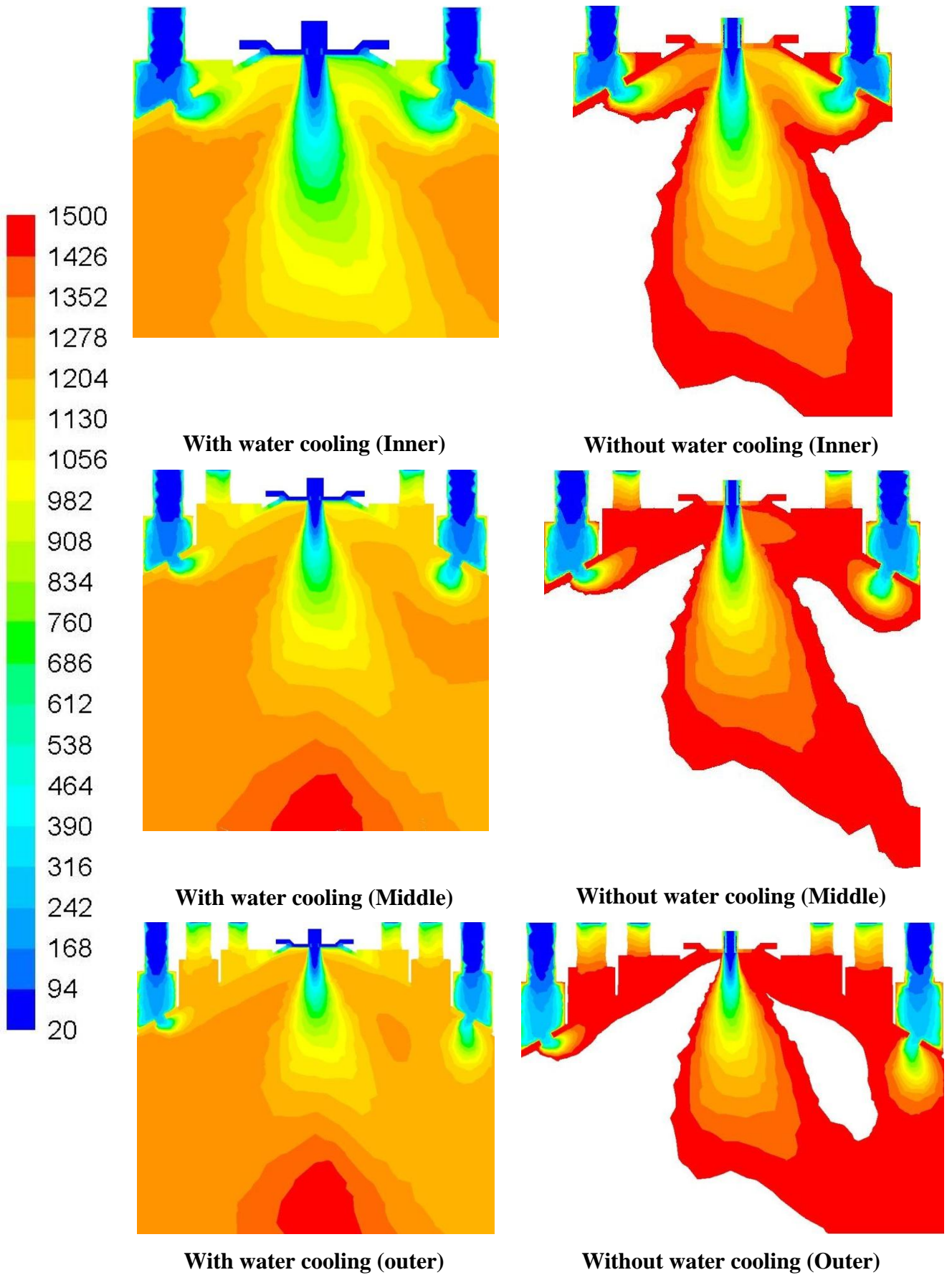


Fig. C3: Effect of different positions of primary air inlet on temperature near nozzle

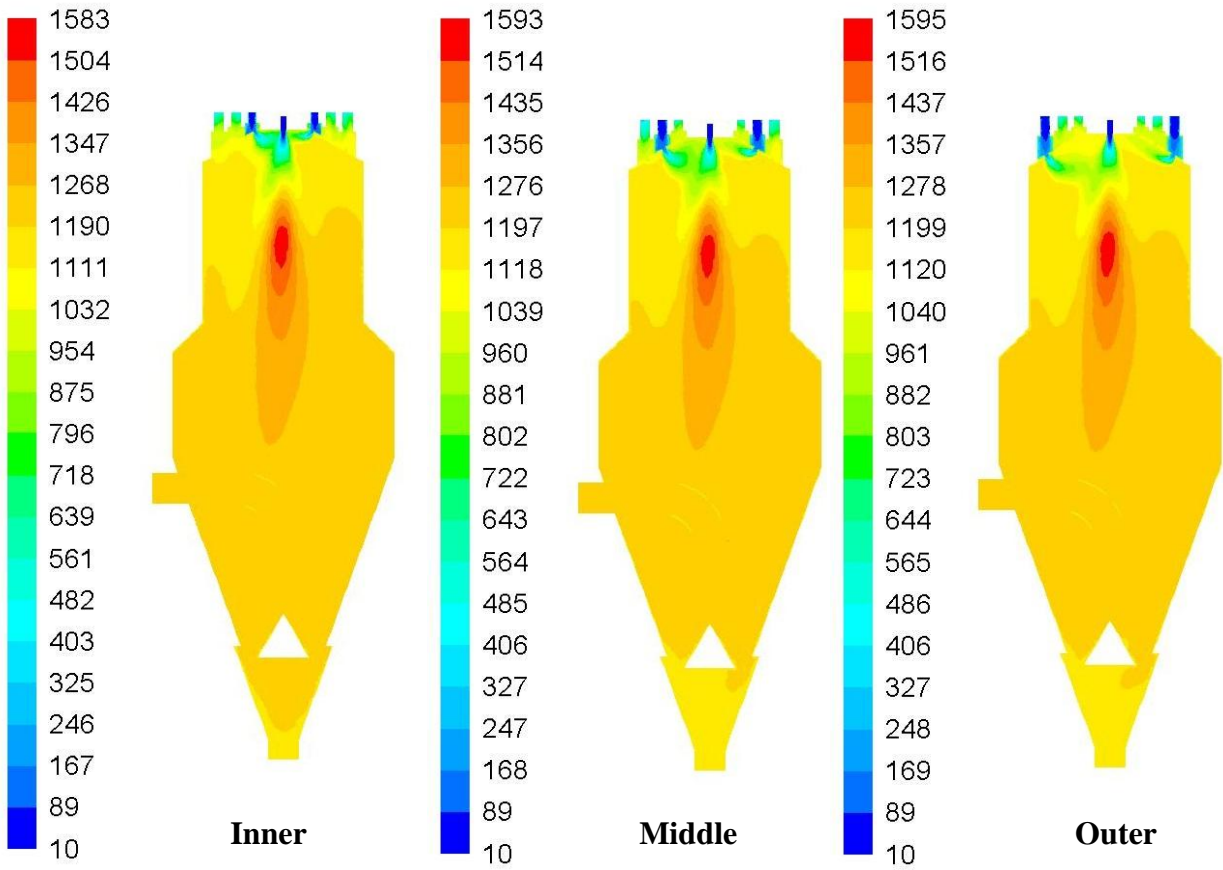


Fig. C4: Effect of heat flux from top of the furnace and different positions of primary air inlet

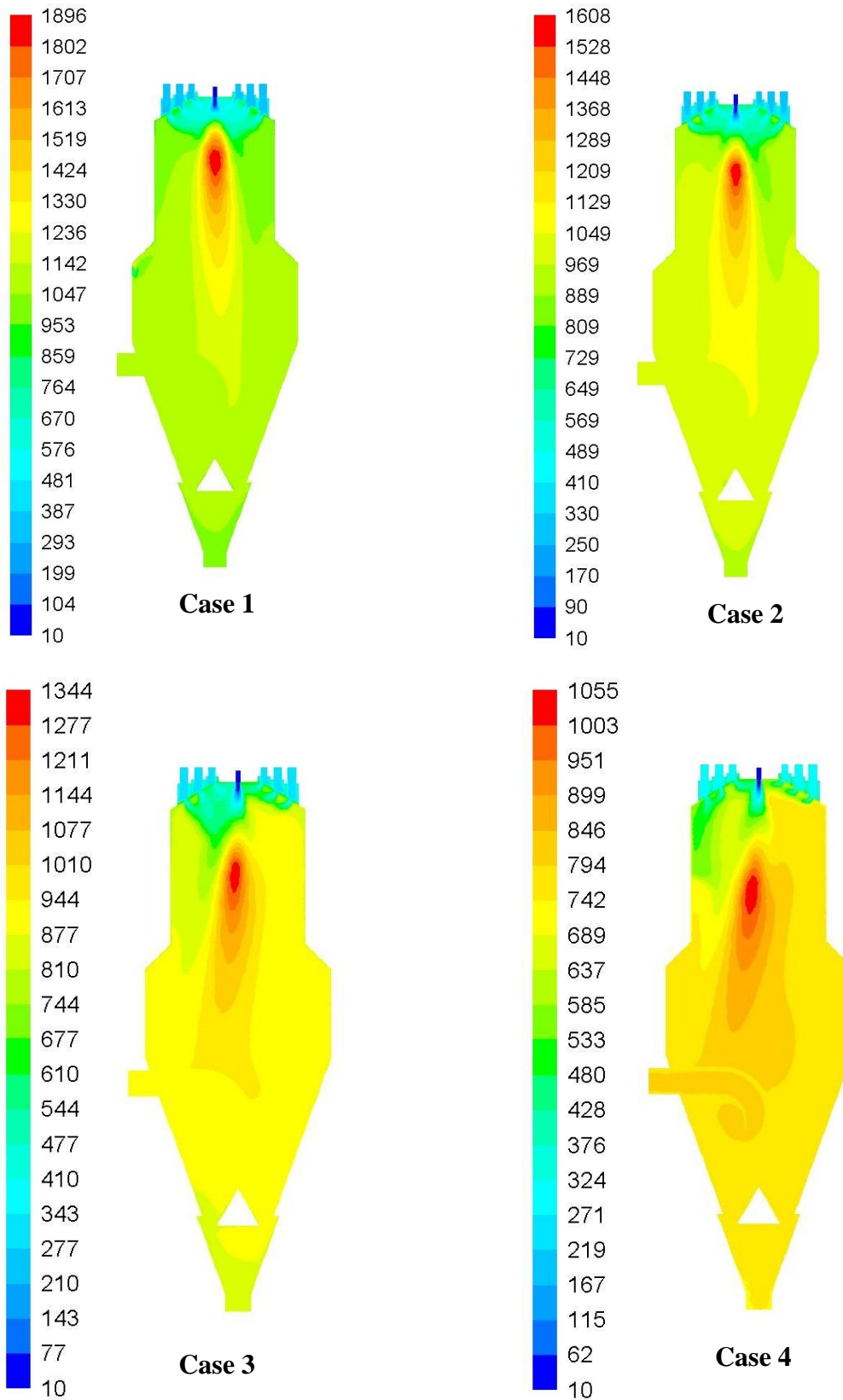


Fig. C5: Temperature profile for different cases of nozzle air flow rates (case of air cooling)

Appendix D: Contours of flue gases (Chapter 7)

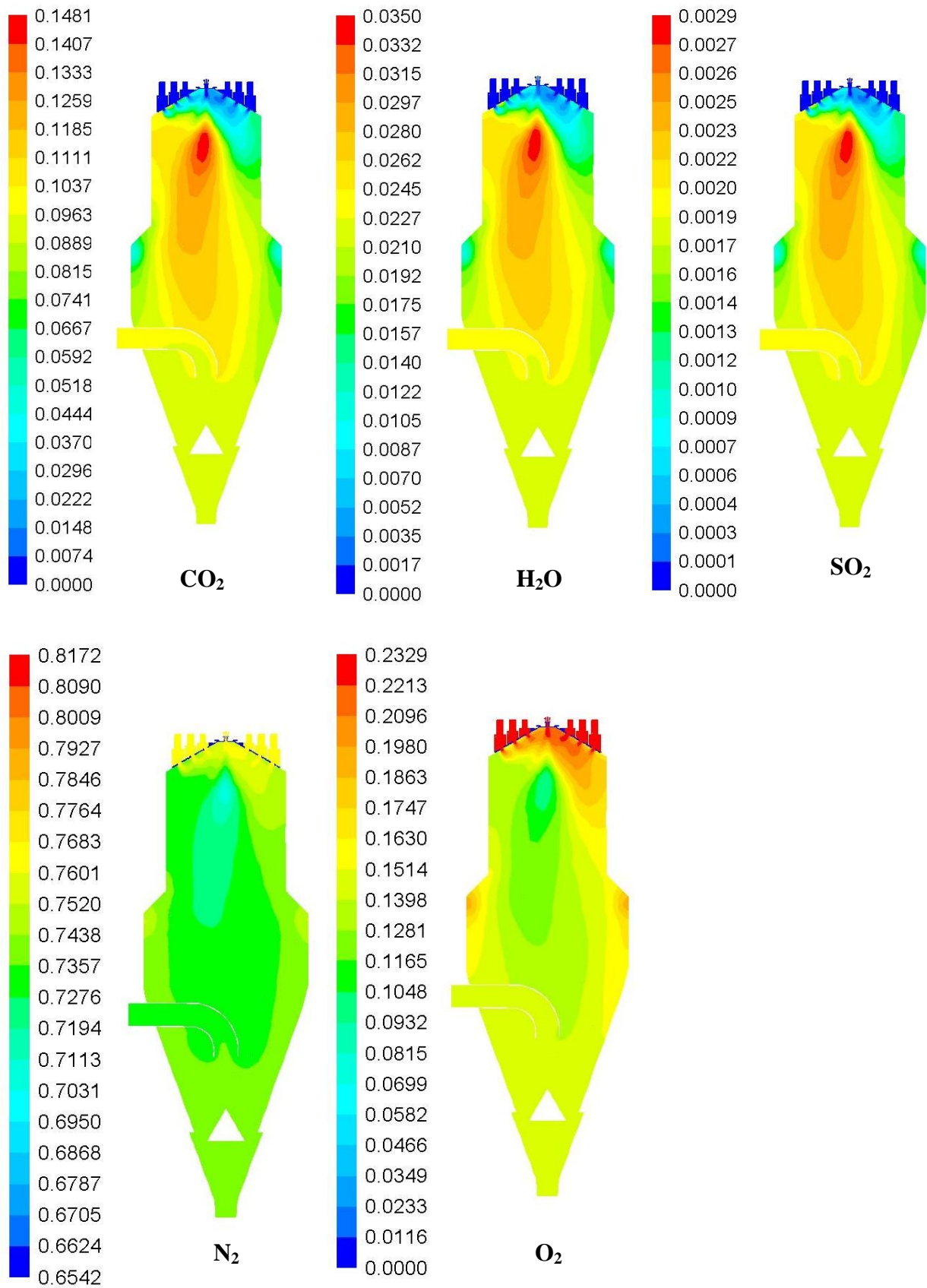


Fig. D1: Mass fractions of combustion gases

Appendix E: List of CFD simulations

Table E1: List of CFD simulations and modeling approaches (Digital files)

Simulation ID	Description	Chapter
EXL 1	Species balance model for different solid fuels	2
Sim-N1 D1	Simulations for Nozzle 1 with Data Set 1	4
Sim-N1 C	Simulations for Nozzle 1 with coarse mesh	4
Sim-N1 F	Simulations for Nozzle 1 with fine mesh	4
Sim-N2 C	Simulations for Nozzle 2 with coarse mesh	4, 5
Sim-N2 F	Simulations for Nozzle 2 with fine mesh	4, 5
Sim-N3 C	Simulations for Nozzle 3 with coarse mesh	4, 5
Sim-N3 F	Simulations for Nozzle 3 with fine mesh	4, 5
Sim-N4 C	Simulations for Nozzle 4 with coarse mesh	4, 5
Sim-N4 F	Simulations for Nozzle 4 with fine mesh	4, 5
MAT 1	Mass and energy balance for Nozzle 1 to Nozzle 4	4, 5
Sim-N2 D1	Simulations for Nozzle 2 with Data Set 1	5
Sim-N3 D1	Simulations for Nozzle 3 with Data Set 1	5
Sim-N4 D1	Simulations for Nozzle 4 with Data Set 1	5
Sim-N1 D2	Simulations for Nozzle 1 with Data Set 2	5
Sim-N2 D2	Simulations for Nozzle 2 with Data Set 2	5
Sim-N3 D2	Simulations for Nozzle 3 with Data Set 2	5
Sim-N4 D2	Simulations for Nozzle 4 with Data Set 2	5
Sim-N2 P2	Simulations for Nozzle 2 with average fuel particle size 2 μm	5
Sim-N2 P10	Simulations for Nozzle 2 with average fuel particle size 10 μm	5
Sim-N2 P20	Simulations for Nozzle 2 with average fuel particle size 20 μm	5
Sim-N3 P2	Simulations for Nozzle 3 with average fuel particle size 2 μm	5
Sim-N3 P10	Simulations for Nozzle 3 with average fuel particle size 10 μm	5
Sim-N3 P20	Simulations for Nozzle 3 with average fuel particle size 20 μm	5
Sim-N2 D3	Simulations for Nozzle 2 with Data Set 3	5
Sim-N2 D4	Simulations for Nozzle 2 with Data Set 4	5
Sim-N2 D5	Simulations for Nozzle 2 with Data Set 5	5
Sim-N2 C1 CA	Simulations for sectional increase (CA) in Nozzle 2 (Case 1)	5
Sim-N2 C1 FTA	Simulations for sectional increase (FTA) in Nozzle 2 (Case 1)	5
Sim-N2 C2 CA	Simulations for sectional increase (CA) in Nozzle 2 (Case 2)	5
Sim-N2 C2 FTA	Simulations for sectional increase (FTA) in Nozzle 2 (Case 2)	5
Sim-N2 C3 CA	Simulations for sectional increase (CA) in Nozzle 2 (Case 3)	5
Sim-N2 C3 FTA	Simulations for sectional increase (FTA) in Nozzle 2 (Case 3)	5
Sim-N2 C4 CA	Simulations for sectional increase (CA) in Nozzle 2 (Case 4)	5
Sim-N2 C4 FTA	Simulations for sectional increase (FTA) in Nozzle 2 (Case 4)	5

Simulation ID	Description	Chapter
Sim-N1 NA1	Simulations for optimization of Nozzle 1 Case 1	6
Sim-N1 NA2	Simulations for optimization of Nozzle 1 Case 2	6
Sim-N1 NA3	Simulations for optimization of Nozzle 1 Case 3	6
Sim-N1 NA4	Simulations for optimization of Nozzle 1 Case 4	6
Sim-N1 PA1	Simulations for different primary air inlet positions (Without losses)	6
Sim-N1 PA2	Simulations for different primary air inlet positions (Water cooling)	6
Sim-N1 H	Simulations with heat losses and different primary air inlet positions	6
Sim-N1 H1	Simulations with heat losses to ambient Case 1	6
Sim-N1 H2	Simulations with heat losses to ambient Case 2	6
Sim-N1 H3	Simulations with heat losses to ambient Case 3	6
Sim-N1 H4	Simulations with heat losses to ambient Case 4	6
Sim-N1 Exp	Simulations with operating conditions of experimental analysis	7
Sim-N2 WT	Simulations with Nozzle2 for comparison with calculated results	7

List of Own Publications and Student Theses

Journal/conference publications

1. Farid, M. U., A. Bück, W. Heineken, M. Gohla and N. Zobel. 2017. Study on nozzle design for combustion of solid materials with low melting points. Applied Thermal Engineering. 115:832-859.
2. Farid, M. U., A. Bück, W. Heineken, M. Gohla and N. Zobel. 2017. Fuel nozzle design for the combustion of materials with low melting point: A CFD modeling study. Proceedings of 18th Forschungskolloquium am Fraunhofer (IFF), November 25, 2016. ISSN 2191-8783.
3. Farid, M. U., A. Bück, W. Heineken, M. Gohla, N. Zobel and C. Keichel. Simplification of fuel nozzle for PFC combustion of solid materials with low melting point: A CFD modeling study. (In progress).

Oral/poster presentations in conferences/colloquia

1. Farid, M. U., A. Bück, W. Heineken, M. Gohla and N. Zobel, 2015. A new technology for the combustion of materials with low melting points. 2015. 10th European Congress of Chemical Engineering (ECCE 10), September 27, 2015 to October 01, 2015, Nice, France. (Poster)
2. Farid, M. U., A. Bück, W. Heineken, M. Gohla and N. Zobel, 2016. Eine neue Technologie zur Verbrennung von Materialien mit niedrigem Schmelzpunkt. 2016. Jahrestreffen der ProcessNet-Fachgruppen Energieverfahrenstechnik und Abfallbehandlung und Wertstoffrückgewinnung, February 23-24, 2016 at Frankfurt am Main, Germany. (Oral)
3. Farid, M. U., A. Bück, W. Heineken, M. Gohla and N. Zobel, 2016. CFD study on different nozzle designs for the combustion of pulverized material (A new technology for the combustion of materials with low melting points). International Congress on Particle Technology, April 19-21, 2016, Nürnberg, Germany. (Poster)
4. Farid, M. U., A. Bück, W. Heineken, M. Gohla and N. Zobel. 2016, Fuel nozzle selection for pulverized (waste) combustion plant: A CFD modeling study. IFF Business Colloquium, August 18, 2016, Fraunhofer (IFF) Magdeburg, Germany. (Oral)

Student thesis

1. Shaikh, F. M., 2016. Modeling of combustion process for solid fuels. Master thesis, Otto von Guericke University, Magdeburg, Germany.

Curriculum Vitae

Personal Information

Name	Muhammad Usman Farid
Date of birth	May 07, 1990
Place of birth	Sahiwal, Pakistan

Education

2005-2007	H.S.S.C. (F.Sc. Pre-Engineering), Government College Sahiwal, Pakistan
2007-2011	B.Sc. Agricultural Engineering, University of Agriculture, Faisalabad, Pakistan
2011-2013	M.Sc. (Hons.) Agricultural Engineering, University of Agriculture, Faisalabad, Pakistan
2014-present	PhD Process Engineering, Chair of Thermal Process Engineering, Otto von Guericke University, Magdeburg, Germany

Work Experience

2012-2013	Assistant Executive Engineer, Department of Farm Machinery and Power, Faculty of Agricultural Engineering and Technology, University of Agriculture, Faisalabad, Pakistan
From 2013	Lecturer, Department of Structures and Environmental Engineering, University of Agriculture, Faisalabad, Pakistan